Automated High-Throughput Experimentation for a Fast and Reliable Bioprocess Development

Automatisiertes Experimentieren im Hochdurchsatz
für eine schnelle und zuverlässige Bioprozessentwicklung

Von der Fakultät für Maschinenwesen der Rheinisch-Westfälischen Technischen Hochschule Aachen zur Erlangung des akademischen Grades eines Doktors der Ingenieurwissenschaften genehmigte Dissertation

vorgelegt von

Martin Kunze

Berichter: Universitätsprofessor Dr.-Ing. Jochen Büchs
Universitätsprofessor Dr. rer. nat. Karl-Erich Jaeger

Tag der mündlichen Prüfung: 04.06.2019

Aspects of this thesis have been published previously:

1) Kunze, M.; Huber, R.; Gutjahr, C.; Müllner, S.; Büchs, J. (2012) Predictive tool for recombinant protein production in Escherichia coli shake-flask cultures using an on-line monitoring system. Biotechnol. Prog. 2012, 28(1):103

2) Kunze, M.; Roth, S.; Gartz, E.; Büchs, J. (2014) Pitfalls in optical on-line monitoring for high-throughput screening of microbial systems. Microbial Cell Factories 2014, 13:53

3) Kunze, M.; Lattermann, C.; Diederichs, S.; Kroutil, W.; Büchs, J. (2014) Minireactor-based high-throughput temperature profiling for the optimization of microbial and enzymatic processes. Journal of Biological Engineering 2014, 8:22

4) Wewetzer, S.J.; Kunze, M.; Ladner, T.; Luchterhand, B.; Roth, S.; Rahmen, N.; Kloß, R.;Costa e Silva, A.; Regestein, L.; Büchs, J. (2015) Parallel use of shake flask and microtiter plate online measuring devices (RAMOS and BioLector) reduces the number of experiments in laboratory-scale stirred tank bioreactors. Journal of Biological Engineering 2015, 9:9

5) Mühlmann, M.; Kunze, M.; Ribeiro, J.; Geinitz, B.; Lehmann, C.; Schwaneberg, U.; Commandeur, U.; Büchs, J. (2017) Cellulolytic RoboLector – towards an automated high-throughput screening platform for recombinant cellulase expression. Journal of Biological Engineering 2017, 11:1

Aspects were further presented at conferences as oral presentations:

6) Kunze, M.; Schmidt, T.; Fischer, R.; Commandeur, U.; Büchs, J. (2012) Application of high-throughput screening methods for the development of improved enzymes for cellulose degradation. Achema 2012, Frankfurt a.M.

7) Kunze, M.; Roth, S.; Bock, S.; Büchs, J. (2012) Kombinierte Kultivierung in Kleinkultursystemen als Alternative zum Laborfermenter für die Bioprozessentwicklung. 30. DECHEMA-Jahrestagung der Biotechnologen und ProcessNet-Jahrestagung 2012, Karlsruhe

8) Kunze, M.; Schmidt, T.; Fischer, R.; Commandeur, U.; Büchs, J. (2012) How an automated screening system can support the enzyme evolution, selection and production process for cellulose degradation. ESBES + ISPPP 2012, Istanbul (Turkey)

I. Abstract

The demand for feasible bioprocesses is continuously increasing in order to realize new production pathways, convert yet unconsidered raw materials, and allow new or advanced product portfolios. One bioprocess of major interest over the last years is the production of fuels or chemicals from biomass. One key process within this production chain is the degradation of recalcitrant cellulose to better processible soluble sugars, and cellulases are key players in the hydrolyzation of cellulose. To identify best working cellulase candidates and their production hosts a reliable screening procedure is necessary. Therefore, a robotic platform is presented, the so called "Cellulolytic RoboLector". Automated upstream, downstream, and analytical process steps in high-throughput are described and evaluated using different microbial and enzymatic candidates as model systems.

One key technique within the RoboLector system, the BioLector device, allows for high-throughput online monitoring of process relevant parameters via optical methods. During the extensive work with the BioLector, some yet undiscovered pitfalls were identified which might mislead the user of such techniques and cause incorrect results. Solutions are presented to overcome these obstacles either by mathematical correction or experimental modifications.

Finally, a unique system for rapid determination of temperature dependent reaction kinetics for microbial and enzymatic reactions is presented. The combination of an optical on-line monitoring device with a customized temperature control unit for 96 well microtiter plates allows high-throughput temperature profiling.

Taking altogether, this work gives an extensive overview how novel automated high-throughput protocols for bioprocess development and characterization are designed, realized, and evaluated.

II. Kurzfassung

Ob für die Realisierung neuer Produktionsrouten, die Nutzung bisher ungenutzter Rohstoffe oder die Schaffung neuer oder erweiterter Produktportfolios: Der Bedarf an rentablen biotechnologischen Prozessen hat über die letzten Jahre und Jahrzehnte kontinuierlich zugenommen. Ein prominentes Beispiel dafür ist die Produktion von Kraftstoffen oder anderen Chemikalien aus Biomasse. Ein Schlüsselprozess dabei ist der Aufschluss schwer abbaubarer Cellulose zu leichter zu verarbeitenden, löslichen Zuckermolekülen. Entsprechende Enzyme, Cellulasen, spielen dafür eine zentrale Rolle. Zur Identifikation geeigneter Enzymkandidaten sowie zugehöriger Expressionsorganismen ist ein aussagekräftiges Screening-System unerlässlich. Dafür wurde die in dieser Arbeit präsentierte Roboter-Plattform entwickelt: Der so genannte “Cellulolytische RoboLector”. Das System ermöglicht die Durchführung von Upstream- und Downstream-Prozessen, sowie verschiedene Analysemethoden im Hochdurchsatz. Seine Einsatzfähigkeit wurde anhand verschiedener mikrobieller und enzymatischer Modellsysteme gezeigt.

Zentrales Element des RoboLector’s ist der BioLector, welcher die Echtzeiterfassung prozessrelevanter Parameter mittels optischer Methoden im Hochdurchsatz erlaubt. Im Laufe der experimentellen Arbeiten zeigten sich bisher unentdeckte Fallstricke beim Einsatz der Technologie, die u.U. zu verfälschten Daten führen und den Nutzer falsche Schlüsse ziehen lassen. Zur Vermeidung wurden Lösungen dafür erarbeitet, basierend auf mathematischen Korrekturen oder experimentellen Anpassungen.

Zu guter Letzt wurde ein einzigartiges System entwickelt, um temperaturabhängige Kinetiken mikrobieller und enzymatischer Reaktionen im Hochdurchsatz bestimmen zu können. Dabei erlaubt die Kombination eines optischen Online-Monitoring-Systems mit einem speziell konstruierten Temperaturkontrollsystem für Mikrotiterplatten individuelle Temperaturprofile über 96 Kavitäten.

Zusammenfassend gibt diese Arbeit einen ausführlichen Überblick darüber, wie fortschrittliche automatische Protokolle zur Entwicklung und Charakterisierung biotechnologischer Prozesse erstellt, umgesetzt, und evaluiert werden.

III. Contents

IV. List of Figures

V. List of Tables

1. Introduction

Over the last years and decades, the demand for feasible bioprocesses is continuously increasing in order to realize new production pathways, convert yet unconsidered raw materials, and allow new or advanced product portfolios. However, respective process development is still laborious and time consuming since bio-catalytic processes, enzymatic or microbial, are rather complex compared to chemical reactions. Consequently, the right development strategy is essential to succeed. Today, it is already consensus that fast track process development starts with screening experiments covering a broad range of process conditions and reaction components. Thereby, the smallest possible experimental scale is preferred, in order to save material and enable a certain degree of parallelization. Consequently, miniaturization and high-throughput experimentation are often heard buzzwords in today's labs. Even apparently well understood and characterized processes like recombinant protein production with a common host organism like *Escherichia coli* (*E. coli*), might be much more challenging than expected. As *E. coli* is well defined with respect to its genome and metabolism, it is a favored host organism for recombinant protein production. However, many processes for recombinant protein production run under suboptimal conditions caused by wrong or incomplete information from an improper screening procedure, because appropriate screening systems are still lacking in process development departments.

To point this out, 16 clones of the same *E. coli* strain with foreign gene sequences, encoding for different target proteins, were cultivated in a typical auto-induction medium, containing glucose, lactose, and glycerol, to identify relationships between metabolic activity and target protein production. Therefore, the oxygen transfer rate (OTR), determined on-line in shake flasks by applying a respiration activity monitoring system (RAMOS) device, was used to

characterize the metabolic state of the recombinant organisms. All 16 clones showed a remarkably different respiration activity, biomass, and protein formation under induced conditions. However, the clones could be classified into three distinct types, and correlations could be made between OTR patterns and target protein production. With the acquired knowledge it was subsequently possible to modify the auto-induction medium in order to increase the productivity. For two of the three types, a decrease of the target protein was observed, after the optimal harvest time had passed. Furthermore, additional glucose accelerated the production process for one clone, whereas, for another clone, lactose addition led to higher volumetric product yields. This shows that individual process knowledge is necessary to decide for optimal process conditions specific for each individual strain.

One bioprocess of major interest over the last years is the production of fuels or chemicals from biomass. Lots of effort was invested to make the chemical and energetic potential of plant material accessible. One key process within this production chain is the degradation of recalcitrant cellulose to better processible soluble sugars. Cellulolytic enzymes, or cellulases, are key player in the hydrolyzation of cellulose. Unfortunately, this reaction is slow and a bottleneck in the process chain from biomass to intermediates and final products due to low activities of the enzymes. To overcome this draw back, a lot of effort is put into the area of protein engineering, to modify these enzymes by directed evolution or rational design. Huge clone libraries are constructed and have to be screened for improved variants. Thereby, inconsistencies might lead to wrong or incomplete information from an improper screening procedure as described before and, hence, distort the screening results.

Automated high-throughput screening is the method of choice to tackle this experimental effort, but up to now only a few process steps are adapted to automated platforms and little attention has been turned to the reproducibility of such screening experiments. For the example of cellulase production in microbial cultures and subsequent enzyme

characterization, this work demonstrates how manual experiments for gaining essential information about bioprocesses can be adapted to automated handling in order to allow fast and reliable data generation. Therefore, an extended robotic platform is presented, the so called “Cellulolytic RoboLector”, to conduct automated high-throughput screenings of clone libraries including pre-culture synchronization and biomass specific induction. Automated upstream, downstream, and analytical process steps are described and evaluated using different microbial and enzymatic candidates as model systems. Conventional protocols for media preparation, inoculation and cultivation, cell lysis, and cellulase activity assays are successfully adapted to automatable high-throughput protocols.

One key technique within the RoboLector system is the BioLector device, a cutting edge technology mainly applied for high-throughput screening of microbial systems. The technology is simple to handle and offers various options of optical online measurements. The parallelization and small scale in microtiter plates allow economical high throughput and, hence, to screen many parameters in reasonable time. Special microtiter plates with optodes for dissolved oxygen tension (DOT) and pH measurement allow detailed insights to microbial cultivations. Furthermore, fluorescent proteins as fluorescent tags made the tracking of cellular proteins in-vivo a routine task. All these tools significantly contribute to the understanding of bioprocesses. However, during the extensive work with the BioLector as part of the advanced RoboLector system, some yet undiscovered pitfalls were identified which might mislead the user of such techniques. It became obvious that fluorescent proteins can interfere with other optical signals leading to incorrect results. Consequently, it became necessary to characterize these effects in detail and present possibilities how such adverse effects can be corrected or minimized. This can be done either by mathematical procedures or modification of the measuring method. Additionally, it is shown how morphological changes of microbial cells can affect the biomass on-line monitoring via scattered light.

By applying the “Cellulolytic RoboLector” a broad spectrum of different operating parameters can be investigated in order to find suitable cellulase candidates and production conditions. However, temperature is one of the most important bioprocess parameters. Unfortunately, systems for rapid determination of temperature dependent reaction kinetics are rare and not yet available for integration to automated systems. Obviously, there is a need for a high-throughput screening procedure of temperature dependent process behavior. Even though, well equipped micro-bioreactors are a promising approach, sufficient temperature control is quite challenging and rather complex. In this work, a unique system for high-throughput temperature profiling is presented combining an optical on-line monitoring device with a customized temperature control unit for 96 well microtiter plates. By exposing microtiter plates to specific temperature profiles, high-throughput temperature optimization for microbial and enzymatic systems in a micro-scale is realized. For single well resolved temperature measurement fluorescence thermometry was used, combining two fluorescent dyes. Thereby, the real time monitoring of the microbial and enzymatic reactions with the BioLector technique provides extensive data output. To evaluate this novel system the temperature optima for different microorganisms regarding growth and recombinant protein production were determined. Furthermore, a cellulase cocktail as a representative for enzymes was investigated applying a fluorescent activity assay. Even though, the developed temperature profiling system is not yet ready for complete automation, a future integration into the RoboLector platform is desirable and possible.

Taking altogether, this work gives an extensive overview how novel automated high-throughput protocols for bioprocess development and characterization are designed, realized, and evaluated. Finally, the presented techniques deliver reliable data about critical process parameters. And even though, this work focusses on the production and characterization of recombinant cellulases, several procedures and methods are simple to adapt to alternative demands. Combined with the possibility of adding or changing equipment, this makes the

RoboLector system a universal automated high-throughput screening system for bio-catalytic processes.

2. Chapter I - Predictive tool for recombinant protein production in *E. coli* shake flask cultures using an on-line monitoring system

2.1. Background

Recombinant DNA technology is a common tool for producing many different types of recombinant proteins such as enzymes, hormones and cytokines. Many of these recombinant proteins are produced using genetically modified *Escherichia coli*, because this bacterium is well known, allows easy introduction of foreign genes, grows fast on inexpensive media and requires no complicated fermentation equipment. The economic feasibility of heterogeneous protein production processes depends on two things: Acquiring high cell densities and high concentrations of target protein per cell. Unfortunately, these two requirements are not always given. In fact, there are several studies about how recombinant proteins actually affect the host organism, whereby these proteins may inhibit cell growth [1]. To avoid this, controllable expression systems have been developed to separate cell growth and protein formation in two consecutive phases [2]. After high biomass concentrations are obtained in a fermenter, the foreign gene can be subsequently induced by environmental factors such as temperature [3], dissolved oxygen tension [4] or particular medium components [5]. An easy and comfortable approach to induce protein production at the proper time is to apply auto-induction media [6-8]. The auto-induction method works as follows: First, the production of the target protein is repressed by the primary carbon source (often glucose) of the organism. This repression initially guarantees undisturbed microbial growth yielding high cell densities. Once this repressing substrate is fully depleted, the target protein production begins.

Even though effective tools such as inducible expression systems and auto-induction media exist, the production of recombinant proteins influences the host organism's metabolism. For many heterologous proteins, their overproduction leads to a metabolic burden [9-12], which is

defined as the amount of resources withdrawn from the host's metabolism. Lee and Ramirez [13] assumed that an additional load to the host's metabolism affects the cell growth in different ways. They mentioned typical behaviors where type 1 is not affected by the protein formation, for type 2 the cell growth rate decreases after induction but recovers later on, and type 3, where the cells cannot regenerate from the shock caused by the induction. However, detailed knowledge about this is still lacking. Phenomena such as metabolic burden and its effects on final product yields are still poorly understood, because of the lack of appropriate monitoring systems. An on-line system is described for quantifying the metabolic burden in a 50 L bioreactor where the respiratory activity is determined via exhaust gas analysis and biomass formation via ammonia consumption for pH control [12,14]. Nonetheless, such fermentations require considerable equipment, chemicals and time. Huber et al. [15] presented a system for monitoring the influence of recombinant protein production on microscale, using a technique for scattered light and fluorescence measurement in shaken microtiter plates developed by Samorsky et al. [16] and Kensy et al. [17]. Conventional microtiter plates, however, run under process conditions which are not always comparable to those for larger scales, in particluar in terms of oxygen transfer. Furthermore, for a direct on-line measurement only proteins with special properties, e.g. fluorescence, are suitable.

In this work the recombinant protein production of *E. coli* was investigated in shake flasks. The oxygen transfer rate (OTR), as determined by the RAMOS (**R**espiration **A**ctivity **MO**nitoring **S**ystem), developed by Anderlei et al [18,19], was used as the characteristic parameter for measuring the metabolic state of the bacteria. Sixteen clones of *E. coli* K12 SCS1 bearing gene sequences for different foreign model proteins were studied. They were cultivated in an auto-induction medium to investigate the influence of heterogeneous protein formation to the host's respiration behavior. Consequently, the generated results were used to modify the auto-induction medium in order to increase target protein yield.

2.2. Material & Methods

2.2.1. Organism

For all experiments the *E. coli* K12 strain SCS1 (Stratagene, USA) was used. Its genotype is *rec*A1 *end*A1 *gyr*A96 *thi*-1 *hsd*R17 (r_K^+ m_K^-) *sup*E44 *rel*A1. Sixteen clones, cited as PR01-16, have been kindly provided by Protagen AG (Germany), randomly chosen from a hEx1 cDNA library developed by Büssow et al. [20]. These clones express different human model proteins from fetal brain tissue. SCS1 cells contain the plasmid pSE111 with the *arg*U^+ gene to supply a rare t-RNA for arginine that improves expression of some target genes, the *lac*I^Q gene to supply an additional *lac* repressor to reduce basal expression and a gene encoding for kanamycin resistance. The used expression plasmid pQE30NST (Qiagen, Germany, GenBank accession no. AF074376) harbors the sequence for the target protein controlled by a T5 promoter under the control of a pair of *lac* operators. According to the manufacturer's specification the vector is classified as low-copy plasmid with a copy number of approximately 20-30 per cell. Target proteins are equipped with N-terminal His_6-tags for affinity purification or antibody recognition [21]. Additionally, pQE30NST encodes for resistance to ampicillin.

2.2.2. Media and Solutions

For growth under non-inducing conditions, *Terrific Broth* medium (TB medium) consisting of 12 g/L tryptone, 24 g/L yeast extract, 12.54 g/L K_2HPO_4, 2.31 g/L KH_2PO_4 and 5 g/L glycerol (all ingredients from Roth, Germany) dissolved in water was used. The pH-value was 7.2±0.2 without adjustment.

For experiments under induced conditions, the *OvernightExpress*™ Instant TB medium (OnEx, Novagen, Merck Bioscience, Germany) was applied. OnEx is a commercially

available ready-made auto-induction medium. It consists of complex components similar to TB medium and the additional carbon sources glucose, lactose and glycerol. Similar media are available from Invitrogen™ (Magic Media™, Germany) and ForMedium™ (AIM, UK). For preparing the standard medium 60 g granulate and 12.6 g glycerol were dissolved in water and filled up to 1 L without pH-adjustment. HPLC analysis of the medium indicated a glucose concentration of 0.5 g/L and a lactose concentration of 2 g/l. After autoclaving, 100 mg/L ampicillin and 50 mg/L kanamycin were added to each medium under sterile conditions.

The OnEx auto-induction medium works as followed: glucose is the preferred carbon source and represses expression, lactose acts as the inducer of the recombinant expression system and glycerol is an additional energy source. The values from HPLC analysis are in agreement with data of Studier [7], where the design of a similar auto-induction medium is described. The working principle of this medium is that glucose is preferentially used as carbon source. During this initial growth phase no other carbon source is metabolized. During this time the production of the recombinant proteins is repressed as a result of catabolite repression of alternative carbon utilization pathways [22] and binding interactions between *lac* repressors and *lac* operators [23]. This allows an undisturbed growth of the microorganisms to high cell densities in the early stages of the cultivation. The depletion of glucose leads to a shift towards lactose import and, therefore, to the initiation of the recombinant protein expression.

2.2.3. Cultivation

For all cultivations, shake flasks with a nominal volume of 250 mL and equipped with a cotton plug were filled with 10 mL of medium. Cultures were grown at 37 °C by using an orbital shaker with a shaking diameter of 50 mm at a shaking frequency of 350 rpm. For pre-cultivation 10 mL TB medium in shake flask were inoculated with 20 µl from a cryo-culture and cultures were grown for 8-10 h.

Experiments with OTR determination were performed with the in house built **R**espiration **A**ctivity **MO**nitoring **S**ystem (RAMOS) in modified shake flasks. Commercial versions are available from Kühner AG (Switzerland) and Hitec Zhang (Germany). To acquire samples for offline analysis, conventional shake flasks were used in parallel. To start the cultivation the medium was inoculated from a pre-culture to an initial Optical Density (OD_{600}) of 0.1.

2.2.4. Analysis

Oxygen transfer rate

The OTR during the cultivations was measured using the RAMOS. This device analyzes the oxygen concentration in the gas headspace of the shake flask with an oxygen sensor [18,19]. For the measurement the system uses a continually repeated cycle consisting of a rinsing and a measuring phase. During the rinsing phase (10 min), a controlled air flow is led through the shake flasks to adjust the equilibrium of the gas phase. The air flow is adjusted in such a way that the gas composition in the headspace of the RAMOS flasks is equal to that in conventional shake flasks equipped with a cotton plug [24]. Subsequently, the inlet and outlet valves that are connected to the modified shake flasks are closed to start the measuring phase (5 min). In the sealed system the depletion of oxygen can be measured by the oxygen sensor on the top of each flask. The slope of this depletion corresponds to the OTR.

Biomass

To follow microbial growth, OD_{600} was determined from samples with a spectrophotometer at a wavelength of 600 nm (Uvikon 922A, Kontron Instruments, Italy) in 1.5 mL PS semi-micro-cuvettes (Plastibrand®, Brand GmbH, Germany) with a filling volume of 1 mL. Samples were diluted to keep the OD_{600} in the linear range from 0.05 to 0.5. Fresh medium was used for dilution and as a blank.

Substrates and metabolites

The concentrations of the carbon sources glucose, lactose and glycerol were determined by HPLC (Ultimate 3000, Dionex, USA) equipped with a Carbohydrat PB2+ column (300 x 8 mm, CS Chromatographie Service, Germany). The column was eluted with filtered and degassed water at a flow rate of 0.6 mL/min and a temperature of 85 °C. A detector with refractive index measurement was used (Shodex RH1, Showa Denko Europe GmbH, Germany).

Acetate was measured by HPLC (Dionex, Germany) equipped with a Organic Acid-Resin column (250 x 8 mm, CS Chromatographie Service, Germany). The eluent was 5 mM H_3PO_4 at a flow rate of 0.6 mL/min and 60 °C. Peaks were detected by recording the refractive index (Skodex RI-71, Showa Denko Europe, Germany) or UV-absorbance at 220 nm with a diode array detector (UVD340S, Dionex, Germany). In both cases, the sample volume was 20 µL. For data analysis, the software Chromeleon (Dionex, Germany) was applied.

Recombinant protein

The recombinant proteins were determined by sodium dodecylsulfate polyacrylamide gel electrophoresis (SDS PAGE). After measuring the OD_{600} of the culture, samples were centrifuged at 14000 rpm for 10 min. Subsequently, the supernatant was removed, and the pellet was re-suspended with water to an OD_{600} of 25. To 40 µL of this suspension, 140 µl of 2-fold concentrated sample buffer (E-PAGE Loading Buffer, Invitrogen, Germany) and 20 µl dithiothreitol (DTT) were added before shaking the mixture for 10 min at 1000 rpm and 70 °C in a thermos shaker. For analysis, the SDS PAGE device (Invitrogen, Germany) was equipped simultaneously with up to two gels (4-12 % Bis-Tris, Invitrogen, Germany). The transferred volumes were 20 µL for the prepared samples and 15 µL for the protein marker (Roti®-Mark Standard, Roth, Germany). The process was operated under the suggested standard settings of the manufacturer (running time 35 min, maximum current 200 V, maximum power 0.25 W).

The gels were stained in Simply Blue Staining Solution (Invitrogen, Germany) at 37 °C and shaken at 60 rpm overnight and were subsequently washed in water at the same temperature and shaking conditions for 2 h.

For quantitative analysis of the SDS-gels by densitometry, 1D gel analysis within the software TotalLab TL100 (Nonlinear Dynamics Ltd., UK) was used under the following conditions: I) Lane creation was done automatically; II) Background subtraction using rolling ball method with a radius of 100; III) Band detection by using a minimum slope of 100. The resulting percentage of the target protein's band quantifies the recombinant protein fraction as part of the entire cell proteins (P_{rec}/P_{tot}, [%]). Assuming that biomass consists of 50 % proteins the overall volumetric product yield (Y_P) of the cultivation can be estimated by multiplying P_{rec}/P_{tot} and 50 % of biomass (OD_{600}) as it can be seen from equation 2.1.

$$Y_P = P_{rec} / P_{tot} \cdot 0.5 \cdot OD_{600} \qquad \text{(Eq. 2.1)}$$

2.3. Results and Discussion

2.3.1. Cultivation under non-induced conditions

To cultivate the *E. coli* clones without inducing protein formation, the complex TB medium was applied, whereby glycerol served as the main carbon source. In the first experiment, eight different clones of *E. coli* SCS1 (PR01-08) were cultivated in the RAMOS device that measures online the respiratory activity. As shown in Fig. 2.1, the OTR curves of all the clones depicted a very similar respiration behavior having an exponential increase with a maximum OTR of 65 to 75 mmol/L/h at 6 h. Afterwards there was a sharp drop in the OTR to nearly 0 mmol/L/h indicating that all of the original carbon sources in the medium were exhausted and no further respiration could be observed until the end of the experiment. For the clones PR09-16 the the same growth behavior was observed in an additional experiment (data not shown). SDS-PAGE analysis showed that no significant amounts of target proteins for all 16 clones were produced (data not shown).

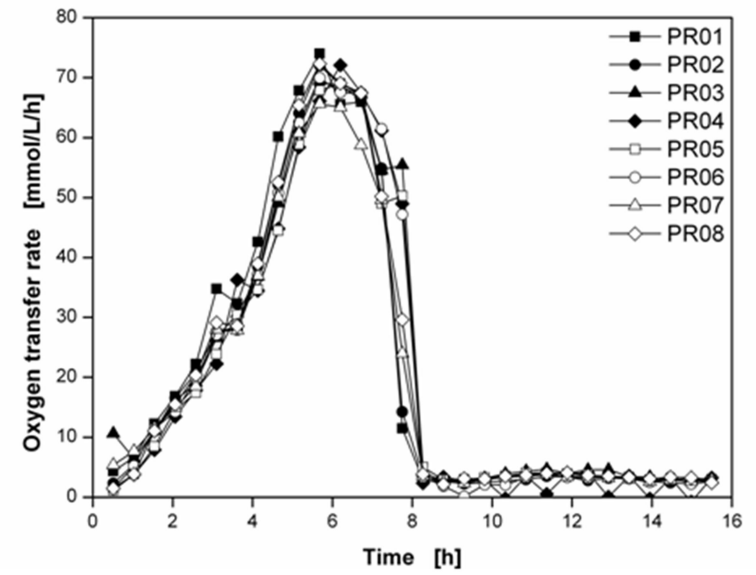

Fig. 2.1 - Oxygen transfer rate during the cultivation of 8 clones of *E. coli* SCS1 in non-inducing TB medium. Conditions: 250 mL flask, filling volume 10 mL, shaking frequency 350 rpm, shaking diameter 50 mm, 37 °C.

The OTR curves in Fig. 2.1 illustrate the typical growth of *E. coli* in TB medium as described earlier by Losen et al. [25]. The maximum OTRs of 65 to 75 mmol/L/h observed here are in good agreement with results from other works where *E. coli* was cultivated under similar conditions. Palmen et al. [26] reached a value of 60 mmol/L/h with a slightly lower shaking frequency of 320 rpm. A value of 65 mmol/L/h for a cultivation in a synthetic medium was e.g. also reported by Scheidle et al. [27]. There are no indications for limiting or inhibitory factors. Although these *E. coli* clones bear plasmids with different gene sequences for recombinant proteins, these variations apparently have no influence on the organism's respiration under non-inducing conditions. This fact indicates that combining the applied host organism with this vector system results either in no or only very low basal expression. The unintended induction, as it was described for some complex media by Grossmann et al. [28], was not observed in TB medium used during these experiments. Also, inhibitory effects caused by plasmid replication were not observed. Therefore, the low copy number of the applied vector system might be positive, as it was reported before that increased copy numbers can lead to decreased growth rates [29,30].

2.3.2. Cultivation in auto-induction medium

To cultivate *E. coli* SCS1 under induced conditions, 16 clones were cultivated in the OvernightExpress™ TB auto-induction medium (OnEx). Even though OnEx and TB medium are both complex media with glycerol as the major carbon source, it must be considered that there are significant differences in their compositions, resulting in different OTR curves. On the one hand the glycerol concentration in TB medium is much lower, on the other hand OnEx contains the additional carbon sources glucose and lactose.

Fig. 2.2-A shows the OTR curves during the cultivation of *E. coli* SCS1 in the inducing OnEx medium. Unlike the similar respiration patterns under non-induced conditions (Fig. 2.1), the

OTR curves in Fig. 2.2-A indicate a great difference in respiration under induced conditions. The variation in the metabolic activity of *E. coli* indicates that the DNA sequence encoding the target protein and varying from clone to clone indeed affect the host cells in quite different ways. The clones showing different OTR patterns can be classified into three distinct types:

- *Type 1* (Fig. 2.2-A, white background, *E. coli* clones PR08, 11, 15, 16)

  This type showed an exponential increase in OTR from the beginning up to the time point when the maximum oxygen transfer capacity OTR_{max} of the culture system under the applied operating conditions of 67 mmol/L/h was reached, indicated by a shift to a horizontal plateau. The increase was only shortly interrupted at a time of 4-5 h. After 11-12 h the initial carbon sources were depleted so that the OTR dropped sharply. The subsequent peak was caused by the metabolism on acetate which was produced and accumulated in the earlier stages of the cultivation as it is shown in following experiments (Fig. 2.3-A).

- *Type 2* (Fig. 2.2-A, light grey back ground, *E. coli* clones PR01, 02, 04, 05, 06, 07, 10, 12, 13, 14)

  For these clones the first exponential increase of OTR was followed by a phase of more or less constant or even slightly decreasing OTR. This course apparently resulted from the recombinant protein being produced that led to a strong metabolic burden for the organisms, thereby inhibiting their respiration. The duration of this phase differed from clone to clone and ranged from 6 to 12 h. Subsequently, another exponential respiration phase occurred until a maximum OTR of 67 mmol/L/h was observed. At this level there was either no or only a short period of oxygen limitation. This implied that the cells could regenerate themselves and continue to grow well. As the final peak indicates, acetate was also formed during the cultivation and metabolized after the depletion of glucose, lactose and glycerol, as explained in more detail in Fig. 2.3-A.

- *Type 3* (Fig. 2.2-A, grey background, *E. coli* clones PR03, 09)

  After the first exponential respiration phase, these clones showed a continuous decrease in OTR under the applied experimental conditions and no further increase was detected until the end of the fermentation. In this case the negative effect of the recombinant protein formation was so strong that the cells could not recover.

To quantify the recombinant proteins, the cells were analyzed by SDS PAGE (Fig. 2.2-B). Only 9 of the 16 clones depicted clear product bands (PR01, 02, 03, 04, 05, 09, 10, 11, 13). It was yet unclear why some of the clones (PR06, 07, 08, 12, 14, 15, 16) did not show recombinant protein, even though their OTR curves indicated a deviation from non-induced conditions. One reason might be that the synthesized product was subsequently degraded by proteolysis so that no protein remained after 24 h of cultivation. Another explanation might be that the DNA sequence for the target protein was only transcribed to mRNA and *E. coli* was not able to translate it to the protein. In this case the bacterial growth could have been inhibited by the overloaded transcription system. It is important to consider that Fig. 2.2-B is only a snapshot at the end of the cultivation, as it is routinely performed in many laboratories. Therefore, this conventional endpoint determination may not give a complete picture about what actually happens during the cultivation.

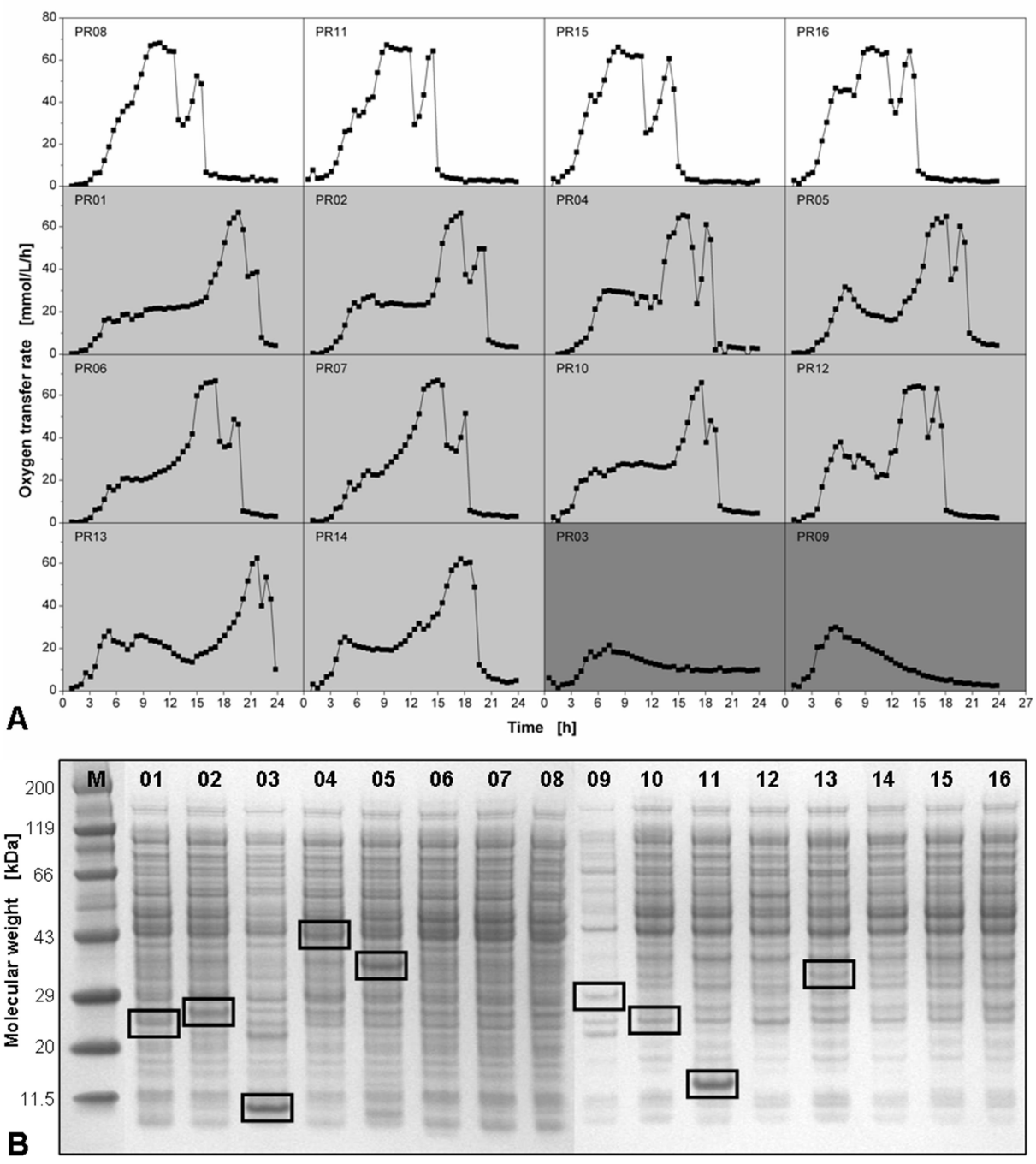

Fig. 2.2 - Oxygen transfer rate during the cultivation (A) and SDS PAGE analysis showing protein per biomass after 24 h cultivation (B, target protein framed, M=protein marker) of sixteen clones of *E. coli* SCS1 expressing different recombinant target proteins in OvernightExpress™ auto-induction medium with 3 different growth behaviors observed. Type 1 (white background); Type 2 (light grey background); Type 3 (dark grey background). Conditions: 250 mL flask, filling volume 10 mL, shaking frequency 350 rpm, shaking diameter 50 mm, 37 °C.

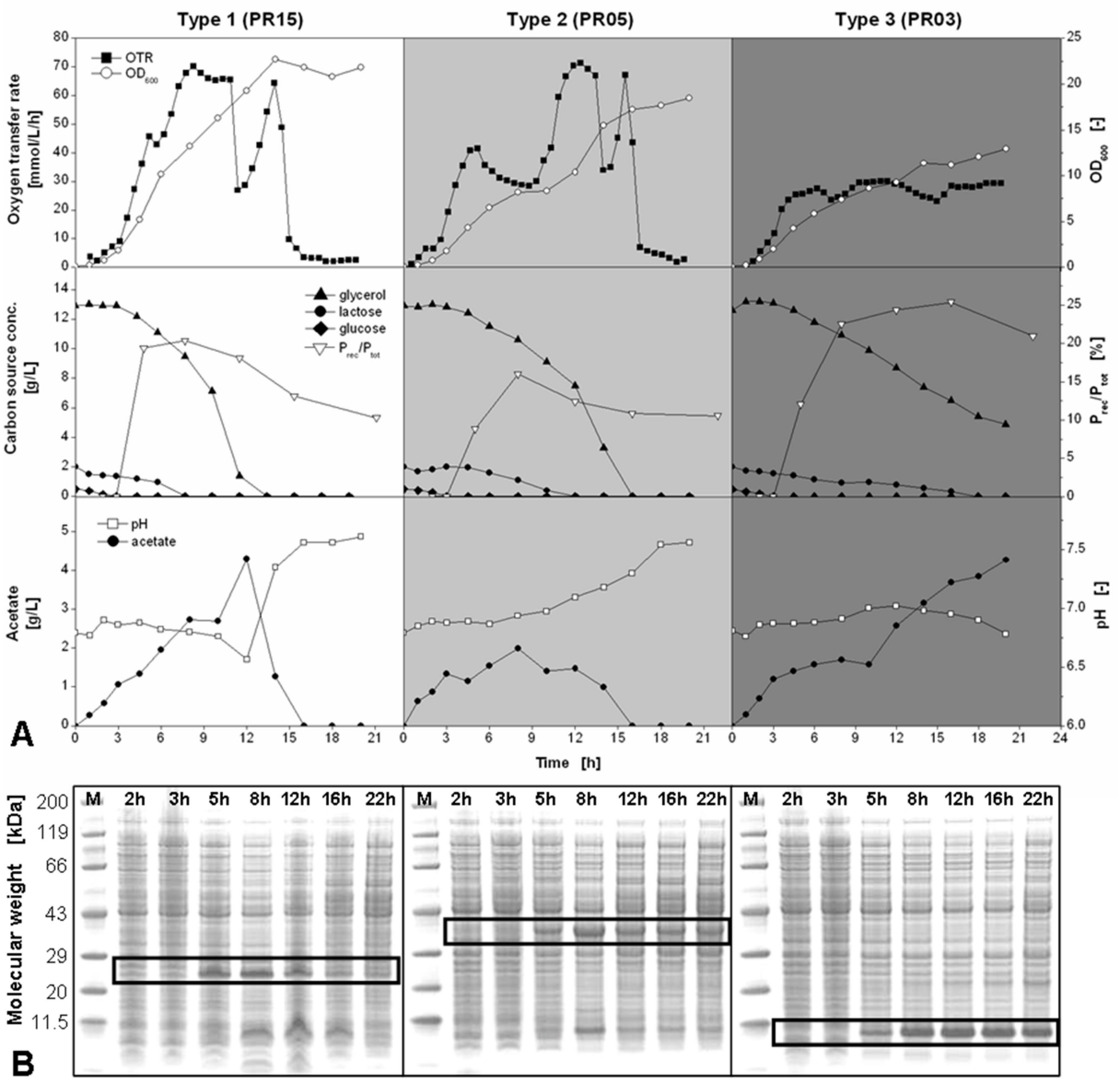

Fig. 2.3 - Characteristic growth parameters (A) and SDS PAGE analysis showing protein per biomass after 2, 3, 5, 8 12, 16 and 22 h cultivation (B, target protein framed, M=protein marker) of three clones of *E. coli* SCS1 with different growth behavior during the cultivation in OvernightExpress™ auto-induction medium. Type 1 (white background); Type 2 (light grey background), Type 3 (dark grey background). Conditions: 250 mL flask, filling volume 10 mL, shaking frequency 350 rpm, shaking diameter 50 mm, 37 °C.

For further characterizing the aforementioned clone types, one clone from each group was chosen for an additional RAMOS experiment with parallel offline analysis of biomass (OD_{600}), sugar consumption, acetate production and pH-value from conventional shake flasks (Fig. 2.3-A). It is obvious that clone PR15, representing type 1, started with an exponential

respiration phase where only glucose was consumed. After glucose was depleted, lactose and glycerol were consumed in parallel. This fact does not agree with an earlier report where lactose and glycerol are consumed one after another [31]. After 7 h, the OTR reached its maximum, and the following oxygen limitation caused a change to linear biomass formation. The insufficient oxygen supply also led to an increase in the acetate concentration to a maximum of 4.5 g/L and a minimal pH-value of 6.5 after 12 h. The strong decrease in the pH-value indicates that the buffer capacity of the medium was depleted. After 12 h, all initially added carbon sources were exhausted, and the OTR dropped. As mentioned before, the subsequent OTR-peak was caused by acetate utilization leading to further respiration activity. As a consequence of acetate consumption and ammonia release from amino acids in the complex medium being metabolized, pH increased to a higher value of 7.6. After 16 h no further change in the concentrations was observed.

PR05, representing type 2, showed a shorter exponential respiration phase in the beginning of the cultivation. Due to the depletion of glucose and the induction by lactose, the OTR and cell growth rate slightly decreased. Contrary to type 1 (PR15), the consumption of lactose and glycerol was slower. After 9 h, all of the lactose was consumed. Thus, unaffected cell growth was again possible resulting in an exponential increase in OTR and OD_{600}. Moreover, after 14 h also residual glycerol in the medium was depleted. PR05 produced considerably less acetate during cultivation than PR15 because there was no extensive oxygen limitation. In addition, the pH did not decrease because of the lower acetate formation and the sufficient buffer capacity in the medium for these experimental conditions.

PR03, representing type 3 clones, depicted initial exponential increase of OTR on glucose, followed by a phase of constant OTR and weak cell growth until the end of the cultivation after 22 h. Compared to PR05 and 15, lactose and glycerol were consumed much slower. After 16 h no more lactose was found in the medium, and cell growth did not resume, as it

was observed for type 2 clones even though glycerol was not depleted. Acetate was formed during the entire cultivation. This must have been caused by the overflow metabolism, because no oxygen limitation was present under the applied process conditions.

Fig. 2.3-B shows the formation of the recombinant proteins during the cultivation for PR15, 05 and 03. It can be seen that the protein formation behavior of the 3 types differed tremendously. They all have in common that no target protein was formed during the first 3 h of cultivation. This shows the effect of the auto-induction medium where glucose in the medium initially repressed protein production to avoid an interference with cell growth in the beginning of the cultivation. After 5 h of cultivation the respective proteins were found for all 3 clone types. It can be seen that type 3 (PR03) was continuously producing its protein over the whole process time. The analysis by densitometry showed a constant high level of 21-25 % for the target protein fraction (Fig. 2.3-A, P_{rec}/P_{tot}) after 8 h cultivation. This correlates very well with the slow consumption of lactose and inhibited cell growth. PR05, representing type 2, showed the maximum quantity of recombinant protein per cell after 8h. The corresponding value for P_{rec}/P_{tot} was 16 %. At this time lactose was depleted, and the second exponential growth phase started with the residual glycerol as the sole carbon source. Therefore, the following decrease in the protein content per cell was caused by an increase in non-induced biomass and a “dilution” of the target protein in the cells. After 16 h, when no carbon source was left in the medium and the growth stopped, the protein concentration remained constant at a much lower level resulting in a P_{rec}/P_{tot} level of 10 %. PR15, representing type 1 clones, was able to form its target protein in the time range from 5 to 12 h, as shown in Fig. 2.3-B. In this time the percentage of the target protein reached a maximal value of 20 %. However, after 8 h another protein band of lower molecular weight was found. At the end of the cultivation, both these proteins disappeared. Presumably, the recombinant protein was the target of proteolytic degradation where the aforementioned smaller protein

was the first degradation product. This effect was observed for another type 1 clone, too, since PR16 showed good productivity until 16 h of cultivation but no target protein at all after 24 h (data not shown). For clone PR03 and PR 05 no such degradation was found since PR03 showed a constant high productivity until the end of the cultivation and PR05 had a constant product level per cell over the last 6 h. This demonstrates that some of the proteins were more prone to proteases than others, thereby verifying the assumption of proteolytic degradation mentioned before. It is, therefore, extremely important to characterize the end of the production for each individual clone or strain by on-line monitoring and to take the sample at this time point for product quantification.

It is known, that cells containing expression plasmids that confer resistance to ampicillin can readily be overgrown by cells that have lost the plasmid, particularly if the target protein is stressful to the host. The enzyme β-lactamase can be secreted to the medium where it inactivates all of the ampicillin by the time a culture has become visibly turbid [32]. Thus, cells that have lost plasmid can overgrow cells that are capable of producing target protein and, therefore, leading to an increasing OTR but decreasing product yield. Such overgrowth may well be responsible for the second increase in the OTR patterns of type 2 clones. Nevertheless, the following results (Fig. 2.6, Fig. 2.7) indicate, that the second increase of the OTR is not due to overgrowth of the cultures by cells that have lost plasmid.

As mentioned in the background section, there are several publications about the influence of recombinant protein formation on the metabolism of the expression host. Similar to the three clone types described above, also Lee and Ramirez [13] reported on such a different behavior with three distinct types, where the additional load to the host's metabolism affects the cell growth in different ways. Their hypothesis agrees very well with the phenomena observed in this work. However, the reason for this different behavior is yet unclear. Büssow et al. [33] already reported that for the applied cDNA library, from which our clones were selected, no

significant correlation was found between the expressions results and either the protein size or the mean net charge. Further investigations within this work excluded that the protein size, 10-55 kDa in this case, the isoelectric point, 6.45-11.35, the hydrophobicity, indicated by the grand average of hydropathy value and reaching from -0.899 to -0.003, and the aliphatic index, which indicates for the fraction of aliphatic amino acids in the proteins and reaches from 37.06 to 97.66 for the here used proteins, are responsible for the observed phenomena (ExPASY, Switzerland, data not shown). An explanation for the different expression types might be the different codon usages of *E. coli* proteins and the target proteins. Resulting insufficiencies of the tRNA pool can lead to differences in the microbial growth and recombinant protein formation [34].

By using conventional screening protocols, especially in microtiter plates and shake flasks, the cultivation and product formation are evaluated via few data points, originating mostly from endpoint analysis. The data presented here show that the results at the end of the experiment often do not reflect the real course of the process. In contrast, the on-line OTR signal from RAMOS gives important information over the whole fermentation time. Interestingly, for PR05 and PR03 representing clone type 2 and 3 respectively, a direct relationship of the product formation and the OTR patterns could be observed. Whereas PR03 shows a constant inhibited respiration activity due to slow continuous protein production, the OTR curve of PR05 indicates the optimal point for terminating the process and harvesting the cells to have the maximum product yield without loss of time and resources. Consequently, RAMOS is a good tool to select and characterize most favourable clones with respect to biomass and target protein production. Additionally, it enables a rough prediction of the expression result without performing costly and laborious offline analysis.

2.3.3. Modification of the auto-induction medium

Since the applied auto-induction medium OnEx is a commercially available product, it was developed to suit a great variety of applications. Nonetheless, Blommel et al. [31] already reported that due to the multiple carbon sources present in the medium, their relative amounts critically contribute to the outcome of the auto-induced process. This was also confirmed in this work. In particular, clone PR05, representing clone type 2, is a good example for the suboptimal medium composition. In addition, also the product formation with clone PR03, representing type 3, shows potential for improvement. Consequently, the OnEx auto-induction medium was modified to optimize the production process and to validate the concept of using RAMOS as a screening tool for recombinant protein production.

Glucose concentration

The first aim was to accelerate the product formation in type 3 clone PR03 to increase the space time yield. By applying the approach of higher glucose concentrations, the time of induction was shifted to a later point in order to reach higher dell densities before the target protein production started. As reported before, the time of induction can strongly influence the result of cell growth and protein formation [5,15,35]. Increasing the glucose concentration of the auto-induction medium should lead to more inducible cells and, hence, to a higher product yield in an earlier stage of the process. This makes, of course, only sense, if culture conditions are selected which provide high levels of maximum oxygen transfer capacity. Otherwise a higher biomass concentration only results in a stronger oxygen limitation. With conventional OnEx, the glucose concentration amounted to 0.5 g/L. This medium was supplemented with additional glucose, resulting in final concentrations of 1 to 5 g/L. In Fig. 2.4-A the OTR curves for the respective cultivations are depicted. The unmodified medium showed the typical curve for type 3 clones with an exponential increase in the beginning and subsequent slightly decreasing OTR until the end of the cultivation. With 0.5, 1.5 and 4.5 g/L additional

glucose, the OTR level after the first exponential phase increased from 2 mmol/L/h to 28, 32 and 49 mmol/L/h, respectively, due to increased biomass before the induction by lactose set in. Surprisingly, the OTR patterns for additional 0.5 and 1.5 g/L glucose looked similar to those of type 2 clones (Fig. 2.2) with a constant level until 18 h followed by another exponential increase. With 4.5 g/L more glucose there was a further change of the OTR profile, comparable to that of type 1, with only a short interruption of the exponential growth and a long phase of oxygen limitation. The OD_{600} in non-modified OnEx medium was 9.8 after 10 h of cultivation (Fig. 2.4-B). The value for the medium with the additional 0.5, 1.5 and 4.5 g/L glucose rose to 11.0, 13.8 and 15.7, respectively. In a later phase the biomass in the conventional medium increased with a constant growth rate, whereas for the medium variants with additional 0.5 and 1.5 g/L glucose a higher growth rate after 17 h was observed when the OTR increased again. With 4.5 g/L more glucose this effect occurred even earlier, indicated by a strong increase of OD_{600} in the time from 10 to 15 h.

Fig. 2.4-B and the SDS gels in Fig. 2.4-C show that the amount of recombinant protein per cell during cultivation was different for the tested medium variants. Non-modified OnEx had a nearly constant product level over the whole time with P_{rec}/P_{tot} of 22-24 %. In the media with 0.5 and 1.5 g/L more glucose the biomass specific product yield decreased after 17 h from more than 20 % to 12 % at the end. This fact suits very well to the growth and expression behavior of type 2 clones (Fig. 2.3), where the growth rate again increased when the inducer lactose in the medium was depleted, causing the growth of non-induced cells and, therefore, leading to a "dilution" of the product inside the cells. Additional 4.5 g/L glucose resulted in a strong decrease of the product yield so that after 15 h almost no recombinant protein was found. Apparently, the maximal level of the target protein occurred already within the first 10 h. So the optimal harvest point for this medium variant would have been earlier. By considering the overall product yield (Eq. 2.1) it can be seen that conventional OnEx

showed a maximum of 188 a.u. at the end of the cultivation. With 1.5 g/L additional glucose the maximal value of 182 a.u. was already achieved after 17 h.

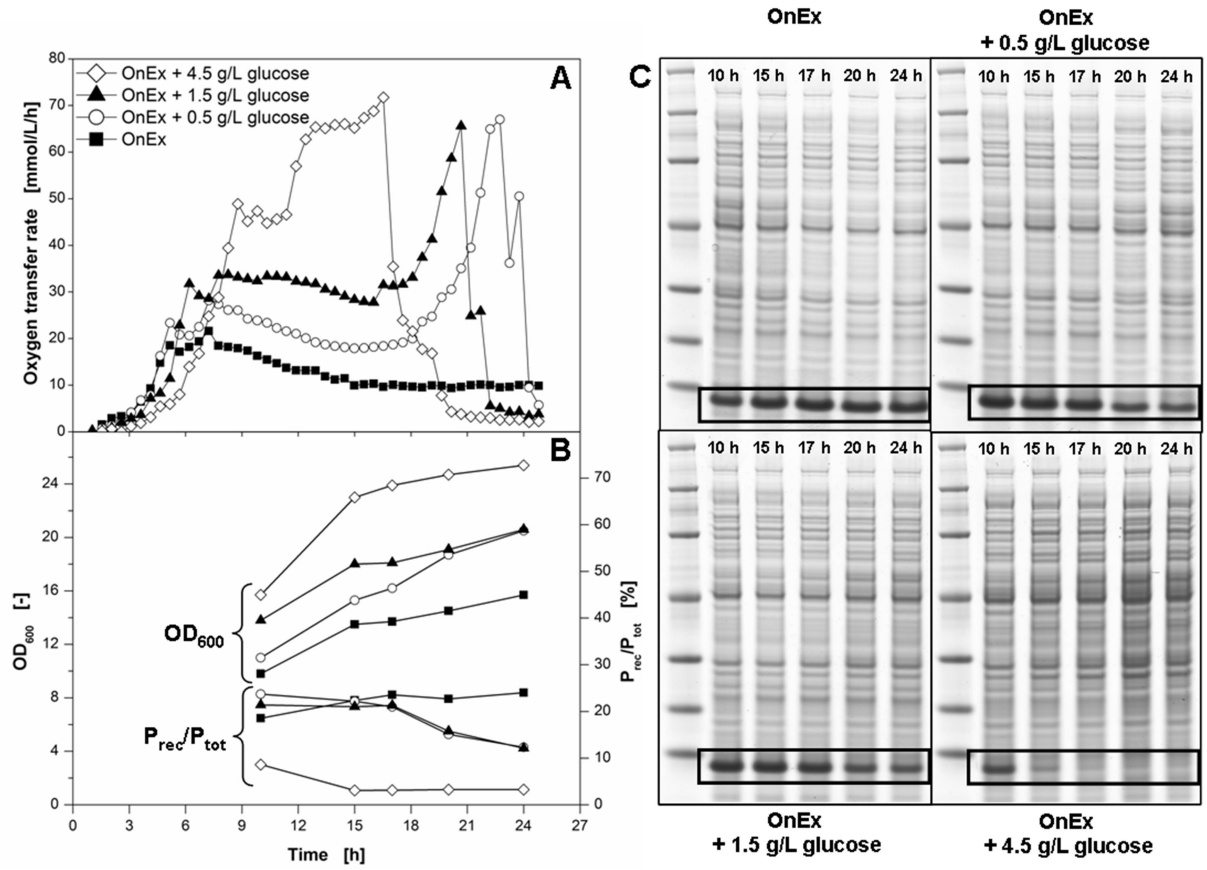

Fig. 2.4 - OTR (A), OD_{600} and recombinant protein fraction per biomass analyzed by densitometry (B) and SDS PAGE analysis showing protein per biomass (C, target protein framed, M=protein marker) during the cultivation of *E. coli* SCS1 PR03 in OvernightExpress™ auto-induction medium with varied glucose concentration. Conditions: 250 mL flask, filling volume 10 mL, shaking frequency 350 rpm, shaking diameter 50 mm, 37 °C.

Altogether, it was proven that additional glucose in the medium led to the desired aim. In fact, higher biomass yields in the early stages of cultivation were obtained due to a longer undisturbed growth phase in the beginning. As a consequence, the time point of the maximal product yield and, therefore, the optimal harvest point were shifted to an earlier time. Furthermore, the results show a strong dependency of growth and expression behaviour on the medium composition. By adding more glucose to the medium, *E. coli* PR03 changed from a

type 3 to a type 2 clone and it can be assumed that a further increase (more than 5 g/L) even might result in the change to type 1.

Glycerol concentration

Another modification of the auto-induction medium involved the cultivation without glycerol. In Fig. 2.3-B it was shown for clone PR05 that glycerol in the medium caused the growth of non-induced cells after lactose was depleted and product formation subsided, thereby resulting in a smaller yield of recombinant protein per biomass. By omitting glycerol, this second growth phase should be avoided.

Fig. 2.5-A compares the cultivations with and without glycerol in the medium. For the glycerol containing medium the typical OTR curve of clone type 2 was obtained. The medium lacking glycerol showed a completely different respiration behavior without any indications of recombinant protein production. The respiration rather resembled that in non-inducing TB medium (Fig. 2.1). In this medium there was a strong increase in the OTR to a maximum level of 65 mmol/L/h and a subsequent drop when all carbon sources in the medium were depleted. The SDS gel image and densitometric analysis in Fig. 2.5-B supports the assumption that there was no significant protein formation during the cultivation without glycerol. Whereas a strong product band was formed in the conventional OnEx medium (P_{rec}/P_{tot}= 7.8 %), it was remarkably lower for the modified medium (P_{rec}/P_{tot}= 5.1 %). Additionally, the biomass yield was much lower without glycerol, resulting in a strong decrease of the overall volumetric product yield (Eq. 2.1) from 82 a.u. for the non-modified medium to 30 a.u. in the glycerol free variant. Apparently, glycerol acted as an additional substrate during the protein production, and, therefore, decelerated the consumption of the inducer lactose. Without glycerol in the medium, lactose as the sole carbon source after glucose depletion was metabolized so quickly that the inducing function of lactose did not work properly. Thus, totally omitting glycerol cannot be recommended. Consequently,

finding the right glycerol concentration for each particular clone is important to achieve the maximal target protein yield. The optimal glycerol concentration would be found if there was no further increase in the OTR, representing the growth of non-induced cells, as it was obtained here after 9 h (Fig. 2.5-A, OnEx).

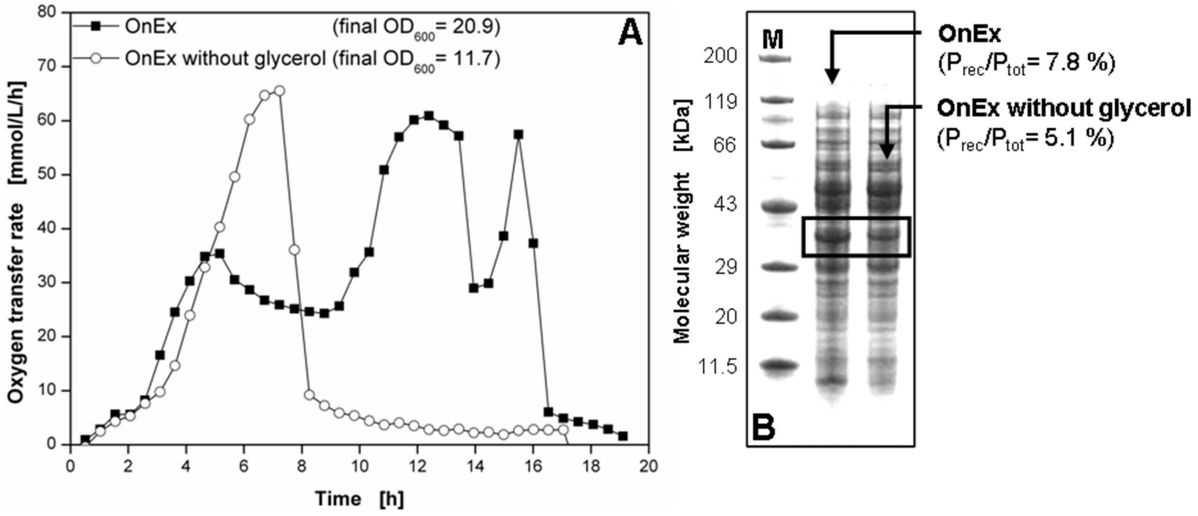

Fig. 2.5 - OTR during the cultivation (A) and SDS PAGE analysis showing protein per biomass after 19 h of cultivation (B, target protein framed, M=protein marker) of *E. coli* SCS1 PR05 in OvernightExpress™ autoinduction medium with and without glycerol. Conditions: 250 mL flask, filling volume 10 mL, shaking frequency 350 rpm, shaking diameter 50 mm, 37 °C.

Lactose concentration

Another optimization strategy for maximizing the product yield was to increase the lactose concentration in order to extend the target protein formation phase and avoid the growth of non-induced cells. An additional 2 and 6 g/L lactose was, respectively, supplemented to the conventional OnEx medium so that the final concentration corresponded to twice and four-times that of the original concentration of 2 g/L. The RAMOS results are depicted in Fig. 2.6-A. The unmodified OnEx medium again showed the typical OTR curve of type 2 clones. As it was intended, the increased lactose concentration caused a longer protein formation phase. An additional 2 g/L lactose led to an extension of this phase from 4 h to 8 h. The additional 6 g/L lactose extended the production phase to 16 h with no subsequent growth of non-induced

cells. Interestingly, the the duration of the OTR plateau at around 25 mmol/L/h (time of protein formation) correlates very well with the lactose concentration. The double and 4-fold amount of the inducer lactose resulted in production times that were two-times and four-times longer, respectively, as judged from the OTR curves. The SDS gel image and densitometric data in Fig. 2.6-B support these results, whereby stronger product bands were found with increasing lactose concentrations and P_{rec}/P_{tot} increased from 7.8 % with no added lactose to 10.3 % and 12.1 % with 2 and 6 g/L more lactose, respectively. Even though more substrate was available to the cells, the final biomass (OD_{600}) slightly decreased with rising lactose concentration, indicating that more resources were withdrawn from growth to product formation. Taking all together, the overall volumetric product yield (Eq. 2.1) increased from 100 a.u. in Onex to 125 and 138 a.u. in Onex with 2 and 6 g/L additional lactose. In addition to the band of the target protein another one of lower molecular weight (~10 kDa) occurred in the gel. The reason for that is yet unclear.

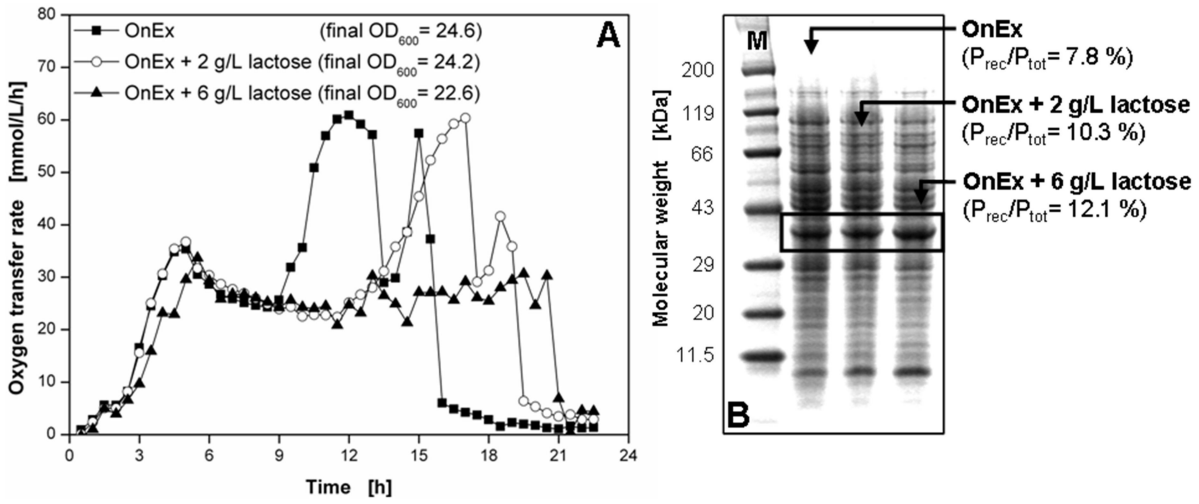

Fig. 2.6 - OTR during the cultivation (A) and SDS PAGE analysis showing protein per biomass after 18 h of cultivation (B, target protein framed, M=protein marker) of *E. coli* SCS1 PR05 in OvernightExpress™ autoinduction medium with varied lactose concentration. Conditions: 250 mL flask, filling volume 10 mL, shaking frequency 350 rpm, shaking diameter 50 mm, 37 °C.

Fig. 2.7 illustrates in more detail the different growth and target protein production behaviour for conventional OnEx and OnEx containing 6 g/L more lactose. In addition to the OTR, Fig. 2.7-A also depicts the respective OD_{600} curves. It can be seen that the OD_{600} curves were identical to each other up to 8 h. Subsequently, the OD_{600} curve for unmodified OnEx medium increased stronger, thereby, indicating a higher growth rate due to the missing target protein formation after inducer depletion. The final OD_{600} value after 19 h for the unmodified medium is 10 % higher than that for the modified one. However, comparing Fig. 2.7-B and C (see frames) shows that additional lactose strongly promoted recombinant protein formation. Without additional lactose, the protein amount per cell reached its maximum after 6 to 8 h with 12.4 % of target protein. Thereafter, it decreased until it stayed constant after 14 h (P_{rec}/P_{tot}= 8.3 %) when the OTR dropped, thus indicating that no carbon source was left in the medium. This clearly shows that the growth of non-induced cells is responsible for the lower product yield. With additional lactose this phenomenon was avoided by extending the protein formation phase until 18 h (Fig. 2.7-C). After 6 h the biomass specific product yield had already reached its maximum and remained nearly constant at 14 % until the end of the cultivation after 19 h. It can be assumed that during protein production the glycerol from the medium was fully consumed so that growth and protein production stopped at the same time point. This led to a constant high level of the desired protein in the cells until the end of the cultivation. As a further advantage, additional 6 g/L lactose in the medium prevented an oxygen limitation during the process and, therefore, the production of potentially inhibiting by-products.

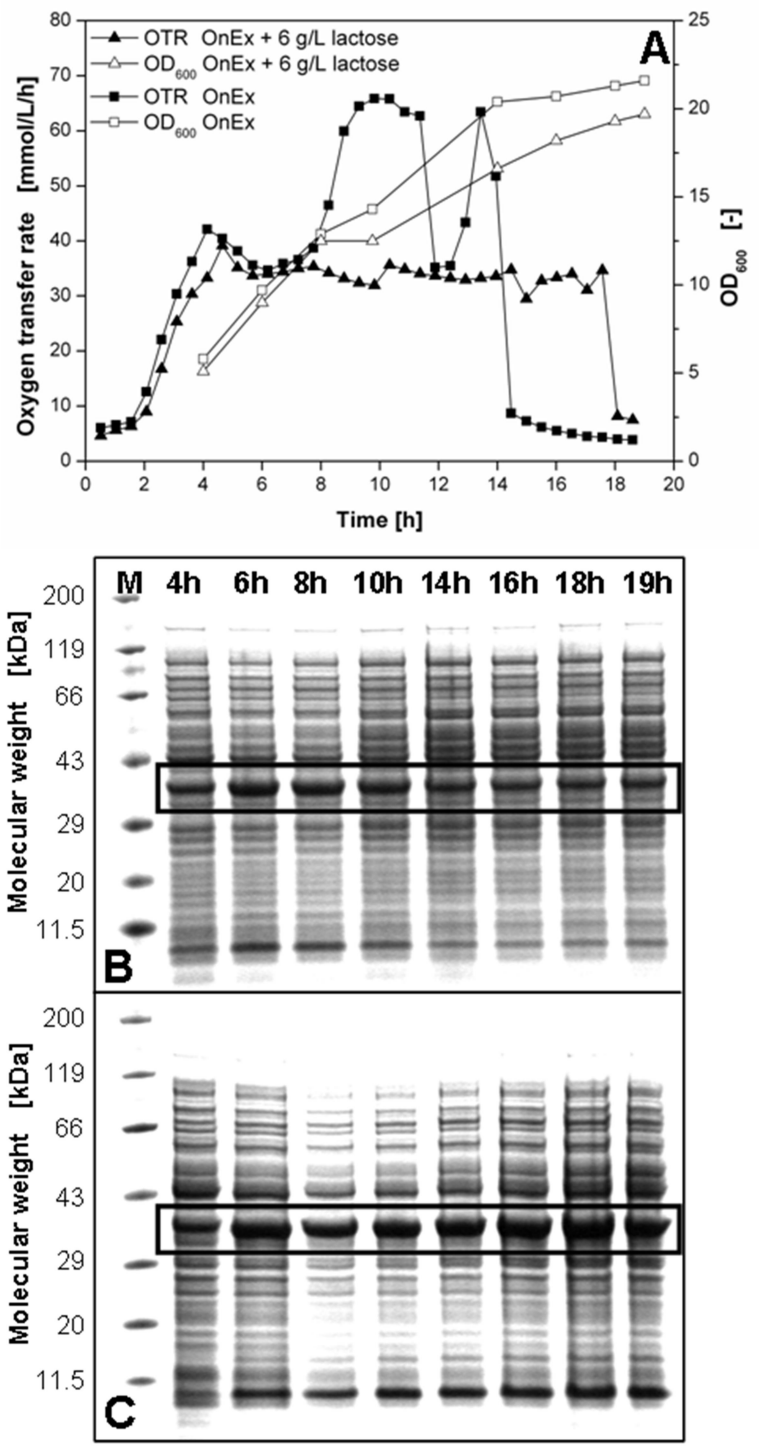

Fig. 2.7 - OTR and OD_{600} during the cultivation (A) and SDS-PAGE analysis showing protein per biomass after 4, 6, 8, 10, 14, 16, 18 and 19 h of cultivation (target protein framed, M=protein marker) of *E. coli* SCS1 PR05 in conventional OvernightExpress™ autoinduction medium (B) and with additional 6 g/L lactose (C). Conditions: 250-mL-flask, filling volume 10 mL, shaking frequency 350 rpm, shaking diameter 50 mm, 37 °C.

The results presented in Fig. 2.6 and Fig. 2.7 also prove that the overgrowth by cells having lost their plasmid is not responsible for the second increase of the OTR and the corresponding decrease of the biomass specific protein yield. Since with additional lactose in the medium a constant high product yield was observed until the end of the cultivation the appearance of non-induced cells in the conventional auto-induction medium is more likely.

Consequently, adding lactose to the medium is a simple and inexpensive way to increase the product yield. For a further increase, a lactose fed-batch would be desirable. It was already shown that an appropriate feeding strategy can lead to, both, higher biomass and biomass specific product yield [36]. Taking the results of the glycerol experiments (Fig. 2.5) into consideration, it is recommended to use both lactose and glycerol as carbon sources for the feeding solution. Otherwise, lactose would be consumed so fast that the induction would be ineffective.

2.4. Conclusion

It was found that among the sixteen examined *E. coli* SCS1 clones there was a great variance with respect to respiration activity and target protein production, despite using the same recombinant expression system. However, it was possible to classify them into three distinct types. Correlations between OTR, indicating metabolic activity, and the recombinant protein formation could be established. Phases of lower OTR were identified as strong production phases, whereas exponential increases of the OTR indicated undisturbed cell growth with low productivity.

It must be considered that the results shown in this work are not yet focused on a detailed quantitative characterization of the relationship between OTR, microbial growth and recombinant gene expression. For that purpose an in depth statistical analysis would be necessary. However, very similar qualitative differences in respiration and expression behaviour were also found for other clone banks in our laboratory. In fact, this work gives a first mechanic understanding how respiration activity, biomass formation and recombinant protein formation interact. It allows rough predictions about the productivity of a particular clone without costly offline analysis. Furthermore, this knowledge can be used to optimize process conditions. Several strategies have been demonstrated to increase the productivity by varying the medium composition, in particular the carbon sources glucose, glycerol and lactose. Currently, investigations are performed to develop a tailor-made screening protocol for the three different expression types.

Unlike conventional shake flask techniques in which only endpoint concentrations of e.g. biomass and product are measured, using the RAMOS device has the following advantages:

- It is fast, allowing relatively immediate measurement (e.g. every 30 minutes, depending on the settings of the device) of the relevant parameter OTR, characterizing the metabolic state of the microorganism;
- It is non-invasive: the cultures need not to be disturbed during cultivation and
- It reduces the need for sampling, since from the OTR curves relevant sampling points can be defined on-line.

This study also shows that unexpected phenomena such as the observed ones are hardly detectable using conventional screening protocols. This might lead to wrong assumptions about the selection of production strains, process parameters, the optimal point of harvest and, ultimately, to wasted resources. Since screening protocols differ from working group to working group [37], the results found might give important hints for investigations in the field of recombinant protein expression with *E. coli*.

Up to now, the reason for the here observed phenomena is yet unclear, since there was no correlation between the expression behavior and parameters like protein size, mean net charge, isoelectric point, hydrophobicity and aliphatic index. Therefore, future investigations should also focus on the recombinant protein properties and their influence to the microbial growth and expression behavior. Furthermore, it hasn't been investigated how plasmid stability and plasmid loss under the applied conditions affects the expression result. Due to the selective pressure in a microbial culture, cells may reduce their plasmid copy number or even lose the gene of interest within the plasmid. That would shift the metabolism from production to growth due to a lower metabolic burden and, consequently, lead to lower product yields. Thus, measuring plasmid contents, e.g. by flow cytometry, could give further important information for a more detailed understanding of the respiration and expression behaviours observed in this study.

2.5. Nomenclature

a.u.	Arbitrary units
E. coli	*Escherichia coli*
HPLC	High performance liquid chromatography
OD_{600}	Optical density at 600 nm
OnEx	OvernightExpress TB auto-induction medium
OTR	Oxygen transfer rate
OTRmax	Maximum oxygen transfer rate
P_{rec}/P_{tot}	Percentage of recombinant protein from total protein content in *E. coli*
RAMOS	Respiration Activity Monitoring System
SDS PAGE	Sodium dodecylsulfate polyacrylamide gel electrophoresis
TB	Terrific broth
Y_P	Volumetric product (recombinant protein) yield

2.6. References

1. Bonomo J,Gill RT. Amino acid content of recombinant proteins influences the metabolic burden response. Biotechnology and Bioengineering 2005; 90: 116-126.

2. Makrides SC. Strategies for achieving high-level expression of genes in Escherichia coli. Microbiological Reviews 1996; 60: 512-&.

3. Yabuta M,Onaimiura S,Ohsuye K. Thermo-Inducible Expression of a Recombinant Fusion Protein by Escherichia-Coli Lac Repressor Mutants. Journal of Biotechnology 1995; 39: 67-73.

4. Khosla C,Curtis JE,Bydalek P,Swartz JR,Bailey JE. Expression of Recombinant Proteins in Escherichia-Coli Using an Oxygen-Responsive Promoter. Bio-Technology 1990; 8: 554-558.

5. Neubauer P,Hofmann K,Holst O,Mattiasson B,Kruschke P. Maximizing the Expression of a Recombinant Gene in Escherichia-Coli by Manipulation of Induction Time Using Lactose as Inducer. Applied Microbiology and Biotechnology 1992; 36: 739-744.

6. Sreenath HK,Bingman CA,Buchan BW,Seder KD,Burns BT,Geetha HV,Jeon WB,Vojtik FC,Aceti DJ,Frederick RO,Phillips GN,Fox BG. Protocols for production of selenomethionine-labeled proteins in 2-L polyethylene terephthalate bottles using auto-induction medium. Protein Expression and Purification 2005; 40: 256-267.

7. Studier FW. Protein production by auto-induction in high-density shaking cultures. Protein Expression and Purification 2005; 41: 207-234.

8. Tyler RC,Sreenath HK,Singh S,Aceti DJ,Binginan CA,Markley JL,Fox BG. Auto-induction medium for the production of [U-N-15]- and [U-C-13, U-N-15]-labeled proteins for NMR screening and structure determination. Protein Expression and Purification 2005; 40: 268-278.

9. Bentley WE,Mirjalili N,Andersen DC,Davis RH,Kompala DS. Plasmid-Encoded Protein - the Principal Factor in the Metabolic Burden Associated with Recombinant Bacteria. Biotechnology and Bioengineering 1990; 35: 668-681.

10. Bhattacharya SK,Dubey AK. Metabolic Burden as Reflected by Maintenance Coefficient of Recombinant Escherichia-Coli Overexpressing Target Gene. Biotechnology Letters 1995; 17: 1155-1160.

11. Glick BR. Metabolic Load and Heterologous Gene-Expression. Biotechnology Advances 1995; 13: 247-261.

12. Hoffmann F,Rinas U. On-line estimation of the metabolic burden resulting from the synthesis of plasmid-encoded and heat-shock proteins by monitoring respiratory energy generation. Biotechnol Bioeng 2001; 76: 333-340.

13. Lee J,Ramirez WF. Mathematical-Modeling of Induced Foreign Protein-Production by Recombinant Bacteria. Biotechnology and Bioengineering 1992; 39: 635-646.

14. Schmidt M,Viaplana E,Hoffmann F,Marten S,Villaverde A,Rinas U. Secretion-dependent proteolysis of heterologous protein by recombinant Escherichia coli is connected to an increased activity of the energy-generating dissimilatory pathway. Biotechnology and Bioengineering 1999; 66: 61-67.

15. Huber R,Ritter D,Hering T,Hillmer AK,Kensy F,Muller C,Wang L,Büchs J. Robo-Lector - a novel platform for automated high-throughput cultivations in microtiter plates with high information content. Microbial Cell Factories 2009; 8: -.

16. Samorski M,Muller-Newen G,Büchs J. Quasi-continuous combined scattered light and fluorescence measurements: A novel measurement technique for shaken microtiter plates. Biotechnology and Bioengineering 2005; 92: 61-68.

17. Kensy F,Engelbrecht C,Büchs J. Scale-up from microtiter plate to laboratory fermenter: evaluation by online monitoring techniques of growth and protein expression in Escherichia coli and Hansenula polymorpha fermentations. Microb Cell Fact 2009; 8: 68.

18. Anderlei T,Büchs J. Device for sterile online measurement of the oxygen transfer rate in shaking flasks. Biochemical Engineering Journal 2001; 7: 157-162.

19. Anderlei T,Zang W,Papaspyrou M,Büchs J. Online respiration activity measurement (OTR, CTR, RQ) in shake flasks. Biochemical Engineering Journal 2004; 17: 187-194.

20. Büssow K,Cahill D,Nietfeld W,Bancroft D,Scherzinger E,Lehrach H,Walter G. A method for global protein expression and antibody screening on high-density filters of an arrayed cDNA library. Nucleic Acids Research 1998; 26: 5007-5008.

21. Büssow K,Nordhoff E,Lubbert C,Lehrach H,Walter G. A human cDNA library for high-throughput protein expression screening. Genomics 2000; 65: 1-8.

22. Hogema BM,Arents JC,Bader R,Postma PW. Autoregulation of lactose uptake through the LacY permease by enzyme IIA(Glc) of the PTS in Escherichia coli K-12. Molecular Microbiology 1999; 31: 1825-1833.

23. Wong P,Gladney S,Keasling JD. Mathematical model of the lac operon: Inducer exclusion, catabolite repression, and diauxic growth on glucose and lactose. Biotechnology Progress 1997; 13: 132-143.

24. Mrotzek C,Anderlei T,Henzler HJ,Büchs J. Mass transfer resistance of sterile plugs in shaking bioreactors. Biochemical Engineering Journal 2001; 7: 107-112.

25. Losen M,Frolich B,Pohl M,Büchs J. Effect of oxygen limitation and medium composition on Escherichia coli fermentation in shake-flask cultures. Biotechnology Progress 2004; 20: 1062-1068.

26. Palmen TG,Nieveler J,Frolich B,Treffenfeldt W,Pohl M,Büchs J. Physiological relation between respiration activity and heterologous expression of selected benzoylformate decarboxylase variants in Escherichia coli. Microbial Cell Factories 2010; 9: 76.

27. Scheidle M,Dittrich B,Klinger J,Ikeda H,Klee D,Büchs J. Controlling pH in shake flasks using polymer-based controlled-release discs with pre-determined release kinetics. BMC biotechnology 2011; 11: 25.

28. Grossman TH,Kawasaki ES,Punreddy SR,Osburne MS. Spontaneous cAMP-dependent derepression of gene expression in stationary phase plays a role in recombinant expression instability. Gene 1998; 209: 95-103.

29. Mason CA, Bailey JE. Effects of plasmid presence on growth and enzyme activity of Escherichia coli DH5alpha. Appl Microbial Biotechnol. 1989;32:54-60.

30. Valenzuela MS, Ikpeazu EV, Siddiqui KAI. E. coli growth inhibition by a high copy number derivative of plasmid pBR322. Biochem Biophys Res Commun. 1996;219:976-883.

31. Blommel PG,Becker KJ,Duvnjak P,Fox BG. Enhanced bacterial protein expression during auto-induction obtained by alteration of lac repressor dosage and medium composition. Biotechnology Progress 2007; 23: 585-598.

32. Jacoby GA. AmpC beta-Lactamases. Clinical Microbiology Reviews 2009; 22: 161-+.

33. Büssow K,Scheich C,Sievert V,Harttig U,Schultz J,Simon B,Bork P,Lehrach H,Heinemann U. Structural genomics of human proteins--target selection and generation of a public catalogue of expression clones. Microbial Cell Factories 2005; 4: 21.

34. Terpe K. Overview of bacterial expression systems for heterologous protein production: from molecular and biochemical fundamentals to commercial systems. Applied Microbiology and Biotechnology 2006; 72: 211-222.

35. Donovan RS,Robinson CW,Glick BR. Review: Optimizing inducer and culture conditions for expression of foreign proteins under the control of the lac promoter. Journal of Industrial Microbiology 1996; 16: 145-154.

36. Hoffman BJ,Broadwater JA,Johnson P,Harper J,Fox BG,Kenealy WR. Lactose Fed-Batch Overexpression of Recombinant Metalloproteins in Escherichia-Coli Bl21(De3) - Process-Control Yielding High-Levels of Metal-Incorporated, Soluble-Protein. Protein Expression and Purification 1995; 6: 646-654.

37. Berrow NS,Büssow K,Coutard B,Diprose J,Ekberg M,Folkers GE,Levy N,Lieu V,Owens RJ,Peleg Y,Pinaglia C,Quevillon-Cheruel S,Salim L,Scheich C,Vincentelli R,Busso D. Recombinant protein expression and solubility screening in Escherichia coli: a comparative study. Acta Crystallogr D Biol Crystallogr 2006; 62: 1218-1226.

3. Chapter II: Cellulolytic RoboLector – Towards an automated high-throughput screening platform for recombinant cellulase expression

3.1. Background

Since fossil resources are limited, many current research projects are investigating the utilization of renewable resources to ensure the sustainable production of platform chemicals and biofuels [1]. Most of these approaches have focused on producing alcohols from starch-containing plant material which competes with the food supply chain. Moreover, these approaches waste most of the plant biomass. New research is focusing on utilizing ligno-cellulose as the prime raw material for biofuel production [2–4] and constructing new biocatalysts for this purpose [5].

As the cellulose de-polymerization performed by different kinds of cellulases is the rate-limiting step for the whole hydrolysis [6, 7], efficient cellulases have to be identified and characterized regarding their performance. Mutagenesis procedures are a common way to modify existing enzymes in order to improve their properties. Typically, such modifications end up in huge libraries of enzyme variants which need to be further investigated [8]. For this task an efficient screening process is essential [6, 9]. To handle this immense workload, a high-throughput screening (HTS) system is necessary, which combines a miniaturized mode of operation with an advanced automation concept [10].

Automated high-throughput (HT) concepts for single steps such as measurement of optical density, pH, metabolites [11], protein purification [12–14] and different enzyme activity assays [11, 15, 16] have been reported. More advanced HT concepts combine single methods to a semi or even fully automated operation. Dörr et al. [17] recently presented a robotic platform for HT enzyme library screening. It enables automated colony picking, at-line

monitoring of biomass growth, induction, subsequent enzyme purification steps and biochemical assay. However, this platform lacks in an on-line monitoring tool to follow the biomass growth without interruption of shaking. In particular, constant oxygen transfer rates are necessary for reproducible cultivations. Huber et al. [18] combined the BioLector technology [19] and a robotic liquid handling system to overcome this issue. A similar set-up was later used by Hemmerich et al. [20] who performed an on-line monitored fed-batch clone screening of *Pichia pastoris*. However, the automation was restricted to the feeding and harvest procedure. Both, the preculture and the subsequent enzyme activity assay was conducted manually. A more complex clone screening was carried out with *C. glutamicum* by Unthan et al. [21]. They integrated an automated biomass triggered sampling with subsequent separation of supernatant by centrifugation and a following freezing step. An independent assay was used for the analysis of samples. Unfortunately, no conditioning of the preculture was attempted since these authors inoculated directly from cryo cultures into the main culture. Additionally, there was no further information about the generation of replicates. It's important to distinguish technical replicates from biological replicates. A small standard error in technical replicates doesn't reflect the reliability of the whole experimental procedure. It only gives information about the reliability of the last measurement step. Moreover, there is a difference in using one microtiter plate (MTP) for producing replicates at the same time and the repetition of a whole experiment in many plates at different times. The big challenge is the comparability of screening results amongst different plates. Clone screening commonly starts from 96well cryo cultures whose biomass concentrations are not individually determined or adjusted. Without the application of on-line measurement tools, this typically leads to a usually non-recognized difference in onset of growth, when comparing different variants. Thereupon, especially microorganisms which have to be induced undergo non-comparable enzyme expression [22, 23].

In this study, an automated and reliable HT system is presented which is able to realize all necessary steps for a complete screening of cellulolytic enzymes. The applied methods focus especially on preculture synchronization and controlled induction of clone libraries which is a prerequisite to obtain a fair comparison of all screened variants. Based on the RoboLector system described before [18], an extended version was constructed to realize more complex operations. Furthermore, existing methods for protein purification and cellulase characterization were adapted to and optimized for miniaturized HT operation with a special focus on automated handling. In several application examples, the potential of the extended cellulolytic RoboLector system is demonstrated. Single steps were evaluated using different *E. coli* and *K. lactis* strains. While *E. coli* usually cannot secrete recombinant proteins, *K. lactis* possesses a secreting system. This leads to a more complex downstream process for *E. coli*. In this study, 46 mutants of *E. coli* expressing celA2 were used for the final evaluation of the screening procedure. A *K. lactis* mutant library screening was not part of this study.

3.2. Material & Methods

3.2.1. Microorganisms

The applied microorganisms with their respective vectors for recombinant protein expression as well as their selection markers are specified in Tab. 3.1.

Tab. 3.1 - Applied microorganisms for the expression of recombinant proteins

Target protein	Organism	Strain	Vector	Selection marker	Inducer	Supplier
FbFP	*E.coli*	BL21 (DE3)	pRhotHi-2	Kanamycin	Lactose	1
cel8H-mCherry	*E. coli*	BL21 (DE3) pLys	pET-22b(+)	Ampicillin	Lactose	2
celA2	*E. coli*	BL21 (DE3)	pET-28a(+)	Kanamycin	IPTG	3
cel5A	*E. coli*	LMG194	pBAD	Ampicillin	L-arabinose	2
cel5A	*K. lactis*	GG799	pKlac1	-	Galactose	2

Supplier:

1. *Institute of Molecular Enzyme Technology (IMET), Heinrich-Heine-University Düsseldorf, Germany*
2. *Institute of Biotechnology, RWTH AachenUniversity, Germany*
3. *Institute of Molecular Biotechnology (Bio VII), RWTH AachenUniversity, Germany*

The *E. coli* clone library for the expression of cel5A variants was created by random mutagenesis applying the JBS dNTP-Mutagenesis Kit (Jena Bioscience, Jena, Germany). This method is based on the incorporation of mutagenic dNTP analogs, such as 8-oxo-dGTP and dPTP, into an amplified DNA fragment by PCR. The mutagenic dNTPs are eliminated by a second PCR step in the presence of the four natural dNTPs only, resulting in a rate of mutagenesis of up to 20% (according to user manual). The *E. coli* clone library for the expression of celA2 variants was created by directed evolution applying a simultaneous site-saturation mutagenesis at positions 288, 299 and 300. Similar libraries were constructed and investigated by Lehmann et al. [24]. For both libraries, active variants where picked from LB

agar plates supplemented with 0.125% (w/v) Azo-CMC. Active transformants were identified by halos on the agar plate.

3.2.2. Media & cultivation

For *E. coli* expressing FbFP, cel8H-mCherry, and cel5A terrific broth (TB) medium [25] consisting of 12 g L^{-1} tryptone, 24 g L^{-1} yeast extract, 12.54 g L^{-1} K_2HPO_4, 2.31 g L^{-1} KH_2PO_4, and 5 g L^{-1} glycerol (all ingredients from Roth, Germany) dissolved in water was used for pre-culture. The pH value was 7.2±0.2 without adjustment. If not stated differently, 10 mL of TB medium in a 250 ml shake flask were inoculated with 50 µL from a cryoculture for *E. coli* pre-cultivation, and cultures were grown for 8 h at 350 rpm (shaking diameter 50 mm) and 37°C. For main culture, OvernightExpress™ (OnEx) medium was used for auto-induction of the FbFP strain. Besides this, the cultivation conditions were identical to the pre-culture. For expression of cel8H-mCherry, a modified TB medium was used containing varied amounts of glucose and lactose in addition to 5 g L^{-1} glycerol (see Tab. 3.2). The cultivation was performed within a 96well MTP (Greiner Bio-One GmbH, Frickenhausen, Germany) with 200 µL filling volume and a shaking frequency of 1000 rpm (shaking diameter 3 mm) at 37°C. The plates were sealed with gas-permeable seals (AB-0718, Thermo Scientific, Dreieich, Germany).

For the pre- and main cultivation of *E. coli* expressing celA2 and cel5A a modified Wilms and Reuss medium (henceforth referred as Wilms-MOPS medium) was used [26]. It consists of 5 g L^{-1} $(NH_4)_2SO_4$, 0.5 g L^{-1} NH_4Cl, 3.0 g L^{-1} K_2HPO_4, 2 g L^{-1} Na_2SO_4, 0.5 g L^{-1} $MgSO_4 \cdot 7H_2O$, 0.01 g L^{-1} thiamine hydrochloride, 41.85 g L^{-1} 3-(N-morpholino)-propanesulfonic acid (MOPS, 0.2 M), and 1 mL L^{-1} trace element solution. This trace element solution consists of 1.98 g L^{-1} $CaCl_2 \cdot 2H_2O$, 0.54 g L^{-1} $CoCl_2 \cdot 6H_2O$, 0.48 g L^{-1} $CuSO_4 \cdot 5H_2O$, 41.76 g L^{-1} $FeCl_3 \cdot 6H_2O$, 0.3 g L^{-1} $MnSO_4 \cdot H_2O$, 0.54 g L^{-1} $ZnSO_4 \cdot 7H_2O$, 33.39 g L^{-1} Na_2EDTA

(Titriplex III). As carbon source 15 g L^{-1} glucose were added for celA2 expression, for cel5A 20 g L^{-1}. The pH was adjusted with 5 M NaOH to a value of 7. Pre- and main culture were performed within a 96well MTP (Greiner Bio-One GmbH, Frickenhausen, Germany) and sealed with xPierce^{TM} film (Z722529, Sigma-Aldrich, Munich, Germany). The expression of cel5A in *E. coli* was induced after 2 h of main culture with 0.2 [m/v] L-arabinose from a 40-fold stock solution. Expression of celA2 was individually induced after exceeding the scattered light value of 10 a.u. by automated adding of IPTG, resulting in a final concentration of 0.1 mM. Depending on the clone's resistance 50 µg mL^{-1} kanamycin or 100 µg mL^{-1} ampicillin were added to all the media from a 1000-fold concentrated stock solution.

Tab. 3.2 - Varied composition of auto-induction media and their abbreviations for the recombinant expression of the cel8H-mcherry fusion protein in *E. coli*.

Abbreviation	Glycerol [g L^{-1}]	Glucose [g L^{-1}]	Lactose [g L^{-1}]
5052	5	0.5	2
512	5	1	2
522	5	2	2
532	5	3	2
516	5	1	6
5110	5	1	10

For *Kluyveromyces lactis* (*K. lactis*) pre-cultures yeast extract peptone (YP) medium was used, consisting of 10 g L^{-1} yeast extract, 20 g L^{-1} tryptone (both Carl Roth, Karlsruhe, Germany) and 10 g L^{-1} glucose [27]. 10 mL of this medium were inoculated with 50 µL from a *K. lactis* cryoculture, and cultures were grown for 12 h at 350 rpm (shaking diameter 50 mm) and 30°C in a 250 ml shake flask. The main cultures were performed in YP medium containing 10-100 g L^{-1} galactose instead of glucose. Thereby, galactose served as carbon source and inducer for recombinant protein expression. The cultivation was conducted within so-called Flower Plates (MTP-48-BOH, Lot. 1202, m2p labs, Germany), equipped with

optodes for on-line monitoring of the dissolved oxygen tension (DOT). Flower Plates were sealed manually with gas-permeable seals (AB-0718, Thermo Scientific, Dreieich, Germany).

All MTP cultivations were performed applying the BioLector technique [19]. For this purpose, the commercial device from m2p-labs (Beasweiler, Germany) was used. Microbial growth and formation of fluorescent proteins were on-line monitored. Wavelengths and gain factors for all optical signals are listed in Tab. 3.3. For scattered light and fluorescence measurement the initial light intensity (I_0), which is mainly attributed to such factors as the media background or the type of the MTP, was subtracted from the original measured data ($I-I_0$).

Tab. 3.3 - Optical signals and applied setup for BioLector on-line monitoring

Optical signal	λ_{ex} [nm]	λ_{em} [nm]	Gain
Biomass (scattered light)	620	-	20
DOT	520	600	60
mCherry fluorescence	580	610	60
FbFP fluorescence	450	492	60

3.2.3. Offline analysis

OD_{600} was determined via a Genesys 20 photometer (Thermo Scientific, Dreieich, Germany) in 1.5 mL micro cuvettes (PS, Plastibrand, Roth, Karlsruhe, Germany). For values higher than 0.5 the samples were appropriately diluted with 0.9 % [m/v] NaCl solution.

For FbFP fluorescence quantification, 100 µl of the respective sample were transferred to a cavity of a 96 well MTP (Greiner Bio-One GmbH, Frickenhausen, Germany). The

measurement was done applying the BioLector system with parameters listed in Tab. 3.3. Each presented value is the average of at least 10 consecutive measuring values.

SDS-PAGE - After measuring the OD_{600} of the culture, samples were centrifuged at 18000 g for 10 min. Subsequently, the supernatant was removed, and the pellet was re-suspended in water to an OD_{600} of 25. To 40 µL of this suspension, 140 µL of twofold concentrated sample buffer (E-PAGE Loading Buffer, Invitrogen, Germany) and 20 µL of 1 M dithiothreitol (AppliChem GmbH, Darmstadt, Germany) were added before shaking the mixture for 10 min at 1000 rpm and 70°C in a thermo shaker (MKR 10, HLC Biotech, Bovenden, Germany). For analysis, the SDS-PAGE device (Invitrogen, Germany) was equipped simultaneously with up to two gels (4–12% Bis-Tris, Invitrogen, Germany). The transferred volumes were 20 µL for the prepared samples and 15 µL for the protein marker (RotiVR -Mark Standard, Roth, Germany). The process was operated under the suggested standard settings of the manufacturer (running time 35 min, maximum current 200 V, and maximum power 0.25 W). The gels were stained in Simply Blue Staining solution (Invitrogen, Germany) at 37°C and shaken at 60 rpm overnight and were subsequently washed in water at the same temperature and shaking conditions for 2 h.

4-MUC assay – The endoglucanase activity of the recombinant protein celA2 was measured manually with the already established fluorescence-based 4-methylumbelliferyl-β-D-cellobioside (4-MUC) assay [24]. Some adaptions were made. A 50x 4-MUC stock solution (0.5 mM) was prepared by dissolving the reagent in potassium phosphate buffer (0.1 M, pH 6.5) and stored at 4°C. 40 µL of disrupted cells and 90 µL of a diluted 4-MUC solution (1.67x) were transferred separately into a 96well MTP (flat-bottom, black/clear, BD Falcon, USA), sealed with a clear sealing tape (EN77.1, Roth, Germany) and preheated to 30°C. After the pre-incubation, 60 µL of the 4-MUC solution were mixed with the disrupted cells. Subsequently, the reaction mixture was incubated at 30°C for 20 min in a Synergy 4

Microplate Reader (BioTek, Winooski, VT, USA). The increase in fluorescence was measured at Ex/Em=365/455 nm in intervals of one minute. For evaluation, a calibration curve, fluorescence versus 4-methylumbelliferone concentration (0.3-300 µM), was recorded in the same phosphate buffer and a final volume of 100 µL. Specified activity values for all measured clone variants refer to the volumetric activity within the culture broth.

3.2.4. RoboLector system

The applied automated HTS platform RoboLector is identical to the system described by Huber et al. (2009). For this work, it was extended by the following components which are commercially available from Hamilton Robotics GmbH (Martinsried, Germany): cooling carrier (PLT_CAR_L5C), MTP heater shakers (HHS), on-deck vacuum station (BVS). The extended setup is illustrated in the layout scheme in Fig. 3.1-A. The cooling carrier was operated with a controllable recirculation cooler (FL300, Julabo, Seelbach, Germany) located under the robotic platform and connected via flexible tubes. It allows temperature set points from -20°C to 40°C. To keep the tubes from ice coating, set temperatures lower than -5°C were avoided for long-term experiments. Due to heat transfer phenomena, set temperatures and final temperatures in MTP wells differ from each other. The respective relationship was identified by experiments. For 96well deep well plates (DWP, 2.2 mL, sterile, square wells, Corning/Axygen Scientific) it is described by eq. 3.1.

$$T_{well} = 0.75 \cdot T_{set} + 6.50°C \qquad \text{(Eq. 3.1)}$$

Similar experiments were performed for the heater shakers, too. The respective relationship for 96well DWPs is described by eq. 3.2. The maximum set temperature was 110°C. Well temperatures were determined by a CheckTemp 1 precision thermometer (G0021, Roth, Karlsruhe, Germany).

$$T_{well} = 0.78 \cdot T_{set} + 6.45°C \qquad \text{(Eq. 3.2)}$$

The vacuum station was operated by a vacuum pump (ME 4C VARIO, Vacuubrand, Wertheim, Germany) equipped with pressure sensor and control unit. All devices are controlled by the VENUS three software of the pipetting robot (Microlab STAR, Hamilton Robotics, Martinsried, Germany).

3.2.5. High-throughput biomass separation

For the HT separation of whole cells or cell fragments, microfiltration was performed applying the on-deck vacuum station of the RoboLector (Fig. 3.1-A, no. 7a-b) with AcroPrep™ 96 Filter Plates (3.0 µm Glass Fiber/0.2 µm Bio-Inert membrane, modified hydrophilic nylon, 1 mL, part no. 5053, Pall Life Sciences, Ann Arbor, MI, USA). For the filtration an underpressure of 0.5-0.6 bar was applied. Previous experiments revealed that a filtration time of 30 min is sufficient for the complete filtration of cultivation samples with volumes up to 600 µL and OD_{600} values up to 20. For all HT filtration experiments, full plate occupancy was ensured for a homogeneous vacuum distribution.

3.2.6. Enzyme extraction

For *E. coli* cell lysis and protein extraction, the commercial kit BugBuster® 10x Protein Extraction Reagent (70921, Merck-Millipore, Darmstadt, Germany) was used. It is a detergent based mixture with a small amount of lysozyme. For the standard protocol, samples were filled in 1.5 mL tubes, biomass was separated via centrifugation for 5 min at 18000 g (centrifuge 1-15K, rotor 12024-H, Sigma), and the supernatant removed with a pipette. For re-suspension, the 10x Protein Extraction Reagent was diluted in acetate buffer (to 1x) and a volume equal to the original sample volume was added to the pellet. After 30 min of

incubation at 900 rpm and room temperature, samples were centrifuged again for 5 min at 18000 g. The resulting supernatant containing the target protein was stored at 4°C. It must be noticed that this protocol is not in accordance with the manufacturer's guidelines since it was optimized for internal use. For the HT protocol, cultivation samples were given directly to a multiwell filter plate for microfiltration. For protein extraction, 11 µL of 10x Protein Extraction Reagent was added to each 100 µL sample volume. After 30 min of incubation at 900 rpm and room temperature, the filter plate was automatically transported by the gripper to the on-deck vacuum station of the RoboLector and filtration performed as described for microfiltrations. The filtrate was collected in a 96well DWP and, if necessary, stored at 4°C.

3.2.7. Cellulase activity assays

Azo-CMC assay

Azo-CMC is a commercially available substrate for endo-1,4-β-glucanases (Megazyme, Bray, Ireland). All working solutions were prepared as given by the manufacturer's instructions. Only the acetate buffer's pH was adjusted to 4.8 instead of 4.6. For the standard protocol of the assay, 0.5 mL enzyme sample were added to 0.5 mL Azo-CMC solution in a 5 mL tube. Both, enzyme and substrate solution were pre-heated to the incubation temperature of 45°C. Incubation was done for 10 min at 900 rpm, before adding 2.5 mL precipitant solution. After thorough manual mixing, the sample was incubated at RT for 10 min. Precipitated non-hydrolyzed substrate was separated by centrifugation at 18000 g for 10 min. For measurement, 100 µL of supernatant were transferred to a flat-bottom MTP (9293.1, Roth, Germany) and absorbance was determined at 590 nm in a Synergy 4 Microplate Reader (BioTek, Winooski, VT, USA). For the HT protocol, 0.2 mL of the enzyme sample were added to 0.2 mL Azo-CMC solution in a 96well DWP. Both, the MTP containing the samples and the MTP with the substrate solution were pre-heated on the heater shakers (Fig. 3.1-A,

no.6) for 15 min at 45°C. After the incubation for 10 or 20 min, respectively, at 900 rpm, 1 mL precipitant solution was added. Mixing was done by threefold repeatedly aspirating and ejecting the solution with the pipetting robot. After 10 min incubation at RT, 300 µL of the solution were transferred to an AcroPrep^{TM} 96 Filter Plate (0.2 µm Bio-Inert membrane, modified hydrophilic nylon, 350 µL, part no. 5042, Pall Life Sciences, Ann Arbor, MI, USA) placed on the vacuum station of the RoboLector. For complete filtration, an underpressure of 0.5-0.6 bar was applied for 15 min. To ensure homogeneous vacuum distribution, filtrations were performed with full plate occupancy. For measurement, 100 µL of filtrate were transferred from the receiver plate to a flat-bottom MTP and absorbance was determined at 590 nm in a Synergy 4 Microplate Reader (BioTek, Winooski, VT, USA). To determine calibration curves, a commercially available endo-1,4-β-D-glucanase (EGII) from *Trichoderma longibrachiatum* was used (E-CELTR, Megazyme, Bray, Ireland). By dilution in 0.1 M acetate buffer, measuring solutions were prepared with cellulase activities of 100-1000 mU ml^{-1}.

CMC hydrolysis

For CMC hydrolysis under HT conditions, 500 µL of enzyme samples were given to 500 µL of a pre-heated solution of 10 g L^{-1} CMC in 0.1 M acetate buffer in a 96well DWP on a heater shaker of the RoboLector system. After incubation at 900 rpm and 45°C, samples were either transferred to a DWP plate on the cooling carrier and stored at 4°C or directly analyzed via PAHBAH test.

PAHBAH test

For the performance of the PAHBAH reaction, the respective working solution was prepared directly before performing the test by mixing one part of reagent A and nine of reagent B. The working reagent remains stable for only a few hours. For reagent A, 5 g 4-hydroxybenzoic acid hydrazide, 30 mL H_2O (dist.), and 5 mL HCl (37 %) are mixed and filled up to 100 mL with H_2O (dist.). For reagent B, 12.5 g trisodium citrate, 1.1 g $CaCl_2$, and 20 g NaOH are dissolved in 500 mL H_2O (dist.) and filled up to 1 L with H_2O (dist.). Both reagents are stable for approximately 3-4 weeks. For the standard protocol, 75 µL sample were mixed with 150 µL working reagent in a 2 mL tube and incubated for 10 min at 900 rpm and 100°C on a thermo mixer (MHR23, HLC Biotech, Bovenden, Germany). After cooling to room temperature, 100 µL were transferred to a flat-bottom MTP (9293.1, Roth, Germany) and absorbance was measured at 410 nm (Synergy 4 Microplate Reader, BioTek, Winooski, VT, USA). For calibration, reference standards with 0-0.5 g L^{-1} glucose in 0.1 M acetate buffer were used. For the HT protocol, 75 µL sample were given to 150 µL pre-heated working reagent in a 96well DWP and incubated for 10 min at 900 rpm and 85°C on a heater shaker of the RoboLector system. Afterwards, 100 µL were transferred to a flat-bottom MTP and absorbance was measured at 410 nm. For calibration, reference standards containing 10 g L^{-1} CMC and 0-0.5 g L^{-1} glucose in 0.1 M acetate buffer, as well as pure buffer were used. The absorbance difference for a buffer with 10 g L^{-1} CMC and pure buffer was subtracted from each measuring value.

3.3. Results & discussion

3.3.1. Extended RoboLector HTS platform

To meet the demands for an automated HTS of cellulase expression, the original RoboLector system [18] had to be extended. Fig. 3.1-A shows the layout of the robotic platform equipped with its different components. The conventional RoboLector system contained the custom-built BioLector on-line monitoring system (1), a carrier for pipetting tip storage (2), a carrier for the storage of different MTPs (3) with an additional position to park the iSwap gripping tool (4), and a waste bag for used tips and MTPs (8). With this setup a sufficient upstream process including media preparation, inoculation, cultivation (including on-line monitoring) as well as automated sampling is possible. But, it lacks possibilities for further sample processing like storage, purification and analysis. Therefore, additional components had to be added to the robotic platform. For tempering tasks, two further tools were integrated. A cooling carrier with five MTP positions (5) connected to a controllable recirculation cooler allows storage of samples and chemicals at low temperatures. With two MTP shakers (6), heat treatment at temperatures up to 110°C can be performed. Furthermore, the RoboLector system was extended by a vacuum filtration module for micro- and ultrafiltration steps in special multiwell filter plates. The filtration module consists of the vacuum chamber (7a), also containing the filtrate receiver plate, and a parking position for the chamber's lid (7b). The components 2-8 are commercially available from Hamilton Robotics GmbH (Martinsried, Germany).

Fig. 3.1-B shows the schematic protocol for automated HTS experiments with the necessary process steps for cellulase expression, purification and quantification. Depending on the experiment's needs, single steps can, of course, be skipped. The screening process can be classified into three major phases: upstream, downstream, and analysis. The upstream part starts with the preparation of the cultivation medium direct in the cultivation MTP from up to

15 supplied stock solutions stored in DWPs on the cooling carrier (step I). Thereby, the combination of automated medium preparation and cultivation in MTPs allowed to compare different media or to investigate the influence of one or more medium components in short time. Subsequently, the medium is inoculated from a prepared MTP containing the preculture which is shaken on a MTP shaker to ensure a homogeneous suspension (step II). The inoculated cultures are then cultivated under defined conditions in the BioLector system, accompanied by optical on-line monitoring of relevant fermentation parameters such as biomass and product formation, DOT and pH (step III, [19, 28]). If necessary, chemicals can be added to the cultures by the pipetting robot at pre-defined times, e.g. inducing chemical compounds to start product formation. At pre-defined time points, samples can fully automatically be taken (step IV) and stored in MTPs on the cooling carrier for further processing (step V). Both, the adding of substances as well as taking samples cause only short interruptions of the cultivation process so that no negative influences are observed.

The upstream phase ends when the cultivation is finished and final samples are taken and stored. The subsequent downstream processing is focused in this work on the elimination of cell material from the cultivation samples. The fact that the target enzyme is either produced intracellular or secreted to the medium dictates which route is taken to gain a cell free cellulase solution. For extracellular enzymes a microfiltration step applying multiwell filter plates with a maximum pore size of 0.2 µm is sufficient to remove all microbial cells and cell fragments (step VII). Afterwards, the corresponding filtrate contains the soluble target enzyme. Intracellular cellulases need a preceding extraction step (step VI). This is done by chemical cell lysis since mechanical procedures or sonification are not applicable for HT processing on a liquid handling robot platform. After the enzyme release by chemical cell lysis, the remaining cell fragments are removed by microfiltration as described earlier for secreted enzymes. It must be considered that the resulting filtrate contains all other soluble components from the cultivation step. But since this work focused on the expression of

cellulases and not on their detailed characterization, these impurities are accepted due to the fact that all investigated enzyme candidates are affected in the same way.

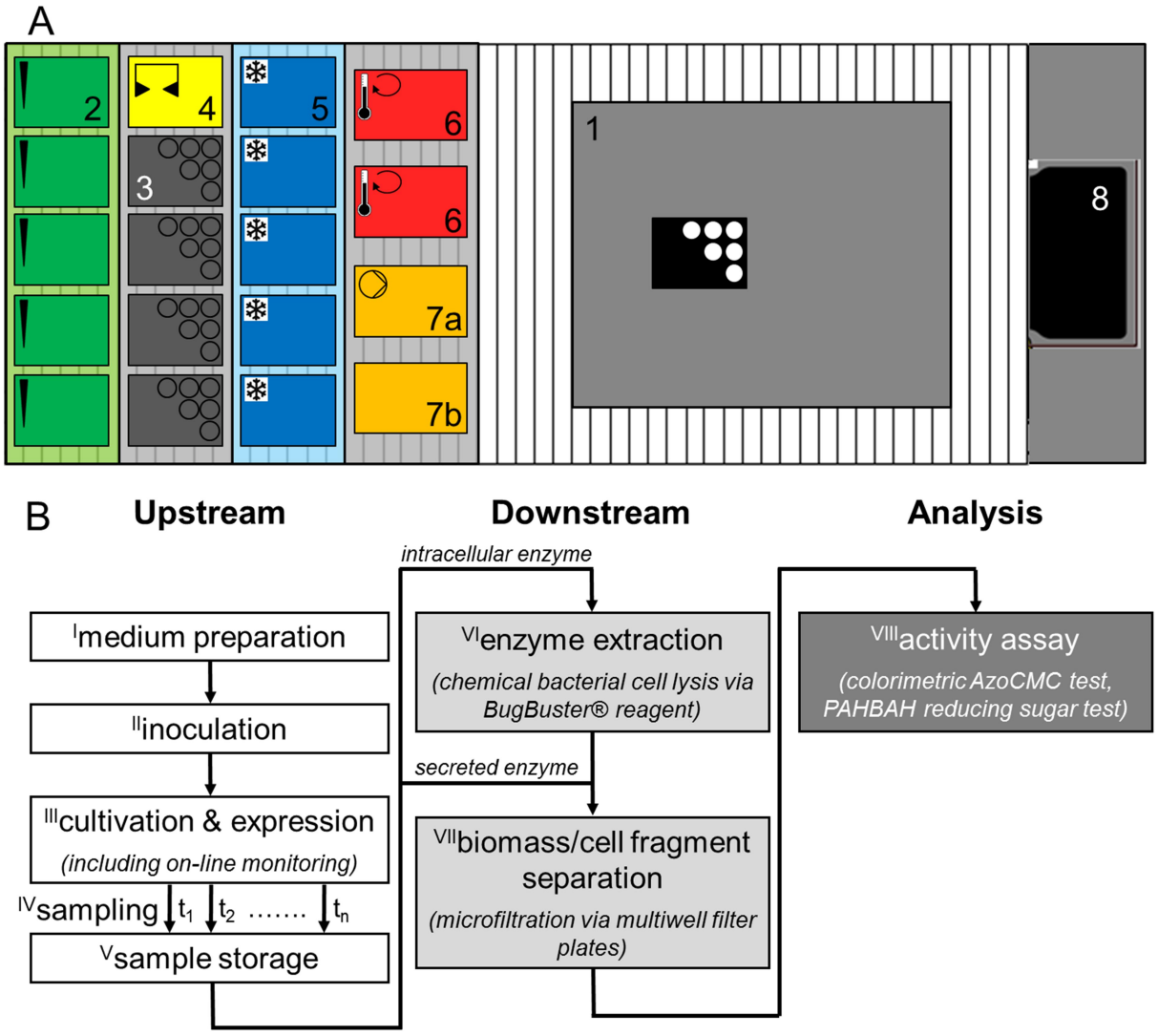

Fig. 3.1 - Automated HTS of recombinant cellulase expression applying the RoboLector platform. (A) Layout of the automated HTS RoboLector platform: 1) Customized BioLector on-line monitoring device; 2) Pipetting tip carrier for up to 5x 96 tips; 3) Carrier with 4 MTP storage positons; 4) Gripping tool parking position; 5) Cooling carrier for storage of up to 5 MTPs containing samples and/or chemicals; 6) Heater shakers (2x) for MTPs; 7a) Vacuum filtration module for one filter MTP with vacuum chamber, 7b) Lid parking position; and 8) Waste bag. (B) Schematic protocol for an automated HTS procedure for recombinant cellulase expression with processing steps I-VIII.

The sample analysis aims for the activity measurement of expressed cellulases. Therefore, two methods for cellulase activity measurement were adapted for automated HTS. The colorimetric Azo-CMC test quantifies a blue dye which is released during cellulase driven CMC hydrolysis. According to the manufacturer's instructions, this method is most effective for endoglucanases. Nevertheless, the applicability for cellobiohydrolases was proved within this work (data not shown). Alternatively, the reducing sugar assay PAHBAH can be used for cellulase quantification [29, 30]. Additionally, a third assay was applied for cellulase activity determination applying the fluorescent dye releasing substrate 4-MUC. This assay was not performed automatically yet, due to its fast and simple manual procedure. However, a full automation would be easy to realize with a sample amount of less than 48 wells.

The control of the robot system is based on a modular structure. Each processing step has its own routine. Depending on the demands of the experiment, all necessary steps can be combined. In this way, the flexible use of the system is ensured and routine programming is simplified. On the other hand, it might be disadvantageous that several steps cannot be operated in parallel, eventually causing increased processing times.

Several process steps from Fig. 3.1-B were not yet designed for a liquid handling robot platform, namely enzyme extraction (VI), biomass separation (VII) and the cellulase activity assays (VIII). Consequently, modifications were necessary for down-scaling and automation. Fig. 3.2 compares schematically the standard lab protocols with the modified protocols for an application on the extended RoboLector system. In the following text, these modifications are described in detail.

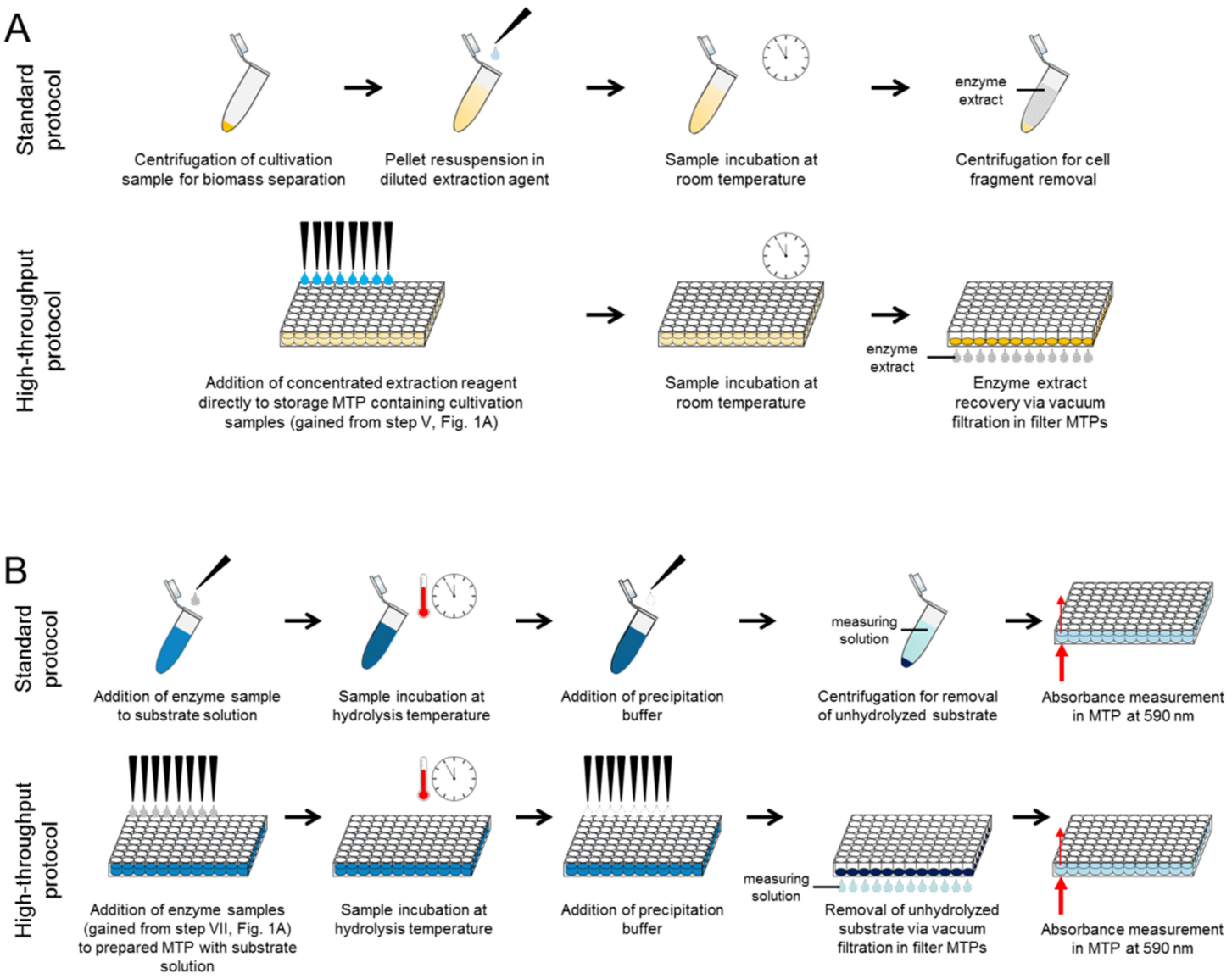
A
Standard protocol
Centrifugation of cultivation sample for biomass separation
Pellet resuspension in diluted extraction agent
Sample incubation at room temperature
enzyme extract
Centrifugation for cell fragment removal
High-throughput protocol
Addition of concentrated extraction reagent directly to storage MTP containing cultivation samples (gained from step V, Fig. 1A)
Sample incubation at room temperature
enzyme extract
Enzyme extract recovery via vacuum filtration in filter MTPs
B
Standard protocol
Addition of enzyme sample to substrate solution
Sample incubation at hydrolysis temperature
Addition of precipitation buffer
measuring solution
Centrifugation for removal of unhydrolyzed substrate
Absorbance measurement in MTP at 590 nm
High-throughput protocol
Addition of enzyme samples (gained from step VII, Fig. 1A) to prepared MTP with substrate solution
Sample incubation at hydrolysis temperature
Addition of precipitation buffer
measuring solution
Removal of unhydrolyzed substrate via vacuum filtration in filter MTPs
Absorbance measurement in MTP at 590 nm

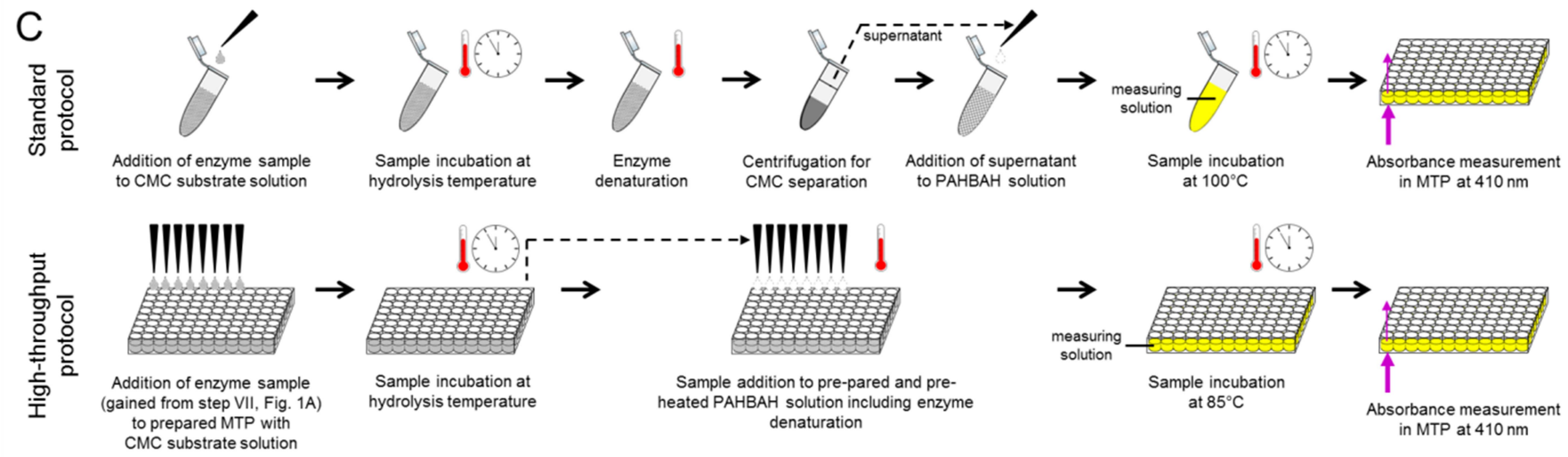

Fig. 3.2 - Schematic comparison of conventional protocols and modified protocols adapted for HT application in MTPs. A) Extraction of recombinant enzymes/proteins from *E. coli* by chemical cell lysis applying BugBuster® reagent. B) Colorimetric AzoCMC assay for cellulase activity measurement. C) PAHBAH test for quantification of reducing sugars after CMC hydrolysis.

3.3.2. Recombinant protein extraction

For the extraction of recombinant proteins from *E. coli* cells, chemical cell lysis was chosen applying the BugBuster® reagent kit. In Fig. 3.2-A the standard protocol according to the operator's manual is compared with the modified HT protocol for automated handling. The conventional procedure applying 1.5 mL tubes started with a centrifugation step of cell suspension gained from a cultivation sample to separate biomass from the fermentation medium. After removal of the supernatant the cell pellet was re-suspended applying the extraction reagent. Therefore, the supplier is offering a 10fold concentrated solution which was appropriately diluted. After incubation at RT the mix was centrifuged again to remove solid components such as cell fragments. The resulting supernatant contained the target protein in soluble form. In contrary, the HT protocol was performed in 96well MTPs. Since centrifugation was not possible on the RoboLector platform, the respective steps had to be replaced. An alternative is microfiltration applying multiwell filter plates. In this way, whole cells and cell fragments can be sufficiently removed from liquid media. But as it turned out, complete re-suspension of cell pellets after the filtration was not possible due to a resistant filter cake. Consequently, the first two steps of the conventional protocol, namely biomass separation and re-suspension, were replaced by only one step. Therefore, the 10fold concentrated extraction reagent solution was not diluted but given directly to the cultivation sample including biomass and liquid medium. Nevertheless, the final reagent concentration before incubation was equal to the conventional protocol since the fermentation medium served as solvent. After sample incubation on a heater shaker (Fig. 3.1-A, no. 6) at RT all solid components were removed by microfiltration applying 96well filter plates equipped with a membrane of 0.2 µm pore size on the vacuum filtration module (Fig. 3.1-A, no. 7a). The resulting filtrate in the receiver plate contained the target protein in soluble form. To simplify the process and save material and time, all steps were performed in the same MTP.

Consequently, in this case the filter plate served for sample storage, the extraction reaction and, finally, for cell fragment separation.

To validate the modified HT protocol, samples from a cultivation of *E. coli* expressing the fluorescent protein FbFP were treated with both protocols and the extraction results were determined by fluorescence measurement and SDS-PAGE analysis (Fig. 3.3). For fluorescence measurement, the fluorescence intensity of the original cell suspension was used as a reference so that the first column in Fig. 3.3-A shows a relative FbFP fluorescence of 100 %. In the corresponding lane of the SDS-PAGE gel in Fig. 3.3-B a prominent band (framed) can be seen, indicating the target protein. For the comparison of the standard and the HT protocol, three fractions which occur during the extraction process were analyzed: the cell suspension after the incubation with the extraction reagent, the pellet after cell fragment removal and the supernatant or filtrate, respectively, after cell fragment removal. For the standard protocol it can be seen that both, cell suspension after the extraction and supernatant after biomass removal, show relative fluorescence intensities around 100 %. The SDS-PAGE gel confirms these measurements, showing strong bands for the target protein (framed) in both fractions. Almost no fluorescent target protein was found in the residual pellet. This means that the standard protocol works properly. The HT protocol shows similar results. The cell suspension after extraction gives a fluorescence intensity of 90 %, the filtrate after cell fragment removal 74 %, and the retained cell fragments a very low value of 7 %. The SDS-PAGE gel is in good agreement with these values.

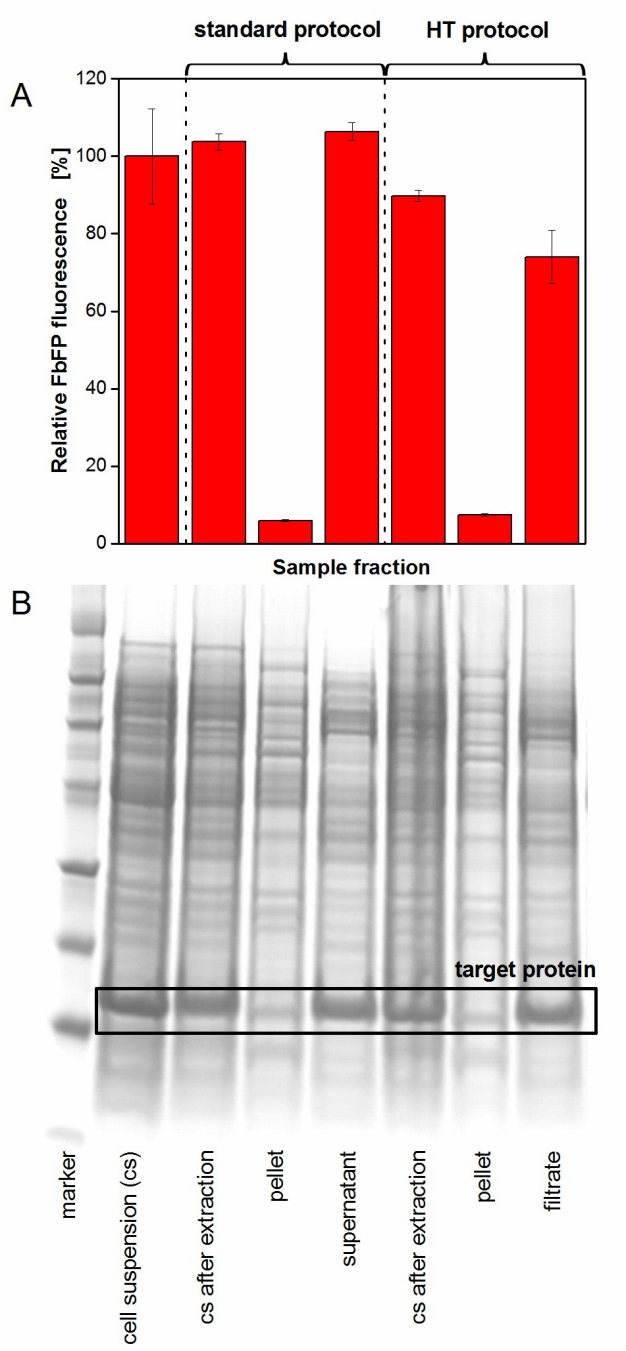

Fig. 3.3 - Extraction of the fluorescent model protein FbFP from *E. coli* BL21(DE3) pRhotHi-2 comparing the standard and HT protocol (according to Fig 2A). A) Fluorescence measurement of different fractions occurring during the extraction procedure applying the BioLector technique. Error bars indicate standard deviation of three simultaneously performed extraction experiments. B) SDS-PAGE analysis of different fractions occurring during the extraction procedure. Target protein FbFP framed. Conditions: Cultivation in 10 mL OnEx auto-induction medium, 250 ml shake flask, n=350 rpm, d_0=50 mm, 37ºC. Extraction with BugBuster 10x Protein Extraction Reagent.

Even though, the measured values, especially those for the fraction containing the target protein, are lower for the HT protocol, the applicability for the RoboLector system could be shown since the majority of the target protein was found in the filtrate. It must be considered, that fluorescence measurement depends on many factors such as pH and ion concentrations [31]. After the extraction from the protecting cells, the FbFP was exposed to the respective environment. Since the medium composition slightly differed in the standard and HT protocol, the protein's fluorescence might be affected leading to inaccurate results. The SDS-PAGE gel, on the other hand, shows very similar bands for the target protein for both protocols.

3.3.3. Colorimetric Azo-CMC test

Assays applying dyed substrates are a convenient way to quantify enzymatic activity. For cellulases, Azo-CMC is a well-established substrate which releases a blue dye during hydrolysis. Subsequently, cellulase activity can be easily determined via absorbance measurement. However, this assay wasn't yet applied for automated HTS. One reason for this might be the difficult handling with a pipetting robot. Fig. 3.2-B shows the manually performed standard protocol as well as the modifications of the assay procedure to adapt it for the application on the RoboLector platform. For comparison, starting point was the addition of an enzyme sample to the ready prepared and pre-heated Azo-CMC substrate solution. The standard protocol was performed in 5 mL tubes. For incubation, the filled tubes containing 0.5 mL preheated enzyme sample and 0.5 mL preheated substrate solution were shaken on a tube shaker for 10 min at 45°C (hydrolysis temperature). Subsequently, the reaction was stopped by adding 2.5 mL precipitation buffer. To remove the precipitated non-hydrolyzed substrate, samples were centrifuged for 10 min at 18000 g and 100 µL of supernatant (measuring solution) was transferred to a MTP for absorbance measurement. Thereby, it was critical to

leave the unstable pellet unaffected since dispersed particles falsify the measurements. For the HT application, the assay was adapted to 96well DWPs. After addition of 200 µL enzyme samples to the DWP placed on the heater shaker containing 200µL pre-heated Azo-CMC solution, the plate was incubated for 10 min at 45°C at 900 rpm. By adding 1 mL precipitation buffer, the hydrolysis reaction was stopped. At this point, it was challenging to remove the precipitated substrate. On the one hand, the RoboLector is lacking a centrifuge. On the other hand, the reduction of the reaction volume due to the assay adapted to DWPs made it very difficult for the pipetting robot to remove a sufficient volume of supernatant without affecting the pellet. Considering the available hardware, a promising approach was microfiltration applying multiwell filter plates. It turned out that a membrane with a pore size of 0.2 µm was sufficient to retain the precipitated substrate particles (data not shown). After the filtration, 100 µL of the filtrate was transferred from the receiver plate to the final MTP for absorbance measurement in a MTP reader. It should be noticed that the MTP reader is not yet integrated into the RoboLector platform. Transport and measuring were done manually. Nonetheless, these steps could be automated in the foreseeable future.

To validate the modified HT protocol, calibration curves were determined with a commercially available endoglucanase. The relationship between enzyme activity and measured absorbance is shown in Fig. 3.4, comparing the manual standard protocol and the HT protocol at varied incubation times. It becomes obvious that the standard protocol (triangles) gives consequently higher values than the HT protocols. Better mixing conditions in the 5 mL tubes and, consequently, an improved substrate access for the enzyme might be the explanation. Nevertheless, a linear relationship is ensured for enzyme activities up to only 400 mU mL^{-1}, before the curve runs into saturation. On the contrary, the HT protocol with 10 min incubation (circles) shows a linear trend up to 1000 mU mL^{-1}. However, the narrow measuring range for the absorbance is rather disadvantageous. To face this problem, the incubation time was increased to 20 min (squares). In this way, the measuring range was more

than doubled and measurements of high cellulase activities up to 1000 mU mL^{-1} were still possible. By looking at the respective standard deviations it must be stated that the accuracy of the HT protocols was much better compared to the manual standard protocol. This fact was ascribed to the filtration process which is much more efficient for the separation of the precipitated non-hydrolyzed Azo-CMC than centrifugation. Therefore, it was possible to adapt the colorimetric Azo-CMC assay for application on the RoboLector platform by modifying the assay procedure and optimizing the process parameters.

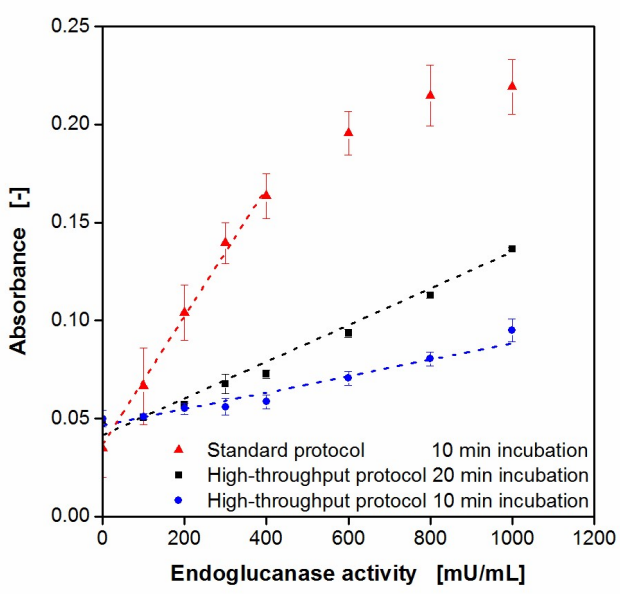

Fig. 3.4 - Calibration curves for the AzoCMC cellulase activity assay comparing the standard protocol and HT protocol at varied incubation times (according to Fig. 3.2-B). Error bars indicate standard deviation of three simultaneously performed assays. Assay conditions: incubation for 10 min in 5 mL tubes, V_L=1 mL, n=900 rpm, d_0=3 mm (standard protocol). Incubation for 10/20 min in 96well DWP, V_L=400 µL, n=900 rpm, d_0=3 mm (HT protocol). 0.2 g L^{-1} Azo-CMC in 0.1 M acetate buffer (pH=4.8), endoglucanase (EGII) from *Trichoderma longibrachiatum*, 50ºC, absorbance measurement at 590 nm.

3.3.4. PAHBAH reducing sugar assay

An alternative way to determine enzyme activity is the quantification of reaction products, which are reducing sugars for cellulases. The PAHBAH test is an already established assay to detect reducing ends. Even though applications in MTP applying a pipetting robot were reported earlier [32], a fully automated protocol has not been described so far. Fig. 3.2-C compares the standard manual test to the modified version for application on the RoboLector system. For comparison, the starting point was the addition of an enzyme sample to the ready prepared and pre-heated substrate solution. Exemplarily, CMC was chosen as substrate for cellulolytic enzymes. The standard protocol was performed in 1.5 mL tubes. For hydrolysis, the filled tubes containing 0.5 mL enzyme sample and 0.5 mL substrate solution were incubated on a tube shaker at 45°C (hydrolysis temperature). By heating the samples up to 100°C, enzymes were inactivated and the hydrolysis reaction stops. The following centrifugation causes the separation of long-chained CMC molecules in a viscous pellet from the less dense solution containing the short-chained sugar molecules in the supernatant. Subsequently, 75 µL supernatant was added to a tube containing 150 µL PAHBAH solution. After incubation at 100°C for 10 min, samples were cooled to RT and 100 µL is transferred to a MTP for absorbance measurement. Since the assay quantifies reducing ends of released sugars, glucose was used for calibration. One glucose molecule possesses one reducing end that is detected by the assay. Therefore, released sugars are specified as glucose equivalents. For the HT application the assay had to be simplified and adapted to 96well DWPs. After addition of enzyme samples to the DWP placed on the heater shaker containing the pre-heated CMC solution, the plate was incubated for up to 5 hours at hydrolysis temperature with shaking. Subsequent transferring of the hydrolysis samples to the DWP containing pre-heated PAHBAH reagent (at 85°C) combined enzyme deactivation and the simultaneous start of the PAHBAH reaction. After incubating at 85°C for 10 min, 100 µL samples were transferred to a MTP for absorbance measurement while cooling to RT. As already discussed for the

AzoCMC assay, the transport to and measuring in the MTP reader was done manually. In contrast to the standard protocol, no separation of the long-chained CMC molecules was done after hydrolysis due to the unavailability of a centrifuge. In doing so, not only the reducing sugars in the supernatant were quantified but the increase of reducing ends during the hydrolysis of CMC. It must be considered that this only works out for low CMC concentrations since the sum of CMC reducing ends and those resulting from the hydrolysis must be within the linear range of the PAHBAH calibration.

To validate the modified HT protocol, calibration curves with glucose were determined, comparing the standard protocol at varied temperatures with the HT protocol. Subsequently, the modified protocol was applied to follow CMC hydrolysis over time by measuring the reducing ends in terms of glucose equivalents. The results are depicted in Fig. 3.5. The calibration curves in Fig. 3.5-A reveal very similar results for all three variants with a linear trend for glucose concentrations up to 0.5 g L^{-1}. For the standard procedure, a temperature decrease during PAHBAH incubation from 100°C (triangles) to 85° (circles) just caused slightly lower absorbance values at lower glucose concentrations. The temperature decrease became necessary since the maximum set temperature of the heater shakers is 110°C. According to eq. 3.2, this limits the incubation temperature in 96well DWP to 85°C. Nevertheless, the PAHBAH test turned out to be reliable even at decreased temperatures. Mellitzer et al. [32] described a slight shift of the linear detection range to higher sugar concentration at lower temperatures. While it ranged from 0.01-1.4 mM (1.8 mg L^{-1}-252.2 mg L^{-1}) at 95°C, it shifted to values of 0.12-2.45 mM (21.6 mg L^{-1}-441.4 mg L^{-1}) at 80°C. These results were confirmed under the modified HT conditions since the measuring values are almost identical with those of the standard protocol at 85°C. The corresponding calibration curve (squares) shows a very good linear trend for sugar concentrations up to 0.5 g L^{-1}. It should be noted that for the calibration applying the HT protocol each sample contained 10 g L^{-1} CMC in addition to the glucose. For comparability with the standard protocol, the

absorbance value for 10 g L^{-1} CMC and 0 g L^{-1} glucose was subtracted from each value. Consequently, the PAHBAH test for reducing sugar detection could be successfully adapted to an automated HT handling on the RoboLector platform.

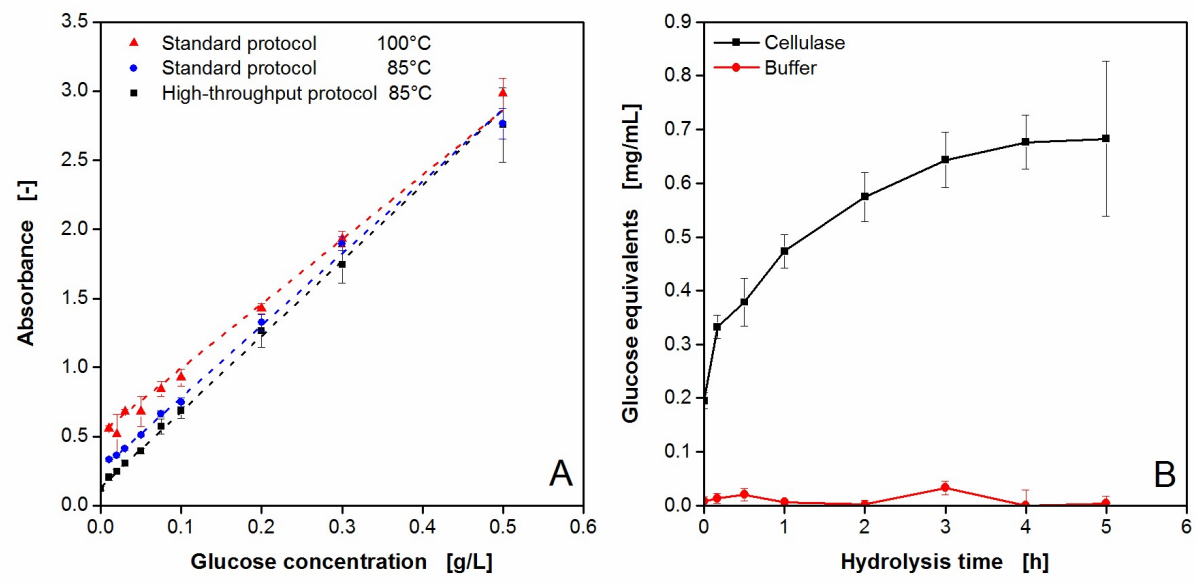

Fig. 3.5 - Adapting the reducing sugar assay PAHBAH for cellulose hydrolysis to automated HT conditions (according to Fig. 3.2-C). A) Calibration curves for the PAHBAH test comparing the standard protocol in tubes at varied incubation temperature and the HT protocol in MTPs. Conditions: Incubation in 1.5 ml tubes for 10 min, V_L=225 µL, n=900 rpm, d_0=3 mm, 100/85°C (standard protocol). Incubation in 96well DWP for 10 min, V_L=225 µL, n=900 rpm, 85°C (HT protocol). Absorbance measurement at 410 nm. Error bars indicate standard deviation of three simultaneously performed assays. B) Glucose equivalent formation during the hydrolysis of CMC incubated with 600 mU cellulase (EGII from *Trichoderma longibrachiatum*) or pure buffer solution measured via PAHBAH reducing sugar assay. Error bars indicate standard deviation of three simultaneously performed assays. Hydrolysis conditions: 96well DWP, V_L=200 µL, 10 g L^{-1} CMC in 0.1 M acetate buffer, pH=4.8, 45°C, n=900 rpm, d_0=3 mm. PAHBAH assay conditions according to the HT protocol described for Fig. 3.5-A.

The novel tool was used to follow CMC hydrolysis by a fungal endoglucanase. Therefore, EGII from *T. longibrachiatum* was incubated with CMC solution in a 96well DWP on the heater shaker of the RoboLector. At pre-defined time points, samples were taken automatically and stored at 4°C in a MTP on the cooling carrier. In parallel, hydrolysis experiments with pure buffer instead of enzyme solution were performed in the same plate as a reference. After the final samples were taken, all collected samples were analyzed via the

PAHABH test. The results in Fig. 3.5-B show the expected behavior. In the presence of the cellulase, the formation of glucose equivalents over time can be observed, with a steep slope in the beginning and saturation after 4-5 h. Without cellulase almost no sugars were detected over the whole time.

Subsequently, the RoboLector platform was used with the newly developed HT methods to characterize cellulase expression. Experiments were performed focusing on different aspects of cellulase expression and, consequently, requiring procedures of different complexity. In this way, different host organisms and expression systems were investigated and expression conditions were optimized. This was accompanied by a very high information content. The presented examples give an overview about the application possibilities and capabilities of the extended RoboLector system.

3.3.5. Expression study of *K. lactis* for cellulase production

For the first example, the behavior of the yeast *K. lactis* for the extracellular expression of recombinant endoglucanase cel5A from *T. reesei* was investigated. Therefore, the complex YP medium was automatically supplemented with different concentrations of galactose, which serves as substrate and at the same time as inducer. Subsequently, the media were transferred to a 48well Flower Plate and inoculated from the provided preculture. All these actions were performed via the pipetting robot. After sealing the plate and transporting it to the BioLector's climate chamber, the cultivation was started. Up to now, automated plate sealing is not possible. But, it could be performed with the integration of the necessary equipment, which is commercially available, into the RoboLector system. Another task which requires manual intervention is the positioning of MTPs in the BioLector. The very tight holding mechanism cannot be handled with the robotic gripping tool. Hence, the development of a new mechanism controllable by the RoboLector software would be advantageous for

further automation. Via optical on-line monitoring, microbial growth (scattered light) and DOT were determined over time, shown in Fig 6A and 6B, respectively. It can be seen that all cultures started growing exponentially after a *lag* phase of 5-6 h, thereby showing almost identical growth rates until 12 h of cultivation. This is accompanied by an inverse decrease of the DOT signals. After 14 h, the culture with 10 g L^{-1} galactose reached the stationary phase, whereas it took 16 h and 19 h for the cultures with 25 g L^{-1} and 50 g L^{-1} galactose, respectively. The simultaneous increase of the DOT signal indicates the complete consumption of the primary substrate galactose. The three curves show no distinct signs of limitation. This is confirmed by the DOT signals which show minimum values of 63 and 16 % for 10 and 25 g L^{-1} galactose, and only a short period of oxygen limitation for 50 g L^{-1}. Also inhibitions, e.g. caused by osmotic stress or recombinant protein productions, seem not to be apparent. Contrary to that, the culture with 100 g L^{-1} galactose showed a first decrease in the growth rate after 12 h. The reason for this is not yet clear. Oxygen limitation can be excluded since the DOT at this time was still higher than 50 %. Nevertheless, a short interruption in the DOT decrease could be observed at this time, too. In the following, microbial growth slightly recovered before becoming linear after 17.5 h due to an oxygen limitation. After 21 h, the DOT signal started increasing before another drop at 22 h accompanied by a further increase of the biomass signal, albeit with decreased growth rate. *K. lactis* is known to produce ethanol under oxygen limitation or as a product of overflow metabolism. Consequently, the second decrease of the DOT signal is due to the utilization of ethanol which was formed from galactose in the earlier stages of the cultivation. This phenomenon was described before [33]. After 25 h, the culture enters the stationary phase and the DOT recovers again.

For the quantification of cellulase production, samples were taken automatically, starting after 8 h of cultivation when the cultures had already entered the exponential growth phase. For sampling, whole wells of the cultivation plate in the BioLector were sacrificed and the cell

suspension was transferred to the storage plate on the cooling carrier. In this case, a multiwell plate for microfiltration served for storage at 4°C. After the final samples were taken, the filter plate with the samples was transported to the vacuum station, filtration was done, and the cell-free permeate was collected in a receiver DWP for subsequent analysis via Azo-CMC assay. Since the enzyme is secreted from the host cells, no further extraction step was necessary. The results in Fig. 3.6-C show that all cultures had a strongly growth related cellulase production behavior. With the beginning of exponential growth, cellulase activity started increasing in the same way, reaching higher final activity values with higher initial galactose concentrations. However, an increase to 100 g L^{-1} galactose didn't result in further improvement. Interestingly, cellulase production did not stop with biomass formation, but it continued until the DOT signal was fully recovered. Consequently, *K. lactis* had the ability for recombinant protein expression, even though the inducing component in the medium was depleted. Earlier reported carbon storage mechanisms might be the explanation for this phenomenon [34].

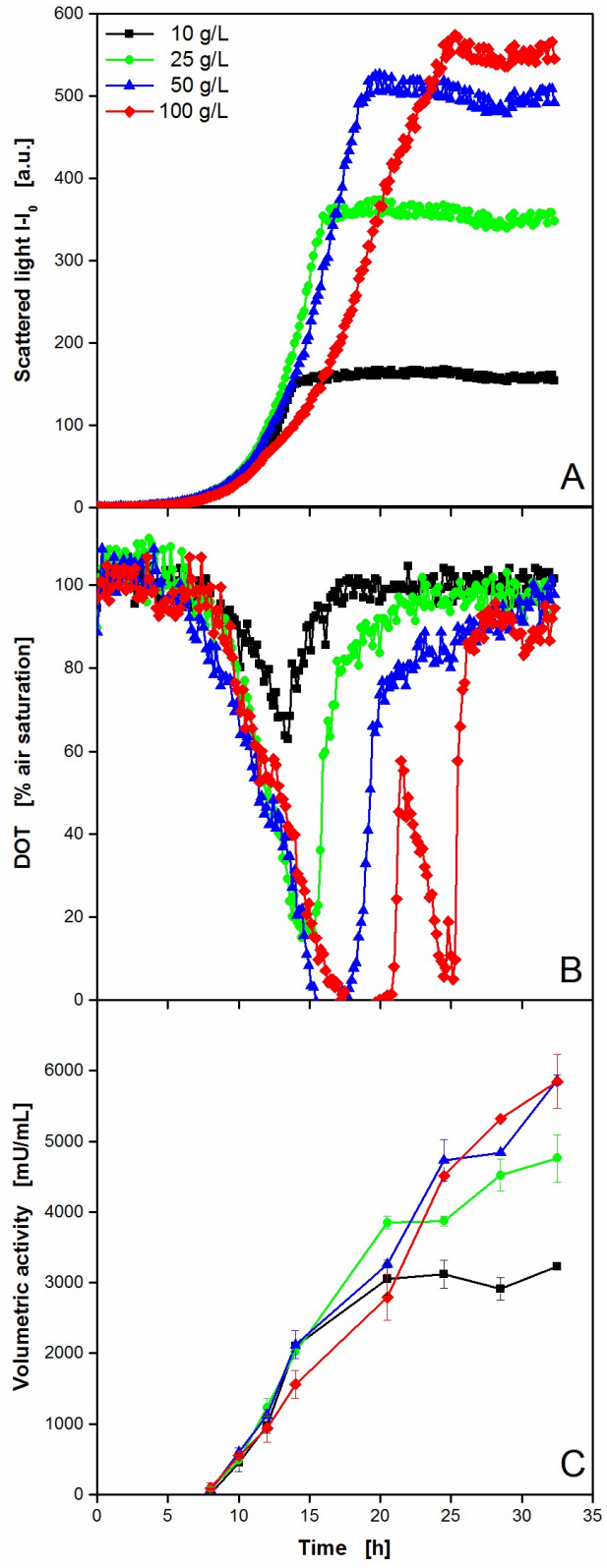

Fig. 3.6 - Expression study of *K. lactis* expressing recombinant endoglucanase cel5A from *Trichoderma reesei* at varied medium composition applying the RoboLector system. Cultivation and on-line monitoring of microbial growth (via scattered light, A) and DOT (B) at varied galactose concentrations. The data were derived from representative single experiments. They are in very good agreement with preliminary, non-automated characterization experiments focusing on growth kinetics and final product yield (data not shown). C) Automated offline analysis of volumetric cellulase activity applying the AzoCMC assay. Error bars indicate standard deviation of three simultaneously performed assays. Cultivation conditions: 48well Flower plate, YP medium containing galactose as carbon source, V_L=1 ml, n=1500 rpm, d_0=3 mm, 30°C. Activity assay conditions: incubation in 96well DWP, 0.2 g L^{-1} Azo-CMC in 0.1 M acetate buffer (pH=4.8), V_L=400 µL, n=900 rpm, d_0=3 mm, 50 ºC, absorbance measurement at 590 nm.

The results enable a comparison of biomass and product formation under consideration of the used substrate (Tab. 3.4). Taking the culture with 10 g L^{-1} galactose as a reference, it can be seen that an increase of the substrate concentration led to a decrease of the yields for biomass and product formation. Even though, the maximum yield for cellulase production was found for all cultures after 20 h, it was highest with 50 g L^{-1} galactose. Consequently, for a later application of the *K. lactis* expression system for endoglucanase production, priorities need to be defined in order to choose the optimal substrate concentration, thereby considering the factors time, substrate costs, and desired product concentration. The respective yields are an important parameter which influences how to run an industrial process. Therefore, the RoboLector system with its novel capabilities can deliver a good data base for making decisions.

Tab. 3.4 - Relative yield coefficients for the expression study with K. lactis expressing recombinant endoglucanase cel5A from Trichoderma reesei with varied galactose concentration. The data were derived from representative single experiments. $Y_{X/S}$ = Biomass yield on substrate, $Y_{P/S}$= Product yield on substrate, STY= Space time yield.

Galactose conc. [g L^{-1}]	Relative $Y_{X/S}$ [%]	Relative $Y_{P/S}$ [%]	Relative max. product STY [%]
10	100	100	100 (after 20 h)
25	89	59	124 (after 20 h)
50	63	36	152 (after 20 h)
100	34	18	145 (after 20 h)

3.3.6. Auto-induction medium optimization for cellulase-expressing *E. coli*

In a second exemplary study, the recombinant expression of the highly salt tolerant and thermostable endoglucanase cel8H from *Halomonas sp66-4* in *E. coli* was attempted to be improved by optimizing the carbon source composition of the applied auto-induction medium. Besides with the original carbon source glycerol, the complex TB medium was enriched with different amounts of glucose and lactose for auto-induction. This approach works as follows: glucose is the preferred carbon source and represses recombinant protein expression to ensure undisturbed initial growth. After glucose depletion lactose is taken up and acts as the inducer of the expression system. Glycerol is an additional energy source. It is consumed in parallel to lactose [33, 35, 36]. It was attempted to vary the time point of induction and the inducer concentration in order to influence the product formation [18, 36]. For a convenient quantification of the cellulase formation, the target protein was linked to a fluorescent mCherry reporter tag. The experiment started with the fully automated composition of the medium variants from a carbon source free TB medium and stock solutions for glucose, lactose, and glycerol directly in a 48well Flower Plate for cultivation. Subsequently, all wells were inoculated from the provided pre-culture. After sealing the plate and its transport to the BioLector, the cultivation was started. Via optical on-line monitoring, microbial growth (scattered light) and cellulase production (mCherry fluorescence) were determined over time. The results for six exemplary wells (out of 48) are shown in Fig 7A and 7B. The legend for the code numbers is given in Tab. 1. It can be seen that all cultures start growing exponentially after a *lag* phase of 1.5 h, thereby showing identical growth rates until 3.5 h of cultivation. At this time, the growth in medium 5052, became slower compared to the other cultures. This is not surprising, since 5052 has the lowest glucose concentration which leads to the earliest time of lactose uptake and, consequently, to the induction of the recombinant protein expression. It is known that this can cause a metabolic burden to the host organism and, hence, inhibiting its growth [36]. Higher glucose concentrations allow a longer

undisturbed growth and, therefore, shift the inhibition phase to a later time. For of 1 g L^{-1} (see 512, 516, and 5110) this was after approx. 5h, whereas no clear growth inhibition occured with 2 and 3 g L^{-1} glucose (see 522 and 532). Comparing the curves for the media 516 and 5110, the effect of induction by lactose on growth becomes visible. Where 6 g L^{-1} lactose caused inhibition until 7.5 h, it took until 8.5 h with 10 g L^{-1} lactose. The final scattered light values differ among the investigated conditions as a result of several factors, e.g. the varied total carbon source amounts, growth inhibition, and varying product formation. It was reported before, that the red mCherry fluorescence affects the scattered light measurement at 620 nm which means that higher fluorescence intensities cause higher scattered light values [37]. When interpreting the BioLector signals, this should be taken into consideration. Consequently, the low final biomass signal for medium 512 is most likely a result of low recombinant protein expression (comp. Fig. 3.7-B).

In accordance with the biomass formation, the cellulase production behavior differed among the media. The first medium showing an increase of the fluorescence signal after 3.5 h was the standard medium 5052, due to lowest glucose concentration. As expected, all media with 1 g L^{-1} glucose (512, 516, 5110) followed simultaneously after approx. 5h, before those with higher concentrations (522, 532) started product formation after 6 h. As observed for microbial growth, no differences occurred for 2 and 3 g L^{-1} glucose. Compared to the rapid increase of all other media, the expression in the standard medium 5052 was rather slow. This can be explained by less biomass at the time of induction and the following stronger growth inhibition. Consequently, less producing host cells were available over the whole cultivation time. Nevertheless, the final product concentration was comparable to those media with 2 and 3 g L^{-1} glucose and even slightly higher than for 1 g L^{-1}. It has to be mentioned, that lactose was used as substrate, too. As a consequence, the same amount of lactose is utilized faster if more cells are present. This leads to an earlier depletion of the inducer lactose and, hence, to

an earlier stop of cellulase expression. This assumption is proved by the curves for 516 and 5110, where additional lactose caused the highest measured target protein formation.

To countercheck the fluorescence values, samples were taken at the end of the cultivation and enzyme activity was determined by CMC hydrolysis and subsequent PAHBAH test applying the HT protocol with the RoboLector system. Therefore, the cell suspension was directly transferred to a 96well microfiltration plate. Since the target protein was expressed intracellularly it was extracted from the *E. coli* cells applying the HT protein extraction protocol described before (Fig. 3.2-A). Subsequently, filtrate samples were used for HT CMC hydrolysis and reducing sugars were quantified by PAHBAH reaction. With the measured values, the volumetric cellulase activity was calculated. One unit was defined as 1 µmol of glucose equivalents produced per minute of reaction time. In Fig. 3.7-C, the final mCherry fluorescence intensities are compared to the final volumetric enzyme activities. Signals went hand in hand since higher fluorescence values are accompanied by higher activities and vice versa. The best result was found for medium 5110, showing approx. 20 % more product formation than the standard medium 5052. Additionally, the data showed that the specific activity of the cellulase did not change with the varied medium composition for enzyme production.

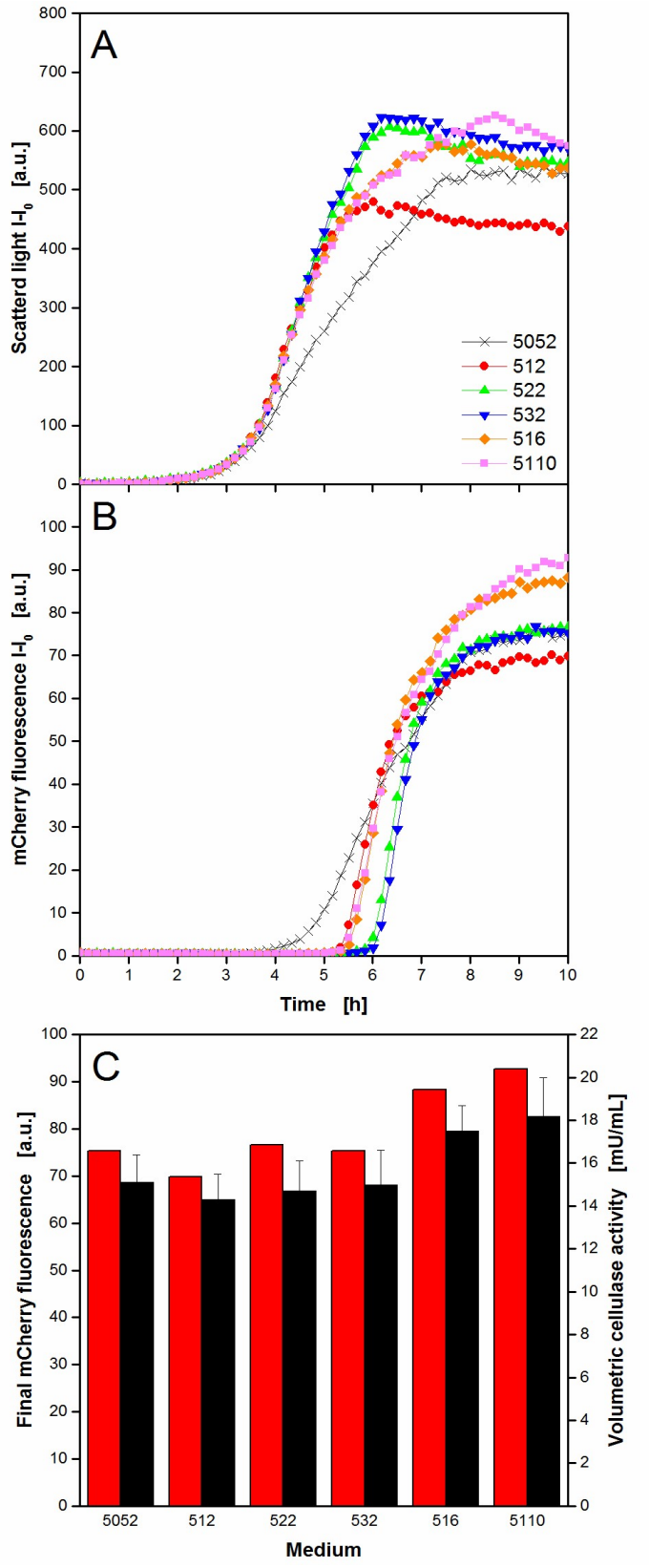

Fig. 3.7 - Auto-induction medium variation for *E. coli* expressing recombinant extremophile endoglucanase cel8H from *Halomonas sp.* tagged with fluorescent mCherry applying the RoboLector system. Cultivation and on-line monitoring of microbial growth (via scattered light, A) and recombinant cellulase expression (via mCherry fluorescence, B) for different auto-induction medium compositions (see Tab. 2). C) Final mCherry fluorescence and volumetric cellulase activity applying the PAHBAH reducing sugar assay for different auto-induction medium compositions. Error bars indicate standard deviation of three simultaneously performed assays. Cultivation conditions: 96well MTP, TB medium with glycerol (5 g L^{-1}) and varied glucose (0.5-3 g L^{-1}) and lactose (2-10 g L^{-1}) concentrations, V_L=200 µl, n=1000 rpm, d_0=3 mm, 37°C. Hydrolysis conditions: incubation in 96well DWP for 60 min, V_L=200 µL, 10 g L^{-1} CMC in 0.1 M acetate buffer, pH=5, 45°C, n=900 rpm, d_0=3 mm. PAHABH assay conditions: incubation in 96well DWP for 10 min, V_L=225 µL, n=900 rpm, d_0=3 mm, 85°C, absorbance measurement at 410 nm.

This example showed how the RoboLector system can conveniently be used to optimize a cellulase production process. The combination of fully automated medium composition, on-line monitoring of biomass and product formation, and final activity measurement allows for fast process characterization and a good data base for further process development. For this goal, the fluorescent tag on the enzyme is a valuable tool to gain kinetic information. Furthermore, the very sensitive PAHBAH test even allows the detection of rather low activities of the highly salt tolerant enzyme cel8H. Such enzymes gain more and more attention since bioprocesses often run under harsh conditions. Cel8H is still active at very high salt loads and, hence, an interesting candidate for future research [38]. Among other measures, elevated expression levels as achieved with the medium optimization can help to improve the feasibility of a potential biomass conversion process.

3.3.7. Semi-automated primary clone bank screening

The data in Fig. 3.8 was observed from a primary clone bank screening for the expression of 95 variants of endoglucanase cel5A from *T. reesei* in *E. coli*. The enzyme variants were created by random mutagenesis. The screening protocol consists of a three step cultivation including two pre-cultivations and a main cultivation with automated induction after 2 h. All cultivation steps were online monitored regarding microbial growth via scattered light measurement. At the end of the cultivation, samples were automatically taken and processed for the final determination of cellulolytic activity. The experiment started by transferring 200 µL of the respective media from the supply plate on the cooling carrier to each well of the 96well MTP for cultivation placed on the cooling carrier, too, and sealed with the xPierce film allowing for pipetting tip penetration. Three cultivation plates were in use for the whole experiment. The first plate was filled with TB medium for the first pre-culture, whereas the second and third plate were filled with WilmsMOPS medium for the second pre-culture and main culture, respectively. Consequently, this procedure requires an exchange of the MTP

within the BioLector. Unfortunately, a removal of the MTP from the climate chamber is not possible with the robotic system due to the very resistant holding mechanism. Hence, these three transfer steps were conducted manually. After filling the first MTP with media, 96 wells were inoculated with 5 µL from a MTP containing cryocultures. Subsequently, the first pre-cultivation was run overnight. The scattered light signal in Fig. 3.8-A shows a very different growth behavior of the 96 clones, especially, when looking at the duration of the *lag* phase which ranges from approx. 2-9 h. Consequently, the cultures are in different growth phases and reach different cell densities after 14 h cultivation. As control, a clone without the plasmid for recombinant cellulase expression was cultivated in parallel. It shows no biomass formation due to the missing ampicillin resistance. For the inoculation of the second pre-culture, 5 µL from each well of the first pre-culture plate were transferred to the respective wells of the second pre-culture plate. After inoculation of the already prepared media plate standing in a storage position, the plate was manually transferred to the BioLector and the cultivation was continued. From the beginning, all clones show much more unified scattered light curves. Compared to the first pre-cultivation, the differences in *lag* phase and final biomass formation are strongly reduced which approves the effectiveness of the conditioning of the *E. coli* cells during pre-culture one. Moreover, the second pre-cultivation allows the cells to adapt to the mineral medium applied for the main cultivation. After 20 h, the inoculation protocol from pre-culture two was used again to start the main cultivation. As expected, all clones show the same growth behavior in the beginning. After 2 h, the recombinant protein expression was induced by adding 5 µL of concentrated L-arabinose solution. Almost immediately, the scattered light signals start diverging from each other, thereby, indicating for clones with strongly inhibited growth, almost non-affected growth, and various kinds of mixed behavior in between. It is obvious that this phenomenon is related to the recombinant formation of cel5A variants. From earlier reports it is known that different

recombinant proteins affect the host organism in different ways, although, the vector system is identical and the target protein sequence is hardly modified [35,36].

Moreover, the results show that cells originating from a cryoculture need much more time to adapt to a new environment as those derived directly from a previous cultivation and, even though, the medium changed from pre-culture 1 to 2, all clones show very similar growth after the first pre-culture. But still, the here used inoculation strategy is not optimal since cultures from pre-culture 1 were used for inoculation under different conditions. By transferring similar volumes from each well, the initial biomass in pre-culture 2 must have differed to some extent. So it is rather surprising that the growth curves from pre-culture 2 show such a uniform behavior. To undergo this problem in future experiments tools like biomass specific inoculation should be applied [18].

To evaluate the clones regarding their production capabilities, cellulolytic activity was quantified via Azo-CMC test. Therefore, samples were taken automatically at the end of the cultivation. The cell suspensions were directly transferred to a 96well microfiltration plate. Since the target protein was expressed intracellularly it was extracted from the *E. coli* cells applying the HT protein extraction protocol described before. Subsequently, filtrate samples were used for the enzyme test applying the HT protocol described before. In Fig. 3.8-B the volumetric cellulose activities of the 96 clones are depicted in decreasing order. The clone without the plasmid is found in the first column and shows no activity as expected. The reference clone expressing the wild-type variant of cel5A is presented by the second column. The regarding reference activity is marked by a dashed line. It becomes obvious that the enzyme production varies among the 96 clones, thereby proving the effectivity of the random mutagenesis procedure. The majority of the clones shows lower activity compared to the reference clone, which is not surprising since non-directed target sequence modifications

often lead to disadvantageous effects. On the other hand, 10 clones show higher activities what makes them most interesting for further verification experiments.

Taking the final scattered light values of the cultures into consideration allows the determination of the biomass specific cellulase activities. As described in Eq. 3.3, a change in volumetric activity can be caused by a difference in the enzymatic specific activity (term 1), by a difference in the biomass specific activity (term 2) or by a difference in the biomass concentration (term 3).

$$\frac{\mathrm{U}}{\mathrm{mL}} = \frac{\mathrm{U}}{\mathrm{g_{enzyme}}} \cdot \frac{\mathrm{g_{enzyme}}}{\mathrm{g_{biomass}}} \cdot \frac{\mathrm{g_{biomass}}}{\mathrm{mL}} \qquad \text{(Eq. 3.3)}$$

The data in Fig. 3.8-C gives a clear trend of a direct proportionality of volumetric and biomass specific enzyme activity, even though, the values are scattering some more at higher activities. Obviously, the cellulase production is not biomass related in this case. Consequently, higher cellulase activities either originate from higher expression levels in the host cells due to a more beneficial target gene sequence, from enzyme variants with increased specific activities, or from a combination of both effects. For final clearance, enzyme quantification would be necessary. Potential tools and methods are discussed for the following application example.

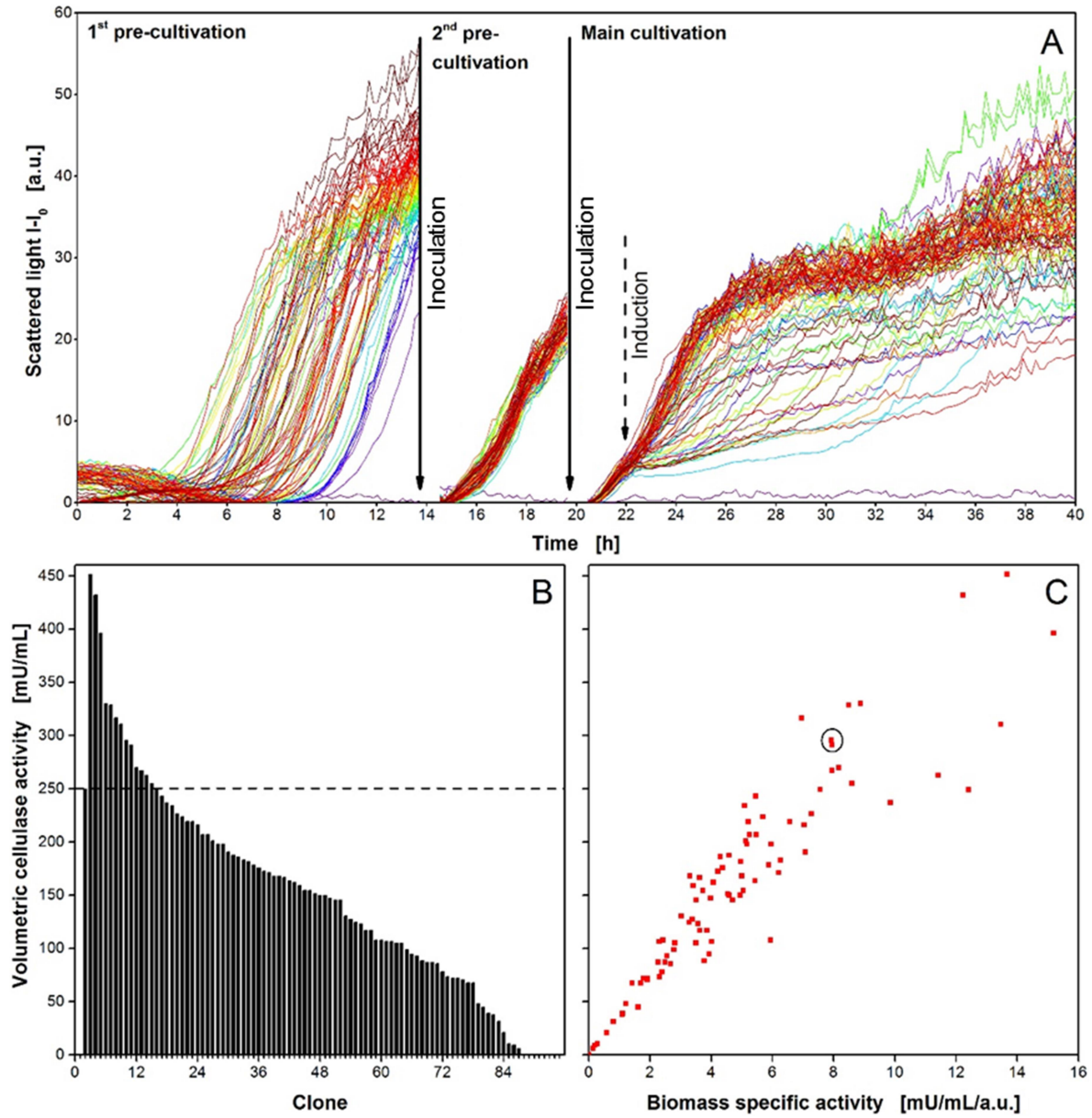

Fig. 3.8 – Semi-automated primary screening of an *E. coli* random mutagenesis clone library expressing variants of endoglucanase cel5A from *Trichoderma reesei* applying the RoboLector system. A) Online biomass signal (monitored via scattered light) for a three step cultivation of 96 *E. coli* clones consisting of two non-induced pre-cultivations and an induced main cultivation. 2nd pre-cultivation and main cultivation were inoculated with 5 µL from the previous cultivation step (solid arrows). B) Volumetric cellulase activity (via AzoCMC assay, according to Fig. 3.2-B) of the supernatant after cellulase extraction (according to Fig. 3.2.-A) from *E. coli* cells of the main cultivation. Reference activity of the clone expressing the original enzyme (clone 1) indicated by dashed line. C) Parity plot comparing volumetric and biomass specific cellulase activities of the supernatants after cellulase extraction from *E. coli* cells of the main cultivation. For calculation of biomass specific activities the final scattered light values of the main cultivation were used. Reference clone expressing the original enzyme indicated by circle. Cultivation conditions: 96well MTP, V_L=200 µL, n=1000 rpm, d_0=3 mm, 1st pre-cultivation in TB medium, 2nd pre-cultivation and main cultivation in WilmsMOPS medium containing 20 g/L glucose, cellulase expression induced by adding 0.2 % [m/v] mM L-arabinoase (dashed arrow). Activity assay conditions: incubation in 96well DWP, 0.2 g/L Azo-CMC in 0.1 M acetate buffer (pH=4.8), V_L=400 µL, n=900 rpm, d_0=3 mm, 50 ºC, absorbance measurement at 590 nm.

3.3.8. Advanced primary clone bank screening

Fig. 3.9 depicts the results of the most complex example performed within this study. The data was generated during a primary clone bank screening for the expression of 46 variants of endoglucanase celA2 in *E. coli*. The enzyme variants were created by directed evolution applying a triple site-saturation mutagenesis [24, 39, 40]. This screening protocol consisted of a two-step cultivation including one pre-cultivation and a main cultivation with automated biomass specific induction. To enable a complete automated cultivation, the first six columns of the plate were used for the pre-culture and the last six columns for the main culture. This avoided the manual transport of MTPs out of the BioLector. For reference, one well in each step of the cultivation was filled with plain medium. Moreover, the wildtype was present two times in both cultivation steps. One served as a non-induced reference.

At the end of the cultivation, the cultures were harvested and used for cell lysis. The already published method to determine celA2 activity in MTP format is the 4-MUC assay [24]. The volumetric activity was calculated from a kinetic measurement of the increase in released fluorescent 4-MU. Therefore, a quick measurement of all micro-wells was necessary. This was not possible within the BioLector since it takes about four minutes to measure 96 wells. Therefore, a manual offline activity assay using a Synergy 4 Microplate reader was chosen for the evaluation of this clone library. But it’s important to consider, that the final assay only measures the volumetric activity. As already discussed for Eq. 3.3, a change in volumetric activity can be caused by a difference in the enzymatic specific activity, by a difference in the biomass specific activity, or by a difference in the biomass concentration. Since the volumetric activity is dependent on these three parameters and only the last term describing the biomass concentration is known from scattered light measurements, it is not possible to distinguish whether the differences are caused by the first or second term.

The scattered light curves of all clones in Fig. 3.9-A show different lag phases within the pre-culture. A time shift of up to four hours within the exponential growth phase was observed when comparing the variants. This is most likely due to fluctuations in the initial cell concentration which are commonly present in cryo-cultures of clone libraries. These differences are then transferred into the culture plate. Moreover, the replication tool which was used to transfer the cells from the cryo-plate to the culture plate plays an important role, as described elsewhere [23]. The asynchronous growth was eliminated after operating the automated biomass specific normalization step shortly after 13 hours. Nevertheless, an automated biomass specific induction was followed which ensures identical induction conditions. As soon as the scattered light exceeded the preset threshold of 10 a. u. the robot induces these specific wells with 10 µL of IPTG, resulting in a final concentration of 0.1 mM. Interestingly, all variants behave the same way after induction and end up with the same biomass concentration at the end of the cultivation. Consequently, similar metabolic burden and similar protein production can be assumed. Integration of this assumption into Eq. 3.3 lead to a direct proportionality of volumetric activity and enzyme specific activity. Thus, an elaborate quantification of the celA2 protein content is not necessary.

After about 14 h of main culture, the cell suspensions were harvested and cell pellets were lysed using BugBuster. The volumetric activity of received crude extract was determined by the fluorescence-based 4-MUC assay. The final clone ranking is depicted in Fig. 3.9-B. Mean values of cellulase activity and error bars coming from three independently conducted HTS are shown. This includes the experiment depicted in Fig. 3.9-A and two more experiments whereof no scattered light curves are shown here. The volumetric activity of the induced wildtype is illustrated as white bar. A six times higher activity was obtained by the best variant when compared to the wildtype. A very small relative standard deviation is observed (wildtype, 5.1 %; best clone, 4.0 %). This confirms a very high reproducibility of the

screening method using the automated pre-culture synchronization and the biomass specific induction. Furthermore, it gives a maximum of standardization accompanied by an on-line monitoring signal to control it. Considering the final scattered light values of the cultures, biomass specific cellulase activities can be determined. Fig. 3.9-C describes the dependency of volumetric activity and biomass specific enzyme activity. Since the biomass concentration was similar for all clones, a completely linear trend was observed.

Dependent on the purpose of the library screening, subsequent enzyme quantification would be necessary to yield the enzyme specific activities. HT affinity chromatography in MTP-format are commercially available for this task, however this leads in most cases to an undesired increase of investment. An easy solution for this problem would be to label the target proteins with fluorescent tags. Term 2 and 3 from Eq. 3.3 would then be known and the enzymatic specific activity could be calculated. However, tags with high molecular weight may stress the host cell metabolism and thus change the target protein expression efficiency or even the enzyme activity. Using smaller tags like tryptophan tags [41] or splitted tags such as the Split-GFP technology [42] could be the method of choice.

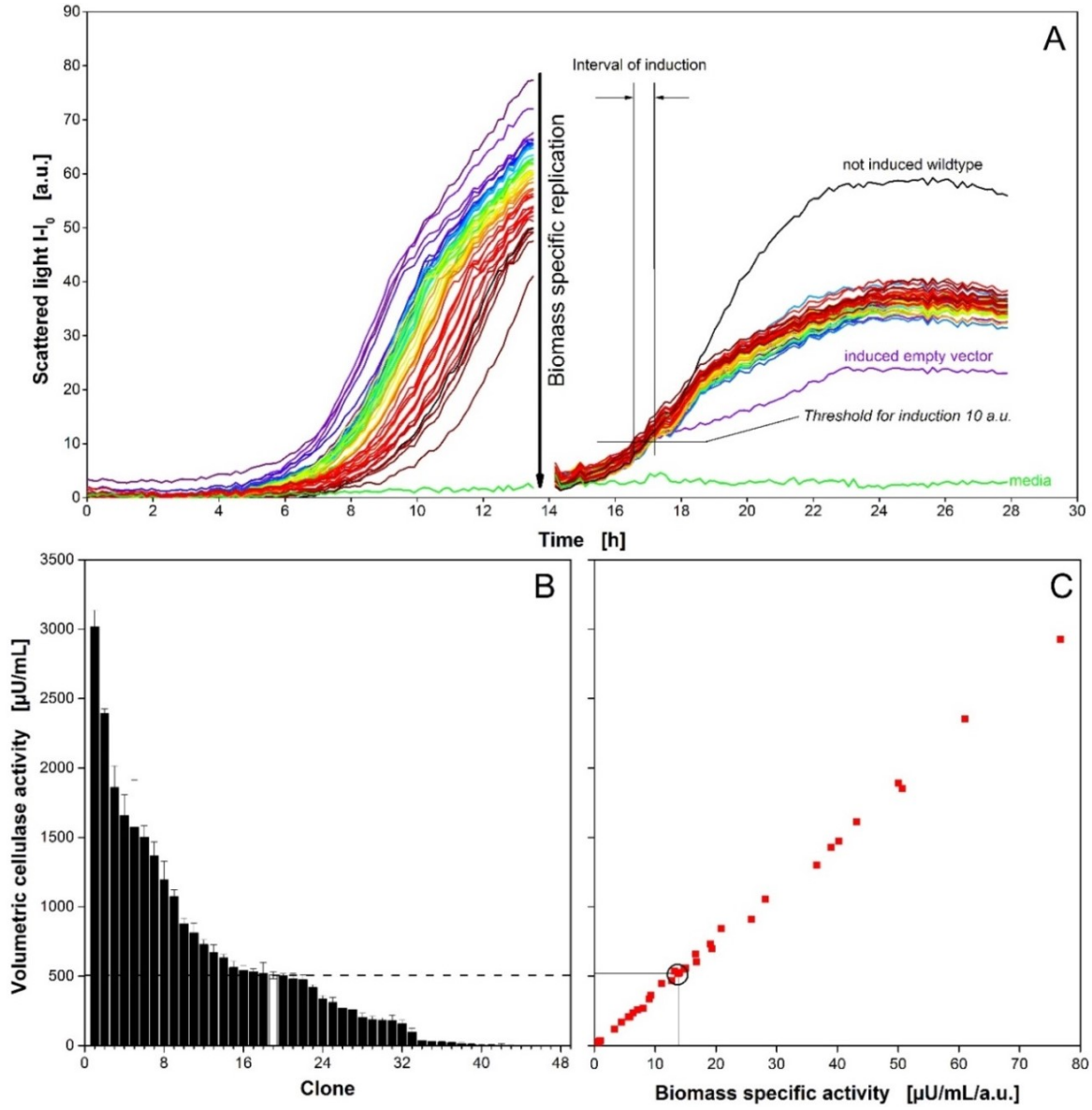

Fig. 3.9 - Primary screening of an *E. coli* random mutagenesis clone library expressing variants of endoglucanase celA2 applying the RoboLector system. A) On-line biomass signal (monitored via scattered light) for a two-step cultivation of 46 *E. coli* clones consisting of one not induced pre-cultivation and an induced main cultivation. Additionally, a not induced wildtype and plain media served as references. The main cultivation was automatically inoculated from the previous cultivation step. B) Volumetric cellulase activity (via 4-MUC assay) of the supernatant after cellulase extraction from *E. coli* cells including standard deviations of three independent main cultivations. Reference activity of the clone expressing the original enzyme indicated by dashed line and white bar. Not induced wildtype and media are depicted as clone no. 47 and 48. C) Parity plot comparing volumetric and biomass-specific cellulase activities of the supernatants after cellulase extraction from *E. coli* cells of the main cultivation. For calculation of biomass specific activities, the final scattered light values of the main cultivation were used. Wildtype clone expressing the original enzyme indicated by circle. Cultivation conditions: 96well MTP, V_L=150 µL, n=995 rpm, d_0=3 mm, pre-cultivation and main cultivation in Wilms-MOPS medium containing 15 g L^{-1} glucose, cellulase expression automatically induced by adding 0.1 mM IPTG after reaching the scattered light threshold of 10 a.u.. Activity assay conditions: incubation in 96well MTP, 0.05 mM 4-MUC solution in potassium phosphate buffer (pH=6.5), V_L=150 µL, 30 ºC, fluorescence measurement at 365/455 nm.

3.4. Conclusion

The RoboLector platform was successfully extended by a cooling carrier, a MTP shaker for heat treatment and a vacuum filtration module. This enables the robot to perform a cellulase screening experiment consisting of upstream, downstream and analysis steps. Some downstream and analysis protocols were adapted from manual handling to a HT protocol suitable for automated handling. This comprises the enzyme extraction step, the Azo-CMC and the PAHBAH cellulase activity assays.

The established methods were successfully applied to investigate the expression of cellulase cel5a in *K. lactis* and to optimize the expression of the endoglucanase cel8H tagged with mCherry in *E. coli*. The results showed how the RoboLector system can conveniently be used to optimize media compositions and analyze the outcome without manual intervention.

The automated HTS of the *E. coli* celA2 library showed the advantage of a biomass specific replication step, to achieve synchronized cultures. A highly parallel biomass growth could be achieved and via biomass specific induction a comparable expression of target protein was secured. A clone ranking revealed a six times higher activity of the best variant, compared to the wildtype.

It was demonstrated that a large variety of methods could successfully be automated on the extended RoboLector platform. The device allows a strongly increased information content compared to screening systems reported so far. The results confirm the feasibility of a reliable and automated HTS on the robotic platform. Up to now, only a small clone library consisting of 46 different variants was screened. The future strategy will be the automation of the whole cellulase screening system with emphasis on the linkages between the already described automated modules and finally screen a large clone library. A comparison of the manual and automated screening is certainly of great interest and will be part of upcoming experiments.

3.5. Nomenclature

4-MUC	4-methylumbelliferyl-β-D-cellobioside
a.u.	Arbitrary unit
Azo-CMC	Carboxymethyl cellulose dyed with Remazolbrilliant Blue
cel5A	Enduglucanase from *Trichoderma reesei*
cel8H-mCherry	Enduglucanase from *Halomonas sp.* tagged with the fluorescent protein mCherry
celA2	Cellulase originally isolated from a metagenome library
CMC	Carboxymethyl cellulose
DNS	3,5-dinitrosalycilic acid
DOT	Dissolved oxygen tension
DWP	Deep well plate
E. coli	*Escherichia coli*
EG	Endoglucanase
Ex	Excitation
Em	Emission
FbFP	Flavin mononucleotide (FMN)-based fluorescent protein
HT	High-throughput
HTS	High-throughput screening
I	Intensity
I_0	Initial light intensity
IPTG	Isopropyl β-d-1-thiogalactopyranoside
K. lactis	*Kluyveromyces lactis*
λ_{em}	Emission wavelength
λ_{ex}	Excitation wavelength
MTP	Microtiter plate
MOPS	3-(N-morpholino)-propanesulfonic acid

PAHBAH	*Para*-hydroxybenzoic acid hydrazide
RT	Room temperature
rpm	Round per minute
SDS-PAGE	Sodium dodecyl sulfate polyacrylamide gel electrophoresis
STY	Space time yield
T	Temperature
TB	Terrific broth
$t_{1;\ldots;n}$	Sampling time
U	Enzyme unit
YP	Yeast extract peptone
$Y_{P/S}$	Product yield from substrate
$Y_{X/S}$	Biomass yield from substrate

3.6. References

1. Fiorentino G, Ripa M, Ulgiati S. Chemicals from biomass: technological versus environmental feasibility. A review. Biofuels, Bioproducts and Biorefining 2016.

2. Ragauskas AJ, Williams CK, Davison BH, Britovsek G, Cairney J, Eckert CA, et al. The path forward for biofuels and biomaterials. Science 2006;311:484–9.

3. Sharma B, Ingalls RG, Jones CL, Khanchi A. Biomass supply chain design and analysis: Basis, overview, modeling, challenges, and future. Renewable and Sustainable Energy Reviews 2013;24:608–27.

4. Hayes DJM. Second-generation biofuels: why they are taking so long. Wiley Interdisciplinary Reviews: Energy and Environment 2013;2:304–34.

5. Dellomonaco C, Fava F, Gonzalez R. The path to next generation biofuels: successes and challenges in the era of synthetic biology. Microbial Cell Factories 2010;9:1–15.

6. Percival Zhang Y, Himmel ME, Mielenz JR. Outlook for cellulase improvement: screening and selection strategies. Biotechnol Adv 2006;24:452–81.

7. Garvey M, Klose H, Fischer R, Lambertz C, Commandeur U. Cellulases for biomass degradation: comparing recombinant cellulase expression platforms. Trends Biotechnol 2013;31:581–93.

8. Wang M, Si T, Zhao H. Biocatalyst development by directed evolution. Bioresour Technol 2012;115:117–25.

9. Chandel AK, Chandrasekhar G, Silva MB, Silverio da Silva S. The realm of cellulases in biorefinery development. Crit Rev Biotechnol 2012;32:187–202.

10. Davids T, Schmidt M, Bottcher D, Bornscheuer UT. Strategies for the discovery and engineering of enzymes for biocatalysis. Curr Opin Chem Biol 2013;17:215–20.

11. Knepper A, Heiser M, Glauche F, Neubauer P. Robotic platform for parallelized cultivation and monitoring of microbial growth parameters in microwell plates. Journal of Laboratory Automation 2014;19:593–601.

12. Meng J, Walter J, Kökpinar Ö, Stahl F, Scheper T. Automated Microscale His-tagged Protein Purification Using Ni-NTA Magnetic Agarose Beads. Chem. Eng. Technol. 2008;31:463–8.

13. Lesley SA. High-throughput proteomics: Protein expression and purification in the postgenomic world. Protein Expression and Purification 2001;22:159–64.

14. Scheich C, Sievert V, Büssow K. An automated method for high-throughput protein purification applied to a comparison of His-tag and GST-tag affinity. BMC Biotechnology 2003.

15. Decker SR, Adney WS, Jennings E, Vinzant TB, Himmel ME. Automated filter paper assay for determination of cellulase activity. Applied Biochemistry and Biotechnology 2003;107:689–703.

16. Navarro D, Couturier M, da Silva G, Berrin J, Rouau X, Asther M, Bignon C. Automated assay for screening the enzymatic release of reducing sugars from micronized biomass. Microb Cell Fact 2010;9:58.

17. Dörr M, Fibinger MP, Last D, Schmidt S, Santos-Aberturas J, Böttcher D, et al. Fully automatized high-throughput enzyme library screening using a robotic platform. Biotechnol Bioeng 2016;113:1421–32.

18. Huber R, Ritter D, Hering T, Hillmer A, Kensy F, Müller C, et al. Robo-Lector – a novel platform for automated high-throughput cultivations in microtiter plates with high information content. Microb Cell Fact 2009;8:42.

19. Samorski M, Müller-Newen G, Büchs J. Quasi-continuous combined scattered light and fluorescence measurements: A novel measurement technique for shaken microtiter plates. Biotechnol. Bioeng. 2005;92:61–8.

20. Hemmerich J, Adelantado N, Barrigón J, Ponte X, Hörmann A, Ferrer P, et al. Comprehensive clone screening and evaluation of fed-batch strategies in a microbioreactor and lab scale stirred tank bioreactor system: application on Pichia pastoris producing Rhizopus oryzae lipase. Microb Cell Fact 2014;13:36.

21. Unthan S, Radek A, Wiechert W, Oldiges M, Noack S. Bioprocess automation on a Mini Pilot Plant enables fast quantitative microbial phenotyping. Microb Cell Fact 2015;14:32.

22. Kensy F, Zang E, Faulhammer C, Tan R, Büchs J. Validation of a high-throughput fermentation system based on online monitoring of biomass and fluorescence in continuously shaken microtiter plates. Microb Cell Fact 2009;8:31.

23. Huber R, Palmen TG, Ryk N, Hillmer A, Luft K, Kensy F, Büchs J. Replication methods and tools in high-throughput cultivation processes - recognizing potential variations of growth and product formation by on-line monitoring. BMC Biotechnol 2010;10:22.

24. Lehmann C, Sibilla F, Maugeri Z, Streit WR, Domínguez de María P, Martinez R, Schwaneberg U. Reengineering CelA2 cellulase for hydrolysis in aqueous solutions of deep eutectic solvents and concentrated seawater. Green Chem. 2012;14:2719.

25. Tartof KD, Hobbs CA. Improved media for growing plasmid and cosmid clones. Focus 1987;9:12.

26. Wilms B, Hauck A, Reuss M, Syldatk C, Mattes R, Siemann M, Altenbuchner J. High-cell-density fermentation for production of L-N-carbamoylase using an expression system based on the Escherichia coli rhaBAD promoter. Biotechnol Bioeng 2001;73:95–103.

27. Hahn-Hagerdal B, Karhumaa K, Larsson CU, Gorwa-Grauslund M, Gorgens J, van Zyl WH. Role of cultivation media in the development of yeast strains for large scale industrial use. Microbial Cell Factories 2005;4:31.

28. Kensy F, Engelbrecht C, Büchs J. Scale-up from microtiter plate to laboratory fermenter: evaluation by online monitoring techniques of growth and protein expression in Escherichia coli and Hansenula polymorpha fermentations. Microb Cell Fact 2009;8:68.

29. Lever M, Powell JC, Killip M, Small CW. A comparison of 4-hydroxybenzoic acid hydrazide (PAHBAH) with other reagents for the determination of glucose. J Lab Clin Med 1973;82:649–55.

30. Moretti R, Thorson JS. A comparison of sugar indicators enables a universal high-throughput sugar-1-phosphate nucleotidyltransferase assay. Anal Biochem 2008;377:251–8.

31. Sarder P, Maji D, Achilefu S. Molecular probes for fluorescence lifetime imaging. Bioconjug Chem 2015;26:963–74.

32. Mellitzer A, Glieder A, Weis R, Reisinger C, Flicker K. Sensitive high-throughput screening for the detection of reducing sugars. Biotechnology Journal 2012;7:155–62.

33. Wewetzer S, Kunze M, Ladner T, Luchterhand B, Roth S, Rahmen N, et al. Parallel use of shake flask and microtiter plate online measuring devices (RAMOS and BioLector) reduces the number of experiments in laboratory-scale stirred tank bioreactors. J Biol Eng 2015;9:2.

34. Dalibor Mijaljica, Mark Prescott, Daniel J. Klionsky, Rodney J. Devenish. Autophagy and vacuole homeostasis: A case for self-degradation? Autophagy 2007;3:417–21.

35. Rahmen N, Fulton A, Ihling N, Magni M, Jaeger K, Büchs J. Exchange of single amino acids at different positions of a recombinant protein affects metabolic burden in Escherichia coli. Microb Cell Fact 2015;14:10.

36. Kunze M, Huber R, Gutjahr C, Müllner S, Büchs J. Predictive tool for recombinant protein production in Escherichia coli Shake-Flask cultures using an on-line monitoring system. Biotechnol Progress 2012;28:103–13.

37. Kunze M, Roth S, Gartz E, Büchs J. Pitfalls in optical on-line monitoring for high-throughput screening of microbial systems. Microb Cell Fact 2014;13:53.

38. Huang X, Shao Z, Hong Y, Lin L, Li C, Huang F, et al. Cel8H, a novel endoglucanase from the halophilic bacterium Halomonas sp. S66-4: molecular cloning, heterogonous expression, and biochemical characterization. J Microbiol 2010;48:318–24.

39. Lan Tee K, Schwaneberg U. Directed evolution of oxygenases: screening systems, success stories and challenges. Combinatorial chemistry & high throughput screening 2007;10:197–217.

40. Wang W, Malcolm BA. Two-stage PCR protocol allowing introduction of multiple mutations, deletions and insertions using QuikChange Site-Directed Mutagenesis. Biotechniques 1999;26:680–2.

41. Siepert E, Gartz E, Tur MK, Delbrück H, Barth S, Büchs J. Short-chain fluorescent tryptophan tags for on-line detection of functional recombinant proteins. BMC Biotechnol 2012;12:65.

42. Santos-Aberturas J, Dörr M, Waldo GS, Bornscheuer UT. In-depth high-throughput screening of protein engineering libraries by split-GFP direct crude cell extract data normalization. Chemistry & Biology 2015;22:1406–14.

4. Chapter III - Pitfalls in optical on-line monitoring for high-throughput screening of microbial systems

4.1. Background

In the field of biotechnology the demand for process development tools is continuously growing. Thereby, the understanding of biotechnological processes is of paramount importance for their development and operation. To face this challenge, the establishment of high-throughput screening techniques became a trend in biotechnology [1, 2]. In this context reactor miniaturization was essential to gain the required degree of experimental throughput. Consequently, miniature stirred bioreactors were developed. Different concepts were presented by various groups over the last years [3-9].

In parallel, microtiter plates (MTP) as shaken reaction systems for microbial and enzymatic reactions became more popular in the last years [10]. To perform these reactions under defined conditions different types of MTP were characterized regarding their mass transfer and hydrodynamic properties [11]. In this way factors such as oxygen transfer [12-15] and mixing [16, 17] were determined. To improve these parameters even new MTPs were developed. The so called Flower Plate was designed to solve the typical problem of oxygen limitation in MTPs by introducing a baffle like structure to each well of the MTP [18]. In this way limitations, especially in mass transfer, could be overcome.

Fluorescent proteins (FPs) are used as versatile in vivo reporters to study gene regulation and protein synthesis, folding, localization, and activity in bacteria and yeast [19-23]. The most widely used FP is the green fluorescent protein (GFP) and its derivatives. By targeted modification of GFP, fluorescence markers have been developed that span the visible spectrum from deep blue to deep red. But one disadvantage of these proteins is their dependence on oxygen for maturing in order to display fluorescence. To face this problem, an

alternative family of fluorescent proteins has been developed, that binds flavin mononucleotide (FMN) as a chromophore [24, 25]. Nowadays, further oxygen independent FPs are available [26].

The combination of MTPs and optical measuring techniques enables the high-throughput monitoring of process relevant parameters during cultivations. The so called BioLector technology allows a continuous and non-invasive on-line monitoring of microbial growth and fluorescence signals without interruption of the shaking process and, hence, the gas-liquid mass transfer [27]. Furthermore, dissolved oxygen tension (DOT) and pH value can be determined via special fluorescent dyes immobilized in sensor spots on the MTP bottom [14, 28, 29]. For both parameters the dual lifetime referencing (DLR) method ensures very high accuracy [30-32]. Taking all together, MTPs as miniature bioreactors can compete with conventional stirred tank reactors regarding their data output. It was also shown that scale-up between the mentioned systems is well possible [33]. Additional to the higher throughput, the easy handling of MTPs makes them perfect for lab automation [3]. The integration of a high-throughput on-line monitoring system, such as the BioLector, to an automated liquid handling robot creates a screening system combining high-throughput experimentation with high information content [34].

In this work we report about typical experiments performed in numerous biotechnological labs, namely the expression of recombinant fluorescent proteins in different host organisms. Important process parameters such as microbial growth, protein formation, DOT and pH value were monitored on-line via optical measurement techniques. During these experiments unexpected pitfalls were identified which might lead to incorrect data about the process. Cultivation results from the bacterium *Escherichia coli* and the yeast *Kluyveromyces lactis*, expressing different FPs, are presented in order to show how fluorescent proteins can influence the optical measuring signals for DOT and pH as well as the scattered light signal

for biomass on-line monitoring. Therefore, different proteins fluorescing at different colors in the visible light spectrum (blue, green, yellow, red) were investigated. Subsequently, methods were found to deal with these interferences. Mathematical correction procedures as well as the modification of the optical measurement technique were performed in order to minimize or avoid the interactions. Furthermore, it was shown that the scattered light signal as on-line biomass indicator is sensitive to morphological changes of the cells. In this work we give an overview of potential sources of errors which may occur in biotechnological experiments if optical methods for the on-line monitoring of bioprocesses are applied. Solution strategies are presented where possible.

4.2. Material & Methods

4.2.1. Microorganisms

The applied microorganisms with their respective vectors for recombinant protein expression as well as their selection markers can be taken from Tab. 4.1.

Tab. 4.1 - Applied microorganisms for the recombinant expression of fluorescent proteins

Target protein	Organism	Strain	Vector	Selection marker	Supplier
-	*E. coli*	BL21 (De3)		-	1
YFP	*E. coli*	BL21 (De3)	pRotHi	Kanamycin	2
FbFP	*E. coli*	BL21 (De3)	pRotHi	Kanamycin	2
mCherry	*E. coli*	BL21 (De3)	pRSet	Ampicillin	1
GFP	*K. lactis*	GG799	pKlac1	-	1

Supplier:
1. *Institute of Molecular Biotechnology (Bio VII), RWTH Aachen University, Germany*
2. *Institute of Molecular Enzyme Technology (IMET), Heinrich-Heine-University Düsseldorf, Germany*

4.2.2. Media & Cultivation

For *E. coli* pre-cultures terrific broth (TB) medium consisting of 12 g L^{-1} tryptone, 24 g L^{-1} yeast extract, 12.54 g L^{-1} K_2HPO_4, 2.31 g L^{-1} KH_2PO_4, and 5 g L^{-1} glycerol (all ingredients from Roth, Germany) dissolved in water was used. The pH value was 7.2±0.2 without adjustment. For the main cultivation of *E. coli* a modified Wilms and Reuss medium (henceforth referred as Wilms-MOPS medium) was used [35, 36]. It consists of 5 g L^{-1} $(NH_4)_2SO_4$, 0.5 g L^{-1} NH_4Cl, 3.0 g L^{-1} K_2HPO_4, 2 g L^{-1} Na_2SO_4, 0.5 g L^{-1} $MgSO_4 \cdot 7H_2O$, 0.01 g L^{-1} thiamine hydrochloride, 20.9 g L^{-1} 3-(N-morpholino)-propanesulfonic acid (MOPS, 0.2 M), 20 g L^{-1} glucose and 1 mL L^{-1} trace element solution. This trace element solution consists of 1.98 g L^{-1} $CaCl_2 \cdot 2H_2O$, 0.54 g L^{-1} $CoCl_2 \cdot 6H_2O$, 0.48 g L^{-1} $CuSO_4 \cdot 5H_2O$, 41.76 g L^{-1} $FeCl_3 \cdot 6H_2O$, 0.3 g L^{-1} $MnSO_4 \cdot H_2O$, 0.54 g L^{-1} $ZnSO_4 \cdot 7H_2O$, 33.39 g L^{-1}

Na_2EDTA (Titriplex III). The pH was adjusted with 5 M NaOH to a value of 7. In dependency on the clone's resistance, 50 µg mL^{-1} kanamycin or 100 µg mL^{-1} ampicillin were added to the medium from a 1000-fold concentrated stock solution. Recombinant protein expression was induced by adding 0.1 mM isopropyl-β-D-thiogalactopyranoside (IPTG) to the culture medium after 6 h of cultivation from a 100-fold concentrated stock solution.

For *K. lactis* pre-cultures yeast extract peptone (YP) medium was used, consisting of 10 g L^{-1} yeast extract, 20 g L^{-1} tryptone and 15 g L^{-1} glucose [37]. The main culture was performed in synthetic yeast nitrogen base (YNB) medium. A commercial formulation was used in 2-fold concentration (Fluka/Sigma-Aldrich, Munich, Germany). The list of ingredients can be taken from the company's user guidelines or from literature [37]. For buffering 0.15 M potassium hydrogen phthalate ($C_8H_5KO_4$) was added. Additional 20 g L^{-1} galactose served as carbon source and inducer for recombinant protein expression.

For *E. coli* pre-cultivation, 10 mL of TB medium in a 250 ml shake flask were inoculated with 50 µL from a cryoculture, and cultures were grown for 8 h at 350 rpm (shaking diameter 50 mm) and 37°C . *K. lactis* pre-culture conditions were the same aside from being grown in YP medium for 12 h at 30°C.

Main cultures were performed applying the BioLector system which allows high-throughput screening of fermentation processes in micro-scale [27, 33]. With this technology relevant process parameters such as microbial growth, formation of fluorescent proteins, DOT and pH value are on-line monitored in shaken microtiter plates without interruption of the shaking process. The used BioLector device was obtained from m2p-labs (Beasweiler, Germany). For cultivation so called Flower Plates (MTP-48-BOH, Lot. 1202, m2p Labs, Germany) were used equipped with optodes for on-line monitoring of DOT and pH value. Wavelengths and gain factors for all optical signals can be seen in Tab. 4.2. For scattered light and fluorescence measurement the initial light intensity (I_0), which is mainly attributed to such factors as the

media background or the type of the microtiter plate, was subtracted from the original measured data ($I-I_0$). All cultivations were performed in triplicate. Parallel cultures were in excellent agreement. The presented results originate from a representative single culture.

Tab. 4.2 - Optical signals and applied setup for BioLector on-line monitoring

Optical signal	**λ_{ex} [nm]**	**λ_{em} [nm]**	**Gain**
Biomass (scattered light)	620	-	20
DOT	505	590	60
pH	485	530	45
YFP fluorescence	510	532	60
FbFP fluorescence	450	492	60
mCherry fluorescence	580	610	60
GFP fluorescence	488	520	100

For the main cultivation of *E. coli*, Wilms-MOPS medium was inoculated from the pre-culture, resulting in an initial OD_{600} of 0.1. The already inoculated medium was then transferred to the wells of the MTP. The cultivation was performed at 37°C, a shaking frequency of 1100 rpm, a shaking diameter of 3mm and a filling volume of 800 µL per well. The plates were sealed with gas-permeable seals (AB-0718, Thermo Scientific, Dreieich, Germany). The conditions for the *K. lactis* main culture were the same aside from being grown in YNB medium at 30°C.

4.2.3. Protein expression and purification

For the production of fluorescent proteins *E. coli* was cultivated in 250 mL shake flasks with 10 mL Wilms-MOPS medium inoculated from pre-cultures at an initial OD_{600} of 0.1. Cultivation took place at 37°C, a shaking frequency of 350 rpm, and a shaking diameter of 50 mm. Protein expression was induced by adding 0.1 mM isopropyl-β-D-thiogalactopyranoside (IPTG) to the culture medium after 6 h of cultivation. After 24 h of cultivation, OD_{600} was determined and the cells were harvested by centrifugation in 50 mL Falcon tubes at 4000 rpm. Subsequently, the intracellular fluorescent protein was extracted by using the BugBuster® Protein Extraction Reagent (Novagen®/Merck, Darmstadt, Germany) in accordance with the manufacturer's guidelines. The resulting supernatant, containing the target protein, was then concentrated in ultrafiltration tubes with an exclusion size of 10 KDa (VIVSPIN 20, Sartorius Stedim BioTech, Göttingen, Germany) at 4000 rpm to approx. one tenth of the original volume and afterwards diluted with the same volume of storage solution containing 10 mM NaCl and 10 mM NaH_2PO_4. The purified proteins were stored at 4°C.

4.2.4. Spectral analysis

Absorption spectra of YFP, FbFP and mCherry were determined on a FP-6300 fluorescence spectrometer (Jasco, Groß-Umstadt, Germany) with 2 mL purified protein solution in a 3.5 mL quartz glass cuvette (Type 101-QS, Precision Cell Quartz SUPRASIL®, Hellma, Müllheim, Germany). The absorption spectra were recorded by scanning from 350 nm to 650 nm.

2D fluorescence spectra were determined on a FluoroMax-4 spectrofluorometer (HORIBA Jobin Yvon, München, Germany) with 2 mL *E. coli* cell suspension in a 3.5 mL quartz glass cuvette (Type 101-QS, Precision Cell Quartz SUPRASIL®, Hellma, Müllheim, Germany).

Cell suspensions originated from cultivations for protein expression described earlier. The spectra were recorded by scanning excitation and emission wavelengths from 300 to 750 nm.

4.2.5. Fluorescent proteins in-vitro experiments

For in-vitro experiments purified fluorescent proteins were used. For the detailed investigation of the influence on the DOT signal the particular protein solution (preparation described before) was used to create solutions of different fluorescence intensity. Therefore, the stock solution was diluted with the storage solution containing 10 mM NaCl and 10 mM NaH_2PO_4. 800 µL of samples prepared in this way were added to each well of the MTP which was shaken at a frequency of 1100 rpm and a shaking diameter of 3 mm at 37 °C. To ensure DOT values of 0 and 100 % air saturation, the climate chamber of the BioLector was aerated with nitrogen or pressurized air, respectively. In this way Φ_0 and Φ_{100} were measured, and the parameter K_{SV} was determined applying Eq. 4.1. Finally, the calibration curve could be calculated due to the Stern-Volmer relationship (Eq. 4.1). The calibration curve between the phase angle and the resulting DOT without interfering fluorescence can be seen in Fig. 4.3-B and C (YFP and mCherry fluorescence intensity of 0 a.u.).

$$\frac{\tau_0}{\tau} = \frac{tan\,\Phi_0}{tan\,\Phi} = 1 + K_{SV} \cdot [DOT] \qquad \text{(Eq. 4.1)}$$

For the corresponding pH experiments the purified protein's stock solutions were diluted in non-dyed CertiPUR® ready-to-use buffers with pH values of 4-9 (Merck, Darmstadt, Germany) to get solutions with varied fluorescence intensity and pH value. After adding the protein solution to the buffer, the pH was measured again. In all cases the measured pH did not deviate more than ±0.2 from the particular buffer pH. In this way the sigmoidal calibration curve in the pH range from 4-9 could be determined which can be seen as black line in

Fig. 4.4-D (mCherry fluorescence intensity of 0 a.u.). For mathematical description the Boltzmann equation (Eq. 4.2a) was modified for the calculation of the pH value from the measured phase angle Φ (Eq. 4.2b).

$$\Phi = \frac{\Phi_{min} - \Phi_{max}}{1 + e^{(pH - pH_0)/dpH}} + \Phi_{max} \qquad \text{(Eq. 4.2a)}$$

$$pH = \ln\left(\frac{\Phi_{min} - \Phi_{max}}{\Phi + \Phi_{max}} + 1\right) \cdot dpH + pH_0 \qquad \text{(Eq. 4.2b)}$$

For DOT reference measurements alternative sensor spots obtained from Presens Precision Sensing (Regensburg, Germany) were used. Sensor spots with (SP-PSt3-NAU-D3-YOP) and without optical isolation (SP-PSt3-NAU-D3-NOP) were fixed with silicone glue to the well bottoms of a Flower Plate without DOT and pH optodes. According measurements were performed in the BioLector device with the same settings applied for conventional DOT optodes from m2p-labs (Tab. 4.2).

For the characterization of the effect of the fluorescent protein mCherry on the scattered light signal for on-line biomass monitoring *E. coli* BL21 (De3) cells without an additional plasmid were used. Cultures were grown at the conditions of *E. coli* pre-cultivation described before, but without the addition of antibiotics, and, finally, the respective OD_{600} was determined. Subsequently, cell suspension, purified mCherry stock solution, and storage solution containing 10 mM NaCl and 10 mM NaH_2PO_4 were mixed in such relations that samples resulted with varied mCherry fluorescene intensity but a constant OD_{600} of 4.9. 800 µL of the samples prepared in this way were added to each well of the MTP which was shaken at a frequency of 1100 rpm and a shaking diameter of 3 mm in the BioLector at 37°C.

4.2.6. Scattered light wavelength scan

For the scattered light wavelength scan *E. coli* BL21 (De3) without an additional vector was used. A cell suspension grown at the conditions of *E. coli* pre-cultivation without the addition of antibiotics was diluted with 0.9 % [m/v] NaCl solution to prepare samples with varied OD_{600} of 0.06-17.4. For the scattered light scan 200 µL of these samples were added to each well of a 96well MTP (lumox^{TM} multiwell plate, Greiner Bio-One GmbH, Frickenhausen, Germany) which was shaken at a frequency of 995 rpm and a shaking diameter of 3 mm at 37°C. The measurements were performed on an in-house constructed BioLector device operated with the FluoroMax-4 spectrofluorometer (HORIBA Jobin Yvon, München, Germany) equipped with an Y-shaped optical fiber (UV-VIS, LEONI Fiber Optics GmbH, Neuhaus-Schierschnitz, Germany). Wavelengths of 200-800 nm were tested.

4.2.7. Offline analytics

For offline biomass quantification the dry cell weight (DCW) and optical density at 600 nm (OD_{600}) were measured. For DCW determination 500 µL of cell suspension were centrifuged at 14000 rpm for 10 min in pre-dried tubes of known weight. Subsequently, the supernatant was removed and the pellet was washed by re-suspending it in 1 mL water and centrifuged as described before. The supernatant was removed again and the tubes with the pellets were dried for 72 h at 80°C before they were weighed. OD_{600} was determined via a Genesys 20 photometer (Thermo Scientific, Dreieich, Germany) in 1.5 mL micro cuvettes (PS, Plastibrand, Roth, Karlsruhe, Germany). For values higher than 0.5 the samples were appropriately diluted with 0.9 % [m/v] NaCl solution.

Galactose concentration in medium was measured by HPLC analysis. After centrifugation of the samples, the supernatant was filtrated through a membrane with 0.2 µm pore size to remove particles. For the measurement the device UltiMate3000 (Dionex, Germany) was used

with an Organic Acid-Resin column (250x8 mm, CS-Chromatographie Service, Langerwehe, Germany). The eluent was 5 mM H_3PO_4 at a flow rate of 0.6 mL min^{-1} and 60°C. Peaks were detected by recording the refractive index (Skodex RI-71, Showa Denko Europe, Germany). For data analysis the software Chromeleon (Dionex, Germany) was applied.

For flow cytometric measurements the Guava EasyCyte Mini Base System (Merck-Millipore, Darmstadt, Germany) was used with a gain factor of 8 and a treshold of 2. For optimal measurement the volumetric cell count should range from 50-500 cells L^{-1}. Samples with higher values were appropriately diluted with 0.9 % [m/v] NaCl solution.

4.3. Results & Discussion

4.3.1. Effect of FPs on DOT and pH optode signals

To show the influence of fluorescent proteins on the optical on-line monitoring of DOT and pH via optodes, three *E. coli* clones expressing different fluorescent proteins were cultivated under non-induced and induced conditions, applying the BioLector technology. For this investigation three proteins with clearly different spectral properties regarding their excitation and emission wavelength were chosen, namely YFP, FbFP and mCherry, emitting light in the yellow, blue and red light spectrum range, respectively. As a reference pure medium without inoculation was tested, too. The results from these experiments can be seen in Fig. 4.1.

Under non-induced conditions the growth behavior of the three clones is almost the same (Fig. 4.1-A). After a *lag* phase of 3 h, cells start growing exponentially. The mCherry expressing clone shows the fastest growth reaching a first maximum after 10.5 h. The clones expressing FbFP and YFP reach this maximum only after 12.5 and 13 h, respectively, thereby showing a slight decrease of the growth rate after 10.5 h. After a short interruption of the exponential growth, all clones have a second increase of the scattered light signal before entering the stationary phase. From earlier experiments it is known that this second growth phase is due to the consumption of the by-product acetate which is a result of oxygen limited conditions and overflow metabolism [35, 38, 39]. Pure medium shows a constant scattered light signal close to 0 a.u. over the whole cultivation time.

In Fig. 4.1-C the production of the fluorescent proteins under non-induced conditions is depicted. As expected, almost no fluorescence was measured for all three clones. Only a small increase could be detected after 9-12 h. These results indicate that leaky expression of the target protein is rather low for these clones in the applied Wilms-MOPS medium.

The DOT curves in Fig. 4.1-E go hand in hand with the scattered light signal in Fig. 4.1-A. After the *lag* time, where the DOT signal remains at a value of about 90 % air saturation, a strong decrease of the DOT occurs as a result of exponential microbial growth. After 9-10 h, the cultivations of all three clones run into an oxygen limitation, indicated by a DOT value of 0 % air saturation, which lasts for about 2 h. Besides the formation of acetate, which was mentioned before, this limitation might also be the explanation for the slightly decreased growth rate in the late exponential growth of *E. coli* YFP and FbFP. The strong DOT increase after the oxygen limitation phase indicates the depletion of the major carbon source glucose in the medium. Consequently, no further respiration is possible so that oxygen is recovered in the medium. However, before the cells entered the stationary phase a second drop of the DOT signal is obtained for all three clones. This decrease, accompanied by an increase of the scattered light signal, is caused by the respiration of acetate accumulated during the cultivation [40]. The complete consumption of this by-product after 12.5, 14.5 and 15 h by *E. coli* mCherry, FbFP and YFP, respectively, leads to the final recovery of the DOT to values of 95-105 % air saturation. It should be noticed that the DOT level for pure medium over the whole time and also for the cultivations in the beginning and in the stationary phase was not at 100 % air saturation as expected. A reason for this might be imprecise calibration parameters given by the manufacturer. Interestingly, *E. coli* YFP and mCherry both ended up at consequently higher DOT values than *E. coli* FbFP and pure medium, which will be explained later.

The curves of the pH values in Fig. 4.1-G show the typical behavior of *E. coli* cultivations. Starting at values of 6.9-7.1 the pH steadily decreases after the *lag* phase due to the consumption of ammonia from the medium and the accumulation of acetate. The curves reach their minimum after 10-11 h. This correlates very well with the time when the DOT increased again as a result of glucose depletion. Hence, exponential growth was terminated and, thereby, ammonium consumption and acetate formation stopped. With the subsequent

respiration of acetate the pH value increased again. The final values are slightly higher than the initial ones. This is not in agreement with values of 6.6-6.8 obtained from offline samples at the end of the experiment.

Compared to the non-induced conditions, the growth behavior of the three investigated clones differs clearly under induced conditions (Fig. 4.1-B). Until a cultivation time of 6 h, the conditions were identical to the experiments without induction. Consequently, no great differences can be obtained in the early phase of the cultivation. After 6 h, 0.1 mM IPTG were added to the medium. From this point, the cultures start varying in their particular growth. Compared to non-induced conditions (Fig. 4.1-A), all clones have a distinct lower growth rate after adding IPTG. This is not surprising due to the fact that the overexpression of a recombinant protein can cause an additional metabolic burden to the host organism [38, 41, 42]. From the curves it is obvious that the perturbed growth occur with some delay and with different strength. While *E. coli* mCherry is poorly affected after 9 h of cultivation, the scattered light signal for the FbFP expressing clone has a much lower slope after this point. The induction effect on *E. coli* YFP is the strongest since it shows the lowest growth rate after already 7 h. It must be considered that these variances between the three clones might also be a result of different cell densities at the time of induction where *E. coli* YFP had the lowest, and mCherry had the highest biomass level. It was reported before that this parameter has a strong influence on the growth and expression behavior of *E. coli* [34]. All clones should have been induced at the same scattered light intensity, but since this was not the focus of this work the more convenient way of a fixed induction time was chosen. What all clones have in common is that the biomass formation recovered over time, so that after 14 h even *E. coli* YFP shows growth rates comparable to these under non-induced conditions. This effect was known before. *E. coli* cells can adapt to the inhibition of recombinant protein expression and recover [38, 43]. In the stationary phase a lower final scattered light intensity was obtained for

all clones indicating that resources from the medium, which usually would have been used for growth, were redirected to the target protein production.

In Fig. 4.1-D it can be clearly seen that significant amounts of the particular fluorescent target proteins were produced by all three clones. Nevertheless, the three curves differ tremendously from each other. The production in *E. coli* YFP starts at 7 h with 1 h delay to the induction and the fluorescence intensity increases steadily for 6 h. Subsequently, a short plateau is formed before the signal increases strongly again after 15 h and reaches its maximum after 17 h. Such a stagnation of the signal followed by a sharp increase is a typical sign for a temporary oxygen limitation. Since YFP is a GFP derivative, it needs oxygen for maturing and generating fluorescence light [24, 25]. In the absence of oxygen the protein might be produced but no fluorescence will be detected. When oxygen becomes available, the accumulated non-matured protein matures at once and a high level of fluorescence light is emitted. For *E. coli* YFP this effect occurs when the culture becomes stationary and no oxygen is needed for growth anymore. *E. coli* mCherry shows a first slight increase of the fluorescence intensity after 10 h of cultivation which means 4 h delay to the induction. Subsequently, the signal shoots to the maximum within 2 h. Also this case can be explained by an intermittent oxygen limitation. Compared to the YFP clone *E. coli* mCherry grew relatively fast in the beginning. Consequently, more oxygen is needed for cell growth and maintenance leading to an earlier depletion of the oxygen supply in the medium. In this way no protein could mature before 10 h. Due to the early appearance of oxygen limiting conditions, the precise starting point of the recombinant protein expression cannot be identified. After 9-10 h, the cell's growth rate slightly decreased so that a certain protein amount was able to fluoresce. Two hours later, when the culture became stationary, all the remaining protein matured within short time. Contrary to YFP and mCherry, FbFP's maturing process is oxygen independent [24, 25]. After 8.5 h, *E. coli* FbFP starts producing the recombinant protein. Compared to the YFP clone, the delay after the induction is with 2.5 h

longer, but from this point a steady increase of the fluorescence intensity can be observed without any conspicuous behavior. The maximum product concentration is reached simultaneously with the stationary phase. It can be concluded that oxygen independent fluorescent proteins simplify the generation of reliable datasets for product formation kinetics. It should be mentioned that undesired oxygen limitation is not only disadvantageous for maturing of GFP and its derivatives but for bioprocess development in general. Besides misleading fluorescence signals, it can cause inhibited growth and unwanted by product formation which decreases the feasibility of a bioprocess. Consequently, oxygen non-limiting conditions should be ensured even in micro-scale experiments. This can be achieved e.g. by increasing the shaking frequency or decreasing the filling volume per well. Performing cultivations in *fed-batch* mode avoids oxygen limitations, too. Controlled release systems [44], enzyme based *fed-batch* media [45], or microfluidic systems for MTPs [40] are convenient solutions. Nonetheless, this study does not aim for kinetic results so that an adjustment of the conditions was not necessary.

In Fig. 4.1-F the corresponding DOT courses are depicted. It can be noticed that to a certain extend they fit qualitatively well to the data of biomass formation and fluorescent protein production. In the beginning, the DOT decreases due to the starting exponential growth. *E. coli* YFP and FbFP show an increase of the DOT after 7 and 9 h, respectively, right at the time when their growth is inhibited by the induction. Simultaneously with the recovery of the microbial growth, the DOT curves start decreasing again before they finally reach the maximum in the stationary phase. *E. coli* mCherry shows a different behavior with a decreasing DOT until a value of 0 % air saturation followed by a 2 h lasting oxygen limited phase and a subsequent increase to its maximum. The reason for this course is the much smaller influence of the induction to this clone's growth and, consequently, a higher oxygen demand over the whole cultivation time. Besides the growth kinetics, this DOT course also approves the assumption that a temporary oxygen limitation is responsible for the late

detection of mCherry discussed earlier and the subsequent strong increase of the fluorescence intensity. Surprisingly, no oxygen limitation can be directly observed in the YFP clone's DOT curve in the time range from 13-15 h which could have caused the plateau and subsequent increase in the YFP fluorescence signal. Completely unexpected are the absolute values delivered by the optical DOT measurement for *E. coli* YFP and mCherry. For the YFP expressing clone DOT values up to 135 % air saturation in the growth inhibited phase at 10 h are observed, and almost 400 % at the end. For mCherry it is even worse since final values of about 1200 % air saturation are reached. For both cultures significant amounts of the fluorescent target protein were detected in parallel to the unrealistic high DOT signals. This fact leads to the assumption that the DOT optodes are strongly influenced by these two proteins. For FbFP no such effect could be observed. Only at the end of the cultivation, the values are slightly higher than those for pure medium.

The pH curves in Fig. 4.1-H reveal further surprise. The typical behavior observed under non-induced conditions was not found anymore. The only similarity is a pH decrease in the beginning. After that, *E. coli* mCherry has a slight increase from 10 h on which becomes steeper after 12 h. The culture ends up at a pH of 7.8. The FbFP expressing clone shows the pH increase already after 8.5 h with a high slope and at 11.5 h the signal was out of the measuring range. The YFP clone's pH value started increasing after 7 h with a short interruption from 13-15 h shortly before leaving the measuring range of pH 9. The final pH values measured offline at the end of the cultivation ranged from 6.7-6.8. So, it becomes obvious again that the unexpected pH courses appear from that time on when the recombinant proteins display their fluorescence. This effect is strongest for FbFP and YFP, but also existent with mCherry.

After the analysis of these experiments, the following points can be concluded:

i) The optical DOT signal is strongly influenced by mCherry fluorescence. Compared to that, the influence of YFP is rather moderate, whereas FbFP has almost no effect.

ii) The optical pH signal is moderately influenced by mCherry, whereas YFP and FbFP seem to have a very strong influence.

The highly parallel experimentation with the BioLector allowed the investigation of several influences and conditions in only one experiment, thereby, saving time and manual effort. From literature, but also from the manufacturer's information, it is known that the on-line monitoring of DOT and pH via optodes can be prone to certain fluorophores. It is astonishing that the influence of the expressed fluorescent proteins is partly so strong, as the measuring principle is not based on intensity but determined by DLR.

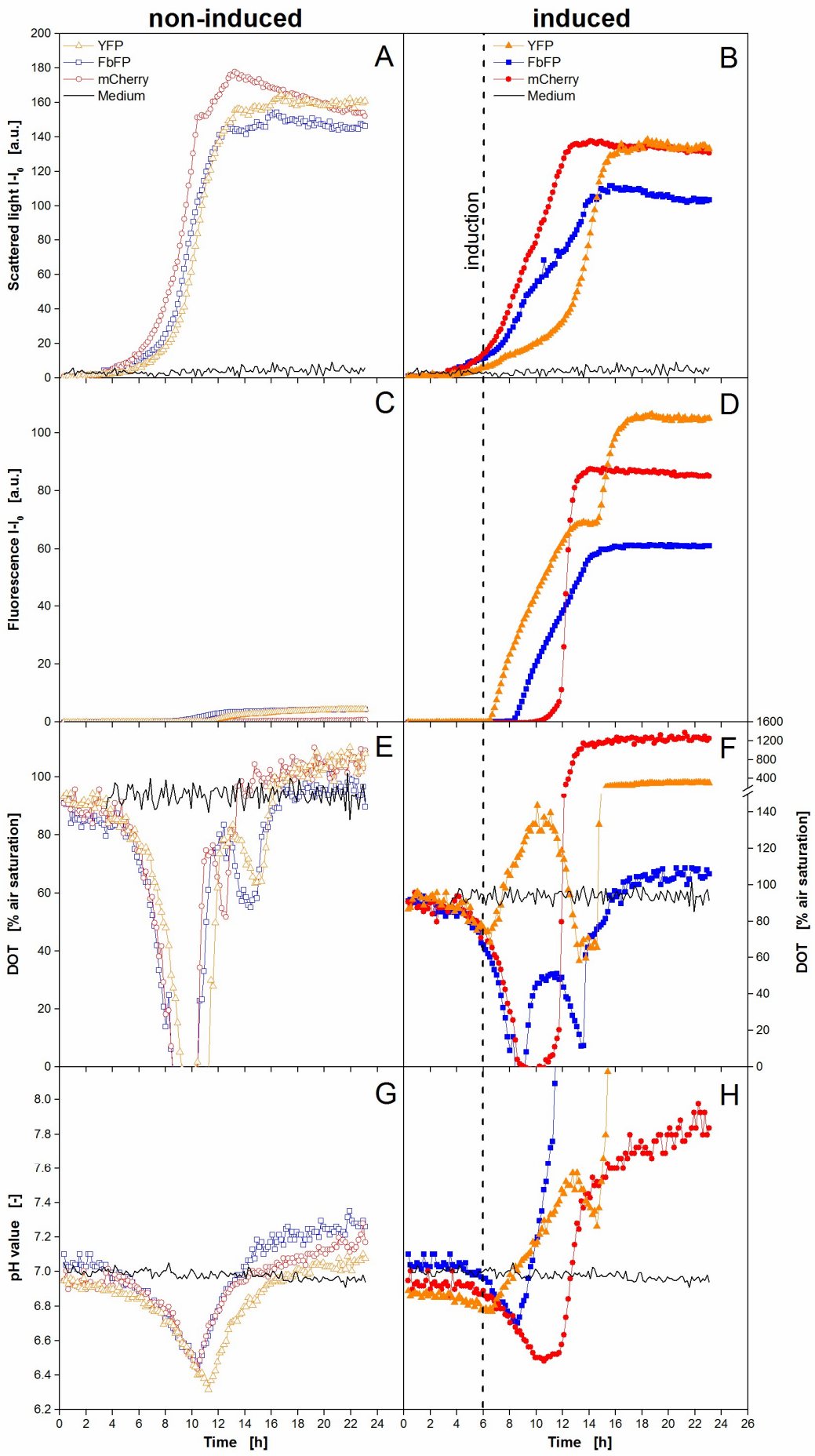
non-induced
induced
YFP
FbFP
mCherry
Medium
A
B
C
D
E
F
G
H
induction
Scattered light I-I0 [a.u.]
Fluorescence I-I0 [a.u.]
DOT [% air saturation]
pH value [-]
Time [h]

Fig. 4.1 - Cultivation of 3 *E. coli* BL21 clones expressing different fluorescent proteins under non-induced (left column, open symbols) and induced conditions (right column, closed symbols) using the BioLector system. Online monitoring of microbial growth (via scattered light), DOT and pH value (via optodes) and fluorescence intensity of the recombinant expressed fluorescent proteins. Note: Altered DOT scale in Fig. 4.1-F at higher values. Cultivation conditions: 48well FlowerPlate with optodes for DOT and pH measurement, V_L=800 µL, n=1100 rpm, d_0=3 mm, 37°C, Wilms-MOPS medium with 20 g/L glucose, induction with 0.1 mM IPTG after 6 h (indicated by dotted line).

With a look at the spectra in Fig. 4.2 it becomes clearer why the here tested fluorescent proteins have such an impact on the DOT and pH measuring signals. In the absorbance spectra of the fluorescent proteins it can be seen that all three proteins are able to absorb light energy at the excitation wavelengths for the DOT and pH optode at 505 and 485 nm, respectively (Fig. 4.2-A, dotted arrows, $\lambda_{ex,DOT}$, $\lambda_{ex,pH}$). This is the prerequisite for fluorescence emission. For influencing the DOT and pH measuring signal there must be emitted fluorescence light in the emission range of the optodes, too. To answer this question, 2D fluorescence spectra of cell suspensions after the expression the particular fluorescent proteins were performed for excitation and emission wavelengths of 300-750 nm (Fig. 4.2-B/C/D). For better visualization the measuring points for DOT and pH are indicated by dotted lines. For YFP (Fig. 4.2-B) it can be seen that these points both lie in the fluorescence range of the protein which explains the effect on both signals. The results of the spectrum for FbFP (Fig. 4.2-C) also prove the phenomena seen before. Since the measuring point for pH is clearly in the fluorescence range there is an according effect on the on-line signal. On the other hand, the DOT measuring point lies further outside, without any consequences for the measurement. The 2D spectrum of the mCherry expressing culture shows two areas of increased fluorescence (Fig. 4.2-D). The DOT measuring point collides with the upper right peak, whereas the pH measuring point lies in the lower left area. Consequently, both signals are prone to interferences with mCherry fluorescence. Surprisingly, the DOT signal is much stronger affected than the pH signal, even though both measuring points are situated in an area of similar mCherry fluorescence intensity. The reason for that is not yet clear.

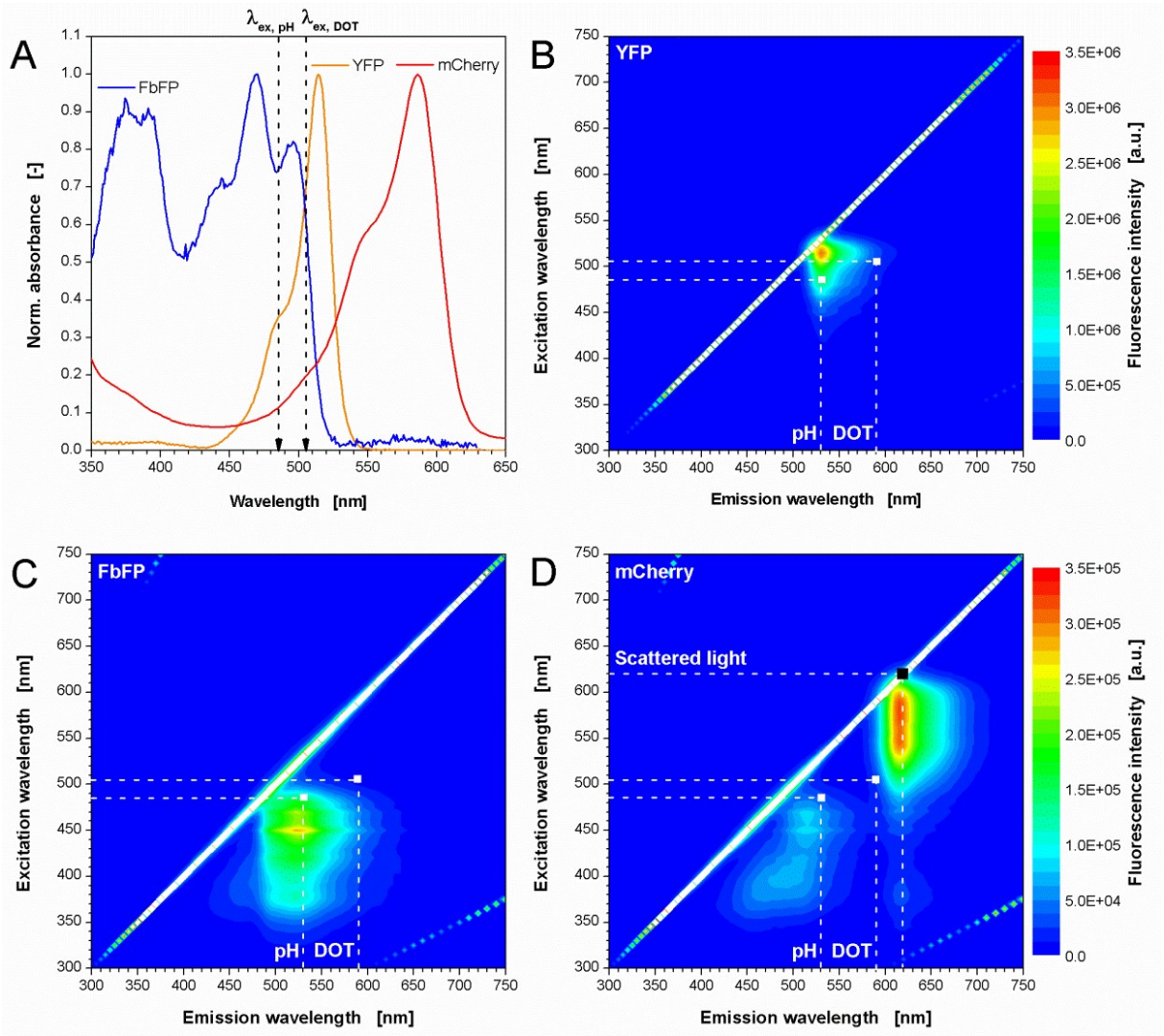

Fig. 4.2 - Absorbance spectra of purified fluorescent proteins (A) and 2D fluorescence spectra of *E. coli* cell suspensions after the expression of the fluorescent proteins YFP (B), FbFP (C) and mCherry (D). Measuring points for optical monitoring of microbial growth (via scattered light), DOT and pH indicated by dotted lines (B-D). Cultivation conditions: 250 mL shaking flask, V_L=10 mL, n=350 rpm, d_0=50 mm, 37°C, 24 h, Wilms-MOPS medium with 20 g/L glucose, induction with 0.1 mM IPTG after 6 h. $\lambda_{ex,pH}$ and $\lambda_{ex,DOT}$ indicate for excitation wavelengths for optical pH and DOT monitoring. Note: Altered color code for Fig. 4.2-B (upper scale) and Fig. 4.2-C and D (lower scale).

4.3.2. Correction of FP's influences on DOT optode

To characterize the interaction between fluorescent proteins and the optical measurement of DOT more in detail, *in-vitro* experiments with purified YFP, FbFP, and mCherry were performed. Therefore, the DOT of solutions with varied fluorescence intensities were determined when aerated with nitrogen or pressurized air. Since no oxygen consumption or formation was apparent in these in-vitro experiments, it can be assumed that the actual DOTs were 0 and 100 % air saturation, respectively. In Fig. 4.3-A it is shown how the phase angle as raw signal for the DOT changes with increasing fluorescence of the three proteins at 0 and 100 % air saturation. As expected from the results before, FbFP has no influence on the DOT signal since it shows a constant phase angle for fluorescence intensities up to 60 a.u. at both DOT values. Contrary to that, the phase angle is clearly dependent on YFP and mCherry fluorescence. In both cases increasing fluorescence intensities lead to decreasing phase angles and, consequently, to misleadingly high DOT measuring values. Interestingly, the relationship between fluorescence intensity and phase angle seems to follow a linear trend. It is also evident that the YFP effect is moderate compared to mCherry. The slope of the decreasing trend lines is lower, and they are almost parallel in the investigated range which means that the influence is similar at DOTs of 0 and 100 %. MCherry, on the other hand, shows a steeper slope of both trend lines which are even converging at fluorescence intensities of 80-90 a.u. A reliable measurement at this point is not possible anymore since almost equal phase angles are measured for 0 and 100 % air saturation.

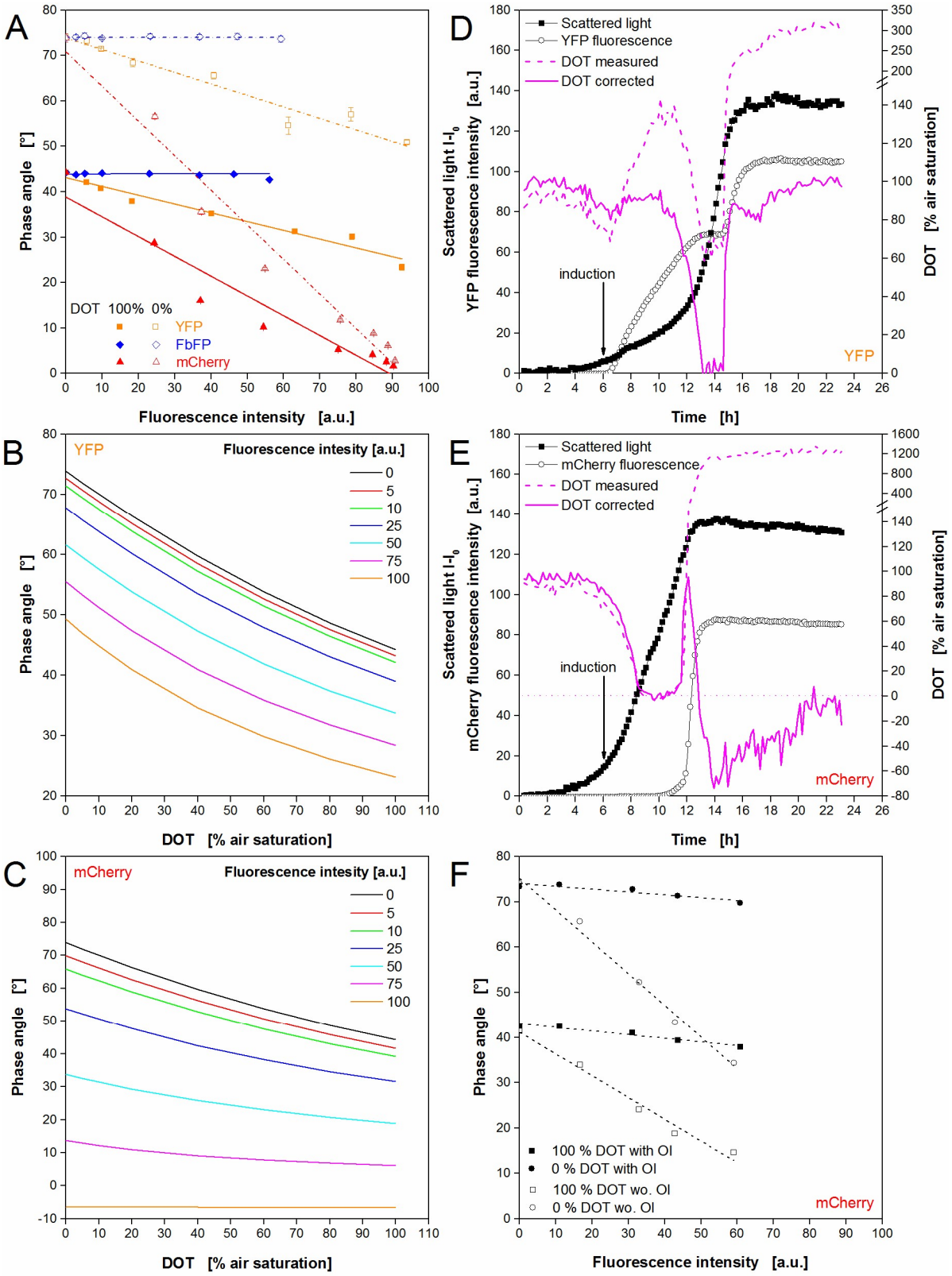

Fig. 4.3 - In-vitro characterization and correction of the influence of different fluorescent proteins on the optical DOT signal. (A) Dependency of the phase angle as raw signal for DOT monitoring from FbFP, YFP and mCherry fluorescence for DOTs of 100% (closed symbols) and 0% (open symbols) air saturation. (B) Change of DOT calibration curve with varied YFP fluorescence intensity. (C) Change of DOT calibration curve with varied mCherry fluorescence intensity. (D) Correction of the online DOT signal for the cultivation of *E. coli* expressing YFP by using

fluorescence dependent calibration curves. (E) Correction of the online DOT signal for the cultivation of *E. coli* expressing mCherry by using fluorescence dependent calibration curves. Note: Altered DOT scale in Fig. 4.3-D and Fig. 4.3-E at higher values. (F) Dependency of the phase angle from mCherry fluorescence for optodes with/without optical isolation (OI). Cultivation conditions: 48well FlowerPlate with optodes for DOT and pH measurement, V_L=800 µL, n=1100 rpm, d_0=3 mm, 37°C, Wilms-MOPS medium with 20 g/L glucose, induction with 0.1 mM IPTG after 6 h (indicated by arrow).

Since the relationship of fluorescence intensity and measured phase angle has a linear trend, it was attempted to use this information to correct the DOT signal. For this purpose, the linear functions (Eq. 4.3a, b) for the trend lines in Fig. 4.3-A were used to determine the parameters Φ_0 and Φ_{100} in dependence on the fluorescence signal.

$$\Phi_0 = m_0 \cdot FI + n_0 \qquad \text{(Eq. 4.3a)}$$

$$\Phi_{100} = m_{100} \cdot FI + n_{100} \qquad \text{(Eq. 4.3b)}$$

By applying these functions in Eq. 4.1, K_{SV} can also be described as fluorescence dependent parameter and fluorescence dependent calibration curves can be determined. In Fig. 4.3-B exemplary calculated calibration curves are depicted for YFP fluorescence intensities of 0-100 a.u. The curve for 0 a.u. is the actual calibration curve when no fluorescence originating from fluorescent protein occurs. Hence, it should correspond to calibration data given by the MTP manufacturer. Unfortunately, some deviations were obtained during the experiments (data not shown). This finding explains also the slightly too low initial DOT values in Fig. 4.1-E and Fig. 4.1-F. The supplier's calibration data delivered initial values of only 90-95 % air saturation, whereas a level of 100 % was expected. Hence, the new evaluated parameters were used for the further work instead of those provided by the supplier. With increasing protein fluorescence the curves shift more and more to lower values. But, they are parallel to each other, which is beneficial for a signal correction, ensuring a sufficient measuring range also at high fluorescence values. Unfortunately, these relations were not found for mCherry.

In Fig. 4.3-C it can be seen how the calibration curves change with increasing mCherry fluorescence. It must be noticed that the curves are not parallel and the measuring range becomes narrower so that at 100 a.u. no difference between a DOT of 0 % and 100 % air saturation can be recognized. Taking a maximum measuring error for the DOT measurement of ±5 % into consideration, a critical level is already reached at fluorescence intensities higher than 50 a.u.. Consequently, beyond this point no reliable determination of the DOT from the phase angle is possible anymore.

In Fig. 4.3-D the before described method of fluorescence dependent calibration curves was used to correct the DOT signal during the cultivation of *E. coli* YFP under induced conditions (comp. Fig. 4.1). The original signal is indicated by the dotted, the corrected curve by a solid pink line. Additionally, the curves for biomass growth (scattered light) and YFP fluorescence are depicted. It can be noticed that the corrected signal differs strongly from the measured one. Even in the beginning, when no fluorescence was present, the corrected curve is slightly higher. The reason for that is the application of self-determined calibration parameters instead of those given by the MTP supplier. In this way, initial DOT values of almost 100 % air saturation are reached as it is expected in the beginning. After 7 h, when the protein fluorescence signal starts increasing, the difference of both curves becomes clearer. The measured DOT signals strongly increased, whereas the corrected signal stayed more or less constant at a level of 90 %. This stagnation of the DOT makes sense since the microbial growth is inhibited by the induction at this time as discussed before. After the regeneration of the growth both DOT courses start decreasing again. But, where the original curve forms a plateau at 65 %, the corrected signal drops to very low values of almost 0 % air saturation, thereby, clearly indicating an oxygen limitation. This correlates very well with the constant fluorescence signal at this time since the lack of oxygen allows no further maturing of the produced YFP. Only after 15 h, when microbial growth came to an end due to the exhaustion of carbon source and oxygen became available again, indicated by a DOT jump, the increase

of YFP fluorescence continued. Shortly before the stationary phase from 15.5-17.5 h, the corrected curve shows a decreasing DOT which is not that present in the original data. As discussed before, this is a clear hint for acetate utilization which would have been missed without the signal correction. The biggest effect shows the signal correction at the end, where the realistic and expected value of 100 % air saturation is reached instead of more than 300 % given by the original measured signal.

In Fig. 4.3-E the same procedure was used to adjust the DOT signal during the cultivation of *E. coli* mCherry under induced conditions (comp. Fig. 4.1). Besides the fact that the corrected signal is again slightly higher than the original signal, which was already discussed for the YFP clone, both curves are almost identical up to 12 h. This is not surprising since mCherry fluorescence is hardly detectable in this time. However, the sudden increase of protein fluorescence after 12 h shows the problem for the signal correction. Within very short time the fluorescence signal rises above the critical level, so that no further mathematical correction makes sense. Consequently, even the data correction in Fig. 4.3-E doesn't provide reasonable values at the end of the fermentation.

To summarize these results, it can be stated that it is possible to minimize the influence of fluorophores on the optical DOT monitoring with mathematical methods. Therefore, a mathematical relationship between the disturbing fluorescence and the measuring signal must be identified. Nevertheless, this method has its limits. I our case, the moderate influence of YFP could be eliminated, but it was impossible for the strong influence of mCherry.

Additional to the mathematical solution, another method was tested to minimize the influence of fluorophores on the optode signal. Sensor spots are available which are equipped with a so called optical isolation. Therefore, a black oxygen permeable polymer layer is immobilized on the upper side of the optode directed to the culture broth in order to block disturbing light influences from above. Such optically isolated optodes were attached with silicone glue on the

bottom of each MTP well replacing the conventional optodes. In addition, a reference sensor spot without optical isolation was investigated. Since it was not possible to mathematically handle the influence of mCherry on the DOT, this protein was used for the following tests. The results are shown in Fig. 4.3-F. The phase angle is depicted in dependency on the fluorescence intensity (comp. Fig. 4.3-A). The effect of the optical isolation is astonishing. The sensors spots without optical isolation (open squares) were again prone to the mCherry fluorescence. The values are correlating very well with those of the conventional optodes from m2p Labs (comp. Fig. 4.3-A for mCherry). Contrary to that, the sensor spots with optical isolation are almost not affected by the fluorescent protein. Both, the curve for 0 % and 100 % air saturation, only show a slight decrease of the phase angle with increasing fluorescence intensity. The small remaining error can easily be corrected with the mathematical procedure described before. Consequently, an optical isolation of the optodes towards the culture broth is strongly recommended when interfering fluorophores occur during fermentation experiments. Unfortunately, the optical isolation is not yet available for the Flower Plate and the manual preparation of complete MTPs with isolated sensor spots is highly laborious.

4.3.3. Correction of FP's influences on pH optode

Due to the fact that not only the DOT signal was disturbed by fluorescent proteins, corresponding investigations were performed for the pH measurement. As described before, solutions with varied pH value and fluorescence intensity for the three proteins YFP, FbFP and mCherry were prepared, and subsequently measured with the BioLector. The determined phase angles from the DLR measurement via optodes as raw signal for the pH value can be seen in Fig. 4.4-A-C. For all three proteins a decreasing trend is observed with increasing fluorescence. The effect seems to differ dependent on the pH value. Low pH values,

represented by higher phase angles, are more prone to the fluorescence than high pH values. As a consequence, the trend lines are converging at certain fluorescence values. For YFP and FbFP these intensities are relatively low at approx. 50 and 30 a.u., respectively. As already observed for the DOT signal before, a reliable measurement of the pH value is not possible beyond these points. And since much higher intensities are reached during the cultivation, namely 105 a.u. for YFP and 60 a.u. for FbFP, a mathematical correction would make no sense for these two proteins. The trend lines for mCherry are converging at a higher fluorescence intensity of approx. 130 a.u., so that a mathematical correction could be successful. By using the linear trend lines in Fig. 4.4-C to describe the phase angle as a function of mCherry fluorescence, it is possible to create fluorescence dependent calibration curves. In Fig. 4.4-D calculated examples for fluorescence intensities of 0-90 a.u. are depicted. As observed before, the curves move to lower phase angles with increasing fluorescence. More disadvantageous is the resulting measuring range. Without mCherry fluorescence the phase angle reaches over approx. 40° for the pH range of 4-9, whereas at an intensity of 90 a.u. it diminishes to 16°. In this case the pH monitoring becomes more prone to deviations. Nevertheless, this method is applied to correct the pH signal during the cultivation of mCherry. Therefore, the linear equations of the trend lines in Fig. 4.4-C are used to determine calibration curves at different fluorescence intensities. The sigmoidal curves in Fig. 4.4-D are mathematically described according to Eq. 4.2b by fitting the parameters Φ_{min}, Φ_{max}, pH_0 and dpH applying the Origin data handling software under standard conditions (OriginLab Corp., Northampton, MA, USA). In this way it became obvious that the fitted parameters in Eq. 4.2b are linear dependent on the fluorescence intensity (data not shown). Subsequently, the resulting linear functions for the parameters were applied in Eq. 4.2b. For convenience reasons the calculations for the correction were done in MS Excel. Fig. 4.4-E shows the results of the procedure. The original signal is indicated by the dotted, the corrected

curve by a solid green line. As a reference three samples were taken during the cultivation for offline determination of the pH value (green diamonds).

Additionally, the curves for biomass growth (scattered light) and mCherry fluorescence are depicted. It is noticed that up to 12 h the measured and the corrected signal are identical as they show the typical pH decrease in the beginning which was already discussed earlier (comp. Fig. 4.1). This is not surprising since mCherry fluorescence is hardly detectable in this time. The sudden increase of fluorescence after 12 h leads also to a rapid increase of the original pH curve from 6.5 to 7.5. The corrected signal instead is much less affected and increases slowly with the time, as it is expected (comp. Fig. 4.1-G). Thereby, the corrected pH values agree very well with the reference offline measurements. Hence, the correction of the pH on-line monitoring was successful.

In summary, it was shown again that it is possible to minimize the effect of a disturbing fluorescence originating from a fluorescent protein also on the pH signal if the influence is not too high. But, it must be mentioned that in this case the detailed characterization of the influence as well as the mathematical steps are more time consuming than in the case of DOT measurement. The method of optical isolation for the pH optode was not tested. But, it reasonable to assume that it will also be beneficial for this application.

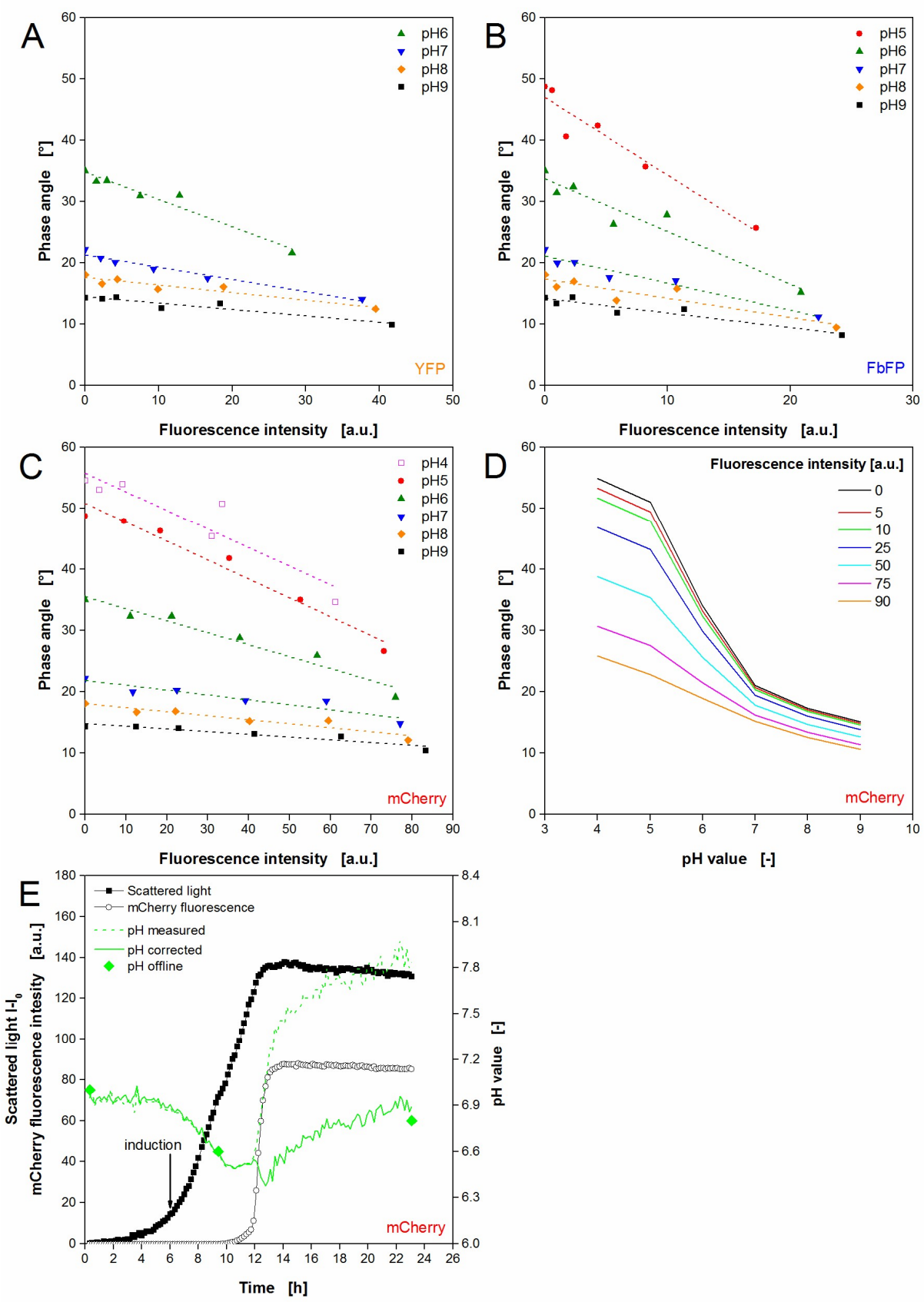

Fig. 4.4 - In-vitro characterization and correction of the influence of different fluorescent proteins on the optical pH signal. (A-C) Dependency of the phase angle as raw signal for pH monitoring from YFP, FbFP and mCherry fluorescence for different pH values. (D) Change of pH calibration curve with varied mCherry fluorescence intensity. (E) Correction of the online pH signal

for the cultivation of *E. coli* expressing mCherry by using fluorescence dependent calibration curves. Cultivation conditions: 48well FlowerPlate with optodes for DOT and pH measurement, V_L=800 µL, n=1100 rpm, d_0=3 mm, 37°C, Wilms-MOPS medium with 20 g/L glucose, induction with 0.1 mM IPTG after 6 h (indicated by arrow).

In addition to the *E. coli* experiments with YFP, FbFP and mCherry, another cultivation with the yeast *K. lactis* expressing GFP was performed. GFP wasn't investigated in *E. coli* since the spectral properties of GFP and FbFP regarding excitation and emission wavelength are close to each other (comp. Tab. 4.2). Moreover, a GFP expressing *E. coli* clone was not available for this work. It must be considered that the recombinant expression in *K. lactis* is lower compared to *E. coli*. Therefore, a much higher gain factor was used for the detection with the BioLector. Consequently, the fluorescence values are quantitatively not comparable. Fig. 4.5 shows the results of the *K. lactis* cultivation with recombinant GFP expression. In Fig. 4.5-A the biomass formation via scattered light is shown in parallel to the corresponding DOT signal. After the *lag* phase of 8 h, the culture starts growing exponentially for 9.5 h. As a consequence, the DOT is decreasing inversely. After 17.5 h, the scattered light signal forms a short plateau and the DOT increases rapidly, indicating the end of the cultivation. Surprisingly, the scattered light shows a second significant increase from 19-26 h. Since the DOT signal already recovered to 100 % air saturation in this time, it is hardly conceivable that further biomass formation occurred in this time. The explanation for this phenomenon was subject of further investigations and is discussed later in this work. Fig. 4.5-B shows the according results for on-line pH monitoring and GFP fluorescence. As a reference, offline samples were taken continuously for additional pH determination via pH electrode. It can be observed that GFP fluorescence starts increasing from the very beginning. This could be expected since the carbon source galactose, which is also the inducer for GFP production, is already present in the medium at the start. The maximum fluorescence intensity of 135 a.u. is reached after 19 h, and then starts decreasing again. After 29 h, it remains constant at a

relatively low level of 33 a.u.. The recombinant protein is obviously degraded right in that time when the second increase of the scattered light signal occurs. The on-line pH signal shows an unexpected behavior, suspiciously similar to the GFP fluorescence. Both signals are increasing, decreasing and stagnating at the same time. Also pH values as high as 6.5 are not typical for yeast cultivations. The offline reference points for the pH substantiate the suspicion that the optical signal is affected by the GFP fluorescence since the offline analysis shows a continuous pH decrease from 5 to 4.4 in the time from 10-18 h. Interestingly, this correlates very well with the first exponential growth phase obtained in Fig. 4.5-A, indicating that no further growth occurred after that. Contrary to the on-line pH signal, the optical DOT measurement seems not to be affected by GFP fluorescence since no unexpected values were detected. Consequently, the influence of GFP is similar to that of FbFP with a strong effect on the pH, but no effect on the DOT optode.

4.3.4. FP's influence on biomass on-line signal

In a set of experiments with *E. coli* mCherry another problem became obvious. By varying the cultivation conditions different amounts of the FP were produced and the fluorescence intensity varied as well. Surprisingly, the wells with the highest fluorescence intensity showed also the highest scattered light intensity indicating the formation of more biomass (data not shown). This was unexpected since overexpression of recombinant proteins usually causes a metabolic burden to the host, and, therefore, leads to decreased microbial growth (comp. Fig. 4.1-A and B). As a consequence, this observation was systematically investigated. Samples were prepared with a constant OD_{600} of 4.9, but varied mCherry fluorescence. From these samples the scattered light intensity was measured in the BioLector (Fig. 4.6-A). The conventional scattered light measurement is performed at 620 nm. At this wavelength it can

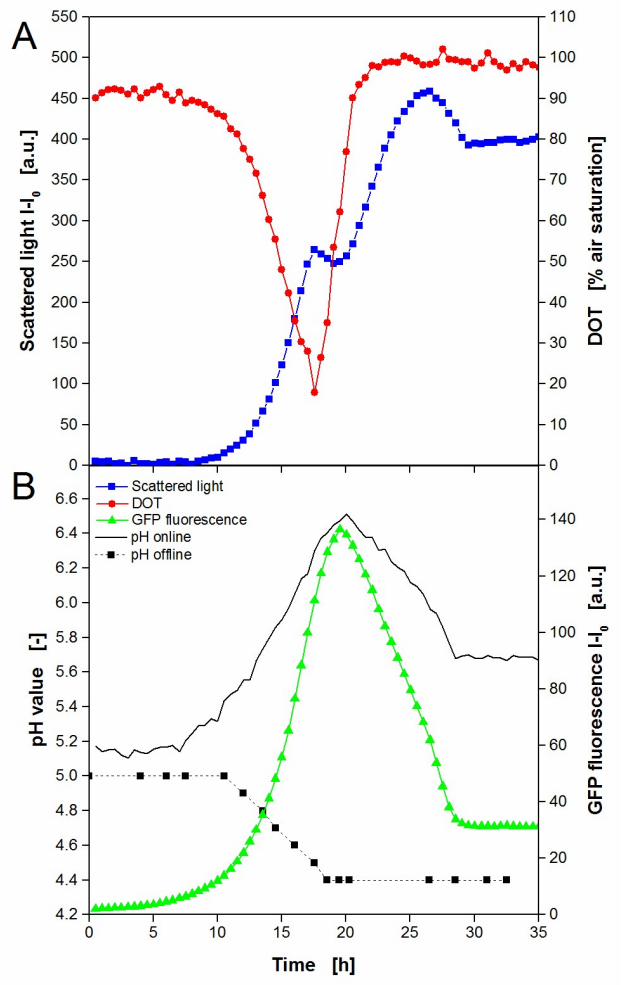

Fig. 4.5 - Cultivation of *K. lactis* GG799 expressing recombinant GFP using the BioLector system. Online monitoring of microbial growth (via scattered light) and DOT (A), pH value and fluorescence intensity of the recombinant expressed GFP. Additional pH measurement of offline samples (B). Cultivation conditions: 48well FlowerPlate with optodes for DOT and pH online measurement, V_L=800 µL, n=1100 rpm, d_0=3 mm, 30°C, YNB medium with 20 g/L galactose as substrate and inducer.

be seen that with increasing mCherry fluorescence intensities also the scattered light signal rises, even though the biomass level is constant in all samples. These results prove the influence of mCherry on the on-line biomass signal. After a look to the 2D fluorescence spectrum of mCherry in Fig. 4.2-D, the reason for the effect becomes clear since the measuring point for scattered light (indicated by dotted lines) is close to the peak maximum of the mCherry fluorescence. Consequently, interferences are very likely.

Subsequently, it was tried to find a solution for this problem. The idea was to shift scattered light measurement to another wavelength which is unaffected by fluorescence of mCherry. To see if this is possible, a scattered light wavelength scan of *E. coli* was performed. Therefore, the scattered light intensity of suspensions with varied biomass level (OD_{600}= 0.06-17.4) was measured at wavelengths of 200-850 nm (Fig. 4.6-B). In principle, all curves are shaped equally like a triangle with a prominent peak at approx. 460 nm. With increasing OD_{600} the curves move to higher scattered light values. This fact is the prerequisite for biomass quantification. At wavelengths below 320 and above 780 nm almost no differences with varied biomass level occur, a reliable biomass monitoring is not possible in these ranges. For the biomass determination via scattered light a linear relationship of OD_{600} and scattered light intensity would be beneficial. Therefore, the scattered light values for varied optical densities at arbitrarily chosen wavelengths of 460, 510, 540, 620 and 700 nm are pointed out in Fig. 4.6-C. For all tested wavelengths it can be recognized that optical density and scattered light are linearly related in the range of OD_{600} values of 2-15. For 620 and 700 nm the linear behavior is also present from 0 on and up to 17.4. The smaller measuring range of the higher wavelength is disadvantageous. At 460 nm it ranges from 200-700 a.u., whereas for 700 nm it's from 50-100 a.u. Consequently, higher wavelengths are more prone to measuring errors. However, Fig. 4.6-A reveals that the measurement at wavelengths of 510 and 540 nm are not independent from mCherry fluorescence. Both signals increase with higher fluorescence intensities. At 450 nm no clear trend can be observed. Contrary to that, the scattered light signal at 700 nm is completely independent of mCherry. Hence, a wavelength higher than 620 nm should be chosen for scattered light measurement in the presence of mCherry fluorescence, but, a compromise must be found ensuring a sufficient measuring range and immunity from interfering fluorescence. Therefore, further wavelengths between 620 and 700 nm should be tested. The 2D spectrum in Fig. 4.2-D inspires the assumption that at 640 nm no interference occurs anymore. Another reason for not shifting to lower wavelengths

is the fact that also other proteins, e.g. cell or medium components, can display certain fluorescence in this spectral range and, thereby, distort the biomass signal.

To sum this up, it must be recognized that also the on-line monitoring of biomass formation via scattered light measurement at 620 nm is prone to fluorescent proteins, namely mCherry. Similar effects for YFP, FbFP and GFP were not noticed. By shifting the measuring wavelength to values higher than 620 nm, this problem can be avoided. If this is not possible due to instrument limitation, alternative reporter proteins should be used. Additionally, a mathematical correction as performed for DOT and pH monitoring could be possible. This approach was not further investigated in this work since a wavelength shift is much more convenient.

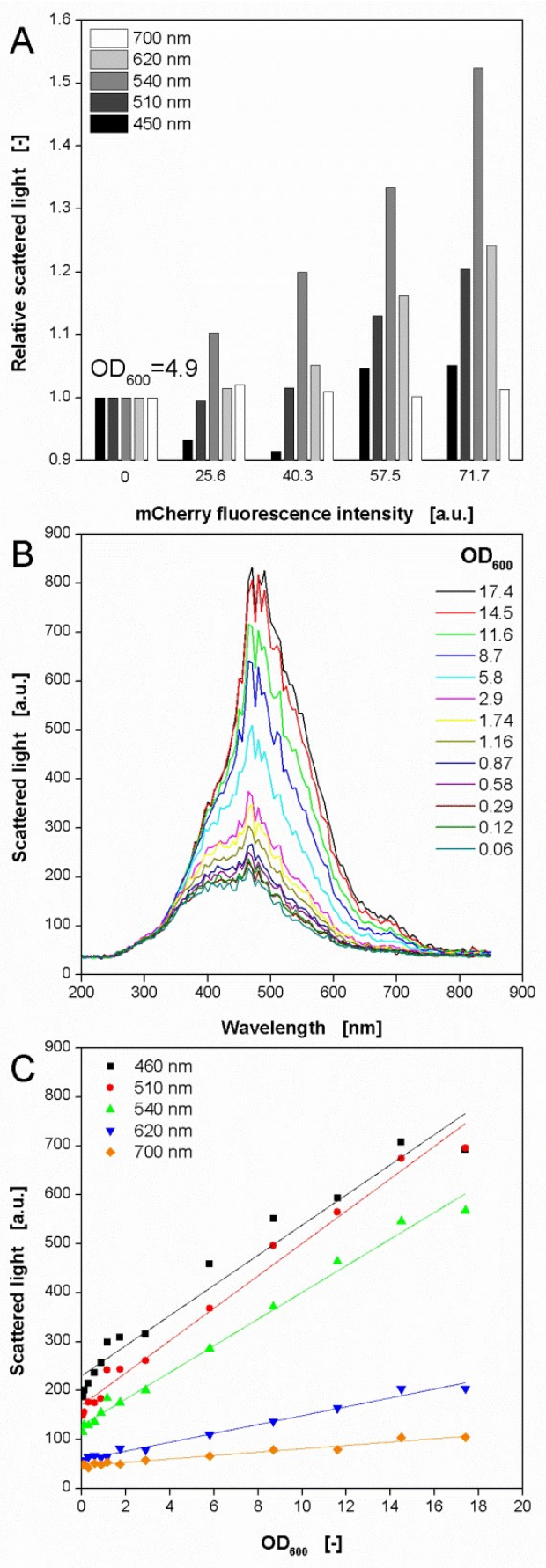

Fig. 4.6 - Characterization of the influence of red fluorescence from mCherry on the scattered light signal for online monitoring of microbial growth. (A) Dependency of the scattered light signal from mCherry fluorescence at different scattered light wavelengths. Different amounts of purified mCherry resulting in increasing fluorescence intensities were added to a suspension of non-induced *E. coli* cells with an OD_{600}=4.9. (B) Scattered light wavelength scan of *E. coli* cell suspensions with varied biomass concentration (OD_{600}). (C) Calibration curves between OD_{600} and scattered light intensity resulting from scattered light wavelength scan (comp. Fig. 4.6-B) at different scattered light wavelengths.

4.3.5. Effect of morphological changes on biomass on-line signal

The results in Fig. 4.5 revealed an unusual behavior of the scattered light signal showing an unexpected second increase of the biomass signal during the cultivation of the yeast *K. lactis*. The signals for DOT and pH value provide no explanation for this phenomenon. The DOT has already returned to 100 % air saturation (Fig. 4.7-A), and also the pH value remains constant at 4.4 (Fig. 4.5-B). Both facts indicate no further growth of the yeast. For further investigation offline samples were analyzed by HPLC for the determination of the galactose concentration which is the carbon source of the medium (Fig. 4.7-A). After the *lag* phase, galactose is consumed in parallel to exponential increase of the scattered light. After 18 h, the substrate is depleted. *K. lactis* cells are known to produce ethanol which can be used as carbon source later on. However, HPLC analysis of the samples revealed no further components which could have been used for further microbial growth. Offline samples were analyzed for the determination of dry cell weight (DCW) and cell number via flow cytometry (Fig. 4.7-B). The DCW increases exponentially from 8-18 h up to 12.5 g L^{-1}. The cell count shows a similar course reaching $2.25 \cdot 10^6$ cells at 20 h. After this time, no significant increase, comparable to that of the scattered light signal, is obtained. All these findings prove the fact that the described phenomenon is not due to microbial growth.

The optical scattered light signal depends on different factors [46]. For the on-line monitoring of biomass concentration the size, surface structure, or granularity of the cells are important parameters. Usually, it is assumed that these parameters do not change significantly during fermentation. To prove this assumption, flow cytometry measurements were performed (Fig. 4.7-C). The forward scatter is mainly attributed to cell size. It can be seen that in the first samples taken after 4, 7, and 14 h (FC1-3) only one population occurs ranging from 10^2-10^3 a.u.. Interestingly, in the following samples a second population of lower cell size (indicated by lower forward scatter intensity) is revealed (FC4-6). Microscopic images of samples from the cultivation were analyzed in parallel (Fig. 4.7-D). At 14 h typically sized

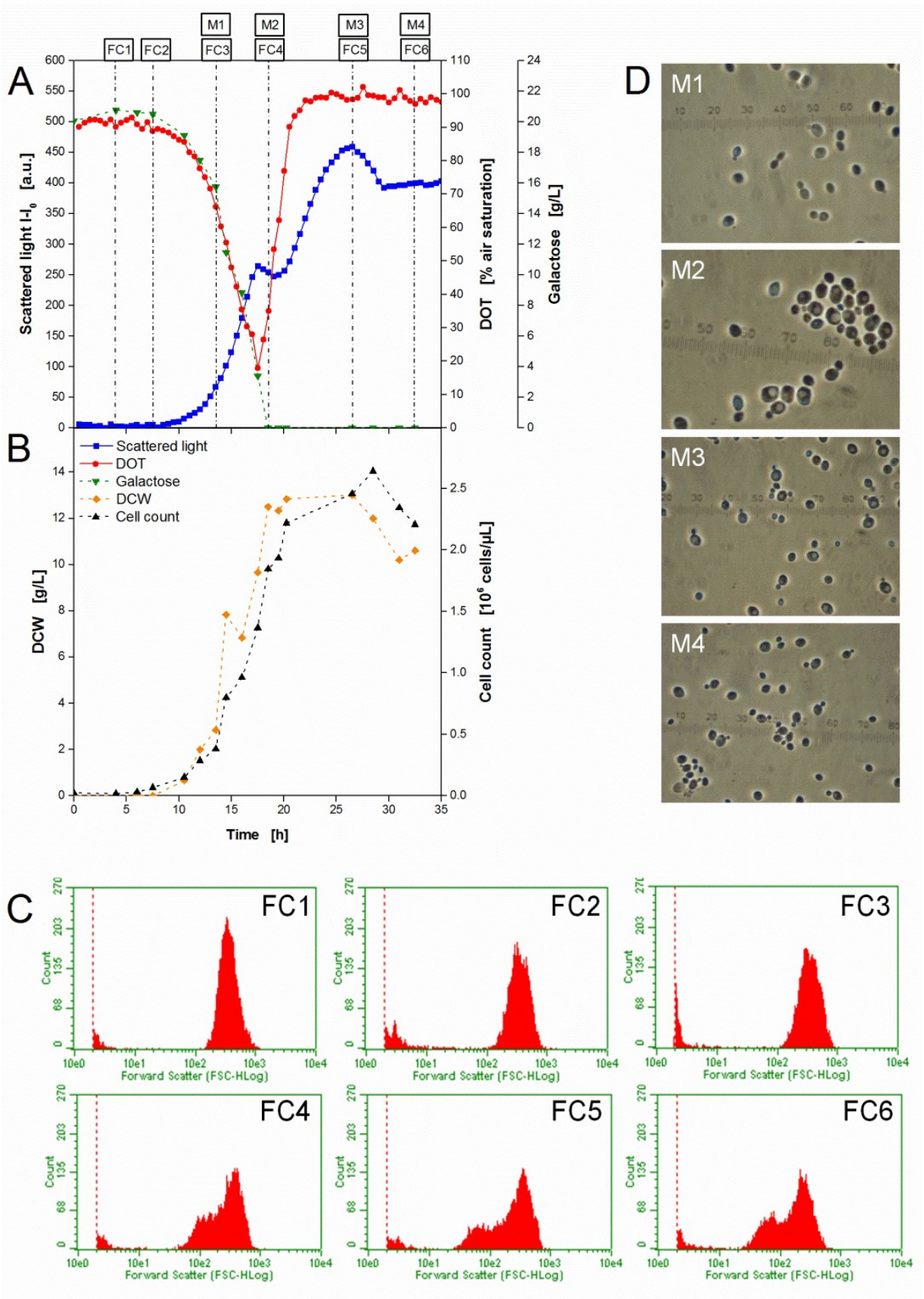

Fig. 4.7 - Cultivation of *K. lactis* GG799 for the investigation of the influence of morphological changes on the scattered light signal for online monitoring of microbial growth. (A) Online measurement of microbial growth (via scattered light) and DOT (via optodes); determination of

galactose concentration in the medium from offline samples (via HPLC). Boxes FC1-6 and M1-4 indicate time points of samples for flow cytometric (C) and microscopic (D) analysis, respectively. (B) Determination of DCW and cell count (via flow cytometry) from offline samples. (C) Forward scatter histograms from flow cytometric analysis at different time points (FC1-6). (D) Microscope images of yeast cells at different time points (M1-4). Cultivation conditions: 48well FlowerPlate with optodes for DOT and pH measurement, V_L=800 µL, n=1100 rpm, d_0=3 mm, 30°C,YNB medium with 20 g/L galactose as substrate and inducer.

yeast cells during the exponential growth are obtained. In the early stationary phase after 18 h, there are still relatively large cells present containing vacuoles. But, in the images M3 and M4 more and more small cells occur. This fact correlates very well with the results from flow cytometry. Finally, it must be concluded that these changes in cell morphology after the depletion of the carbon source galactose are responsible for the unusual behavior of the scattered light signal shown in Fig. 4.7-A. Interestingly, this phenomenon occurred only in the synthetic medium YNB, but not in a rich YPD medium (data not shown).

A similar behavior of the scattered light signal was described before for the yeast *Hansenula polymorpha* [47]. It was also reported that shifts in the subpopulations of the light scatter are often associated with events in the cell division cycle [48]. Measurements on single cell level implied this effect to be associated with a change in morphology and heterogeneity in the cell cycle. Unfortunately, this influence cannot be quantified which makes a correction unfeasible.

4.4. Conclusion

New shaken bioreactor systems like the BioLector are simple to handle, and offer various options of optical online measurements. Thereby, the high level of parallelization and the small scale of cultures in MTPs allow economical high throughput and, hence, to screen many parameters in reasonable short time. Since the development of FPs as fluorescent tags, the tracking of cellular proteins *in-vivo* became routine. The application of all these tools significantly contributes to the understanding of bioprocesses. Nevertheless, overreliance on experimental results provided by high-throughput screening procedures applying optical on-line monitoring can mislead the ordinary user. In this work it was demonstrated how fluorescent proteins can influence the optical signals indicating the DOT and pH value. It was shown that:

- YFP has a moderate effect on the DOT optode, the pH signal is strongly affected.
- FbFP has no effect on the DOT optode, the pH signal is strongly affected.
- MCherry has a strong effect on the DOT optode, the pH signal is moderately affected.
- GFP has no effect on the DOT optode, the pH signal is strongly affected.

With a mathematical correction procedure it was possible to minimize the moderate influences, but strong influences were not correctable in this way. By using sensor spots (optodes) with optical isolation even the very strong influence of mCherry on the DOT signal could be minimized. Consequently, an optical isolation is recommended for all measurements. A further solution might be the use of alternative fluorescent proteins in the future. There are reports about variants with fluorescence in the UV spectrum [49], but also in the NIR range [50]. On the other hand, new fluorescent dyes for pH and DOT sensing became available emitting light in the NIR range [51, 52]. In both ways interferences of optode and protein fluorescence are excluded.

The scattered light signal as indicator for biomass concentration was proved to be prone to different influences, too. On the one hand, mCherry fluorescence leads to increased scattered light values even though the biomass level is constant. By shifting the measuring point for scattered light to wavelengths higher than 620 nm this effect can be avoided. On the other hand, it was observed that morphological changes of cells can cause unexpected scattered light changes. Unfortunately, this effect is hard to quantify and, hence, not correctable.

In summary, it should be noticed that the phenomena reported here refer to typical experiments in biotechnological labs. For this reason these aspects are highlighted in this work to make operators of such valuable systems as the BioLector aware of potential pitfalls and resulting misinterpretations. With the right methods it is possible to uncover existing problems and correct them.

4.5. Nomenclature

Abbreviations

DLR	Dual lifetime referencing
E. coli FbFP	*Escherichia coli* BL21 (De3) pRotHi-FbFP
E. coli mCherry	*Escherichia coli* BL21 (De3) pRSet-mCherry
E. coli YFP	*Escherichia coli* BL21 (De3) pRotHi-YFP
FbFP	FMN-binding fluorescent protein
FMN	Flavin mononucleotide
FP	Fluorescent protein
GFP	Green fluorescent protein
MTP	Microtiter plate
YFP	Yellow fluorescent protein
YNB	Yeast nitrogen base (medium)
YPD	Yeast extract peptone D-glucose (medium)

Symbols

DOT	Dissolved oxygen tension	[% air saturation]
dpH	Step size of sigmoidal pH calibration function	[-]
d_0	Shaking diameter	[mm]
FI	Fluorescence intensity	[a.u.]
I	Measured signal intensity	[a.u.]
I_0	Initial signal intensity	[a.u.]
K_{SV}	Stern-Volmer constant	[-]
m_0	Slope of linear relation between Φ_0 and FI	[° $a.u.^{-1}$]
m_{100}	Slope of linear relation between Φ_{100} and FI	[° $a.u.^{-1}$]
n_0	Offset of linear relation between Φ_0 and FI	[°]
n_{100}	Offset of linear relation between Φ_{100} and FI	[°]
pH_0	Central pH of sigmoidal pH calibration function	[-]
Φ	Phase angle (from DLR measurement)	[°]
Φ_0	Φ at DOT=0 % air sturation	[°]
Φ_{100}	Φ at DOT=100 % air sturation	[°]

Φ_{max}	Final Φ of sigmoidal pH calibration function		[°]
Φ_{min}	Initial Φ of sigmoidal pH calibration function		[°]
$\lambda_{ex,DOT}$	Excitation wavelength for DOT optode		[nm]
$\lambda_{ex,pH}$	Excitation wavelength for pH optode		[nm]
τ	Decay time	[ms]	
τ_0	Decay time at DOT=0 % air saturation		[ms]

4.6. References

1. Micheletti M, Lye GJ: Microscalle bioprocess optimisation. *Curr Opin Biotech* 2006, 17:611-618.

2. Tustian AD, Chhatre S: Speeding the design of bioprocesses. *Chem Eng Prog* 2008, 104:S8-S13.

3. Bareither R, Pollard D: A review of advanced small-scale parallel bioreactor technology for accelerated process development: Current state and future need. *Biotechnol Progr* 2011, 27:2-14.

4. Gill NK, Appleton M, Baganz F, Lye GJ: Quantification of power consumption and oxygen transfer characteristics of a stirred miniature bioreactor for predictive fermentation scale-up. *Biotechnol Bioeng* 2008, 100:1144-1155.

5. Gill NK, Appleton M, Baganz F, Lye GJ: Design and characterisation of a miniature stirred bioreactor system for parallel microbial fermentations. *Biochemical Engineering Journal* 2008, 39:164-176.

6. Lee HLT, Boccazzi P, Ram RJ, Sinskey AJ: Microbioreactor arrays with integrated mixers and fluid injectors for high-throughput experimentation with pH and dissolved oxygen control. *Lab Chip* 2006, 6:1229-1235.

7. Maharbiz MM, Holtz WJ, Howe RT, Keasling JD: Microbioreactor arrays with parametric control for high-throughput experimentation. *Biotechnol Bioeng* 2004, 85:376-381.

8. Puskeiler R, Kaufmann K, Weuster-Botz D: Development, parallelization, and automation of a gas-inducing milliliter-scale bioreactor for high-throughput bioprocess design (HTBD). *Biotechnol Bioeng* 2005, 89:512-523.

9. Weuster-Botz D, Puskeiler R, Kusterer A, Kaufmann K, John GT, Arnold M: Methods and milliliter scale devices for high-throughput bioprocess design. *Bioproc Biosyst Eng* 2005, 28:109-119.

10. Duetz WA: Microtiter plates as mini-bioreactors: miniaturization of fermentation methods. *Trends Microbiol* 2007, 15:469-475.

11. Zhang H, Lamping SR, Pickering SCR, Lye GJ, Shamlou PA: Engineering characterisation of a single well from 24-well and 96-well microtitre plates. *Biochemical Engineering Journal* 2008, 40:138-149.

12. Duetz WA, Ruedi L, Hermann R, O'Connor K, Büchs J, Witholt B: Methods for intense aeration, growth, storage, and replication of bacterial strains in microtiter plates. *Appl Environ Microb* 2000, 66:2641-2646.

13. Hermann R, Lehmann M, Büchs J: Characterization of gas-liquid mass transfer phenomena in microtiter plates. *Biotechnol Bioeng* 2003, 81:178-186.

14. Kensy F, John GT, Hofmann B, Büchs J: Characterisation of operation conditions and online monitoring of physiological culture parameters in shaken 24-well microtiter plates. *Bioproc Biosyst Eng* 2005, 28:75-81.

15. Kensy F, Zimmermann HF, Knabben I, Anderlei T, Trauthwein H, Dingerdissen U, Büchs J: Oxygen transfer phenomena in 48-well microtiter plates: Determination by optical monitoring of sulfite oxidation and verification by real-time measurement during microbial growth. *Biotechnol Bioeng* 2005, 89:698-708.

16. Duetz WA, Witholt B: Effectiveness of orbital shaking for the aeration of suspended bacterial cultures in square-deepwell microtiter plates. *Biochem Eng J* 2001, 7:113-115.

17. Weiss S, John GT, Klimant I, Heinzle E: Modeling of mixing in 96-well microplates observed with fluorescence indicators. *Biotechnol Progr* 2002, 18:821-830.

18. Funke M, Diederichs S, Kensy F, Müller C, Büchs J: The baffled microtiter plate: Increased oxygen transfer and improved online monitoring in small scale fermentations. *Biotechnol Bioeng* 2009, 103:1118-1128.

19. Chudakov DM, Lukyanov S, Lukyanov KA: Fluorescent proteins as a toolkit for in vivo imaging. *Trends Biotechnol* 2005, 23:605-613.

20. Crivat G, Taraska JW: Imaging proteins inside cells with fluorescent tags. *Trends Biotechnol* 2012, 30:8-16.

21. Day RN, Davidson MW: The fluorescent protein palette: tools for cellular imaging. *Chem Soc Rev* 2009, 38:2887-2921.

22. Frommer WB, Davidson MW, Campbell RE: Genetically encoded biosensors based on engineered fluorescent proteins. *Chem Soc Rev* 2009, 38:2833-2841.

23. Giepmans BNG, Adams SR, Ellisman MH, Tsien RY: Review - The fluorescent toolbox for assessing protein location and function. *Science* 2006, 312:217-224.

24. Drepper T, Eggert T, Circolone F, Heck A, Krauss U, Guterl JK, Wendorff M, Losi A, Gartner W, Jäger KE: Reporter proteins for in vivo fluorescence without oxygen. *Nat Biotechnol* 2007, 25:443-445.

25. Drepper T, Huber R, Heck A, Circolone F, Hillmer AK, Büchs J, Jäger KE: Flavin mononucleotide-based fluorescent reporter proteins outperform green fluorescent protein-like proteins as quantitative in vivo real-time reporters. *Appl Environ Microb* 2010, 76:5990-5994.

26. Kumagai A, Ando R, Miyatake H, Greimel P, Kobayashi T, Hirabayashi Y, Shimogori T, Miyawaki A: A bilirubin-inducible fluorescent protein from eel muscle. *Cell* 2013, 153:1602-1611.

27. Samorski M, Müller-Newen G, Büchs J: Quasi-continuous combined scattered light and fluorescence measurements: A novel measurement technique for shaken microtiter plates. *Biotechnol Bioeng* 2005, 92:61-68.

28. Arain S, John GT, Krause C, Gerlach J, Wolfbeis OS, Klimant I: Characterization of microtiterplates with integrated optical sensors for oxygen and pH, and their applications to enzyme activity screening, respirometry, and toxicological assays. *Sensor Actuat B-Chem* 2006, 113:639-648.

29. John GT, Klimant I, Wittmann C, Heinzle E: Integrated optical sensing of dissolved oxygen in microtiter plates: A novel tool for microbial cultivation. *Biotechnol Bioeng* 2003, 81:829-836.

30. Boniello C, Mayr T, Bolivar JM, Nidetzky B: Dual-lifetime referencing (DLR): A powerful method for on-line measurement of internal pH in carrier-bound immobilized biocatalysts. *BMC Biotechnol* 2012, 12.

31. Kocincova AS, Borisov SM, Krause C, Wolfbeis OS: Fiber-optic microsensors for simultaneous sensing of oxygen and pH, and of oxygen and temperature. *Analytical Chemistry* 2007, 79:8486-8493.

32. Kocincova AS, Nagl S, Arain S, Krause C, Borisov SM, Arnold M, Wolfbeis OS: Multiplex bacterial growth monitoring in 24-well microplates using a dual optical sensor for dissolved oxygen and pH. *Biotechnol Bioeng* 2008, 100:430-438.

33. Kensy F, Engelbrecht C, Büchs J: Scale-up from microtiter plate to laboratory fermenter: evaluation by online monitoring techniques of growth and protein expression in Escherichia coli and Hansenula polymorpha fermentations. *Microb Cell Fact* 2009, 8.

34. Huber R, Ritter D, Hering T, Hillmer AK, Kensy F, Müller C, Wang L, Büchs J: Robo-Lector - a novel platform for automated high-throughput cultivations in microtiter plates with high information content. *Microb Cell Fact* 2009, 8.

35. Scheidle M, Klinger J, Büchs J: Combination of on-line pH and oxygen transfer rate measurement in shake flasks by fiber optical technique and Respiration Activity Monitoring System (RAMOS). *Sensors-Basel* 2007, 7:3472-3480.

36. Wilms B, Hauck A, Reuss M, Syldatk C, Mattes R, Siemann M, Altenbuchner J: High-cell-density fermentation for production of L-N-carbamoylase using an expression system based on the Escherichia coli rhaBAD promoter. *Biotechnol Bioeng* 2001, 73:95-103.

37. Hahn-Hagerdal B, Karhumaa K, Larsson CU, Gorwa-Grauslund M, Gorgens J, van Zyl WH: Role of cultivation media in the development of yeast strains for large scale industrial use. *Microb Cell Fact* 2005, 4:31.

38. Kunze M, Huber R, Gutjahr C, Müllner S, Büchs J: Predictive tool for recombinant protein production in Escherichia coli shake-flask cultures using an on-line monitoring system. *Biotechnol Prog* 2012, 28:103-113.

39. Losen M, Frölich B, Pohl M, Büchs J: Effect of oxygen limitation and medium composition on Escherichia coli fermentation in shake-flask cultures. *Biotechnol Prog* 2004, 20:1062-1068.

40. Funke M, Buchenauer A, Schnakenberg U, Mokwa W, Diederichs S, Mertens A, Müller C, Kensy F, Büchs J: Microfluidic BioLector-Microfluidic bioprocess control in microtiter plates. *Biotechnol Bioeng* 2010, 107:497-505.

41. Bentley WE, Mirjalili N, Andersen DC, Davis RH, Kompala DS: Plasmid-encoded protein - The principal factor in the metabolic burden associated with recombinant bacteria. *Biotechnol Bioeng* 1990, 35:668-681.

42. Bhattacharya SK, Dubey AK: Metabolic burden as reflected by maintenance coefficient of recombinant Escherichia coli overexpressing target gene. *Biotechnol Lett* 1995, 17:1155-1160.

43. Lee J, Ramirez WF: Mathematical-modeling of induced foreign protein-production by recombinant bacteria. *Biotechnol Bioeng* 1992, 39:635-646.

44. Jeude M, Dittrich B, Niederschulte H, Anderlei T, Knocke C, Klee D, Büchs J: Fed-batch mode in shake flasks by slow-release technique. *Biotechnol Bioeng* 2006, 95:433-445.

45. Neubauer P, Siurkus J, Panula-Perala J, Neubauer A, Ukkonen K, Krause M, Meyer D, Pelzer S, Eck J, Tegel H, et al: EnBase (TM) - MTP based high-cell-density fermentation for high-throughput and high-content screening. *New Biotechnol* 2009, 25:S161-S161.

46. Brumberger H, Stein RS, Rowell R: Light scattering. *Sci Technology* 1968:34-&.

47. Kottmeier K, Weber J, Muller C, Bley T, Büchs J: Asymmetric division of Hansenula polymorpha reflected by a drop of light scatter intensity measured in batch microtiter plate cultivations at phosphate limitation. *Biotechnol Bioeng* 2009, 104:554-561.

48. Scheper T, Hoffmann H, Schügerl K: Flow cytometric studies during culture of Saccharomyces cerevisiae. *Enzyme Microb Tech* 1987, 9:399-405.

49. Siepert EM, Gartz E, Tur MK, Delbruck H, Barth S, Büchs J: Short-chain fluorescent tryptophan tags for on-line detection of functional recombinant proteins. *BMC Biotechnol* 2012, 12.

50. Shcherbakova DM, Verkhusha VV: Near-infrared fluorescent proteins for multicolor in vivo imaging. *Nat Methods* 2013, 10:751-754.

51. Aigner D, Borisov SM, Petritsch P, Klimant I: Novel near infra-red fluorescent pH sensors based on 1-aminoperylene bisimides covalently grafted onto poly(acryloylmorpholine). *Chemical Communications* 2013, 49:2139-2141.

52. Borisov SM, Nuss G, Klimant I: Red light-excitable oxygen sensing materials based on platinum(II) and palladium(II) benzoporphyrins. *Analytical Chemistry* 2008, 80:9435-9442.

5. Chapter IV - Minireactor-based high-throughput temperature profiling for the optimization of microbial and enzymatic processes

5.1. Background

Bioprocesses, either fermentations or enzymatic catalysis, depend on a number of different operating parameters. Temperature is one of the most important. It is commonly known that processes should be performed under optimal conditions in order to achieve best results, e.g. reaction rates or yields [1]. Thereby, the temperature optimum can be different within one microbial or enzymatic system, either the focus is on growth or product formation [2], on enzyme activity or stability [3, 4].

Over the last decades the number of potential bioprocesses for the production of valuable products increased and this trend continues. Consequently, more and more microbial and enzymatic systems need to be characterized regarding their temperature optima. Conventional methods are disadvantageous in many ways. Repetitive batch cultivations at varied temperatures, either in shake flasks or bench scale bioreactors, provide only a few data points at the expense of relatively high material and time input. The analysis of temperature-specific activities and kinetic parameters of enzymes is traditionally performed in a spectrophotometric way by use of a temperature-controlled water jacketed single cuvettes [5]. Even though the external thermostat provides constant and accurate temperature control over a broad temperature range, the numbers of samples handled for simultaneous reading in such spectrophotometers are usually very limited.

To face these limitations micro-bioreactors (MBR) became a promising alternative, but sufficient temperature control is quite challenging [6]. The simplest way is to use MBRs, e.g. microtiter plates (MTP), in temperature controlled rooms [7] or incubators [8]. Another option

is to link the MBR system to a thermostat system and circulate water through the MBR chamber base [4, 9-11]. The major disadvantage of these systems is their limitation in operating parallel reactors at different temperatures. One exceptional system allows the operation of sixteen parallel small scale reactors equipped with ceramic heating jackets but its use requires costly instrumentation and is focused on chemical reactions [12]. The integration of electrical micro-heaters to the bottoms or walls of MBRs allows individual temperature control of parallel MBRs [13-15]. However, for high-throughput application the required hardware and control become exceedingly complex.

Whilst temperature control is rather challenging in MBRs, temperature measurement is relatively simple. There are several reports on the application of temperature dependent resistances [14-16] or thermocouples [10, 17]. Also thermal or infrared cameras allow temperature determination in MBRs [18, 19]. Furthermore, the so called fluorescence thermometry can be used [11, 20-22]. The combination of a temperature dependent fluorophore and a spectrophotometer is a promising method for high-throughput temperature determination, e.g. in MTPs.

In this work, a system is presented combining the on-line monitoring system BioLector [23, 24] with a customized temperature control unit for 96 well MTPs, thereby, allowing high-throughput temperature optimization for microbial and enzymatic reaction systems in a micro-scale of 200 µL. On the one hand, the BioLector system allows quasi-continuous measurement of optical signals over time representative for microbial growth and product formation or enzymatic activity. On the other hand, the tempering system, consisting of a special thermostating block connected to two thermostats, creates specific temperature profiles over a MTP. For the single well temperature measurement fluorescence thermometry was used. Combining the fluorescent dyes Rhodamin B (RhB) and Rhodamin 110 (Rh110) a reliable assay was established for application with the BioLector technique [21]. After

defining several profiles at different temperature levels, the device was used to characterize microbial and enzymatic systems. The whole temperature profiles and optima for the bacterium *Escherichia coli* and the yeast *Kluyveromyces lactis* regarding growth and recombinant protein production were determined in single shot experiments. Additionally, the commercial cellulase mixture Celluclast as a representative for enzymes was investigated applying a fluorescent activity assay. The results of this temperature high-throughput screening could be used for a mathematical description of the particular temperature dependent behavior of the investigated biological system as an extended Arrhenius model for catalyst activation and deactivation [25].

5.2. Material & Methods

5.2.1. Temperature control unit

The design of the heating block is based on the work of Rachinskiy et al. [4, 9]. It is made of aluminium with tube adapters for the two water circulation systems (Fig. 5.1-C). The circulation system for cooling was operated with the FL300 recirculation cooler (Julabo, Seelbach, Germany) allowing temperature set points from -20°C to 40°C. The flow rate was determined to 2.1 L min^{-1}. The heating water circulation worked with the Ecoline E300 thermostat (Lauda, Lauda-Königshofen, Germany) for temperature set points of 25-100°C. A flow rate of 1.1 L min^{-1} was measured. Both circulation systems were operated with tap water. Temperature set points below 5°C and above 95°C were avoided to prevent the water from freezing or boiling.

5.2.2. On-line monitoring system

The optical measurement technique is identical to that described in the work of Samorski et al. [24]. The in-house constructed device is henceforth referred as BioLector. Wavelengths and gain factors for all optical signals are specified in Tab. 5.1. For all experiments 96well lummox multiwell plates (Greiner Bio-One GmbH, Frickenhausen, Germany) were used.

5.2.3. Temperature determination

For the temperature measurement via fluorescent dyes a mixture of Rhodamin B (RhB) and Rhodamin 110 (Rh110) was used. Before each experiment a fresh measuring solution was prepared from 100-fold concentrated stock solutions of RhB and Rh110, respectively. For these stock solutions dye powder was dissolved in pure methanol yielding a concentration of

Tab. 5.1 - Optical signals and applied setup for on-line monitoring

Optical signal	λ_{ex} [nm]	λ_{em} [nm]	Gain
Rhodamin B fluorescence	485	589	20
Rhodamin 110 fluorescence	485	520	2
Biomass (scattered light)	620	-	20
FbFP fluorescence	460	490	45
GFP fluorescence	485	510	30
4-methylumbellyferone fluorescence	365	455	25

1 g L^{-1} and stored at 4°C. For the measuring solution the two stock solutions were mixed with water and diluted to a final concentration of 10 mg L^{-1}, respectively. 200 µL of the prepared solution were filled into each well of the MTP and shaken at a frequency of 995 rpm at a shaking diameter of 3 mm.

For temperature reference a special in-house constructed PT100 temperature sensor was placed in the arbitrary chosen well A2 of the microtiter plate. The sensor was connected to the serial port of the LAUDA thermostat for data output. Before use the sensor was calibrated with a gauged thermometer.

For the calibration of the fluorescence signal versus the temperature only the well equipped with the PT100 sensor was monitored in order to accelerate the procedure. For each point five consecutive measuring values were averaged. For temperature profiles twelve consecutive measurement cycles of the whole MTP were performed to get the average for each well. The PT100 sensor was placed as reference in well A2. For each specific temperature profile fresh prepared measuring solution with a new determined calibration curve was used.

5.2.4. Microorganisms

The *E. coli* clone expressing FbFP was *E. coli* BL21 (DE3) with the pRhotHi vector and kanamycin resistance supplied by the Institute of Molecular Enzyme Technology (IMET) at the Heinrich-Heine University Düsseldorf (Germany). For alcohol dehydrogenase A (ADH-A, from *Rhodococcus ruber*) expression *E. coli* BL21 (DE3) with the pET22b vector and ampicillin resistance was used supplied by the Department of Chemistry (Organic and Bioorganic Chemistry) at the University of Graz (Austria). For *K. lactis* experiments the strain GG799 with the pKlac1 vector expressing GFP from the Institute of Molecular Biotechnology (Bio VII) at the RWTH Aachen University, Germany) was applied.

5.2.5. Media & cultivation

For *E. coli* pre-cultures terrific broth (TB) medium consisting of 12 g L^{-1} tryptone, 24 g L^{-1} yeast extract, 12.54 g L^{-1} K_2HPO_4, 2.31 g L^{-1} KH_2PO_4, and 5 g L^{-1} glycerol (all ingredients from Roth, Germany) dissolved in water was used. The pH value was 7.2±0.2 without adjustment. For the main cultivation of *E. coli* under non-induced conditions either TB medium or a modified Wilms and Reuss medium (henceforth referred as Wilms-MOPS medium) were used [26, 27]. Wilms-MOPS medium consists of 5 g L^{-1} $(NH_4)_2SO_4$, 0.5 g L^{-1} NH_4Cl, 3.0 g L^{-1} K_2HPO_4, 2 g L^{-1} Na_2SO_4, 0.5 g L^{-1} $MgSO_4 \cdot 7H_2O$, 0.01 g L^{-1} thiamine hydrochloride, 20.9 g L^{-1} 3-(N-morpholino)-propanesulfonic acid (MOPS, 0.2 M), 20 g L^{-1} glucose and 1 mL L^{-1} trace element solution. This trace element solution consists of 1.98 g L^{-1} $CaCl_2 \cdot 2H_2O$, 0.54 g L^{-1} $CoCl_2 \cdot 6H_2O$, 0.48 g L^{-1} $CuSO_4 \cdot 5H_2O$, 41.76 g L^{-1} $FeCl_3 \cdot 6H_2O$, 0.3 g L^{-1} $MnSO_4 \cdot H_2O$, 0.54 g L^{-1} $ZnSO_4 \cdot 7H_2O$, 33.39 g L^{-1} Na_2EDTA (Titriplex III). The pH was adjusted with 5 M NaOH to a value of 7. For experiments under induced conditions either the commercially available ready-made complex auto-induction medium Overnight Express Instant TB medium (OnEx, Novagen®/Merck, Darmstadt, Germany) or a modified

Wilms-MOPS medium was used. OnEx consists of complex components similar to TB medium and the carbon sources glucose, lactose, and glycerol. For preparing the medium 60 g of the commercial granulate and 12.6 g of glycerol were dissolved in water and filled up to 1 L without pH-adjustment. HPLC analysis of the medium indicated a glucose concentration of 0.5 g/L and a lactose concentration of 2 g/L. For the modification of Wilms-MOPS medium in order to get a mineral auto-induction medium 1 g L^{-1} glucose, 4 g L^{-1} lactose and 5 g L^{-1} glycerol where added instead of 20 g L^{-1} glucose as carbon source. Depending on the clone's resistance, 50 µg mL^{-1} kanamycin or 100 µg mL^{-1} ampicillin were added to the medium from a 1000 fold concentrated stock solution.

For *K. lactis* pre-cultures and cultivation under non-induced conditions yeast extract peptone (YP) [28] medium was used, consisting of 10 g L^{-1} yeast extract, 20 g L^{-1} tryptone and 20 g L^{-1} glucose. For cultivations under induced conditions 20 g L^{-1} galactose instead of glucose served as carbon source and inducer for recombinant protein expression.

For *E. coli* pre-cultivation, 10 mL of TB medium in a 250 ml shake flask were inoculated with 50 µL from a cryoculture, and cultures were grown for 8 h at 350 rpm (shaking diameter 50 mm) and 37°C. *K. lactis* pre-culture conditions were the same aside from being grown in YP medium for 12 h at 30°C.

For all main cultivations the respective medium was inoculated from the pre-culture, resulting in an initial OD_{600} of 0.1. 200 µL of the already inoculated medium was then transferred to each of the wells of the MTP. The plates were sealed with gas-permeable seals (AB-0718, Thermo Scientific, Dreieich, Germany). Subsequently, the pre-tempered thermostating block was mounted atop the MTP and both were fixed on the orbital shaker (Kühner AG, Basel, Switzerland) of the BioLector. The cultivation was performed at a shaking frequency of 995 rpm and a shaking diameter of 3mm. For aeration pure oxygen was used. For scattered light and fluorescence measurement the initial light intensity (I_0), which is mainly attributed to

such factors as the media background or the type of the microtiter plate, was subtracted from the original measured data ($I-I_0$).

Reference shake flask cultures were performed in a Respiration Activity Monitoring System (RAMOS) [29, 30] built in-house. Commercial versions of this device are available from Hitec Zang (Herzogenrath, Germany) or Kühner AG (Birsfelden, Switzerland). 10 mL of OnEx medium in a special 250 ml shake flask were inoculated from the pre-culture, resulting in an initial OD_{600} of 0.1. Subsequently, the cultures were shaken at 350 rpm with a shaking diameter of 50 mm at temperatures of 22-37°C with aeration by pressurized air. Cells for ADH-A analysis were harvested in the stationary phase, indicated by the OTR on-line signal of the RAMOS device.

5.2.6. Cellulase experiments

For hydrolysis experiments the substrate 4-methylumbelliferyl-β-D-cellobioside (4MUC) was used in combination with the commercial cellulase mix Celluclast 1.5 L (Novozymes, Bagsvaerd, Denmark). A 0.75 mM stock solution of 4MUC in 0.1 M acetate buffer (pH=4.8) was prepared. The enzyme stock solution contained 5 g L^{-1} of Celluclast crude extract in 0.1 M acetate buffer (pH=4.8). Before starting the experiments, 180 µL of the 4MUC stock solution were filled in each well of a 96 well MTP and pre-heated for 30 min applying the respective temperature profile. Subsequently, 20 µL of the enzyme stock solution were added to each MTP well resulting in final concentrations of 0.6 mM 4MUC and 1 g L^{-1} Celluclast. Since no aeration was necessary, the plate was sealed with a non-permeable foil (AB-0580, Thermo Scientific, Dreieich, Germany). The further procedure was identical to the cultivation experiments in MTPs besides that 4-methylumbellyferone (4MU) fluorescence was the only measuring signal (Tab. 5.1). To calibrate the fluorescence signal, 200 µL of solutions with varied 4MU concentrations were filled in a 96 well MTP and their fluorescence intensity was

measured using the BioLector. The calibration measuring points are average values from three independent measurements.

5.2.7. Offline analysis

OD_{600} was determined via a Genesys 20 photometer (Thermo Scientific, Dreieich, Germany) in 1.5 mL micro cuvettes (PS, Plastibrand, Roth, Karlsruhe, Germany). For values higher than 0.5 the samples were appropriately diluted with 0.9 % [wt/vol] NaCl solution.

The volumetric activity of the produced alcohol dehydrogenase A (ADH-A) was determined at 30°C by following the oxidation of NADH at a wavelength of 340 nm in 96-well microtiter plates (F-profile, Roth, Germany) using a Synergy-4 Multi-Mode Microplate Reader (BioTek Instruments, Germany). For cell disruption of *E. coli* expressing ADH-A, the cell pellet of 500 µL culture broth was suspended in 100 µL BugBuster Protein Extraction Reagent (Novagen, Merck, Germany) adding 1000 U/mL lysozyme (Roth, Germany) and 25 U/mL DNaseI (AppliChem, Germany). Cell disruption was continued according to the manufacturers' specifications obtaining the soluble fraction with dissolved ADH-A. 200 µL reaction mixture (including enzyme solution) were prepared for measurement of ADH-A activity and contained 50 mM Tris buffer (pH 8, RT), 100 mM 2,5-hexanedione, and 0.5 mM NADH (biomol, Germany). By addition of the enzyme solution the reactions were initiated, thereby, applying appropriate enzyme solution amounts to ensure linear decreases of NADH absorbance over 1 min at least. One unit (U) was defined as the amount of enzyme converting 1 µmol cofactor per min.

5.3. Results & Discussion

5.3.1. Development of the instrumentation

The here used measurement setup is a modification of an earlier developed system, the so called Enzyme Test Bench [4, 9]. It combines an optical on-line monitoring system for cultivations and reactions in microtiter plates with a special system for temperature regulation.

The temperature control unit is depicted in Fig. 5.1. It is similar to the heat transfer block of the Enzyme Test Bench for oxygen consuming reactions described by Rachinskiy et al. [9]. During experiments the MTP (side and top views in Fig. 5.1-A) is covered by a perspex frame (side and top views in Fig. 5.1-B) with an inlet and an outlet for aeration. The thermostating block (side and top views in Fig. 5.1-C) is mounted on top. It includes radiators which fit exactly within the well interspaces. Thus, the wells are jacketed by these radiators providing efficient heat transfer between the thermostating block and the MTP wells. The heat transfer properties of the system were specified before [4]. The whole system itself was placed in a temperature controlled environment. To minimize the evaporation, a gas permeable seal is fixed between the MTP and the perspex frame. In this foil a pattern in the radiators' shape is cut. Additionally, the aeration gas is passed through five bubble columns to saturate it with water vapor. A sectional view (A-A-cut in Fig. 5.1-A) of the MTP attached with the perspex frame and thermostating block is shown in Fig. 5.1-D.

The original thermostating block described by Rachinskiy et al. was designed to ensure a homogeneous temperature distribution over the microtiter plate [9]. Contrary to that, in this work the aim was to create a temperature gradient. For this purpose, the thermostating block has two water circulation systems instead of one, each with a separate thermostat (Fig. 5.1-C). If operated at different temperatures a certain temperature profile can be imposed onto the MTP just by heat conductance through the aluminium block (Fig. 5.1-A).

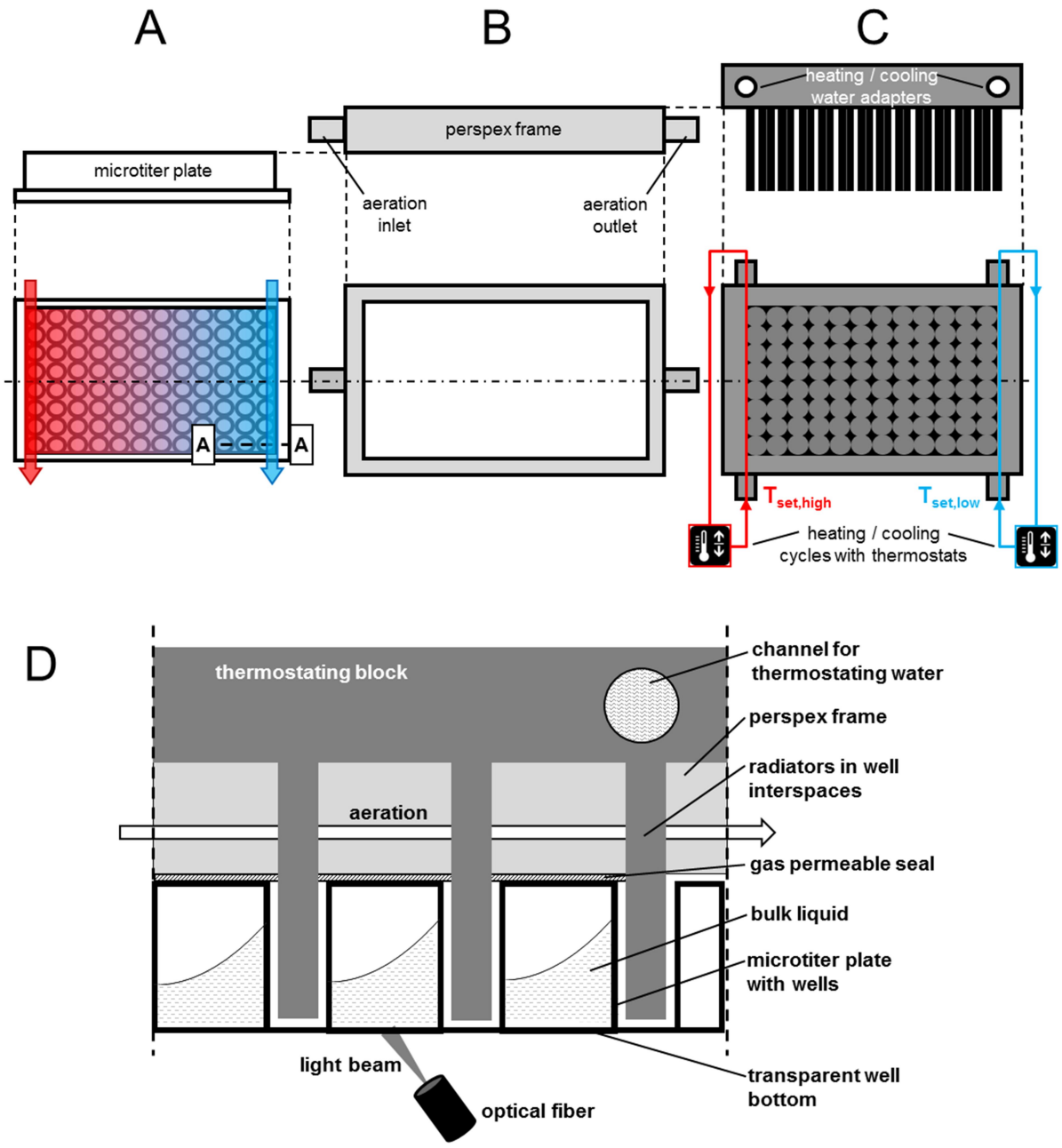

Fig. 5.1 - Scheme of the temperature control unit for temperature profiling in microtiter plates (MTP). (A) Side view on the MTP and top view with schematic illustration of thermostating water flows (arrows) and resulting temperature profile. (B) Side and top view on the perspex frame for aeration (C) Side view on the thermostating block and bottom view with schematic illustration of the heating (red) and cooling (blue) water circulation and their two respective thermostats. $T_{set,high}$ and $T_{set,low}$ stand for thermostat set point temperatures for heating and cooling water, respectively. (D) Cut A-A-view (see Fig. 5.1-A) on the microtiter plate with attached thermostating block and optical measurement.

The advantage of the thermostating block mounted on top of the MTP, compared to systems working e.g. with electrical micro-heaters [9, 23, 34, 36] is that the transparent MTP bottom is still available for optical measurements. The applied on-line monitoring system (indicated by the optical fiber and light beam in Fig. 5.1-D) is similar to the BioLector technique presented before [24]. Thereby, the equipped fluorescence spectrometer allows measurements at different wavelengths. With this setup, microbial growth (via scattered light) or the formation of various fluorescent components is continuously followed in microtiter plates without interruption of the shaking process.

5.3.2. Optical temperature determination in MTPs

To characterize the behavior of microbial or enzymatic systems at different temperatures it is necessary to know the specific temperature in each single well. Equipping each well with a temperature sensor requires a very high degree of instrumentation. Just by using a temperature dependent fluorophore measurements can easily be done with the optical on-line monitoring system. In this work a combination of the fluorescent dyes Rhodamin B (RhB) and Rhodamin 110 (Rh110) was applied, where RhB is the temperature sensitive compound, whereas Rh110 acts as a reference. This measuring principle was described before [21]. In Fig. 5.2-A the fluorescence intensity of both dyes depending on the temperature is shown. Therefore, the thermostating block was tempered only by one thermostat to ensure a constant temperature distribution over the whole MTP. Thermostat set point temperatures from 5-95°C were adjusted. After each temperature shift (dotted vertical lines) the experimental conditions remained unchanged until both fluorescence signals showed constant values. The RhB signal decreases in a step like manner since its fluorescence intensity is decreasing with increasing temperature. After each temperature shift the fluorescence signal drops sharply before it remains constant when the temperature reaches its equilibrium. On the contrary, the

fluorescence intensity of Rh110 is almost constant over the whole time. The slight decrease is due to a bleaching effect which is known to happen to RhB as well. To obtain a reliable measuring signal, the ratio of both fluorescence intensities was calculated [21].

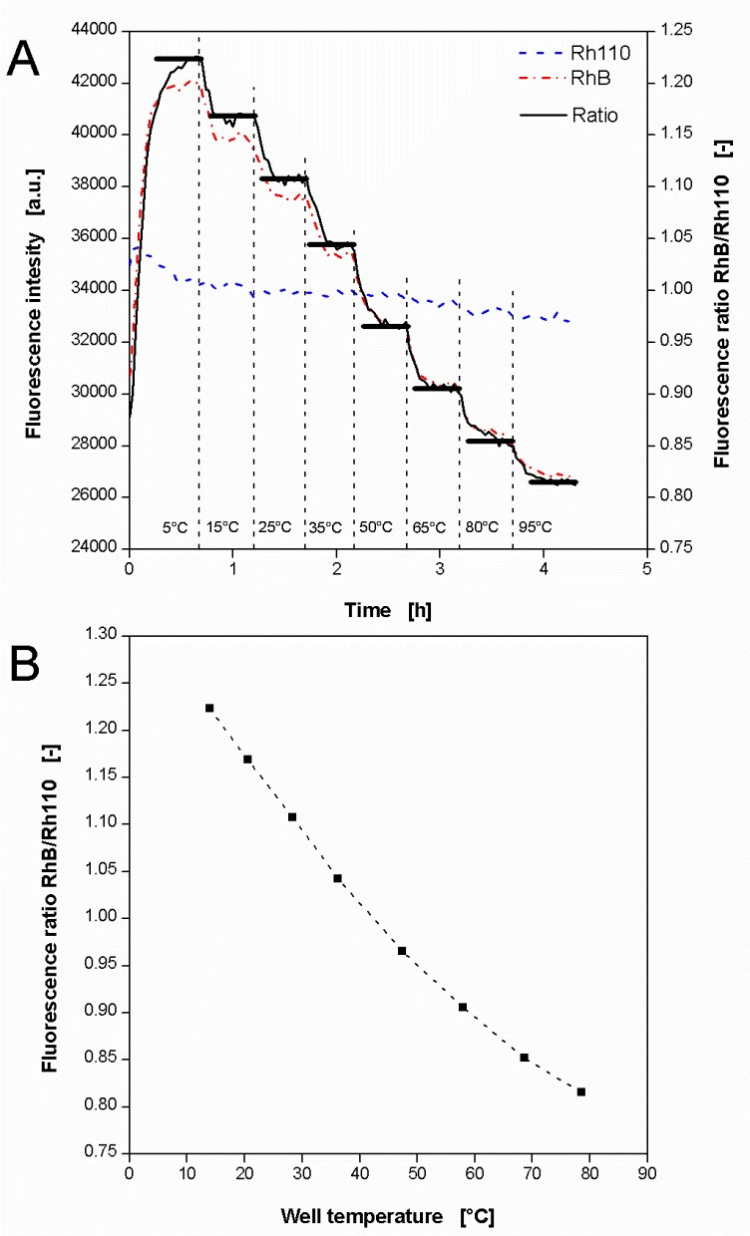

Fig. 5.2 - Optical temperature measurement in MTPs applying a fluorescent assay with the dyes Rhodamin B and Rhodamin 110. (A) Progress of the fluorescence signals of Rhodamin B (RhB) and Rhodamin 110 (Rh110) and their calculated ratio in a single well with varied thermostat set point temperature. Contrary to Fig. 5.1-C heating and cooling circulation systems were operated with one thermostat. (B) Calibration curve of the well temperature (measured via PT100 thermometer) vs. the fluorescence ratio RhB/Rh110. Experimental conditions: 96well MTP, V_L=200 µL, n=995 rpm, d_0=3 mm, RT=37°C.

It must be considered that the thermostat set point temperatures in Fig. 5.2-A and the actual temperatures in the MTP's wells are not identical since heat may be lost to the environment. For this reason, one well was equipped with an in-house constructed PT100 temperature sensor. In this way, the corresponding well temperatures for various RhB/Rh110 ratios were determined. In Fig. 5.2-B the resulting calibration curve is depicted. It is described by a polynomial equation of second degree applying MS Excel. The fluorescence ratios are average values of five measurements in one well. The maximum relative standard deviation was 0.4 %. For further investigation of the measuring accuracy the heating block temperature, as well as the room temperature, was adjusted to 37°C. In this way, a constant temperature of 37°C in each well could be assumed. The regarding measurement of all 96 wells revealed an average value of 37°C with a maximum of 38.7°C and a minimum of 35.6°C. The standard deviation was 0.76°C. The reason for the deviation from well to well cannot be explained completely. Slight deviations in the properties of the transparent microtiter plate bottom are possible which may influence the optical signals. A systematic position effect could be excluded during the experiments.

5.3.3. Temperature profiles

The optical temperature measuring method was then used to characterize the temperature distribution over microtiter plates at varied set point temperatures of the heating and cooling thermostat ($T_{set,high}$, $T_{set,low}$) and at varied room temperature (RT). Fig. 5.3-A the exemplary temperature profile for $T_{set,low}$ of 5°C, $T_{set,high}$ of 50°C and a RT of 30°C is depicted. As expected, the profile shows a clear gradient from the warm right side (column 1) to the cold left side (column12). The highest measured well temperatures were found in the wells A-D of column 1 (T_{max}= 36.2-36.9°C), the lowest values in the wells A-F of column 12 (T_{min}= 20.4-20.8°C). The rest of the wells cover the whole temperature range between T_{min} and T_{max}. Even

though not every MTP row shows exactly the same temperature gradient, a certain repetitive trend can be observed.

By varying the thermostat set temperatures the profile can be shifted to higher or lower temperature ranges. A decrease of $T_{set,high}$ to 40°C results in a temperature range of 17.7-30.3°C, showing that the change of only one set point temperature has influence on both, T_{min} and T_{max} (comp. Fig. 5.3-A and B). This is not surprising since the temperature gradient in the thermostating block itself is strongly dependent on the two set point temperatures of the heating and cooling cycle.

The room temperature has a strong influence to the temperature profile, too. Its increase from 30°C to 37°C resulted in a higher temperature range (comp. Fig. 5.3-A and C). T_{min} increased from 20.4 to 28.0°C, T_{max} from 36.9 to 39.9°C. This effect is mainly attributed to the MTP's bottom which is thermally completely exposed to the environment. Hence, there is a large heat exchange area. This cannot be avoided, e.g. by insulation, because the transparent bottom needs to be accessible for the optical measurement. On the other hand, this effect might be beneficial by making the RT an additional temperature control parameter.

Fig. 5.3-D and E show further profiles at higher temperature levels. By setting the thermostat temperatures to 5 and 60°C, respectively, well temperatures of 30.3-47.3°C can be realized (Fig. 5.3-D). To characterize even thermophilic microbial or enzymatic systems a $T_{set,high}$ of 95°C was chosen (Fig. 5.3-E). In this way a profile with T_{max} of 64.5°C was achieved. T_{min} was 42.1°C. It must be considered that under these conditions the cryostat was not able anymore to ensure a set point temperature of 5°C since the cooling water heated up to much while passing through the thermostating block. To work under defined conditions $T_{set,low}$ was increased to 10°C.

In all determined profiles it is obvious that T_{min} and T_{max} differ strongly from $T_{set,low}$ and $T_{set,high}$, respectively. This is due to heat losses in the temperature control system. Some heat transfer might occur from the tubes of the circulation system. Measurements show that this loss is rather low, e.g. for the profile in Fig. 5.3-C with $T_{set,low}$ of 5°C and $T_{set,high}$ of 50° the temperatures before entering the block were 5.2°C and 49.3°C, respectively. This proves that the tube insulation worked properly. On the contrary, the current version of the thermostating block has no special insulation to the environment. It can be assumed that the exposed aluminum surface is mainly responsible for the observed temperature differences. The non-insulated MTP bottom is responsible for additional heat dissipation as discussed above. The results in Fig. 5.3-F support this argument. Compared to the profile in Fig. 5.3-D the MTP was not shaken during the measurement. Interestingly, the differences between the set point temperatures $T_{set,low}$ and $T_{set,high}$ and the regarding minimal and maximal temperatures T_{min} and T_{max} are smaller. This results in a broader well temperature range of 22.2-51.3°C (comp. Fig. 5.3-D, 30.3-47.3°C). The phenomenon can be explained by a ventilation effect caused by shaking of the MTP. While an insulating air layer may be generated below a non-shaken MTP decreasing the environment's influence, this layer may be lost when the plate starts moving. Nonetheless, for most processes sufficient shaking is absolutely necessary due to mixing and mass transfer requirements.

For all profiles shown in Fig. 5.3 a slight temperature gradient over the MTP rows (A-H) was observed apart from the intended one over the MTP columns. This is not surprising since the heating water enters the thermostating block closest to well A1, such as the cooling water enters closest to well A12. While passing through the block the heating water gets colder and the cooling water warms up. For the profile in Fig. 5.3-C the heating water's temperature decreased by 1.2 K from entry to exit, whereas the cooling water got 0.5 K warmer. Of course these values will differ from one profile to another.

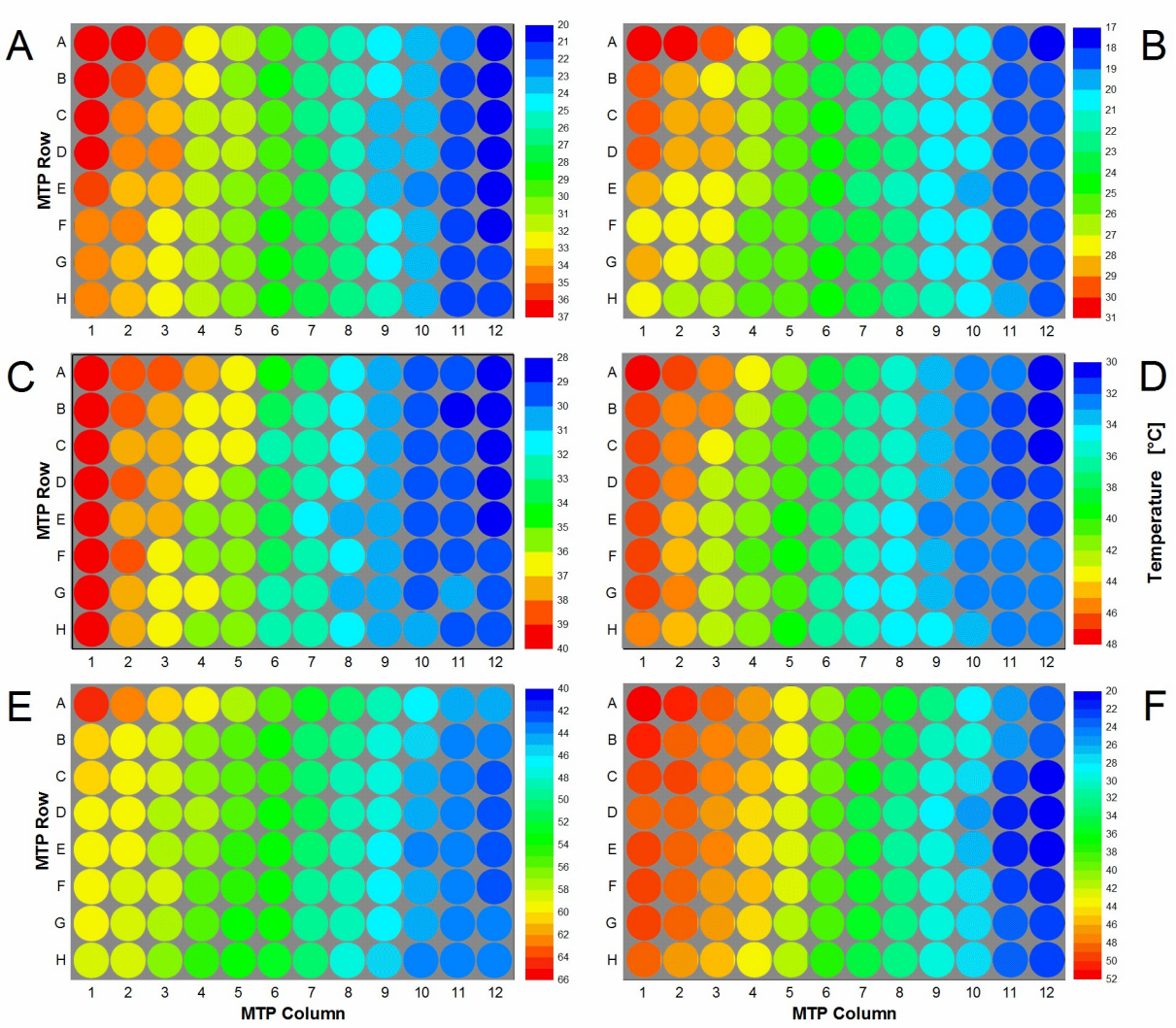

Fig. 5.3 - Exemplary temperature profiles in MTPs at varied room temperature and thermostat set point temperatures. (A) RT=30°C, $T_{set,low}$=5°C, $T_{set,high}$=50°C, n=995 rpm. (B) RT=30°C, $T_{set,low}$=5°C, $T_{set,high}$=40°C, n=995 rpm. (C) RT=37°C, $T_{set,low}$=5°C, $T_{set,high}$=50°C, n=995 rpm. (D) RT=37°C, $T_{set,low}$=5°C, $T_{set,high}$=60°C, n=995 rpm. (E) RT=37°C, $T_{set,low}$=10°C, $T_{set,high}$=95°C, n=995 rpm. (F) RT=37°C, $T_{set,low}$=5°C, $T_{set,high}$=60°C, n=0 rpm. Note: Temperature scale differs from A to F for better visualization of temperature profiles. Experimental conditions: 96well MTP, V_L=200 µL, d_0=3 mm.

5.3.4. Temperature dependence of microbial systems

In the following experiments the information from the temperature profiles (Fig. 5.3) was used to investigate several microbial systems in order to find optimal conditions for biomass formation or recombinant protein expression. Microbial growth (via scattered light) and the formation of fluorescent proteins was followed on-line applying the BioLector technique. To ensure that really the temperature is the limiting factor during the cultivation it was necessary to exclude other limitations. Previous studies showed that the applied media allow non-limiting growth [27, 28, 31]. A critical factor is the oxygen supply. For the applied shaking conditions (200 µL filling volume, 995 rpm shaking frequency, 3 mm shaking diameter) and aeration with pressurized air a maximum oxygen transfer capacity of approx. 0.03 mol L^{-1} h^{-1} was determined (data not shown). This value differs among media depending on their oxygen solubility and diffusion coefficient [32-34]. However, *E. coli* grown in rich medium at 37°C may require maximum oxygen transfer capacities up to 0.1 mol L^{-1} h^{-1} (data not shown). To realize such high transfer rates the aeration was shifted from pressurized air to pure oxygen. In this way, almost the 5-fold maximum oxygen transfer capacity can be achieved and cultivations without oxygen limitation are warranted for all applied media and microorganisms.

An *E. coli* strain expressing a fluorescent model protein (FbFP) as product was investigated (Fig. 5.4). Non-induced (MTP row A,C,E,G) and induced (MTP row B,D,F,H) cultivations were performed in parallel in one MTP. The temperature profile was essentially identical to Fig. 5.3-D. The results of 12 (out of 48) exemplary non-induced cultures in TB medium are shown in Fig. 5.4-A. All cultures begin immediately with their exponential growth without any *lag* phase. After 1 h the curves start spreading indicating different growth rates at different temperatures. The lowest rate is observed at the lowest temperature of 30.3°C. Higher temperatures lead to increased growth rates indicated by steeper curves. The maximum growth rate occurs at temperatures of 41.4-45.3°C. A further increase retarded the

microbial growth again. Due to varied growth rate the time point for reaching the stationary phase differs as well. At 41.4°C the culture became stationary after 4.5 h, whereas it needed twice as long at 30.3°C. Comparing the final scattered light intensities, it can be seen that slightly more biomass was formed at lower temperatures. This might be explained by a higher energy demand for cell maintenance at higher temperatures which withdraws metabolic resources from growth [35]. It was already found that organisms growing at temperatures above their optimal growth temperature show lower cell yields. Thereby, it was postulated that biosynthetic reactions at high temperatures do not keep pace with catabolic reactions [36].

Exemplary curves for growth and product formation under induced conditions are depicted in Fig. 5.4-B and C, respectively. The auto-induction medium OnEx was used which works as follows: glucose is the preferred carbon source and represses recombinant protein expression to ensure undisturbed initial growth. After glucose depletion lactose is taken up and acts as the inducer of the expression system. Glycerol is an additional energy source. The scattered light curves reflect the medium's working principle (Fig. 5.4-B) which was studied before in detail [37]. For all cultures a short *lag* phase (~0.5 h) is followed by a small exponential increase in the scattered light signal after 1.5 h. In this time glucose is consumed allowing undisturbed growth without product formation. As observed for the non-induced cultivations (Fig. 5.4-A) the temperature has no influence on the initial behavior of the cells. After the first exponential growth phase the scattered light signal remains at a constant level indicating no further growth. The reason for this is the induction by lactose after glucose depletion. The recombinant protein expression causes a metabolic burden to the cells and inhibits the microbial growth. After a certain time the biomass signal starts increasing again resulting in a second exponential growth phase. From earlier studies it is known that *E. coli* cultures can recover from the metabolic burden after lactose depletion [37]. The duration of the inhibition phase differs over the curves. It is shortest at 40.9-42.7°C and extends at higher and lower

temperatures. This might be explained with accelerated lactose consumption at the temperatures which are most beneficial for the host organism. Consequently, the cells can recover earlier and grow further on the residual glycerol in the medium. For temperatures higher than 38°C the scattered light curves show an unexpected decrease after their maximum value. The reason for this is not yet clear. Morphological changes of the cells when entering the stationary phase might be one explanation [38]. Another could be related to inclusion body formation. It is known that higher temperatures promote protein precipitation in cells [39]. Additionally, there are reports about the influence of inclusion bodies to the cell's light scatter [40, 41]. Further flow cytometric investigations should be performed to finally clarify this issue. The corresponding product formation was followed by fluorescence measurement (Fig. 5.4-C). After 3 h all cultures started producing the fluorescent protein FbFP and, subsequently, showed a continuous increase of the fluorescence signal. The curve's slope depends on the temperature with the strongest increase at 40.9-42.7°C indicating the highest production rate. As a consequence, the maximum FbFP fluorescence is reached in the shortest time after 9 h. The slowest culture is found at 30.9°C reaching its maximum fluorescence after 17-18 h. These times correlate very well with the biomass signal (Fig. 5.4-B) which indicates that product formation stops with entering the stationary phase. Additionally, not only the production rate differs among the temperatures, but the maximum product concentration, too. The highest level is observed again at 40.9°C revealing the optimal temperature for FbFP production combining the maximum production rate and product concentration.

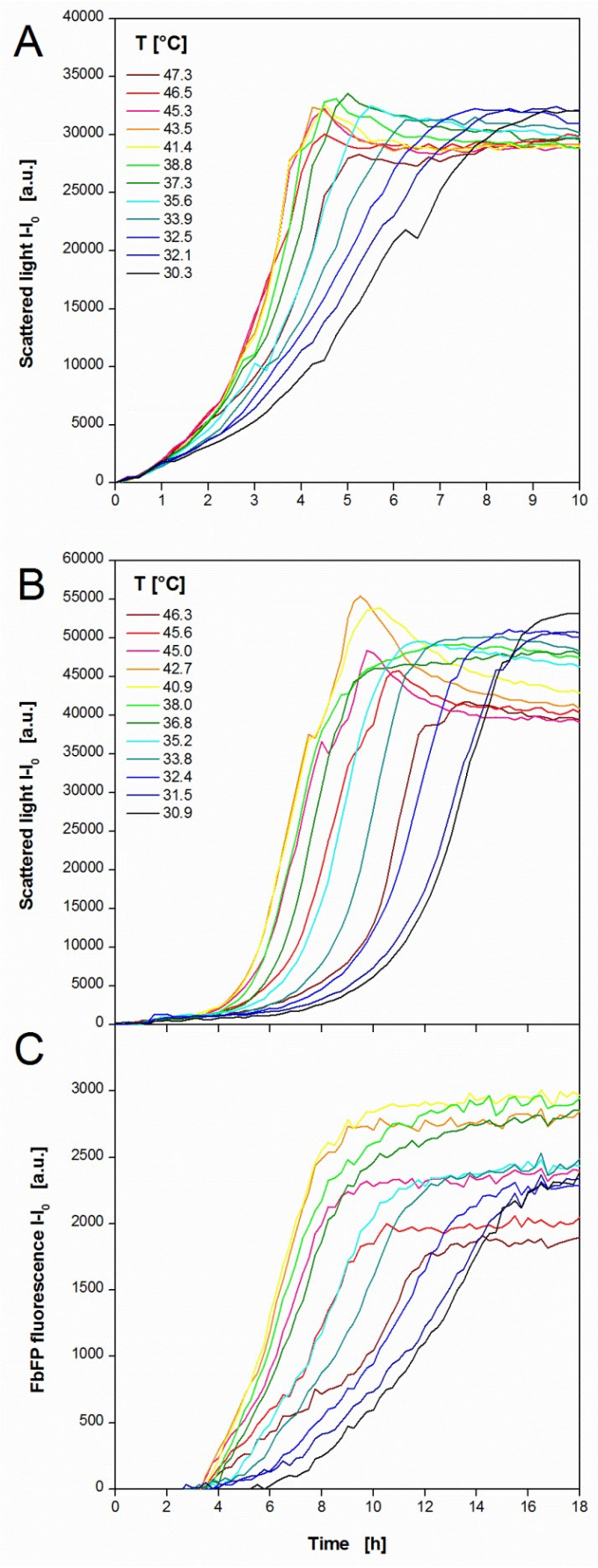

Fig. 5.4 - Cultivation of *E.coli* BL21 expressing the fluorescent protein FbFP applying a temperature profile in a MTP. (A) Cultivation and online monitoring of microbial growth (via scattered light) in complex TB medium without induction. (B) Cultivation and online monitoring of microbial growth and (C) fluorescent protein formation in complex auto-induction OnEx. Culture conditions: 96well MTP, V_L=200 µL, n=995 rpm, d_0=3 mm, aeration with 100% oxygen. Temperature profile: RT=37°C, $T_{set,low}$=5°C, $T_{set,high}$=60°C (comp. Fig. 5.3-D). Data of 12 (from 48) exemplary wells.

As a further microbial system the yeast *K. lactis* expressing GFP as product was investigated (Fig. 5.5). Again, non-induced (MTP row A,C,E,G) and induced (MTP row B,D,F,H) cultivations were performed in parallel in one MTP. The temperature profile was essentially identical to Fig. 5.3-A. The results of 12 exemplary non-induced cultures in YP medium containing glucose as carbon source are shown in Fig. 5.5-A. Contrary to *E. coli*, the cultures show a temperature dependent *lag* phase. The minimum *lag* time of 2 h was observed at 27.2-33.8°C. During the subsequent exponential growth phase also the highest growth rates occur at those temperatures. Shifts to higher or lower temperatures lead to extended lag phases and reduced growth rates. As already observed for *E. coli*, the time point for reaching the stationary phase differs from 9-18 h due to the temperature dependent *lag* phase and growth rate. Again, the final scattered light intensities are higher at lower temperatures as already discussed for *E. coli*.

Contrary to *E. coli*, the growth behavior of *K. lactis* under induced conditions is not much different from that under non-induced conditions (comp. Fig. 5.5-A and B). The substitution of glucose by galactose as carbon source and inducer affects the microbial growth insignificantly. The *lag* phase, the growth rate, and the final biomass concentration show the same temperature dependent behavior as observed for the non-induced *K. lactis* cultures. The product formation shows a slightly different trend (Fig. 5.5-C). All GFP fluorescence signals increase continuously from the beginning. The strongest increase indicating the highest production rate is observed at 31.0-34.9°C meaning that the GFP expression rather than microbial growth favors higher temperatures. Also the final product concentration increases with rising temperature. The reason for the further increase of the GFP fluorescence in stationary phase observed for 34.1 and 34.9°C is yet unclear. A concentration effect due to increased evaporation cannot explain this phenomenon. The determination of the filling volume after the cultivation revealed relatively low volume decreases of 1.1, 4.5, and 7 % at 20.8, 31.0, and 34.9°C, respectively. For this reason, evaporation was not taken into

consideration. Higher temperatures may provoke cell lysis in the stationary phase. As a result free GFP may induce brighter fluorescence in the medium without the barrier of the yeast's cell wall and membrane. Further studies, e.g. by applying flow cytometry, could help to clarify this effect.

For cultivation media it is known that temperature changes may result in pH changes as well, hence, two process parameters are unintendedly varied at once. This might lead to distorted results. The buffers used within this work show rather low changes within the applied temperature profiles with a maximum pH change of 0.2 (0.013 K^{-1}). But for more sensitive systems this effect should be considered by adapting the initial pH to the regarding temperature.

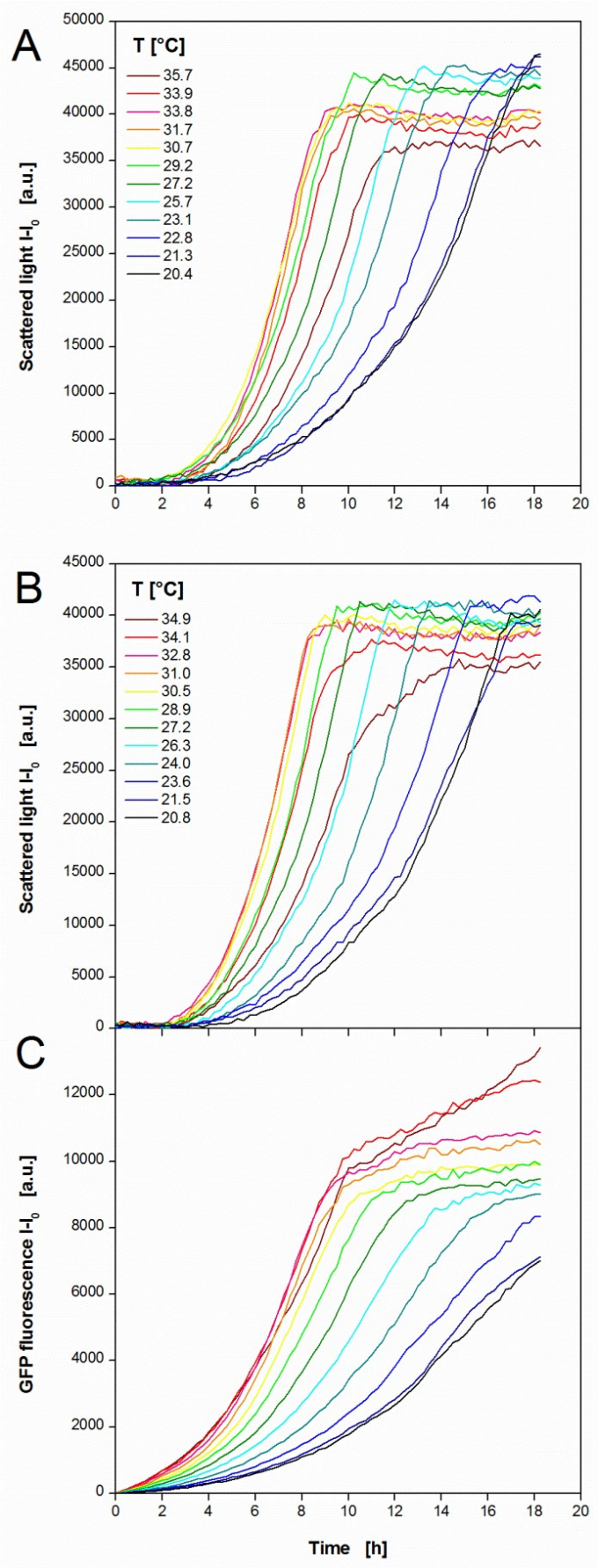

Fig. 5.5 - Cultivation of *K. lactis* GG799 expressing the fluorescent protein GFP applying a temperature profile in a MTP. (A) Cultivation and online monitoring of microbial growth (via scattered light) without induction in complex YP medium containing 20 g/L glucose. (B) Cultivation and online monitoring of microbial growth and (C) fluorescent protein formation in complex YP medium containing 20 g/L galactose as substrate and inducer. Culture conditions: 96well MTP, V_L=200 µL, n=995 rpm, d_0=3 mm, aeration with 100% oxygen. Temperature profile: RT=30°C, $T_{set,low}$=5°C, $T_{set,high}$=50°C (comp. Fig. 5.3-A). Data of 12 (from 48) exemplary wells.

From the before described data sets (Fig. 5.4 and Fig. 5.5) it is already possible to get an idea of the temperature optima for microbial growth and product formation in yeast and bacterial cells. But the high throughput of the MTP yields sufficient data for a more detailed characterization. For biomass formation the maximum growth rate under non-induced conditions was chosen as temperature dependent parameter (Fig. 5.6-A). As expected, the bacterial and the yeast system show a different behavior. *E. coli* in rich TB medium has a maximum growth rate of 0.41 h^{-1} at 43°C. The highest growth rate determined for *K. lactis* in rich YP medium is 0.16 h^{-1} at 32-33°C. In addition, the growth of *E. coli* in the mineral Wilms-MOPS medium was investigated. Compared to the growth in rich TB medium, a higher maximum growth rate of 0.67 h^{-1} was determined but at a lower temperature of 39.5°C. The observed values are in good agreement with earlier studies about *E. coli* [42-45] and *Kluyveromyces* strains [35, 46, 47]. For the product formation the maximum product fluorescence (indicator for product concentration) and the maximum space time yield were exemplary chosen as characteristic values (Fig. 5.6-B and C). Again differences between the microbial systems and cultivation media occur. *K. lactis* has the maximum product fluorescence and highest STY in the same range of 34-35°C which is slightly higher than the temperature for optimal growth. *E. coli* expressing FbFP in the rich auto-induction medium OnEx shows constant high fluorescence values over a relatively broad range from 35-42°C before it drops sharply at higher temperatures. The regarding maximum STY was determined at 41°C. For FbFP production in the mineral auto-induction medium the highest values for fluorescence and STY are observed at 44°C and 40-45°C, respectively.

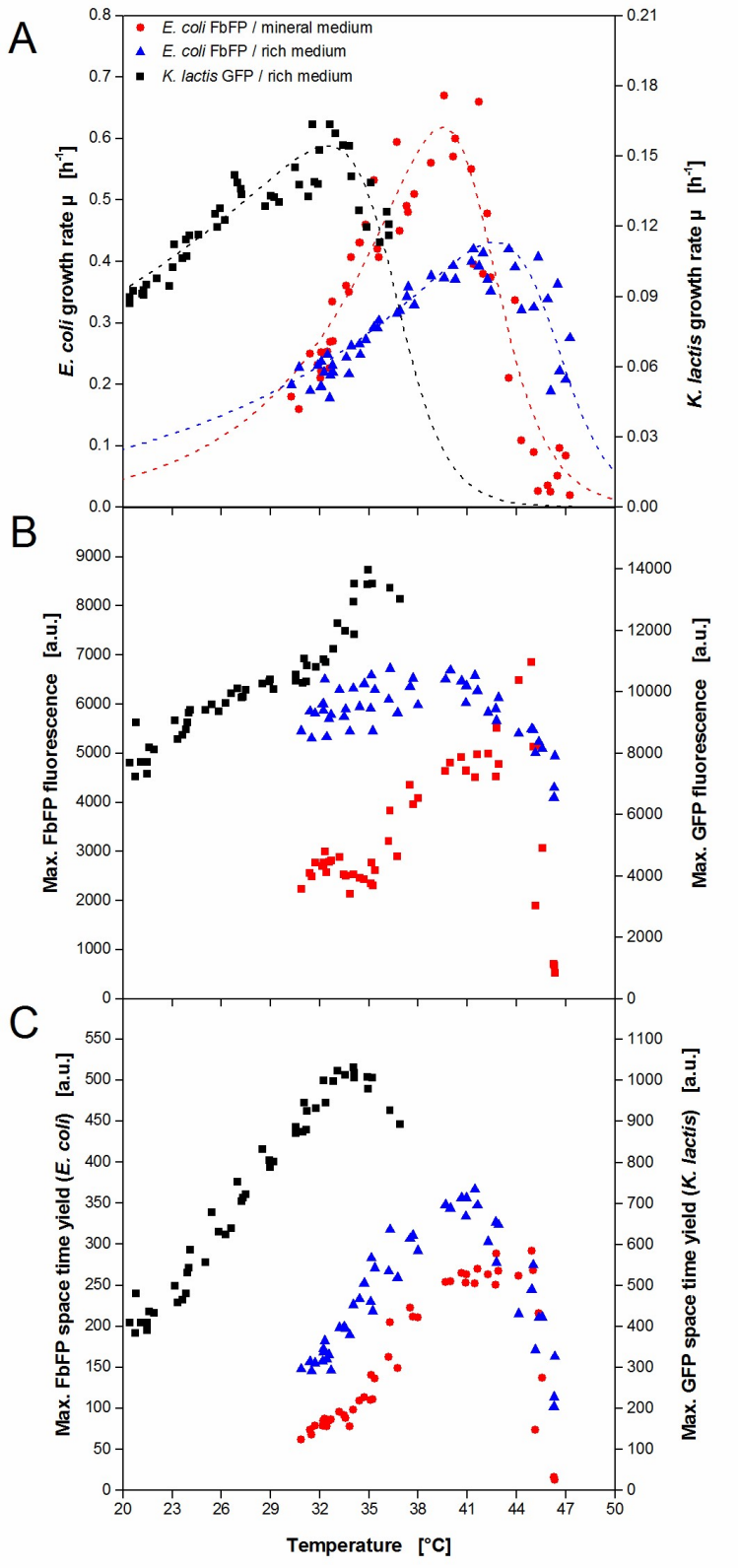

Fig. 5.6 - Determination of the optimal temperature for microbial growth and product formation of *E.coli* and *K. lactis* resulting from temperature profile experiments in MTPs. (A) Temperature dependent growth rate of *E.coli* (in rich and mineral medium) and *K. lactis* (in rich medium) under non-induced conditions. Temperature dependent maximum product formation (B) and maximum STY (C) of *E.coli* producing FbFP (in rich and mineral medium) and *K. lactis* producing GFP (in rich medium) under induced conditions. Dotted lines in A indicate Arrhenius fits due to Eq. 5.1.

An overview of all determined temperature optima is given in Tab. 5.2. The optima for growth and product formation are not in agreement for some of the investigated expression systems. Interestingly, even the medium composition has an influence. Compared to the standard cultivation temperatures of 30 and 37°C for *K. lactis* and *E. coli*, respectively, the determined optima differ to some extent. Consequently, an individual temperature screening is recommended guided by the desired aim of the process.

Tab. 5.2 - Temperature optima for growth and recombinant protein expression of *E. coli* (in rich and mineral medium) and *K. lactis* (in rich medium) under non-induced (ni) and auto-induced (ai) conditions.

Expression system	**Temperature optimum**		
	growth	*product concentration*	*product STY*
E. coli (rich medium)	42°C^{ni}, 43°C^{ai}	35-42°C^{ai}	41°C^{ai}
E. coli (mineral medium)	40.5°C^{ni}, 41.5°C^{ai}	43-44°C^{ai}	40-45°C^{ai}
K. lactis (rich medium)	32°C^{ni,ai}	35°C^{ai}	34°C^{ai}

It is noticed that the measuring points in Fig. 5.6 show some scattering indicating certain measurement inaccuracies. The fluorescence thermometry method has a standard deviation of ±0.76 K (see chapter Temperature profiles) which might be one explanation. Furthermore, it should be considered that the temperature profiles were determined in separate experiments without the microbial reaction system. It was assumed that no significant changes are encountered during cultivations, thereby, neglecting the possibility of produced reaction heat. In future studies, it should be investigated how fluorescence thermometry can be used directly in the reaction system in order to realize temperature real time monitoring. Nonetheless, the high number of measuring points compensates these disadvantages and gives a clear trend.

A typical procedure to describe the temperature dependent behavior of microorganisms and (bio-)catalysts is the Arrhenius plot. An extended version of the Arrhenius equation was used for mathematical modeling (Eq. 5.1).

$$v_{max} = \frac{A\, exp(-E_g/RT)}{1 + B\, exp(-\Delta G_d/RT)} \qquad \text{(Eq. 5.1)}$$

Thereby, the numerator is the classical Arrhenius equation with the numerical constant A and the activation energy E_g describing the typical increase of the growth rate or catalyst activity with increasing temperatures. Assuming that proteins are temperature-denatured and inactivated by a reversible chemical reaction with free energy change (ΔG_d), the nominator describes the behavior beyond the temperature optimum due to the Hougen-Watson expression for catalyst activity [25]. In Fig. 5.7 the data from Fig. 5.6-A for the microbial growth of *E. coli* and *K. lactis* was plotted logarithmically over the reciprocal absolute temperature.

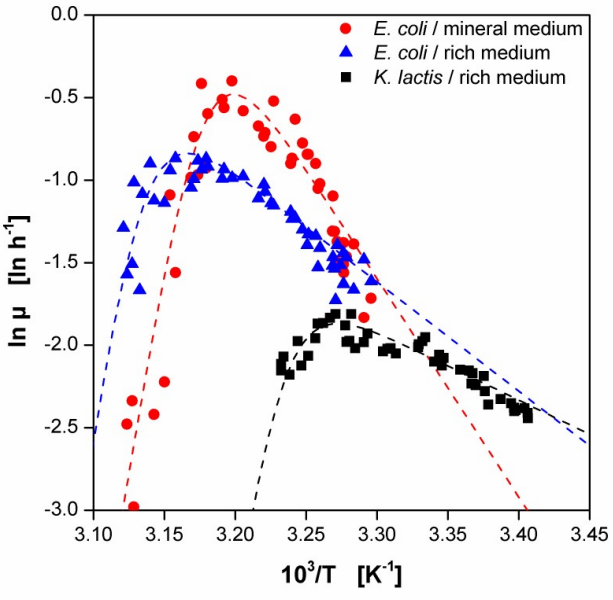

Fig. 5.7 - Characterization of the temperature dependent growth behavior of *E.coli* and *K. lactis* applying the Arrhenius plot. Temperature dependent growth rates of *E.coli* (in rich and mineral medium) and *K. lactis* (in rich medium) under non-induced conditions (comp. Fig. 5.6-A). Dotted lines indicate Arrhenius fits according to Eq. 5.1.

By solving Eq. 5.1 in MS Excel, the parameters for the different investigated microbial systems were determined (Tab. 5.3). The model fit for *E. coli* in rich TB medium reveals an activation energy of 55 kJ mol^{-1} which is in very good agreement with earlier reports [42-44]. Interestingly, *E. coli* in the mineral Wilms-MOPS medium shows a much higher value compared to that in TB medium. *K. lactis* shows a lower value of 34.5 kJ mol^{-1}. Literature values for *Kluyveromyces* strains range from 36.6 to 85.2 kJ mol^{-1} [35, 46, 47]. In contrast to the activation, the deactivation behavior indicated by ΔG_d is similar for all organisms and media.

Tab. 5.3 - Arrhenius model parameters in Eq. 5.1 for the yeast *K. lactis*, the bacterium *E. coli* and the cellulase preparation Celluclast

Parameter		*E. coli* (TB medium)	*E. coli* (Wilms-MOPS)	*K. lactis* (YP medium)	Celluclast
E_g	[kJ mol^{-1}]	55	110	34.5	29
ΔG_d	[kJ mol^{-1}]	549	548	539	579
A	[h^{-1}]	$6 \cdot 10^{8}$	$1.85 \cdot 10^{18}$	$1.3 \cdot 10^{5}$	$1.2 \cdot 10^{4}$
B		$7 \cdot 10^{89}$	$9 \cdot 10^{90}$	$9 \cdot 10^{90}$	$8 \cdot 10^{90}$

As an additional expression system *E. coli* producing a recombinant alcohol dehydrogenase A from *Rhodococcus ruber* (ADH-A) was investigated regarding its temperature behavior. In order to look at a broader temperature range, two experimental sets were performed applying a low and a high temperature profile according to Fig. 5.3-B and D, respectively. In this way, temperatures of 18.1-46.3°C were realized. To avoid excess evaporation at higher temperatures the cultivation was aborted after 20 h when all cultures had entered the stationary phase. The low temperature profile was applied for 27 h. The biomass formation was followed on-line by scattered light measurement (Fig. 5.8-A). As discussed before, the typical growth behavior of *E. coli* in the auto-induction medium OnEx is observed at

temperatures of 27.6-39.7°C. After a temperature dependent *lag* phase of 2-4.5 h a first exponential growth is observed. The subsequent growth inhibition indicated by decreasing slopes of the scattered light curves after 4-7 h was caused by the metabolic burden of recombinant ADH-A expression. As seen for *E. coli* expressing FbFP this growth inhibited production phase takes longer at lower temperatures, e.g. 2 h at 39.7°C and 4 h at 27.6°C. When cells recover from that metabolic load a second exponential increase occurs before the stationary phase is reached. At temperatures below 27.6°C the microbial growth becomes more linear so that product formation is not the prior growth inhibitor, but the temperature. At temperatures higher than 39.7°C almost no growth is detected.

Indicator for the product formation was the volumetric ADH-A activity at the end of the cultivation (Fig. 5.8-B). An on-line signal was not available and sampling during the cultivation was not possible. Furthermore, the cell suspensions of three wells had to be pooled to have sufficient volume for the enzyme activity assay. Thereby, the information about the respective well temperature was beneficial for combining wells of similar temperature. The results of the MTP experiments show a clear trend of increasing volumetric enzyme activities with decreasing temperatures. Maximum values of 7.4 U mL^{-1} were measured at 20-28°C. At the highest temperatures of 42.3 and 45.5°C no product activity was detected. This correlates very well with the on-line biomass signal where almost no growth occurred in this temperature range (comp. Fig. 5.8-A). Taking growth and product formation results together into consideration, a certain trend becomes obvious. Higher temperatures (if not too high) favor bacterial growth but reduce product formation, whereas, at low temperatures the behavior is vice versa. The reference values from the shake flask cultivations do not completely reflect the MTP results. Nevertheless, a similar trend is present with increasing volumetric ADH-A activities at lower temperatures. The maximum activity of 8.5 U mL^{-1} was determined at 22°C.

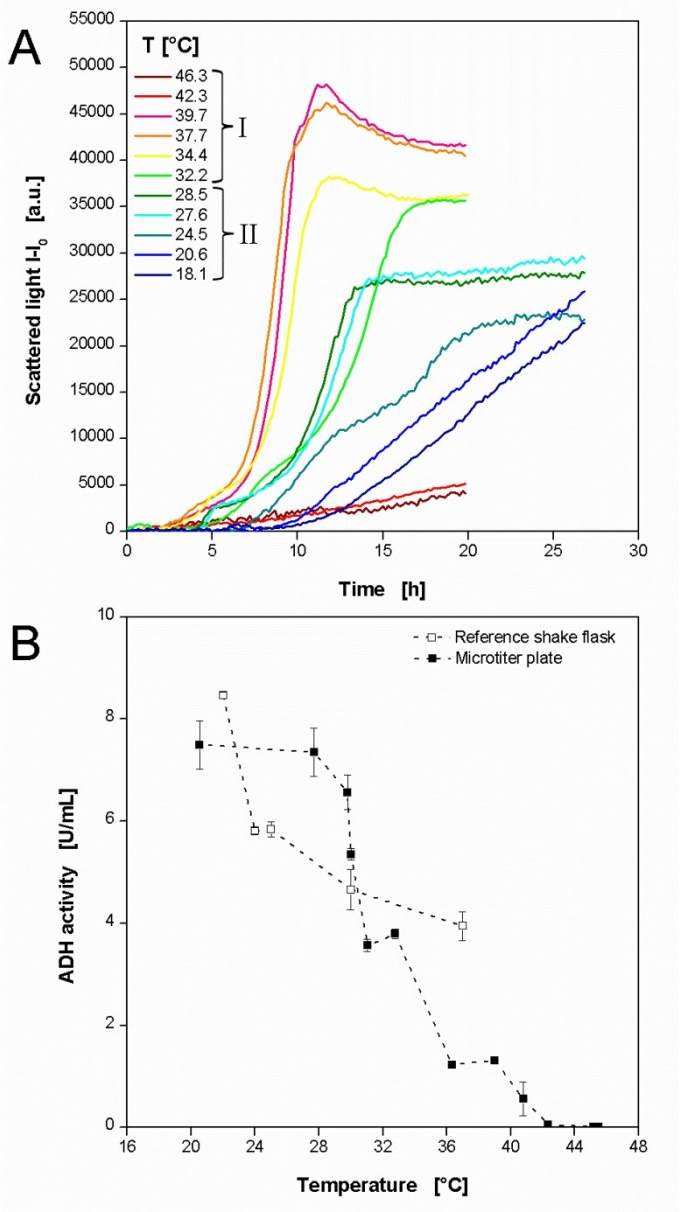

Fig. 5.8 - Cultivations of *E.coli* BL21 expressing the recombinant enzyme ADH-A applying 2 temperature profiles in MTPs. (A) Cultivation and online monitoring of microbial growth (via scattered light) in complex auto-induction medium OnEx. (B) Temperature dependent volumetric activity at the end of the cultivation in the MTP. Reference values from additional cultivations in shake flasks at different temperatures. Culture conditions: 96well MTP, V_L=200 µL, n=995 rpm, d_0=3 mm, aeration with 100% oxygen. Temperature profile I for T=32.2-46.3°C: RT=37°C, $T_{set,low}$=5°C, $T_{set,high}$=60°C (comp. Fig. 5.3-D); Temperature profile II for T=18.1-28,5°C: RT=30°C, $T_{set,low}$=5°C, $T_{set,high}$=40°C (comp. Fig. 5.3-B). Reference cultivation: 250 ml shake flask, V_L=10 mL, n=350 rpm, d_0=50 mm, aeration with air. Online data of 10 exemplary wells.

All these investigations of different microorganisms, expression systems and culture media show how the presented high-throughput temperature profiling helps to find optimal conditions for fermentations. The on-line monitoring feature allows a much more detailed insight to the microbial processes at varied temperature than classical end point analysis, e.g. kinetic parameters such as growth and production rates or space time yields.

5.3.5. Temperature dependence of cellulases

As a candidate for the optimization of enzymatic reactions the commercial cellulase cocktail Celluclast was chosen since it is often used for biomass degradation. The Celluclast cocktail contains a mixture of several cellulases from the fungus *Trichoderma reesei* [48]. In order to follow the enzyme reaction on-line, a substrate, namely 4-methylumbelliferyl-β-D-cellobioside (4MUC), was used. It releases the fluorescent dye 4-methylumbelliferone (4MU) when hydrolyzed by cellulases which can be easily detected with a fluorescence spectrometer. Consequently, the 4MUC assay is commonly used for the high-throughput screening of cellulolytic enzymes [49]. Compared to the microbial systems described before, a higher temperature optimum was expected for the cellulases. Consequently, a profile was chosen providing a higher temperature range of 42-65°C (comp. Fig. 5.3-E).

Twelve exemplary curves resulting from the 4MUC hydrolysis by Cellucalst are depicted in Fig. 5.9-A, whereby, the fluorescence intensity indicates the formation of the product 4MU. For all conditions the typical course of enzymatic reactions is observed with a strong increase of the product concentration in the beginning which runs into saturation after a certain time when no substrate is available anymore. The reaction is strongly temperature dependent. The highest reaction rates are observed at 53.2-56.2°C. Consequently, these curves run into saturation already after approx. 3 h. Furthermore, the highest final product concentrations occur at these temperatures. In the temperature ranges above and below reduced reaction rates

and extended reaction times for complete substrate conversion are observed. Pure substrate showed a constant signal close to 0 a.u., thereby, proving that no substrate reacted in the absence of enzyme. In order to quantify the cellulolytic reaction, the 4MU fluorescence signal was calibrated assuming that each cleaving of a 4MUC molecule releases one 4MU molecule (Fig. 5.9-B). In this way reaction rates as well as final product concentrations can be calculated.

To evaluate the temperature dependent behavior, the initial reaction rate was chosen as indicator and plotted over the respective temperature (Fig. 5.9-C). A maximum initial rate of 0.295 mmol h^{-1} was determined at 55°C. At the lowest checked temperature of 42°C an initial reaction rate of 0.19 mmol h^{-1} was found, close to 0.17 mmol h^{-1} at the highest temperature. A complete enzyme deactivation was not achieved. The optimum temperature is in good agreement with other reports about cellulases [3, 50, 51]. As for microbial systems, the corresponding Arrhenius plot was plotted from these results (Fig. 5.9-D). By fitting the curve in MS Excel, the parameters in Eq. 5.1 for Celluclast were determined (Tab. 5.2). It must be considered, that Celluclast is no single cellulase but a mixture of endoglucanases (EG), cellobiohydrolases (CBH) and β-glucosidases (BG). In literature E_g values of 20-32 KJ mol^{-1} for EGs [52-54], 18-45 KJ mol^{-1} for CBHs [3, 55], and 18-59 KJ mol^{-1} for BGs [55, 56] are reported. The here reported value of 29 KJ mol^{-1} is within these ranges.

It can be stated that the presented high-throughput temperature profiling is a useful tool for enzyme characterization. The technique can easily be applied to other enzyme classes as long as fluorescent assays are available. If necessary, the temperature range can be shifted to either higher or lower levels. Sufficient aeration can be assured as discussed for microbial cultivations. With all these presented features the system allows the investigation of a great variety of biocatalysts: psychro-, meso- or thermophilic; oxygen dependent or not.

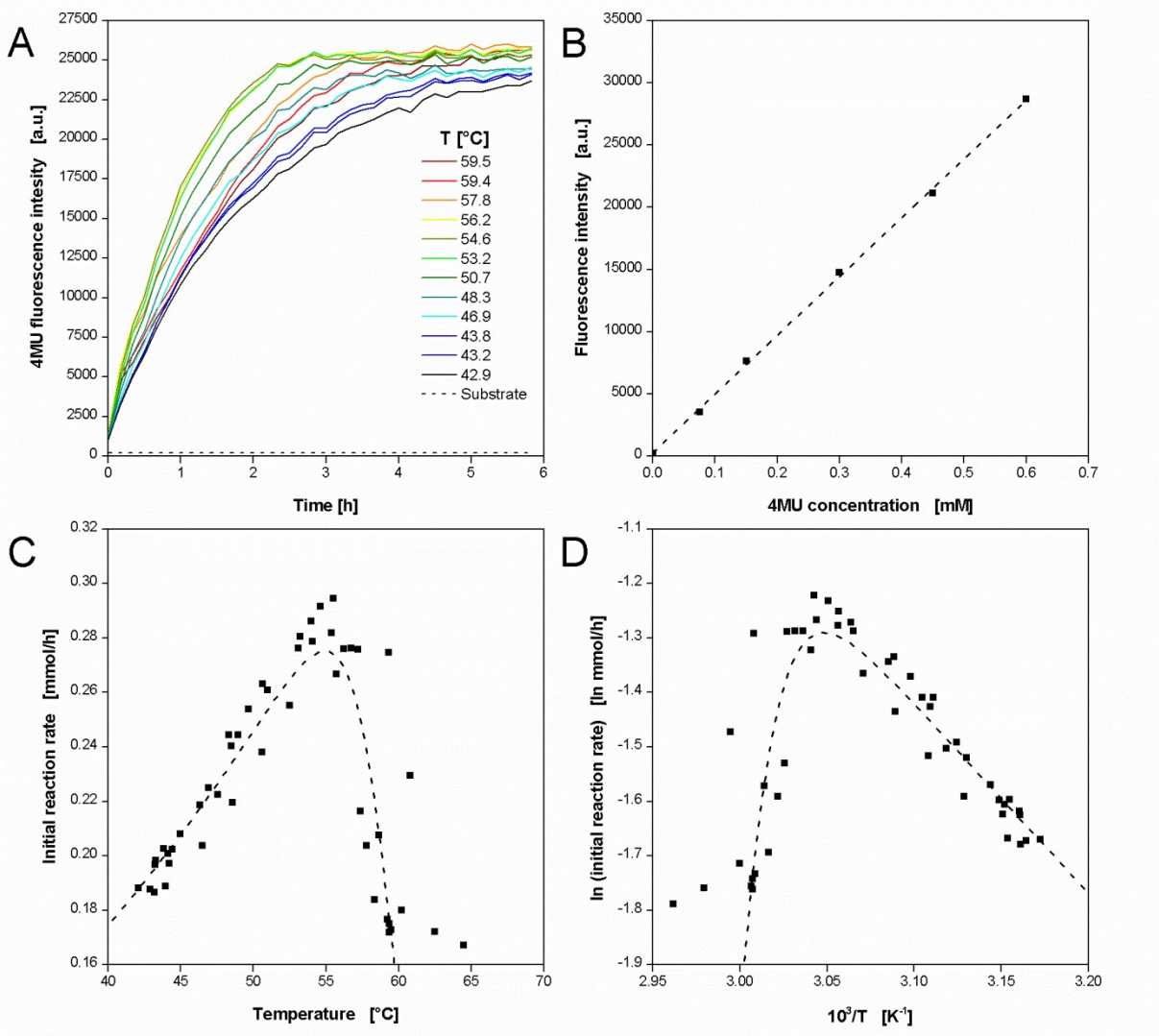

Fig. 5.9 - Enzymatic hydrolysis of 4-methylumbelliferyl-ß-D-cellobioside (4MUC) with cellulase from *T. reseei* (Celluclast) applying a temperature profile in a MTP. (A) Progresses of 4-methyl-umbelliferyl (4MU) fluorescence (λ_{ex}=365 nm, λ_{em}=455 nm) during the hydrolysis of 4MUC at different temperatures. Online data of 12 (from 48) exemplary wells. (B) Calibration curve for fluorescence intensity at varied 4MU concentration. (C) Temperature dependent initial reaction rate and (D) resulting Arrhenius plot of Celluclast. Dotted lines indicate Arrhenius fit. Experimental conditions: 96well MTP, V_L=200 µL, n=995 rpm, d_0=3 mm, 1 g/L Celluclast and 0.6 mM 4MUC in 0.1 M acetate buffer, pH=4.8. Temperature profile: RT=37°C, $T_{set,low}$=10°C, $T_{set,high}$=95°C (comp. Fig. 5.3-E).

5.4. Conclusion

Running bioprocesses at their temperature optima is essential for their economical operation. Unfortunately, systems for rapid determination of temperature dependent behavior are rare. The presented high-throughput screening system for temperature optimization faces this challenge. A novel temperature control system with a customized thermostating block and two thermostats can generate individual temperature profiles in MTPs with relatively simple instrumentation. Three controlling parameters were identified: $T_{set,high}$, $T_{set,low}$ and RT. For temperature measurement a fluorescent assay with two Rhodamin dyes was established for the use in MTPs which allows the convenient determination of temperature profiles in short time. Applying the high-throughput screening system BioLector which is already commercially available, important process parameters, e.g. biomass and product formation, are monitored on-line. The high throughput of the MTP provides sufficient data output for a detailed characterization of temperature dependent behavior. Consequently, the combination of the thermostating block, temperature determination via fluorescence thermometry, and an optical on-line monitoring system provides extensive information about temperature dependent process behavior, e.g. concentrations of biomass or products, growth or reaction rates, space time yields, and others. Representative investigations with microbial and enzymatic systems proved the system's general applicability for various purposes. Thereby, the repetition of the temperature profiles in the MTP rows allows the investigation of several systems in parallel.

During the experiments some potential for improvement became apparent, considering heat dissipation to the surroundings, temperature dependent pH changes, evaporation effects, and sufficient oxygen supply. All these issues can be addressed in future work to achieve most precise results.

The MBR-based high-throughput temperature profiling is a convenient tool for rapid characterization of temperature dependent reaction processes. It allows the fast investigation of numerous conditions, e.g. microorganisms, enzymes, media, and others, in a short time. The simple temperature control combined with a commercial on-line monitoring device makes it a user friendly system.

5.5. Nomenclature

Abbreviations

4MU	4-methylumbellyferone
4MUC	4-methylumbellyferyl.cellobioside
ADH-A	Alcohol dehydrogenase A from *Rhodococcus ruber*
BG	β-glucosidase
CBH	Cellobiohydrolase
EG	Endoglucanase
FbFP	Flavinmononucleotide-based fluorescent Protein
GFP	Green fluorescent protein
MBR	Micro-bioreactor
MTP	Microtiter plate
OD_{600}	Optical density at 600 nm
OnEx	OvernightExpress Instant TB medium
OTR	Oxygen transfer rate
RAMOS	Respiration activity monitoring device
Rh110	Rhodamin 110
RhB	Rhodamin B
RT	Room temperature
TB	Terrific broth medium
YP	Yeast peptone medium

Symbols

A	Numerical constant	$[h^{-1}]$
B	Numerical constant	[-]
E_g	Activation energy	$[kJ\ mol^{-1}]$
I	Measured signal intensity	[a.u.]
I_0	Initial signal intensity	[a.u.]
R	Ideal gas constant ~8.314	$[J\ mol^{-1}\ K^{-1}]$
STY	Space time yield	$[a.u.\ mL^{-1}\ h^{-1}]$
T	Absolute temperature	[K]
T_{max}	Maximum temperature within a temperature profile	[°C]
T_{min}	Minimum temperature within a temperature profile	[°C]
$T_{set,high}$	Set point temperature of heating thermostat	[°C]
$T_{set,low}$	Set point temperature of cooling thermostat	[°C]
ΔG_d	Deactivation energy change	$[kJ\ mol^{-1}]$
μ	Growth rate	$[h^{-1}]$
μ_{max}	Maximum growth rate	$[h^{-1}]$
v_{max}	Maximum reaction rate	$[h^{-1}]$

5.6. References

1. Shuler ML, Kargi F: *Bioprocess engineering : basic concepts.* 2nd edn. Upper Saddle River, NJ: Prentice Hall; 2002.

2. Dragosits M, Frascotti G, Bernard-Granger L, Vazquez F, Giuliani M, Baumann K, Rodriguez-Carmona E, Tokkanen J, Parrilli E, Wiebe MG, et al: Influence of growth temperature on the production of antibody fab fragments in different microbes: A host comparative analysis. *Biotechnology Progress* 2011, 27:38-46.

3. Pardo AG, Forchiassin F: Influence of temperature and pH on cellulase activity and stability in Nectria catalinensis. *Rev Argent Microbiol* 1999, 31:31-35.

4. Rachinskiy K, Schultze H, Boy M, Bornscheuer U, Büchs J: "Enzyme Test Bench," a high-throughput enzyme characterization technique including the long-term stability. *Biotechnology and Bioengineering* 2009, 103:305-322.

5. Zakhartsev MV, Portner HO, Blust R: Environmentally low-temperature kinetic and thermodynamic study of lactate dehydrogenase from Atlantic cod (G-morhua) using a 96-well microplate technique. *Analytical Biochemistry* 2004, 330:10-20.

6. Schäpper D, Alam MN, Szita N, Eliasson Lantz A, Gernaey KV: Application of microbioreactors in fermentation process development: a review. *Anal Bioanal Chem* 2009, 395:679-695.

7. Vervliet-Scheebaum M, Ritzenthaler R, Normann J, Wagner E: Short-term effects of benzalkonium chloride and atrazine on Elodea canadensis using a miniaturised microbioreactor system for an online monitoring of physiologic parameters. *Ecotoxicology and Environmental Safety* 2008, 69:254-262.

8. van Leeuwen M, Heijnen JJ, Gardeniers H, Oudshoorn A, Noorman H, Visser J, van der Wielen LAM, van Gulik WM: A system for accurate on-line measurement of total gas consumption or production rates in microbioreactors. *Chemical Engineering Science* 2009, 64:455-458.

9. Rachinskiy K, Kunze M, Graf C, Schultze H, Boy M, Büchs J: Extension and Application of the ‘‘Enzyme Test Bench’’ for Oxygen Consuming Enzyme Reactions. *Biotechnology and Bioengineering* 2014, 111:244-253.

10. Zanzotto A, Szita N, Boccazzi P, Lessard P, Sinskey AJ, Jensen KF: Membrane-aerated microbioreactor for high-throughput bioprocessing. *Biotechnology and Bioengineering* 2004, 87:243-254.

11. Zhang ZY, Grattan KTV, Palmer AW: Fiber optic thermometry based on fluorescence lifetimes of Cr-3+ doped materials. *Second International Symposium on Measurement Technology and Intelligent Instruments, Pts 1 and 2* 1993, 2101:476-482.

12. Hoogenboom R, Fijten MWM, Brandli C, Schroer J, Schubert US: Automated parallel temperature optimization and determination of activation energy for the living cationic polymerization of 2-ethyl-2-oxazoline. *Macromolecular Rapid Communications* 2003, 24:98-103.

13. Krommenhoek EE, van Leeuwen M, Gardeniers H, van Gulik WM, van den Berg A, Li X, Ottens M, van der Wielen LA, Heijnen JJ: Lab-scale fermentation tests of microchip with integrated electrochemical sensors for pH, temperature, dissolved oxygen and viable biomass concentration. *Biotechnology and Bioengineering* 2008, 99:884-892.

14. Lee HLT, Boccazzi P, Ram RJ, Sinskey AJ: Microbioreactor arrays with integrated mixers and fluid injectors for high-throughput experimentation with pH and dissolved oxygen control. *Lab on a Chip* 2006, 6:1229-1235.

15. Maharbiz MM, Holtz WJ, Howe RT, Keasling JD: Microbioreactor arrays with parametric control for high-throughput experimentation. *Biotechnology and Bioengineering* 2004, 85:376-381.

16. Li X, van der Steen G, van Dedem GWK, van der Wielen LAM, van Leeuwen M, van Gulik WM, Heijnen JJ, Krommenhoek EE, Gardeniers JGE, van den Berg A, Ottens M: Improving mixing in microbioreactors. *Chemical Engineering Science* 2008, 63:3036-3046.

17. Boccazzi P, Zhang Z, Kurosawa K, Szita N, Bhattacharya S, Jensen KF, Sinskey AJ: Differential gene expression profiles and real-time measurements of growth parameters in Saccharomyces cerevisiae grown in microliter-scale bioreactors equipped with internal stirring. *Biotechnology Progress* 2006, 22:710-717.

18. Liu LY, Peng SL, Niu XZ, Wen WJ: Microheaters fabricated from a conducting composite. *Applied Physics Letters* 2006, 89.

19. Yamamoto T, Nojima T, Fujii T: PDMS-glass hybrid microreactor array with embedded temperature control device. Application to cell-free protein synthesis. *Lab on a Chip* 2002, 2:197-202.

20. Fernicola VC, Zhang ZY, Grattan KTV: Investigation of Cr-fluorescence in olivine crystals with potential in fibre optic thermometry. *Sensors and Their Applications Viii* 1997:367-372.

21. Sakakibara J, Adrian RJ: Whole field measurement of temperature in water using two-color laser induced fluorescence. *Experiments in Fluids* 1999, 26:7-15.

22. Sun T, Zhang ZY, Grattan KTV, Palmer AW, Collins SF: Temperature dependence of the fluorescence lifetime in Pr3+:ZBLAN glass for fiber optic thermometry. *Review of Scientific Instruments* 1997, 68:3447-3451.

23. Kensy F, Zang E, Faulhammer C, Tan RK, Buchs J: Validation of a high-throughput fermentation system based on online monitoring of biomass and fluorescence in continuously shaken microtiter plates. *Microbial Cell Factories* 2009, 8.

24. Samorski M, Müller-Newen G, Büchs J: Quasi-continuous combined scattered light and fluorescence measurements: A novel measurement technique for shaken microtiter plates. *Biotechnology and Bioengineering* 2005, 92:61-68.

25. Roels JA: *Energetics and kinetics in biotechnology.* Amsterdam ; New York: Elsevier Biomedical Press; 1983.

26. Scheidle M, Klinger J, Buchs J: Combination of on-line pH and oxygen transfer rate measurement in shake flasks by fiber optical technique and Respiration Activity Monitoring System (RAMOS). *Sensors* 2007, 7:3472-3480.

27. Wilms B, Hauck A, Reuss M, Syldatk C, Mattes R, Siemann M, Altenbuchner J: High-cell-density fermentation for production of L-N-carbamoylase using an expression system based on the Escherichia coli rhaBAD promoter. *Biotechnology and Bioengineering* 2001, 73:95-103.

28. Hahn-Hagerdal B, Karhumaa K, Larsson CU, Gorwa-Grauslund M, Gorgens J, van Zyl WH: Role of cultivation media in the development of yeast strains for large scale industrial use. *Microbial Cell Factories* 2005, 4.

29. Anderlei T, Büchs J: Device for sterile online measurement of the oxygen transfer rate in shaking flasks. *Biochemical Engineering Journal* 2001, 7:157-162.

30. Anderlei T, Zang W, Papaspyrou M, Büchs J: Online respiration activity measurement (OTR, CTR, RQ) in shake flasks. *Biochemical Engineering Journal* 2004, 17:187-194.

31. Losen M, Frolich B, Pohl M, Buchs J: Effect of oxygen limitation and medium composition on Escherichia coli fermentation in shake-flask cultures. *Biotechnology Progress* 2004, 20:1062-1068.

32. Duetz WA, Witholt B: Effectiveness of orbital shaking for the aeration of suspended bacterial cultures in square-deepwell microtiter plates. *Biochemical Engineering Journal* 2001, 7:113-115.

33. Kensy F, Zimmermann HF, Knabben I, Anderlei T, Trauthwein H, Dingerdissen U, Buchs J: Oxygen transfer phenomena in 48-well microtiter plates: Determination by optical monitoring of sulfite oxidation and verification by real-time measurement during microbial growth. *Biotechnology and Bioengineering* 2005, 89:698-708.

34. Maier U, Losen M, Buchs J: Advances in understanding and modeling the gas-liquid mass transfer in shake flasks. *Biochemical Engineering Journal* 2004, 17:155-167.

35. Rajoka MI, Khan S, Latif F, Shahid R: Influence of carbon and nitrogen sources and temperature on hyperproduction of a thermotolerant beta-glucosidase from synthetic medium by Kluyveromyces marxianus. *Applied Biochemistry and Biotechnology* 2004, 117:75-92.

36. Senez JC: Some considerations on energetics of bacterial growth. *Bacteriological Reviews* 1962, 26:95-&.

37. Kunze M, Huber R, Gutjahr C, Mullner S, Buchs J: Predictive tool for recombinant protein production in Escherichia coli shake-flask cultures using an on-line monitoring system. *Biotechnology Progress* 2012, 28:103-113.

38. Kunze M, Roth S, Gartz E, Buchs J: Pitfalls in optical on-line monitoring for high-throughput screening of microbial systems. *Microb Cell Fact* 2014, 13:53.

39. Chalmers JJ, Kim E, Telford JN, Wong EY, Tacon WC, Shuler ML, Wilson DB: Effects of temperature on Escherichia coli overproducing beta-lactamase or human epidermal growth factor. *Appl Environ Microbiol* 1990, 56:104-111.

40. Hedhammar M, Stenvall M, Lonneborg R, Nord O, Sjolin O, Brismar H, Uhlen M, Ottosson J, Hober S: A novel flow cytometry-based method for analysis of expression levels in Escherichia coli, giving information about precipitated and soluble protein. *Journal of Biotechnology* 2005, 119:133-146.

41. Lavergne-Mazeau F, Maftah A, Cenatiempo Y, Julien R: Linear correlation between bacterial overexpression of recombinant peptides and cell light scatter. *Appl Environ Microbiol* 1996, 62:3042-3046.

42. Herendeen SL, Vanbogelen RA, Neidhardt FC: Levels of major proteins of Escherichia coli during growth at different temperatures. *Journal of Bacteriology* 1979, 139:185-194.

43. Johnson FH, Lewin I: The growth rate of E. coli in relation to temperature, quinine and coenzyme. *Journal of Cellular and Comparative Physiology* 1946, 28:47-75.

44. Mohr PW, Krawiec S: Temperature characteristics and Arrhenius plots for nominal psychrophiles, mesophiles and thermophiles. *Journal of General Microbiology* 1980, 121:311-317.

45. Ratkowsky DA, Olley J, Mcmeekin TA, Ball A: Relationship between temperature and growth-rate of bacterial cultures. *Journal of Bacteriology* 1982, 149:1-5.

46. Rajoka MI, Khan S, Shahid R: Kinetics and regulation studies of the production of beta-galactosidase from Kluyveromyces marxianus grown on different substrates. *Food Technology and Biotechnology* 2003, 41:315-320.

47. Toyoda T, Ohtaguchi K: Effect of temperature on D-arabitol production from lactose by Kluyveromyces lactis. *Journal of Industrial Microbiology & Biotechnology* 2011, 38:1179-1185.

48. Jäger G, Wu ZJ, Garschhammer K, Engel P, Klement T, Rinaldi R, Spiess AC, Büchs J: Practical screening of purified cellobiohydrolases and endoglucanases with alpha-cellulose and specification of hydrodynamics. *Biotechnology for Biofuels* 2010, 3.

49. Ko KC, Han Y, Cheong DE, Choi JH, Song JJ: Strategy for screening metagenomic resources for exocellulase activity using a robotic, high-throughput screening system. *J Microbiol Methods* 2013, 94:311-316.

50. Karlsson J, Siika-aho M, Tenkanen M, Tjerneld F: Enzymatic properties of the low molecular mass endoglucanases Cel12A (EG III) and Cel45A (EG V) of Trichoderma reesei. *Journal of Biotechnology* 2002, 99:63-78.

51. Krishna SH, Rao KCS, Babu JS, Reddy DS: Studies on the production and application of cellulase from Trichoderma reesei QM-9414. *Bioprocess Engineering* 2000, 22:467-470.

52. Busto MD, Ortega N, Perez-Mateos M: Characterization of microbial endo-beta-glucanase immobilized in alginate beads. *Acta Biotechnologica* 1998, 18:189-200.

53. Saqib AA, Farooq A, Iqbal M, Hassan JU, Hayat U, Baig S: A thermostable crude endoglucanase produced by Aspergillus fumigatus in a novel solid state fermentation process using isolated free water. *Enzyme Res* 2012, 2012:196853.

54. Xiao ZZ, Wang P, Qu YB, Gao PJ, Wang TH: Cold adaptation of a mesophilic cellulase, EG III from Trichoderma reesei, by directed evolution. *Science in China Series C-Life Sciences* 2002, 45:337-343.

55. Steinweg JM, Jagadamma S, Frerichs J, Mayes MA: Activation energy of extracellular enzymes in soils from different biomes. *PLoS One* 2013, 8:e59943.

56. Siddiqui KS, Saqib AAN, Rashid MH, Rajoka MI: Carboxyl group modification significantly altered the kinetic properties of purified carboxymethylcellulase from Aspergillus niger. *Enzyme and Microbial Technology* 2000, 27:467-474.

6. Summary & Outlook

The results in chapter I show that unexpected phenomena regarding non-uniform growth and protein expression are hardly detectable using conventional screening protocols. This might lead to wrong assumptions about the selection of production strains, process parameters, the optimal point of harvest and, ultimately, to wasted resources. Since screening protocols differ from working group to working group, the results found might give important hints for investigations in the field of recombinant protein expression with *E. coli*. In fact, this work gives a first mechanic understanding how respiration activity, biomass formation and recombinant protein formation interact. It allows rough predictions about the productivity of a particular clone without costly offline analysis. Furthermore, this knowledge can be used to optimize process conditions.

Up to now, the reason for the here observed phenomena is yet unclear, since there was no correlation between the expression behavior and parameters like protein size, mean net charge, isoelectric point, hydrophobicity and aliphatic index. Therefore, future investigations should also focus on the recombinant protein properties and their influence to the microbial growth and expression behavior. Furthermore, it hasn't been investigated how plasmid stability and plasmid loss under the applied conditions affects the expression result. Due to the selective pressure in a microbial culture, cells may reduce their plasmid copy number or even lose the gene of interest within the plasmid. That would shift the metabolism from production to growth due to a lower metabolic burden and, consequently, lead to lower product yields. Thus, measuring plasmid contents, e.g. by flow cytometry, could give further important information for a more detailed understanding of the respiration and expression behaviours observed in this study. In order to deal with such phenomena in a future screening process, it

might be feasible to develop a tailor-made screening protocol for each of the three different expression types.

For such screening protocols, the extended RoboLector system is a valuable tool since methods like automated media preparation, biomass specific replication and induction, as well as automated sampling and analysis help to run screenings under competitive conditions. For now, it was demonstrated in chapter II that a large variety of methods could successfully be automated on the extended RoboLector platform. This enables the robot to perform a cellulase screening experiment consisting of upstream, downstream and analysis steps. The device allows a strongly increased information content compared to screening systems reported so far. The results confirm the feasibility of a reliable and automated HTS on the robotic platform. A comparison of the manual and automated screening is certainly of great interest and will be part of upcoming experiments. Furthermore, the method spectrum shall be further extended in order to meet the increasing demands to a screening process. For example, the downstream process might be intensified by using chromatographic procedures for protein purification and buffer exchange. Depending on the target protein's properties, new analytical methods need to be developed, either activity assays for enzymes or methods for high-throughput protein quantification, e.g. chromatographic approaches or capillary gel electrophoresis. Up to now, feasibility of the system was shown only for small clone libraries consisting of maximum 96 different variants were screened in a sequenced mode. The future strategy will be the automation of the whole cellulase screening system with emphasis on the linkages between the already described automated modules and finally screen larger clone libraries in routine. Since this will cause enormous data amounts, which cannot be handled by human operators anymore, methods have to be established for automated data acquisition, analysis, and management. For this, an advanced lab information management system (LIMS) combined with bio-informatic approaches would allow the fast output of key results, the best

possible data overview and security, and, maybe most important for research issues, the recognition of certain patterns from comprehensive comparisons of data sets from numerous experiments. This might give further insights for a mechanistic understanding of bio-processes.

New shaken bioreactor systems like the BioLector as centerpiece of the RoboLector platform are simple to handle, and offer various options of optical online measurements. Thereby, the high level of parallelization and the small scale of cultures in MTPs allow economical high throughput and, hence, to screen many parameters in reasonable short time. Since the development of FPs as fluorescent tags, the tracking of cellular proteins *in-vivo* became routine. The application of all these tools significantly contributes to the understanding of bioprocesses. Nevertheless, overreliance on experimental results provided by high-throughput screening procedures applying optical on-line monitoring can mislead the ordinary user. In chapter III it was demonstrated how fluorescent proteins can influence the optical signals indicating the DOT and pH value. In summary, it should be noticed that the phenomena reported here refer to typical experiments in biotechnological labs. For this reason these aspects are highlighted in this work to make operators of such valuable systems as the BioLector aware of potential pitfalls and resulting misinterpretations. With the right methods it is possible to uncover existing problems and correct them. Besides experimental changes like the use of alternative fluorescent reporters or optical isolation of sensor spots, the mathematical correction algorithms overserved here might be directly implemented to device's data analysis software in the future to allow an automated correction. Alternatively, the correction could be done with a single software tool or integrated to a laboratory information management system (LIMS).

Running bioprocesses at their temperature optima is essential for their economical operation. Unfortunately, systems for rapid determination of temperature dependent behavior, one of the

most important process parameters, are rare. The presented high-throughput screening system for temperature optimization in chapter IV faces this challenge. The micro-bioreactor based high-throughput temperature profiling is a convenient tool for rapid characterization of temperature dependent reaction processes. It allows the fast investigation of numerous conditions, e.g. microorganisms, enzymes, media, and others, in a short time. The simple temperature control combined with a commercial on-line monitoring device makes it a user friendly system. A novel temperature control system with a customized thermostating block and two thermostats can generate individual temperature profiles in MTPs with relatively simple instrumentation. Applying the high-throughput screening system BioLector which is already commercially available, important process parameters, e.g. biomass and product formation, are monitored on-line. The high throughput of the MTP provides sufficient data output for a detailed characterization of temperature dependent behavior. Consequently, the combination of the thermostating block, temperature determination via fluorescence thermometry, and an optical on-line monitoring system provides extensive information about temperature dependent process behavior. Representative investigations with microbial and enzymatic systems proved the system's general applicability for various purposes. However, during the experiments some potential for improvement became apparent, considering heat dissipation to the surroundings, temperature dependent pH changes, evaporation effects, and sufficient oxygen supply. All these issues should be addressed in future work to achieve most precise results. Finally, measures should be taken to integrate the tool to the RoboLector platform in order to perform the temperature screening experiments fully automatic.

Appendix

A. List of Appendix Figures

B. Comparability of process conditions in RAMOS shake flasks and shaken microtiter plates

In Chapter I (2) exclusively RAMOS data are presented to demonstrate the non-uniform behavior of recombinant protein expressing *E. coli* clones. To close that gap between RAMOS derived respiration data and optical BioLector online data, systematic studies were performed to show the comparability of both cultivation systems.

1. Maximum oxygen transfer rate as comparability factor

It is possible to obtain equal cultivation conditions in microtiter plates and shake flasks. Therefore, it is important to guarantee equal maximum oxygen transfer capacity (OTR_{max}) values. This fact is especially important in case of oxygen limitation. Fig. A 1 illustrates the dependency of the OTR_{max} value in mmol/L/h on the filling volume in a 48-well Flowerplate® and a 250 mL shaking flask. In case of MTP cultivations different shaking frequencies are also displayed. Encountering all OTR_{max} values obtained for altering volumes and different shaking frequencies in a range of 700 - 1000 rpm in MTPs, a non-linear regression fit was established. The resulting equation for calculating the OTR_{max} value is:

$$OTR_{max} = 4.58 \cdot 10^{-9} \cdot V_L^{-0.7} \cdot n^{1.78} \qquad (Eq.\ A1)$$

V_L	Filling volume (per well)	[mL]
N	Saking frequency	[rpm]

Applying this equation, OTR_{max} values specific for the cultivation of E. coli BL21 (DE3) pRhotHi-2-EcFbFP in WilmsMOPS mineral medium could be calculated for any combination of shaking frequency and filling volume. Exemplary a curve for 1500 rpm and alternating filling volumes (0.6 – 1 mL) is shown in Fig. A 1. These conditions were chosen due to their relevance for following experiments. In order to measure the OTR_{max} of a system, it is

important that the oxygen partial pressure or rather the dissolved oxygen in the medium is equal to zero. Only this condition guarantees that the driving partial pressure or rather the concentration difference is greatest and the actually maximum oxygen transfer capacity can be determined. The required condition is achieved by cultivation under oxygen limitation, wherein the microorganisms consume the dissolved oxygen immediately. Fig. A 1 clearly shows that a decreasing filling volume results in an increasing OTRmax value. Additionally, an increase of the OTRmax value can be obtained by increasing the shaking frequency. From the non-linear fit for a shaking frequency of 1500 rpm for MTPs a filling volume up to 1 mL will not lead to oxygen limitation.

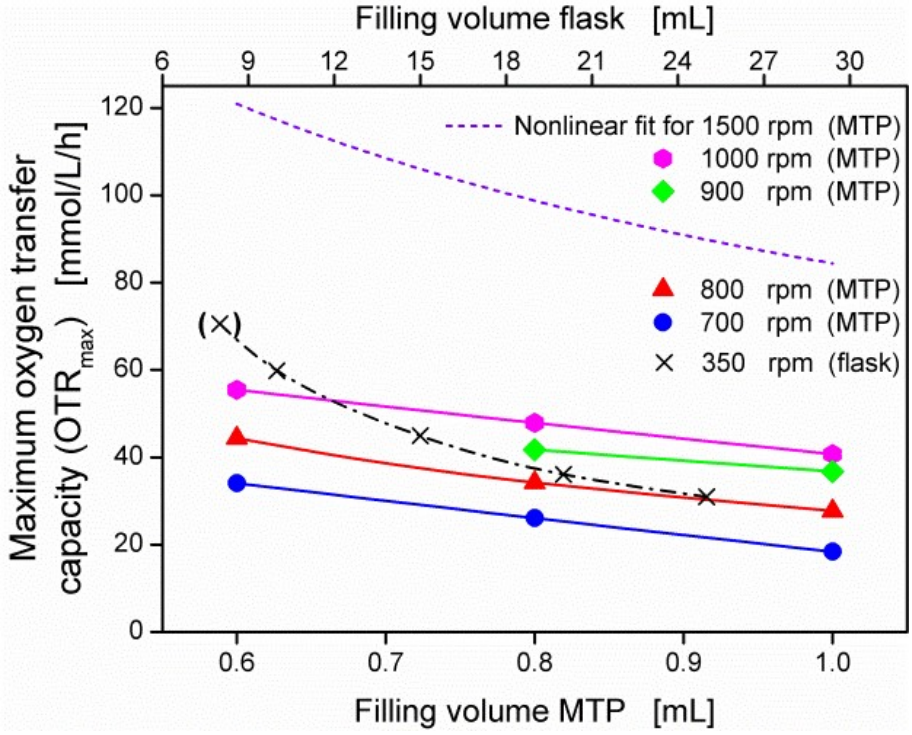

Fig. A 1 - Volume dependency of the maximum oxygen transfer capacity for *E. coli* BL21 (DE3) pRhotHi-2-EcFbFP-His$_6$ in 250 mL shake flasks and 48-well micro titer plates (Flowerplate®). Culture condition in RAMOS: Medium was supplemented with 10 g/L glucose, 250 mL RAMOS shake flasks, V_L = 8 - 25 mL, n = 350 rpm, d_0 = 50 mm, T = 37 °C. Value for 350 rpm and 8 mL is shown in brackets, because an oxygen limitation did not occur at these conditions. Culture conditions for microRAMOS: Medium was supplemented with 20 g/L glucose, 48- well Flowerplates®, V_L = 0.6 -1 mL, n = 700 - 1000 rpm, d_0 = 3 mm, T = 37 °C. To estimate the OTR_{max} values at a shaking frequency of 1500 rpm, a nonlinear fit curve, incorporating all data shown for the micro titer plate in this figure, was calculated, resulting in the following equation $OTR_{max} = 4.58 \cdot 10^{-9} \cdot VL^{-0.7} \cdot n^{1.78}$.

2. Oxygen non-limited cultivations

Fig. A 2 shows the characteristic oxygen transfer rate (OTR) curve for an oxygen unlimited *E. coli* cultivation. Herein, no plateau is visible, but an exponential increases until complete consumption of the substrate after 8 h. Due to substrate depletion, the OTR drops and after a small shoulder develops the curve results in 0 mmol/L/h. While taking a look on the dissolved oxygen tension (DOT) curve displayed in Figure 3A as well, it is proven, that the chosen cultivation conditions for MTP incubation prevent oxygen limitation. At no point a DOT value close to 0 % is reached, more accurate, throughout the cultivation a minimum of 40 % DOT was assured.

Fig. A 2 also shows how well the two cultures in RAMOS (shake flask) and BioLector (MTP) run simultaneously. While the OTR exponentially increases (4-8 h), the DOT decreases exponentially and both curves reach at the same time their maximum (65 mmol/L/h) and minimum (40 %), respectively. Furthermore, an excellent correlation between offline samples taken from separate shake flasks and the online measurements via RAMOS and BioLector is shown. A closer look at Fig. A 2C reveals the end of biomass production (OD_{600}, offline value) at the same point at which the OTR value drops. The end of the exponential biomass production was also detected online by the scattered light (S.L.) intensity. The small increases of the S.L. value after the OTR reached its maximum is most likely due to morphological changes as described earlier in this work.

Between 8.5 - 10 h decreased metabolic activity takes place, recognizable by a small OTR-shoulder with a maximum of 10 mmol/L/h. This shoulder can also be seen in the course of the DOT, which does not rise to 100 % immediately after the minimum at 8 h. Given the fact, that glucose is completely consumed at this point metabolic activity has to takes place using a different substrate. Encountering the offline data shown in Fig. A 2E it becomes clear that during the growth phase acetate was produced due overflow metabolism. Between 8 and

10.5 h the acetate gets consumed leading to the shoulder in the OTR and DOT curve. Production and consumption of acetate was also monitored by the pH value. Starting at a pH value of 7.5 it drops within 8 h to a minimum of 7.0 due to acetate production and rises again to a final value 7.1 as the acetate gets consumed. A decrease of 0.5 pH units is not solely caused by the production of 0.5 g/L of acetate. In addition, dissolved ammonium salt which acts as a kind of an alkaline is taken up by the cells and therefore removed from the medium which fosters the drop of the pH value. In Fig. A 2E the fluorescence tag signal (FbFP) is also plotted and multiplied by a factor of three for better visibility. The residual activity is so low, that it can be neglected.

3. Oxygen limited cultivations

Fig. A 2B shows the course of OTR and DOT for the oxygen limited cultivation of *E. coli* BL21 (DE3) pRhotHi-2-EcFbFP-His6. It can be easily picked up, that the DOT mirrors the curve of the OTR which indicates the simultaneous cultivation progress in both small scale systems. The exponential growth lasts from about 4 h until 7 h and is than immediately interrupted by the missing oxygen supply at an OTR value of 32 mmol/L/h. The plateau of the OTR lasts for 3 h before it decreases to 11.8 mmol/L/h and rises again to a maximum of 24 mmol/L/h and afterwards finally drops to 0 mmol/L/h.

The growth behavior is displayed in Fig. A 2D where from 4 - 7 h the OD_{600} increases exponentially followed by a linear progression until 10.5 h. After the maximum OD_{600} of 10.8 is reached a small drop occurs and afterwards remains at a level of about 9. The same trend can also be recognized for online light scattering measurement in the BioLector device. The further increase after carbon source depletion has already been discussed for oxygen unlimited conditions in a previous paragraph of this section.

The collected offline data are coherent with the metabolic activity suggestions that could be made from the course of the OTR curve. During the first 10 h glucose is consumed completely and up to 2.4 g/L acetate is produced as well as about 0.7 g/L lactate (Fig. A 2F). Due to the high concentration of overflow metabolites a diauxic growth can be observed and as such the second peak of the OTR reaches maximum value of 24 mmol/L/h. The formation of 3.1 g/L of total acid explains the drop of the pH down to 6.4. As for unlimited condition a residual fluorescence signal could be detected which is slightly higher this time but can still be neglected.

In this and the previous described experiment it is shown that parallel batch cultivations with and without oxygen limitation can go synchronous very well in the BioLector and RAMOS devices. The oxygen consumption in both systems is very similar, which is recognizable by the curves of the OTR and DOT. Offline samples from separate shake flasks give insight on the metabolic activities and support what is monitored online with OTR and DOT. This already shows that data derived from the RAMOS shake flask system and shaken microtiter plates in the BioLector can be drictly compared.

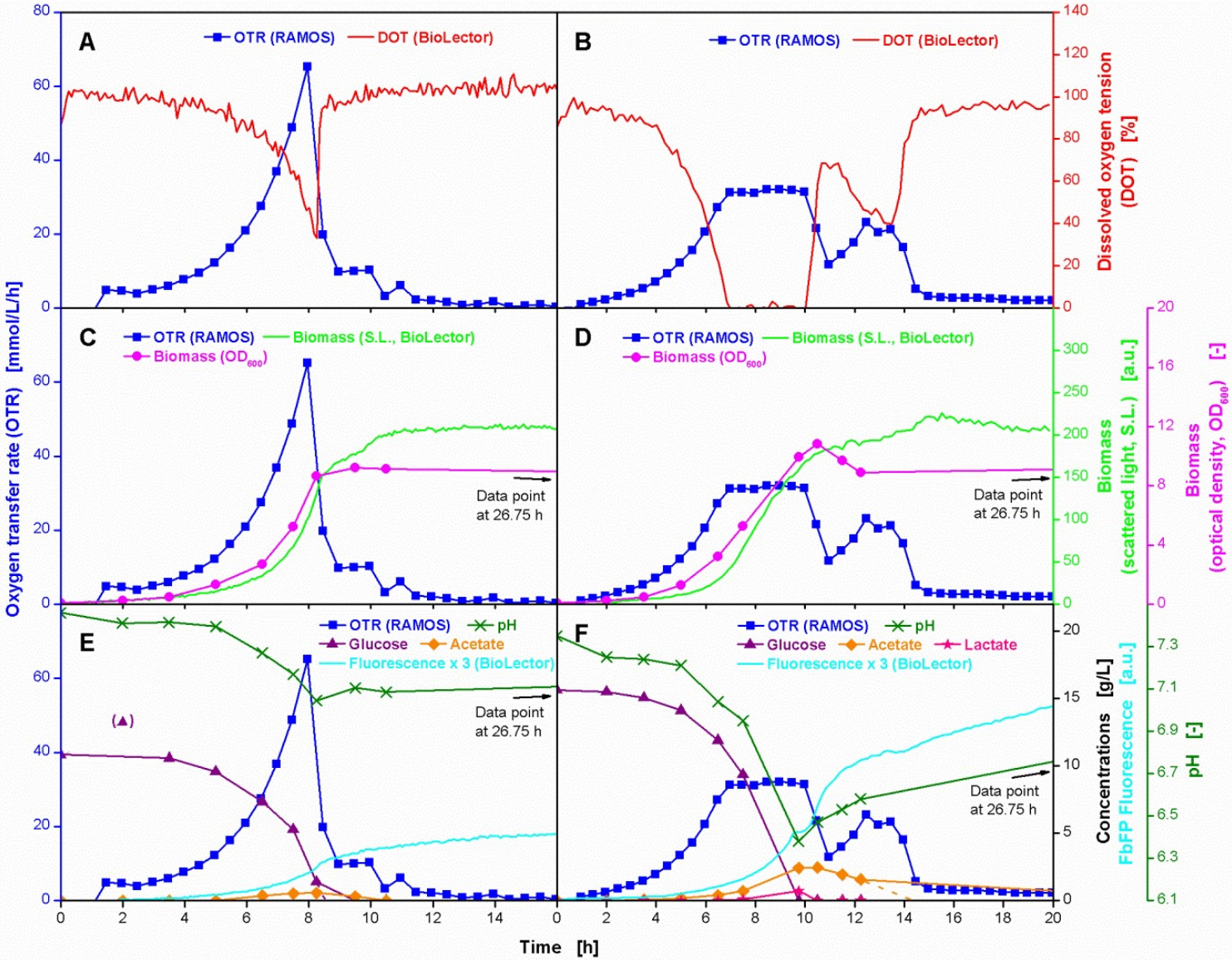

Fig. A 2 - Online and offline data for the fermentation of E. coli BL21 (DE3) pRhotHi-2-EcFbFP-His6 under oxygen unlimited and oxygen limited conditions. Growth without oxygen limitation in WilmsMOPS medium (A, C, E) supplemented with 10 g/L glucose. Culture conditions for RAMOS: 250 mL RAMOS shake flasks, VL = 8 mL, n = 350 rpm, d0 = 50 mm, T = 37 °C. Culture conditions for BioLector: 48well-flowerplate, VL = 1 mL, n = 1500 rpm, d0 = 3 mm, T = 37 °C. Growth under oxygen limited conditions in WilmsMOPS medium (B, D, F) supplemented with 15 g/L glucose. Culture conditions for RAMOS: 250 mL RAMOS shake flasks, VL = 25 mL, n = 350 rpm, d0 = 50 mm, T = 37 °C. Culture conditions for BioLector: 48-well Flowerplates®, VL = 1 mL, n = 800 rpm, d0 = 3 mm, T = 37 °C. For better visibility product fluorescence values in E and F were multiplied by a factor of 3.

4. Diauxic growth and comparability of samples from MTP and shake flasks

As an additional scenario, growth under diauxic conditions was examined using 20 g/L glucose and 1.5 g/L sorbitol as carbon sources. To trigger not only a diauxic but triauxic effect, incubation conditions were chosen, leading to a short oxygen limitation. The experiment was performed at 30 °C to slow down the metabolic activity of *E. coli* to assure good visibility of diauxic growth. As for the previous described experiments, RAMOS, BioLector and separate shake flasks were run in parallel. Furthermore, samples for offline analysis were taken directly from the MTP by using the RoboLector system described in Chapter II (3.2.4).

Comparing the courses of OTR and DOT of RAMOS and RoboLector, respectively, the conformity becomes obvious. As seen before for the non-limited and oxygen limited scenarios the DOT course is a perfect mirror image of the OTR curve. After an exponential growth phase until about 15 h the foreseen oxygen limitation begins and from thereon only linear growth can be observed. These observations made by the course of OTR and DOT can also be verified by the OD_{600} and scattered light intensity (Fig. A 3B). In Fig. A 3B the comparability of offline samples taken from separate shake flasks and MTP is given. The OD_{600} was measured in both samples and the results are displayed as round dots in Fig. A 3B. The line within the dots represents the average of both samples. It is apparent how well the values from both systems align.

Casting an eye on the offline data, the specific maxima and minima of both curves can be easily explained. After 16 h of incubation the first drop in the OTR curve occurs, which is coherent with the depletion of glucose (Fig. A 3C). At this point the cells adapt their metabolic pathways and initiate the consumption of the second substrate sorbitol. Consumption and depletion of the 1.5 g/L sorbitol takes place within only 1 h (16.5 - 17.5 h). Subsequently and partly even simultaneously to sorbitol usage the former produced overflow

metabolite acetate is consumed. This explains rise and fall of the OTR curve between 17.5 h and 20 h. Decrease and increase of the pH value is due to the production and consumption of acetate as well as the uptake of ammonium salts, as previously described.

The results presented here clearly show the comparability of data derived from shake flasks and shaken microtiter plates as long as comparable reaction condtions are ensured. The maximum oxygen transfer rate was proven to be a sufficient comparability factor. The experiments show that the online measurement of the OTR in the RAMOS system perfectly aligns with the online DOT monitoring from the Biolector. The OD_{600} measured in offline samples and the scattered light intensity from the BioLector, both indicators for microbial growth, are in good accordance as long as regular growth in the presence of a carbon source is given.

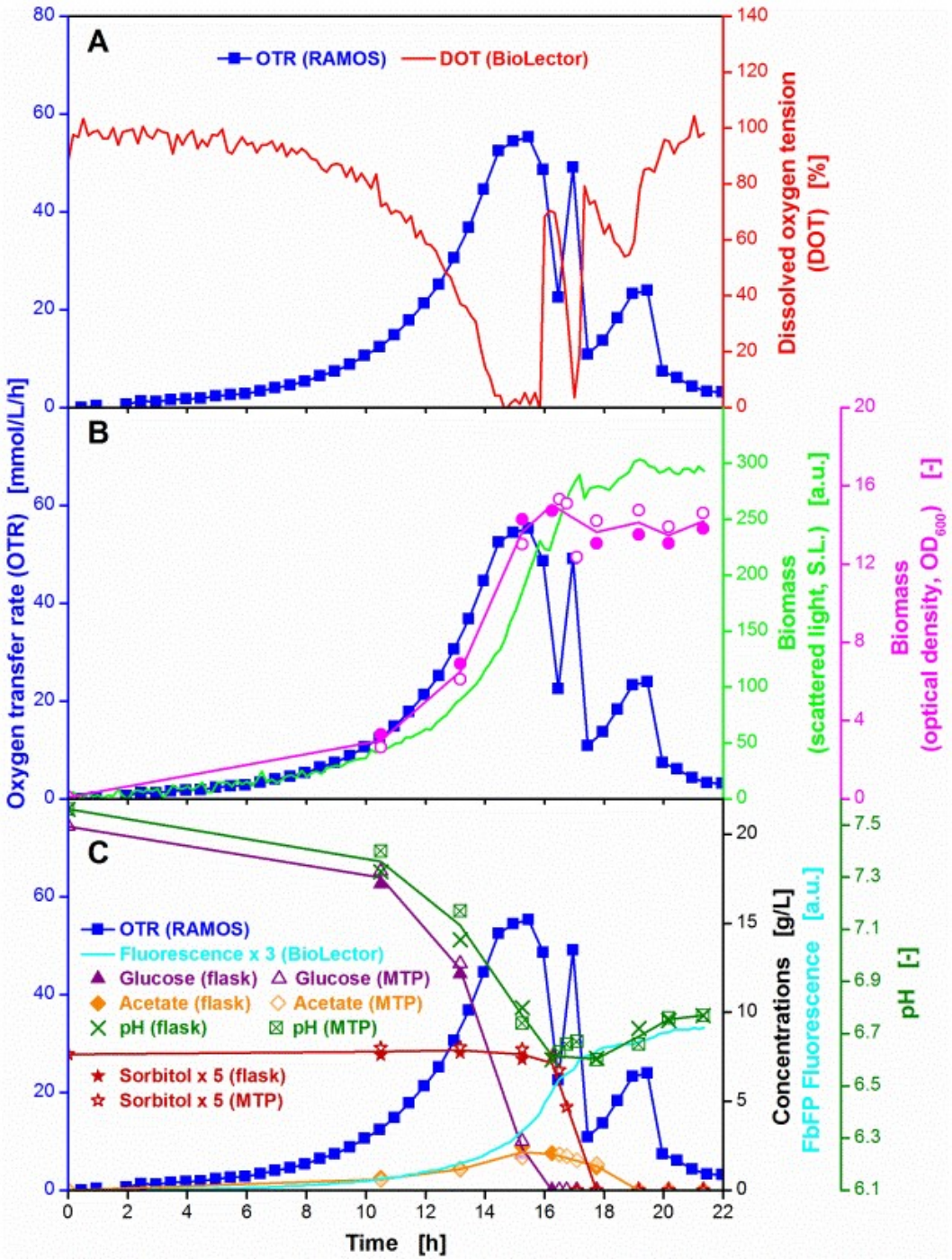

Fig. A 3 - Online and offline data for the fermentation of *E. coli* BL21 (DE3) pRhotHi-2-EcFbFP-His$_6$ under diauxic growth conditions. Diauxic growth in WilmsMOPS-medium supplemented with 20 g/L glucose and 1.5 g/L sorbitol. Culture conditions for RAMOS: 250 mL RAMOS shake flasks, V_L = 12 mL, n = 350 rpm, d_0 = 50 mm, T = 30 °C. Culture conditions for RoboLector: 48-well Flowerplates®, V_L = 0.6 mL, n = 1000 rpm, d_0 = 3 mm, T = 30 °C. Trend lines shown in Fig. 4 B and C for OD_{600}, glucose, acetate, sorbitol and pH are averages of the offline data obtained from 250 mL shake flasks and 48-well micro titer plate. For better visibility the sorbitol concentrations were multiplied with a factor of five and the product fluorescence values by a factor of 3.

5. Material & Methods

Materials

Chemicals were obtained from Sigma-Aldrich (Taufkirchen, Germany), Qiagen (Hilden, Germany), Merck (Darmstadt, Germany), Roth (Karlsruhe, Germany), and Roche Diagnostics (Mannheim, Germany).

Bacterial strain

E. coli BL21 (DE3) pRhotHi-2-EcFbFP-His_6 was bearing the expression plasmid consists of a T7 promoter which is under the control of the lac operator. For screening purposes a kanamycin resistance gene is integrated in the plasmid. As model protein the FMN-based fluorescent protein (FbFP) was used with codon-optimized for *E. coli* as expression host (hence the name EcFbFP) and additionally fused with a His_6-tag to the C-terminus resulting in a recombinant fusion protein with a molecular weight of 16.5 kDa. The EcFbFP encoding gene was cloned into the pRhotHi-2 vector downstream of the T7 promoter and EcFbFP.

Cultivation media

For the growth of *E. coli* two precultivations with different media were necessary. The first preculture was carried out in complex Terrific Broth (TB) medium composed of 12 g/L tryptone, 24 g/L yeast extract, 12.54 g/L K_2HPO_4, 2.3 g/L KH_2PO_4 and 5 g/L glycerol dissolved in deionized water. The pH-value was 7.2 ± 0.2 without adjustment.

Modified WilmsMOPS mineral medium was used for the second preculture and was prepared according to Wilms *et al.* that consisted of 5 g/L $(NH_4)_2SO_4$, 0.5 g/L NH_4Cl, 3 g/L K_2HPO_4, 2 g/L Na_2SO_4, 41.85 g/L (N-Morpholino)-propanesulfonic acid (MOPS), 0.5 g/L $MgSO_4 \cdot 7H_2O$, 0.01 g/L thiamine hydrochloride, 1 mL/L trace element solution [0.54 g/L $ZnSO_4 \cdot 7H_2O$, 0.48 g/L $CuSO_4 \cdot 5H_2O$, 0.3 g/L $MnSO_4 \cdot H_2O$, 0.54 g/L $CoCl_2 \cdot 6H_2O$, 41.76 g/L $FeCl_3 \cdot 6H_2O$, 1.98 g/L $CaCl_2 \cdot 2H_2O$, 33.4 g/L Na_2EDTA (Titriplex III)]. The pH-value was

adjusted to 7.5 with 1 M NaOH. All medium components were sterilized separately by autoclaving or filtration before mixing.

For the main cultivation the same modified WilmsMOPS mineral medium was used as it is described for the second precultivation in the section above. Altered concentrations of carbon sources are stated in the figure description.

To examine diauxic growth behavior modified WilmsMOPS mineral medium was prepared as mentioned for the second preculture but with altered substrate concentrations. No glycerol was added to the medium but a total of 20 g/L glucose and 1.5 g/L sorbitol.

Cultivation parameters

For all main cultivations a master mix was prepared prior to distribution to the respective incubation vessels. Master mix preparation was as follows: The medium for the main cultivation was completed (adding remaining supplements) and the beforehand determined volume of preculture was added to obtain the respectively desired initial optical density.

Precultivations of *E. coli* BL21 (DE3) pRhotHi-2-EcFbFP-His6 were performed in regular 250 mL shake flasks. For the first preculture 10 mL TB-medium containing 50 µg/mL kanamycin was inoculated with 100 µL from a cryo stock (cell solution in 50 % (w/w) glycerol/water). Subsequently the shake flasks were incubated over night at a temperature (T) of 37 °C on an orbital shaker at a shaking frequency (n) of 350 rpm and a shaking diameter (d_0) of 50 mm. As soon as an OD_{600} of 17±3 was reached (6-24 h), the second preculture was started by inoculating 10 mL of modified WilmsMOPS mineral medium supplemented with 10 g/L glucose to an initial OD_{600} of 0.1. Cultivation parameters (T, n, d_0) were kept the same and the culture was incubated over night for 8-11 h until an OD of 9±2 was obtained.

Processing of the main cultures for both *E. coli* strains were identical. For all cultivations a master mix with an initial OD of 0.1 was prepared. Subsequently, the master mix was

apportioned to the RAMOS flasks, separate shake flasks and Flowerplates® (cultivation parameters are described in a later section). The respective volumes are stated in the figure legends. Incubation parameters were T = 37 °C, n = 350 rpm and d_0 = 50 mm, if not otherwise stated.

RAMOS cultivations

The in-house developed Respiration Activity MOnitoring System (RAMOS, for references see Chapter I) allows the online measurement of the oxygen transfer rate (OTR). The resulting characteristic curve gives information about growth and metabolic activity of the investigated organism. All cultivations were conducted in 250 mL flasks modified as described by Anderlei & Büchs (2001) in the RAMOS device with the individually specified culture conditions.

Shake flask cultivations

Shake flask cultivations were carried out in conventional 250 mL Erlenmeyer flasks with the respective filling volume (stated in figure legends) under identical cultivation conditions as described for the main cultivations. At different time points single flasks were removed from the shaker and in total used for sample taking. Carbon source concentrations and byproduct via HPLC, biomass and the pH-value were measured offline.

Microtiter plate cultivations

All microtiter plate (MTP) cultivations were performed in 48 well Flowerplates®. An in house developed device, namely BioLector, was used for online measurement of scattered light (signal for biomass formation) and fluorescence (signal for product formation) during cultivations in microtiter plate scale. Signals were obtained by irradiating every single well with light of a defined wavelength (excitation), and detecting and analyzing the reflected/scattered light or fluorescence. The system is highly suitable for screenings in small

scale (100 – 2000 µL) and offers the opportunity of a non-invasive measurement of biomass formation and fluorescence activity. In combination with special microtiter plates equipped with optodes on the bottom of the MTPs, dissolved oxygen tension (DOT) can also be measured fluorometrically quasi-online and non-invasive. As for the RAMOS experiments, the specific respectively applied cultivation conditions are stated in the figure legends.

OTR_{max} determination

For determination of the maximum oxygen transfer capacity (OTR_{max}) in shake flasks, the main culture of *E. coli* BL21 (DE3) pRhotHi-2-EcFbFP-His6 was grown on modified WilmsMOPS mineral medium containing 10 g/L glucose. While keeping the shaking diameter (50 mm) and the shaking frequency (350 rpm) constant, the filling volume was altered in a range of 8 – 25 mL. A plateau in the resulting curves equals the OTR_{max} value under the respective conditions.

In order to determine the maximum oxygen transfer capacity of a Flowerplate® a modified RAMOS device was used which was first described 2005 by Kensy et al.. The so called MicroRAMOS is capable of measuring the oxygen transfer rate of a culture incubated in a micro titer plate. The cultures were grown in WilmsMOPS mineral medium supplemented with 20 g/L glucose. A high initial optical density (OD_{600}) of 1.0 was established to shorten the lag-phase enabling multiple plateaus with one experimental run. For the determination of OTR_{max} the shaking diameter was kept constant at 3 mm and the shaking frequency as well as the filling volume was altered in a range of 700 - 1000 rpm and 0.6 - 1.0 mL, respectively. The attained plateaus represent the OTR_{max} value of the applied cultivation condition.

C. HTS screening of microbial growth and cellulase cel8H expression in *E. coli* applying mCherry fluorescent tag

In the following figures the final values for scattered light and mCherry fluorescence intensity are presented for the cultivation of *E. coli cel8H-mCherry* in varied auto-induction media combining different amounts of glucose, lactose, and glycerol according to the cultivation conditions described under 3.3.6.

1. Variation of glycerol and lactose concentration at constant glucose

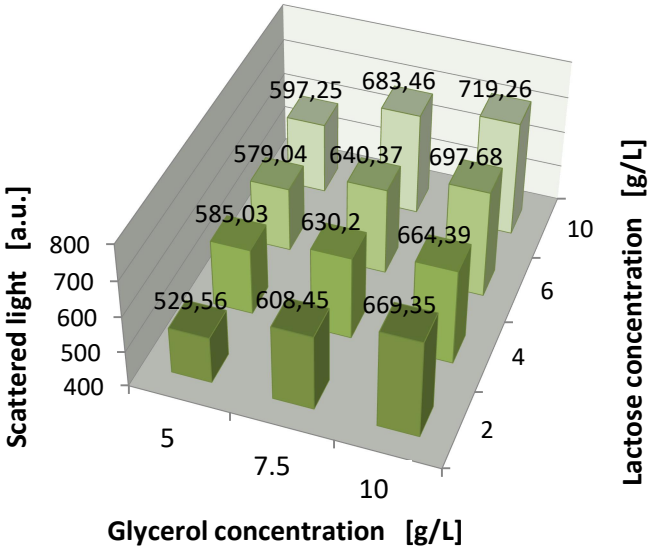

Fig. A 4 – Final scattered light as indicator for microbial growth after the cultivationof E. coli Cel8H-mCherry in auto-induction medium with varied lactose and glycerol concentration. Cultivation in 48-Flowerplate in the BioLector system, 800 µL filling volume, 1100 rpm shaking frequency, 3 mm shaking diameter, 37°C, OnEx medium with 0.5 g/L glucose and varied lactoose and glycerol concentrations.

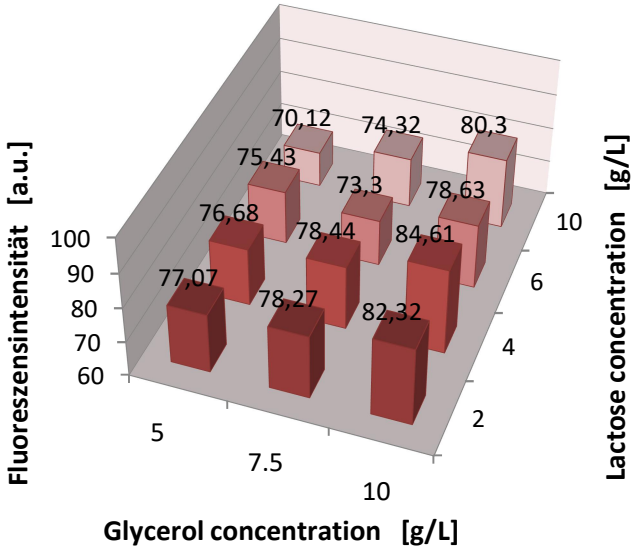

Fig. A 5 - Final mCherry fluorescence intensity as indicator for recombinant protein formation after the cultivationof *E. coli Cel8H-mCherry* in auto-induction medium with varied lactose and glycerol concentration. Cultivation in 48-Flowerplate in the BioLector system, 800 µL filling volume, 1100 rpm shaking frequency, 3 mm shaking diameter, 37°C, OnEx medium with 0.5 g/L glucose and varied lactose and glycerol concentrations.

2. Variation of glycerol and glucose concentration at constant lactose

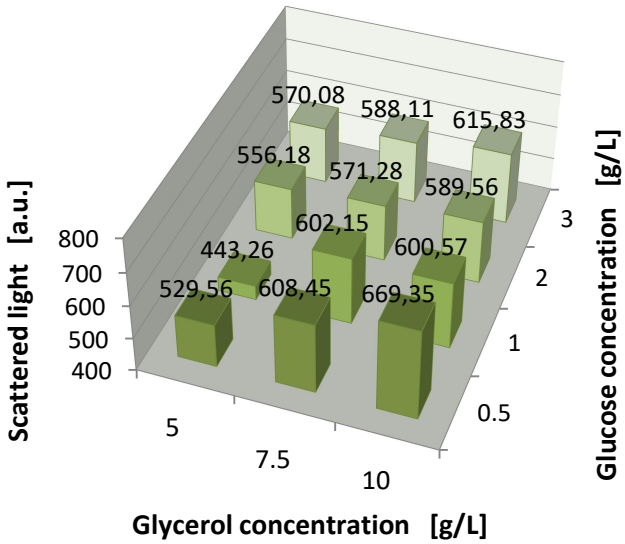

Fig. A 6 - Final scattered light as indicator for microbial growth after the cultivationof E. coli Cel8H-mCherry in auto-induction medium with varied glucose and glycerol concentration. Cultivation in 48-Flowerplate in the BioLector system, 800 µL filling volume, 1100 rpm shaking frequency, 3 mm shaking diameter, 37°C, OnEx medium with 2 g/L lactose and varied glucose and glycerol concentrations.

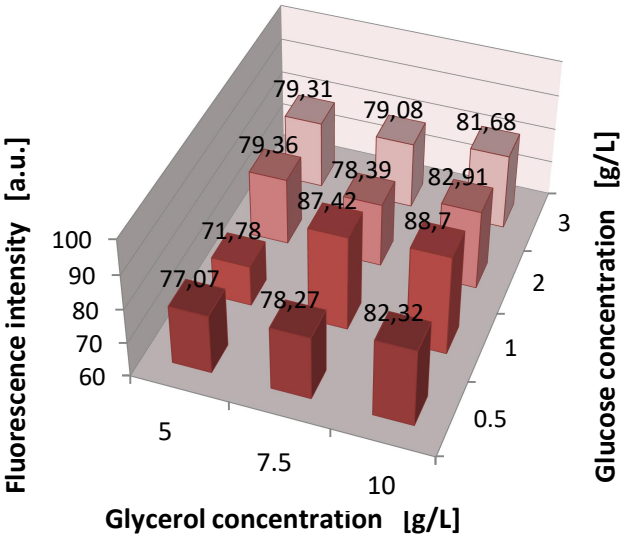

Fig. A 7 - Final mCherry fluorescence intensity as indicator for recombinant protein formation after the cultivationof E. coli Cel8H-mCherry in auto-induction medium with varied glucose and glycerol concentration. Cultivation in 48-Flowerplate in the BioLector system, 800 µL filling volume, 1100 rpm shaking frequency, 3 mm shaking diameter, 37°C, OnEx medium with 2 g/L lactose and varied glucose and glycerol concentrations.

3. Variation of glucose and lactose concentration at constant glycerol

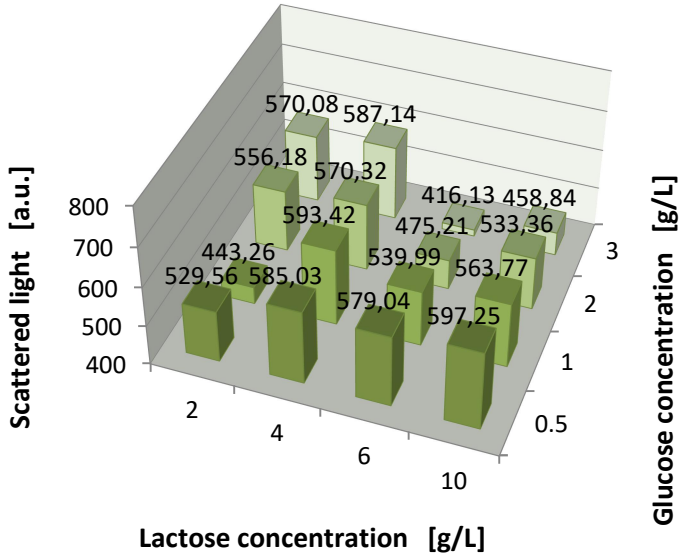

Fig. A 8 - Final scattered light as indicator for microbial growth after the cultivationof E. coli Cel8H-mCherry in auto-induction medium with varied glucose and lactose concentration. Cultivation in 48-Flowerplate in the BioLector system, 800 µL filling volume, 1100 rpm shaking frequency, 3 mm shaking diameter, 37°C, OnEx medium with 5 g/L glycerol and varied glucose and lactose concentrations.

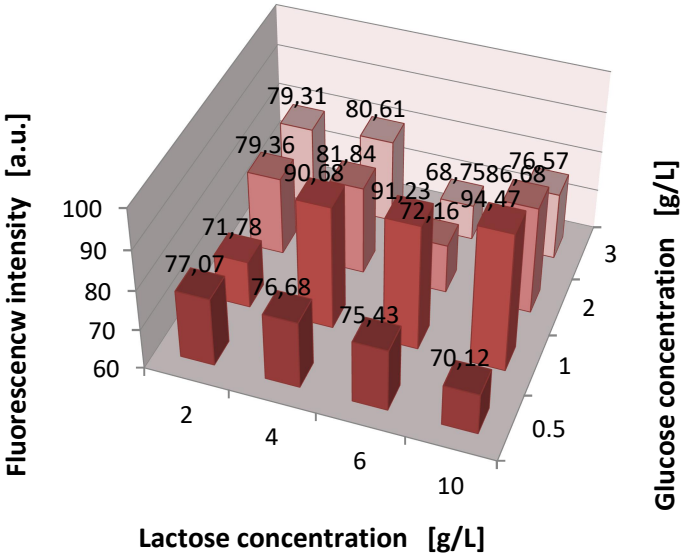

Fig. A 9 - Final mCherry fluorescence intensity as indicator for recombinant protein formation after the cultivationof E. coli Cel8H-mCherry in auto-induction medium with varied glucose and lactose concentration. Cultivation in 48-Flowerplate in the BioLector system, 800 µL filling volume, 1100 rpm shaking frequency, 3 mm shaking diameter, 37°C, OnEx medium with 5 g/L glycerol and varied glucose and lactose concentrations.